Fluorescent Ajoenes as a Mechanistic Probe for Cancer

By:

Jonathan Cotton

Thesis presented for the degree of Master of Science in Chemistry
Faculty of Science
University of Cape Town

December 2010

Supervisors:

Professors Roger Hunter, Mino Caira and Iqbal Parker

Declaration

I declare that this thesis is my own work. Where collaboration with other people has taken place, or material generated by other researchers is included, the parties and/or materials are indicated in the acknowledgements and/or are explicitly stated with the references as appropriate.

This work is being submitted for the Masters of Science in Chemistry at the University of Cape Town. It has not been submitted to any other university for any other degree or examination.

Jonathan Cotton	15 – 12 – 2010
	Date

Dedication

This thesis is dedicated to my loving family - Thank you for all you encouragement and support.

Acknowledgements

To my supervisors Professors Roger Hunter, Mino Caira and Iqbal Parker:

I don't think words alone can express my gratitude towards you. Apart from your support and encouragement, your kindness and mentorship inspired me to love and pursue a career in science. My appreciation for all the time and effort put into this thesis is unquestionably large.

To all the people working in the various laboratories involved with my project, I would like to offer my immense gratitude. Dr Nashia Stellenboom, Dr Yabing Wong, Dr Catherine Kaschula for biological assistance, Dr Dirk Lang for help with scanning laser confocal microscopy, Mr. Mohammed Jaffer for transmission electron microscopy, Lee Trollope, Dyanne Cruickshank, Aneesa Omar, the Hunter group, the Caira group, the Parker group, Noel Hendricks and Pete Roberts – Thank you!

Abstract

This thesis describes the development and synthesis of several novel ajoene mimics. The first of which, (*E/Z*)-1,8-(Bis-*p*-methoxyphenyl)-2,3,7-trithia-octa-4-ene 7-oxide **17**, was developed as a continuation of SAR studies performed by our group, involved the placing *p*-methoxyphenyl groups on the termini of the ajoene pharmacophore. **17** was found to be twenty times more active (IC_{50} = 0.83 ± 0.20) than *Z*-ajoene (IC_{50} = 13.70 ± 2.02) against MDA-MB-231 breast tumour epithelial cells. Despite its high *in vitro* activity, **17** was found to be ineffective at reducing tumour size in the animal studies performed.

Several fluorescently-tagged ajoenes were synthesized with the intention to view the localization of drug in treated cells using scanning confocal laser microscopy (SCLM). The localization of drug was hoped to help elucidate the biological mechanism associated with ajoene's anti-cancer activity. Two dansyl-tagged ajoenes, namely 5-(Dimethylamino)-*N*-(3-((3-(propylsulfinyl)prop-1-enyl)disulfanyl)propyl)naphthalene-1-sulfonamide **30** and 5-(Dimethylamino)-N-(3-((3-(4-methoxybenzylsulfinyl)prop-1-enyl)disulfanyl)propyl) naphthalene-1sulfonamide **32** as well as one fluorescein-tagged ajoene Methyl 2-(6-(3-((3-(4-methoxybenzylsulfinyl)prop-1-enyl)disulfanyl)propoxy)-3-oxo-3*H*-xanthen-9-yl)-4-nitrobenzoate **53** were synthesized. MDA-MB-231 cells treated with **30** and **53** were examined under SCLM. Cells treated with **53** revealed localization of drug in the endoplasmic reticulum (ER).

Attempts to solubilize the ajoene mimics through cyclodextrin (CD) inclusion were unsuccessful. Several inclusion complexes were generated through kneading **17** and **53** with β- and γ-CD, with isostructurality detected from the powder X-ray diffraction (PXRD) patterns.

Abbreviations

Ac	Acetyl
Ac_2O	acetic anhydride
ACCN	1,1'-Azobis(cyclohexanecarbonitrile)
AML	acute myeloid leukemia
Ar	Aromatic
ATM	ataxia-telangiectasia, mutated
Bn	Benzyl
Bp	boiling point
BFP	blue fluorescent protein
Boc	*tert*-butyloxycarbamate
BSA	bovine serum albumin
cat	catalytic
CAN	Ceric ammonium nitrate
CD	cyclodextrin
CDK	cyclin-dependent kinase
CH_3CN	acetonitrile
m-CPBA	meta-Chloroperbenzoic acid
cys	cysteine
DCM	Dichloromethane
DNA	deoxyribonucleic acid
DCC	Dicyclohexylcarbodiimide
DIMEB	2,6-dimethyl-β-cyclodextrin
DMEM	Dulbecco's Modified Eagle Medium
DMF	Dimethyl formamide
DMSO	Dimethyl sulfoxude
d	doublet
dd	doublet of doublets
dt	doublet of triplets
EDTA	Ethylenediaminetetraacetic acid
eq	equivalents
ER	endoplasmic reticulum
Et	Ethyl
EtOAc	ethyl acetate
EtOH	ethanol
FITC	fluorescein isothiocyanate
FBS	fetal bovine serum
g	grams
GFP	green fluorescent protein
GR	(human) glutathione reductase
Hz	Hertz
HOMO	Highest occupied molecular orbital
HPLC	High performance liquid chromatography
HRMS	High resonance mass spectrometry
HSQC	Heteronuclear Single Quantum Coherence
h	hour
IC_{50}	concentration inhibiting 50 % of cell-growth
IR	Infra red spectroscopy
J	Coupling constant
KOH	potassium hydroxide
K_2CO_3	potassium carbonate
LUMO	Lowest unoccupied molecular orbital
MeOH	methanol
MS	Mass spectrometry or Molecular sieves
MHz	Megahertz

m	*meta*
m	multiplet
Me	Methyl
mg	milligrams
$MgSO_4$	magnesium sulfate
mL	millilitres
mmHg	millimetre mercury, torr
mmol	millimole
min	minute
MMP	mitochondrial membrane permeabilization
M.p	Melting point
Ms	Methanesulfonyl
MTT	(3-(4,5-Dimethylthiazol-2-yl)-2,5-diphenyltetrazolium bromide
N_2	nitrogen
NaI	sodium iodide
Na_2S	sodium sulfide
NMR	Nuclear Magnetic Resonance
NaSH	sodium hydrosulfide
o	orthro
p	para
PBS	phosphate buffer solution (pH 7.4)
PMB	*p*-Methoxybenzyl
Ph	Phenyl
q	quartet
ROS	reactive oxygen species
rt	room temperature
s	singlet
SAR	structure-activity relationship
SCLM	scanning confocal laser microscope(y)
SLS	sodium laurel sulfate
TBAI	Tetrabutylammonium Iodide
TEM	transmission electron microscope
THF	Tetrahydrofuran
TLC	Thin layer chromatography
TR	(*T. cruizi)* trypanothione reductase
TRIMEA	(2,3,6-tri-O-methyl)-α-cyclodextrin
TRIMEB	(2,3,6-tri-O-methyl)-β-cyclodextrin
Ts	p-Toluenesulfonyl
TMS	Trimethylsilyl
t	triplet
td	triplet of doublets
UCT	University of Cape Town
UPR	unfolded protein response
UV	ultra-violet
YFP	yellow fluorescent protein
λ_{ex}	wavelength (of light) to excite fluorophore
λ_{em}	wavelength (of light) emitted by fluorophore

Chapter 1: Review of the Biological and Synthetic Aspects of Ajoene and General Background

1.1 Introduction

This thesis describes the synthesis of several fluorescent ajoenes designed for elucidating the biological mechanism of ajoene-induced anti-cancer activity. The project spans several disciplines, thus this chapter will offer an overview of the fundamental concepts and background information relevant to the project.

1.2 Overview of Garlic

From the beginnings of human civilization, people have relied on the healing potential of plants. Garlic or *Allium sativum*, has been widely used to treat ailments ranging from inflammation[1] to fungal infection.[2] Around the 5th century BC, Aristotle and Hippocrates, both of whom were unaware of the potent organosulfur chemistry at work, advocated natural remedies based on garlic extracts.[3] Although other members of the *Allium* family (e.g. onion) also contain organosulfur compounds, their concentrations are typically three times lower than those in garlic.[4]

1.2.1 Organosulfur Compounds Found in Garlic

Intact cloves of garlic contain the allylcysteine sulfoxide alliin (see Scheme 1 i), that upon maceration is converted by the enzyme allinase (stored separately in mesophyll vacuoles) into 2-propenesulfenic acid (step 1). This enzyme and substrate can for example be brought together via mechanical damage i.e. chopping/crushing or via invasion by a pathogen. 2-Propenesulfenic acid is unstable and readily self-condenses to form the thiosulfinate allicin (step 2) as well as several other organosulfur compounds.[5] Allicin continues to be widely studied for its applications as a medicinal agent. It can be synthesized in the laboratory through the oxidation of diallyl disulfide with peracetic acid formed by mixing hydrogen peroxide with acetic acid (see Scheme 1 ii). Allicin is unstable and readily rearranges into more stable products.[4]

Many rearrangement products of allicin possess useful biological activities, similar to allicin. A full description of the organosulfur compounds found in garlic extracts is beyond the scope of this project, however Figure 1 below depicts some the major compounds and their chemical structures.[6]

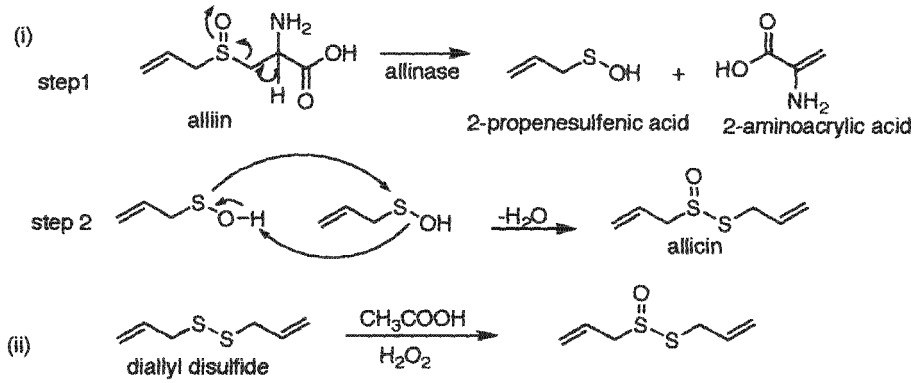

Scheme 1: (i) The formation of allicin from alliin - Step 1, the degradation of alliin into 2-propenesulfenic acid and 2-aminoacrylic acid. Step 2, the self-condensation of 2-propenesulfenic acid into allicin (ii) The chemical synthesis of allicin from diallyl disulfide.

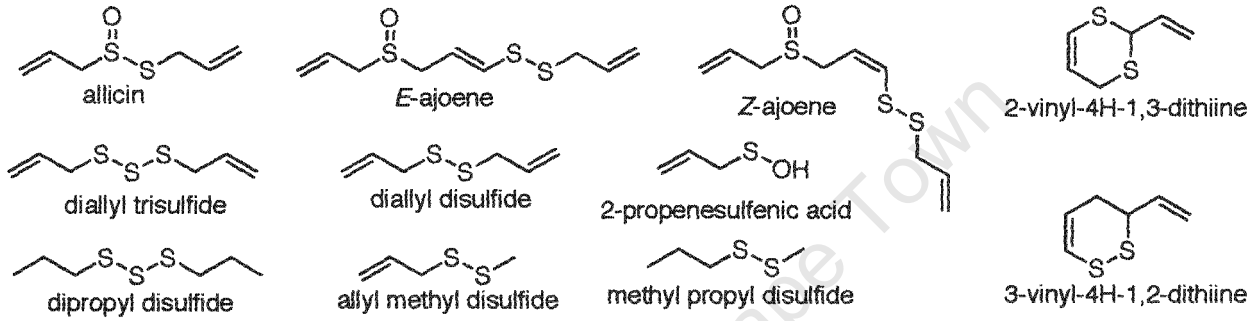

Figure 1: Some of the major sulfur-containing compounds found in garlic extracts.

1.3 Ajoene

Ajoene (*E/Z*-4-5-9-trithiadodeca-1,6,11-triene-9-oxide), a stable rearrangement product of allicin, was first characterized in the 1980s by Block and Apitz-Castro, who postulated that it is formed (see Scheme 2) when two molecules of allicin combine via S-thioallylation to give a sulfonium ion, which can then undergo a Cope-type elimination to form a vinylthionium ion and 2-propenesulfenic acid. The final step involves a Michael-type addition between the two newly formed intermediates, resulting in an *E/Z*-mixture of ajoene.[7]

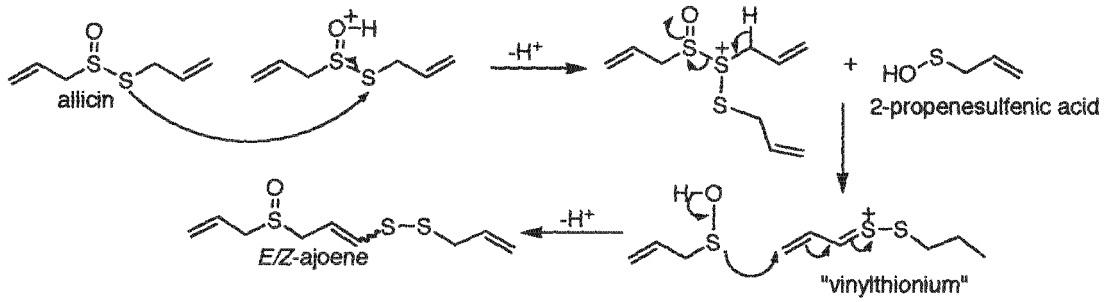

Scheme 2: Rearrangement of allicin to *(E/Z)*-ajoene. The reaction proceeds via the S-thioallylation of allicin, followed by a Cope-type elimination to produce the vinylthionium ion, which undergoes a Michael-type addition with 2-propenesulfenic acid to form *(E/Z)*-ajoene.

A common motif amongst the compounds shown in Figure 1 is the presence of a di- or tri-sulfide backbone, thought to be the pharmacophore of their diverse biological activities. Ajoene stands out from the rest as it is the only compound containing a vinyl disulfide group. The vinyl moiety is thought to labilize the disulfide bond further; possibly giving ajoene enhanced activity compared to other related rearrangement products. Ajoene is more stable than allicin and has been studied over the past 20 years, for its anti-thrombotic activity.[8] Ajoene exhibits a wide range of biological activities and has been used therapeutically to treat a variety of microbial infections, namely: fungal, bacterial and parasitic (trypanosoma and malaria).[9] Ajoene has been shown to lower blood cholesterol and to inhibit the human gastric lipase and lipoxygenase enzymes.[10] However, the key bioactivity of ajoene for this dissertation is its anti-cancer activity.

1.4 Cancer

Cancer is a class of disease in which a group of cells display uncontrolled growth or division and is a result of the cell's ability to evade apoptosis. Cancer is often invasive causing damage to adjacent cells, and is prone to spread to other parts of the body (through metastasis) via blood or lymph vessels. Cancer is a leading cause of death worldwide, accounting for 7.9 million deaths (around 13% of all deaths) in 2007.[11]

1.4.1 Treatment of cancer

In the broad sense, most *chemotherapeutic* drugs work by impairing cell division, effectively targeting fast-dividing cells. Many chemotherapeutic drugs cause cells to undergo apoptosis (see Section 1.4.3) and as these drugs cause damage to cells, they are termed *cytotoxic.*

Common classes of chemotherapeutic drugs include:[12]

1. Alkylating agents – Alkylating agents such as cisplatin are able to alkylate nucleophilic functional groups within the cancer cell, forming covalent bonds with amino, sulfhydryl, carboxyl and phosphate groups, thus impairing cell function.
2. Antimetabolites – Antimetabolites inhibit normal cell division by masquerading as DNA-bases, preventing DNA replication and subsequently mitotic division.
3. Anthracyclines - Chemicals derived from streptomyces, which inhibit DNA and RNA replication.
4. Plant alkaloids – Vinca alkaloids, originally from the Madagascar periwinkle inhibit the assembly of the microtubules, which is essential for cell division. Taxanes, originally derived from the bark of the pacific Yew tree, act to strengthen the microtubule network, preventing separation during anaphase.

The side effects of most chemotherapeutic drugs include suppression of the immune system, fatigue, hair loss, weakness, nausea, gastro-intestinal upset and anemia. Over time, cancer cells develop

resistance to chemotherapeutic treatments[13], and thus there is a constant need to develop new chemotherapeutic agents to combat resistance, while also invoking fewer negative side-effects.

1.4.2 Cell Life-cycle

A common feature amongst all eukaryotes is the need for cellular proliferation. In complex, multi-cellular organisms such as mammals, this process is essential for the maintenance of all tissues and organs needed to sustain life. The cell-cycle (see Figure 2) is thus a series of events leading to cell division and duplication and is a carefully controlled and highly precise process.[14] Each class of anti-cancer pharmaceuticals target specific processes in the cell's growth cycle and thus understanding both the cell's life cycle and the drug's mode of action can enhance the development of new anti-cancer agents.

The cell cycle comprises five stages: The first is the *resting phase* (G_0). The next phase is G_1, in which various enzymes and proteins needed for replication and division are synthesized. The next phase (S) involves the replication of the DNA. The cell undergoes a second growth phase (G_2), in which it experiences high levels of biosynthesis, mainly involving production of the microtubules required for mitotis. The final stage of cell division is *mitosis* (M), which involves the division of the cell into two identical daughter cells.

To ensure proper progression through the cell cycle, cells have developed a series of checkpoints to safeguard them from entering a new phase of development until they have successfully completed the previous one. The cycle is mediated by two classes of regulatory molecules, cyclins and cyclin-dependent kinases (CDKs), that control the progression through the cell cycle.[14]

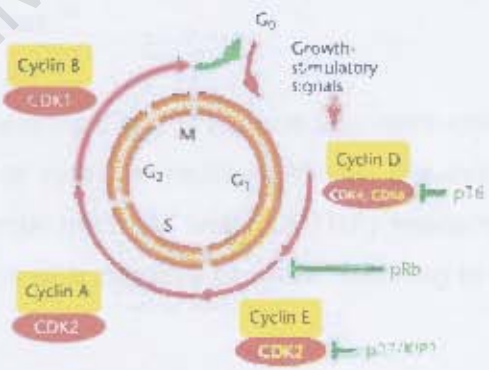

Figure 2: Cell-cycle illustrating critical regulators and checkpoints. Cell cycle consists of G_1, S, G_2 and M phases as indicated with checkpoints in G_1, G_2 and M shown as horizontal green T-bars. Sequential activation of the indicated Cyclin-CDK (cyclin-dependent kinase) complexes drives the cell cycle (red arrows). Cell cycle progression can be blocked by negative regulators such as p16, pRb (retinoblastoma protein) and p27/KIP1 (kinase inhibitor protein 1) or by exit from the cell cycle into G_0 phase. Growth-stimulatory signals can lead to re-entry into the cell cycle.[14]

Growth factor signals stimulate the synthesis of D-type cyclins in the G_1 phase, which then form an active complex with CDK4 and CDK6. The primary substrate of CDK4/6 is the retinoblastoma protein (pRb), which in its active hypophosphorylated form inhibits cell cycle progression by binding and repressing the activity of E2F. The transcription of several genes then occurs in the G_1 to S transition. To facilitate the latter, E-type cyclins are then synthesized and complex with CDK2. Cyclin A then complexes with CDK2 to allow the cell to enter into G_2 and it is at this point that the cell prepares for mitotic division. Microtubule networks are generated through the transcription of tubulin and it is through the complexing of cyclin B and CDK1 that the cell is triggered to undergo mitosis.[14]

1.4.3 Apoptosis

Amongst all vertebrates there is the need for continuous homeostasis of biomass. This is affected by the careful balance between cellular proliferation and apoptosis. Apoptosis by definition is programmed cell death and is essential for life. Apoptosis is an energy-dependent, genetically determined process. It proceeds without resulting in inflammation as compared to necrosis, which is an energy-independent cell death that non-specifically affects cell groups and leads to inflammation. The genetic pathways that control both the proliferation and apoptosis of cells are strictly controlled and consequently, when deranged or mutated, cause auto-immune disease and cancer.[14]

Apoptosis occurs via several molecular pathways, some of which are well defined. Damage sensors such as "*ataxia-telangiectasia mutated*" (ATM) in the nucleus or death receptors associated with the cell membrane, can initiate signaling cascades that activate 'execution machinery', to 'kill' the cell. The two principal pathways are mitochondrial and death-receptor mediated apoptosis. Intimately connected, one pathway often complements and amplifies the other. Both pathways are mediated by a family of cysteine proteases called caspases.[14]

The death receptor pathway is extrinsic and is triggered by extra-cellular stimuli such as growth-factor withdrawal, matrix detachment or cytokine-mediated killing. The extrinsic pathway is initiated when a suitable death ligand (e.g. tumour necrosis factor or TNF) interacts with its corresponding surface-receptor, leading to the activation of a caspase cascade, resulting in the cleavage of proteins essential for cell viability.[14]

The mitochondrial pathway is intrinsic and is triggered by intracellular stimuli such as deoxyribonucleic acid (DNA) damage or osmotic stress. This process is mediated by Bcl-2 proteins, which exist as both pro- and anti-apoptotic varieties. In response to apoptotic signals, proapoptotic *Bcl-2* family proteins such as *Bax* translocate to and alter the permeability of the mitochondrial membrane, leading to cytochrome *c* release and the activation of the caspase cascade. Anti-apoptitic Bcl-2 family members such as Bcl-2 and Bcl-xL counter these effects.[14 15]

1.4.4 Other Causes of Apoptosis

Disturbances in the normal endoplasmic reticulum (ER) functions lead to an evolutionarily conserved cell-stress response.[16] The ER fulfills many cellular functions, with its lumen containing the highest concentration of calcium (Ca^{2+}) in the cell. The lumen is an oxidative environment, critical to the proper folding of many cellular and excreted proteins. Disturbances in the cellular redox regulation cause an accumulation of unfolded proteins in the ER lumen leading to the unfolded protein response (UPR). If the cell cannot restore homeostasis, the UPR triggers apoptosis.[17]

The mechanisms surrounding this induction of apoptosis are poorly understood, but several pathways may be involved. Caspases linked to both the mitochondrial and/or death receptor mediated apoptotic pathways are implicated in the process. The ER has been shown, in a similar fashion to the mitochondria, to release apoptogenic proteins into the cytosol. The release of Ca^{2+} from the ER lumen into the cytosol may also induce apoptosis through enhancing the cellular oxidative environment and by encouraging increasing concentrations of Ca^{2+} to accumulate in the mitochondria.[16 17]

1.5 Anti-cancer Activity of Ajoene

1.5.1 Anti-mutagenic

The first topic of discussion relating to the anti-cancer activity of ajoene is its use as a preventative agent, rather than for treatment. Epidemiological evidence exists linking a dietary intake of garlic with a lowered risk of certain types of cancer.[18] This is most likely attributed to the combined action of many biologically active compounds in garlic. Specifically, ajoene has been shown to inhibit the activation of the known carcinogens benzo[a]pyrene and 4-nitro-1,2-phenylenediamine in *Salmonella typhimurium in vitro*.[19] The full mechanism of action has not been elucidated, but it is likely to proceed via a similar mechanism to other garlic organosulfides. One proposed mechanism is the inhibition of cytochrome P450-dependent monooxygenases responsible for carcinogen activation as well as the induction of phase II detoxification enzymes, which are responsible for accelerated carcinogen detoxification.[20]

1.5.2 Anti-tumor

Since the early 1990s, ajoene has been shown to exert an anti-proliferative effect on growing cancer cell-lines, both *in vitro* and *in vivo*.[21 22]

In vitro, ajoene has been shown to have activity at inhibiting cell growth of cultured mammary, bladder, colorectal, gastric, prostate, lung, pancreatic, lymphoid, skin, hepatic and leukemia cancer cells, with IC_{50} values ranging from 4 - 41 μM.[21, 23] Wagner and coworkers were the first to discover the cytotoxic effects of ajoene, which was twice as active against Burkitt lymphoid BJA-B cells compared with the control cell-line (baby hampster kidney BHK_{21}) as well as human primary fibroblasts.[21 23b] Another

example highlighting the selectivity of ajoene towards malignant cell-lines was reported by Dirsch[24] and coworkers, who demonstrated ajoene's ability to induce apoptosis in human leukemia cells, but not in the blood cells of healthy donors. Contrasting results were obtained by Taylor et al., who did not find any selectivity for tumor versus the non-tumor fibroblast NIH3T3 cell-line. This lack of selectivity may be due to the fact that the NIH3T3 cell-line had been immortalized.[25]

In vivo, ajoene inhibits malignant cell growth in both human and animal models. Thus, ajoene was found be an effective treatment for skin carcinoma in both humans (nodular or basal cell carcinoma) and rodents (xenograft), with a topical application reducing tumor size in over 80% of the human subjects.[26] Ajoene, administered through intraperitoneal injection, has been shown to reduce the size and metastasis of several tumor-lines grown in mice.[23b 23a]

1.5.3 Chemosensitization

Ajoene displays the interesting property of inducing a chemosensitizing effect on cells, reversing resistance to chemotheraputic drugs. Specifically, Hassan has shown that ajoene can enhance the apoptotic effect that drugs such as fludarabine and cytarabine have on resistant acute myeloid leukemia (AML) KG_{1a} cells, presenting the prospect of a combination therapy that requires much lower doses of the toxic chemotherapeutic drugs. It is thought that this effect is related to ajoene's ability to reduce the over-expression of the anti-apoptotic protein Bcl-2 in resistant cell lines.[27 28]

1.6 Signaling Pathways

Dirsch *et al.* has shown that ajoene administered to human promyelocytic leukemia HL-60 cells stimulates the generation of reactive oxygen species (ROS) and NFκB, a common regulatory protein for cellular proliferation.[25 29] After ajoene exposure, these cells showed increased production of intracellular peroxide in a time- and dose-dependent manner, which could be blocked by preincubation with the anti-oxidant *N*-acetylcysteine. Peroxides puts the cell under oxidative stress, resulting in activation of NFκB. It is thought that ROS may induce apoptosis through the interference with signal transduction. The signaling cascades leading to apoptosis utilize ROS as secondary messengers.

The molecular pathway by which ajoene induces apoptosis strongly points to the activation of the mitochondrial-dependent caspase cascade (see Figure 3).[24, 30] Dirsch using the same HL-60 proluekemia cell-line, showed that ajoene-induced apoptosis is dependent on the activation of caspase-3.[24] This activation was measured using a fluorescent DEVD-cleavage assay, when caspase-3-like activity was detected at 4 hours after ajoene treatment. The time-dependent activation of caspase-3-like proteases was then confirmed by monitoring the cleavage of poly(ADP-ribose)polymerase (PARP), a nuclear protein that is cleaved by caspases during apoptosis (Figure 3). It is interesting to note that the HL-60 cell-line expressed functionally inactive CD-95 death receptors,

meaning that the death-receptor mediated apoptotic pathways were not essential for cell ajoene induced apoptosis.

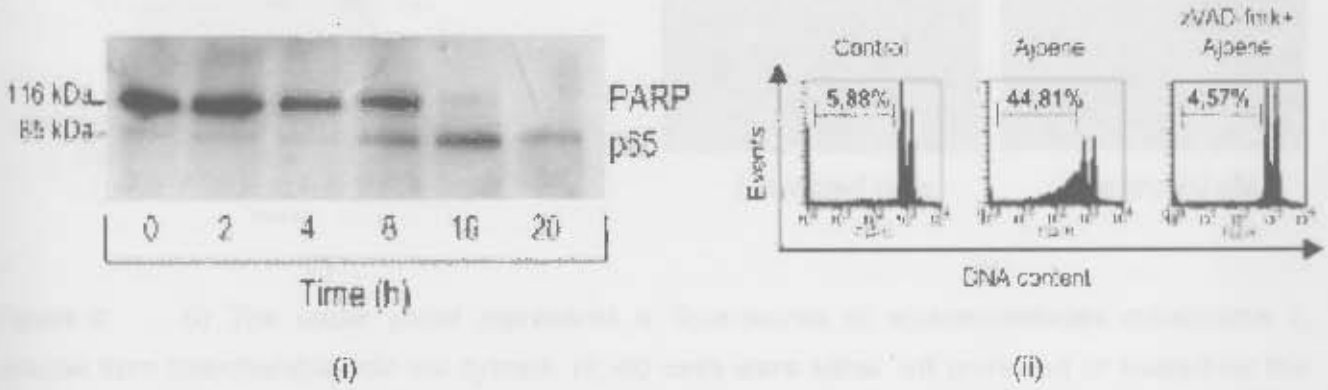

(i) (ii)

Figure 3: (i) Time-dependent cleavage of PARP. HL-60 cells were treated with ajoene (20 μM) for the indicated time. 40 μg of protein was separated using 10 % SDS-PAGE, with anti-PARP used as a detector; (ii) Caspase inhibitor zVAD-fmk inhibits ajoene mediated apoptosis. HL-60 cells were treated with ajoene (20μM, 8 h) or preincubated with zVAD-fmk (100 μM, 1 h) and then incubated in ajoene as above. The nuclei were stained with propidium iodide and DNA content was analyzed by flow cytometry.[15]

Dirsch *et. al.* also showed that ajoene induces mitochondrial membrane permeabilization (MMP) (see Figure 4 i), a key step in cell death. The induction of caspase-3-like activity in the human promyelocytic leukemia (HL-60) cell-line is linked to the release of mitochondrial factors such as cytochrome C. into the cytosol (see Figure 4 ii). Cytochrome C binds to a cytoplasmic protein (Apaf-1) starting a caspase cascade resulting in the loss of mitochondrial transmembrane potential and cell termination. The mechanism does not require JNK (Jun N-terminal Kinases), but is amplified by the inhibition of ERK (extra-cellular signal related kinases).[15,29]

(i) (ii)

Figure 4: (i) The upper panel represents a time-course of ajoene-mediated cytochrome c release from mitochondria into the cytosol. HL-60 cells were either left untreated or treated for the indicated time with ajoene (20 µM) or as positive control with etoposide (Et,17 µM) for 5h. The lower panel reflects a time-course of cytochrome c as it appears in the cytosol of HL-60 cells treated with ajoene (20 µM) for the indicated time. In parallel, at each time-point, cells were preincubated for 1 h with the caspase inhibitor zVAD-fmk (100 µM) and then treated with ajoene (20 µM). Cytosol and mitochondrial fractions were separated by 15% SDS-PAGE and cytochrome c was detected by immunoblot analysis using a monoclonal anti-body; HL-60 cells; (ii) Dissipation of MMP in cells treated with ajoene (20 µM) for 8h, stained with the fluorochrome JC-1 and analyzed by fluorescence microscopy. The red fluorescence reflects the multimer form of JC-1 localized in mitochondria under control (untreated) conditions. The green fluorescence corresponds to monomer JC-1 after ajoene-induced dissipation of MMP.[15]

1.7 The Mode of Action of Ajoene and Possible Drug Targets

The anti-cancer activity of ajoene has been linked to the mitochondrial mediated apoptotic pathways, but the mechanism and drug targets remain unknown. Ajoene contains a vinyl disulfide group, which is likely responsible for its biological activity. Disulfides are well known to behave as thiol oxidizing agents, modifying proteins and enzymes through the thiolation of exposed cysteine residues. This modification can lead to an alteration of enzyme or protein function and eventually cell death. [31]

Ajoene has been shown by Gallwitz and co-workers to act as a covalent inhibitor of both human glutathione reductase (GR) and *T. cruzi* trypanothione reductase (TR). This inhibition was found to be both time- and temperature-dependent. GR was found to react in its reduced state (EH_2) with ajoene to form a mixed disulfide. X-ray crystallography revealed a modification in the active site at Cys-58 (see Scheme 3 i) to form CH_2=CH-CH_2-(SO)-CH_2-CH=CH-S-S-(Cys-58)-GR. The ajoene-sulfoxide was also implicated in H-bonding to the GR active site, highlighting the importance of the sulfoxide in this aspect of ajoene's biological activity, as diallyl trisulfide was not found to inhibit GR. Furthermore, this result implies the *in vivo* regioselective preference of the cysteine sulfhydryl sulfur to nucleophilic attack at the

vinyl-S over the allyl-S, which is counterintuitive since one would expect the vinyl-S to be less electrophilic than the allyl-S in view of the vinyl-S being a better leaving group. Making reference to a PhD thesis, Gallwitz *et. al.* alluded to the reaction between ajoene and free cysteine. It was found that the reaction led to the formation of allyl-S-S-cysteine and a mixed disulfide involving the 1,5-dithiaocta-2,7-diene 5-oxide (Scheme 3 **ii**). Furthermore, when ajoene was reacted with 2 molar equivalents of cysteine (see Scheme 3, **iii**) in a neutral buffer, two products, namely ajocysteine (3-((3-(allylsulfinyl)prop-1-enyl)disulfanyl)-2-aminopropanoic acid) and S-allylmercaptocysteine, were formed.[9] It may be that the spatial and electronic environment in the GR active site pocket facilitates the formation of the less favoured product. Another postulation is that the results of Gallwitz reflect the secondary reaction of an ajoene metabolite with the active site of GR and that the primary reaction with the allyl-S occurs elsewhere.

GR that has been covalently modified by ajoene shows increased oxidase activity. Through the blocking of Cys58, electron density is expected to shift toward the flavin ring, promoting reduction of molecular oxygen. The elevated oxidase activity of ajoene-modified GR, together with its inability to reduce glutathione disulfide, is expected to have a strong impact on the redox status of the cell.[9] It has been shown that free cysteine can form disulfide bridges with both sulfurs of the vinyl disulfide pharmacophore.[20] However, which product(s) are primary (kinetic) ones remains to be established.

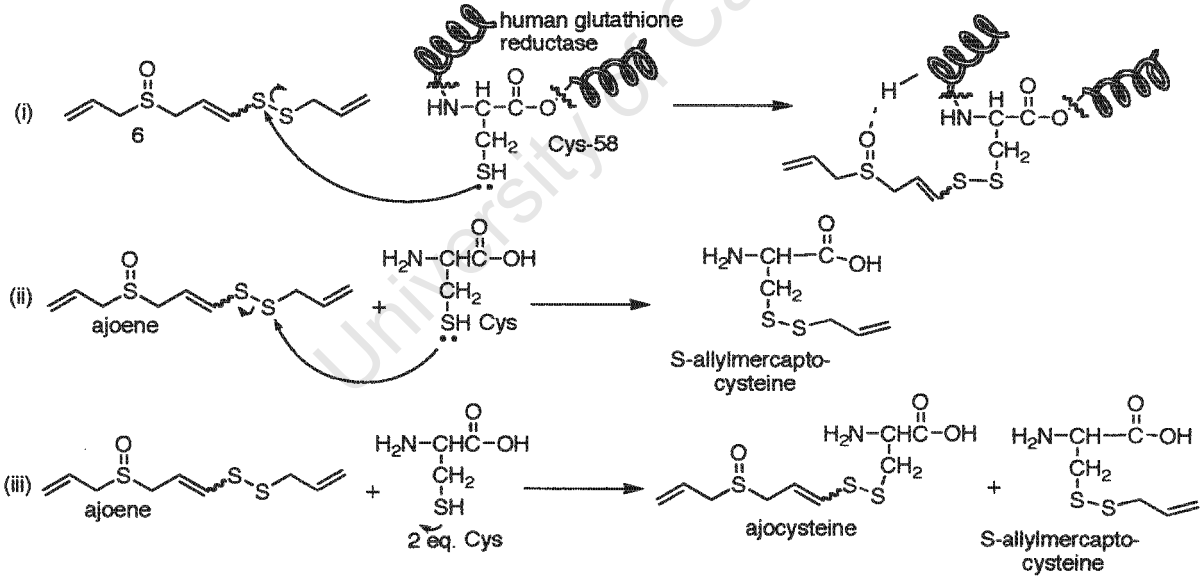

Scheme 3: (i) Ajoene is a covalent inhibitor of glutathione reductase[9]; (ii) Reaction of ajoene with 1 equiv. cysteine; (iii) Reaction of ajoene with 2 equiv. cysteine.[20]

Ajoene has been shown to inhibit a number of enzymes such as lipoxygenase and human gastric lipase, but the molecular mechanism of inhibition has not yet been elucidated.[10] It is possible that the inhibition is associated with a covalent protein modification as described above. The activity may also involve more complicated pathways, such as non-covalent competitive inhibition or radical generation.

It has been proposed that ajoene may also exert an effect by compromising the integrity of cell membranes through various hydrophobic interactions.

Because of its diverse biological activity, it is likely that ajoene has multiple drug targets. There is evidence to link ajoene's biological activity with its ability to interact with and modify proteins e.g. β-tubulin[23a] and $\alpha_4\beta_1$ integrin[32]. Ajoene inhibits platelet aggregation and exerts its anti-thrombotic activity by interacting directly with the fibrinogen receptor GPIIb/IIIa.[33] This effect also implicates integrins as a possible target of ajoene.

Work done by Li *et al.* at Peking University have indicated interesting interactions between ajoene and cellular microtubules, leading to a blocking of cells in the G_2/M phase of the cell cycle. The garlic-derived diallyl trisulfide disrupts microtubule formation in a similar fashion through the oxidative modification of the Cys-12β and Cys-354β residues of the protein constituent of tubulin.[30]

1.8 Fluorescent-labeling

The medical and scientific communities are constantly seeking new techniques for visualizing and understanding biological processes. The ability to attach traceable markers to drugs (and other small molecules) has contributed to the advancement of medicinal chemistry. Knowledge of the movement and localization of the drug in a cell can offer a unique perspective into its activity and function.[34 35]

Fluorescence is an appealing technique as the energy required to excite the fluorophore is often non-destructive to biological samples. Determining the biological mechanism by which a pharmaceutically active compound exerts its activity is difficult. *Frisoli et al.* demonstrated the use of fluorescent compounds to determine the location and tissue concentration of pharmaceutical agents. Through the analysis of data obtained by fluorescent tagging, pharmacokinetic models can be enhanced, resulting in a better understanding of drug activity and better dosimetry.[35]

Fluorescence is a type of luminescence that is mostly associated with cold bodies. The principles of fluorescence (see Figure 5) are similar to any absorption-emission spectral phenomenon. Typically, the energies of excitation and emission are in the visible electromagnetic spectrum. Fluorescence occurs when the molecular absorption of a photon triggers the excitement of an electron from its ground energy state (E_0) to a higher energy level (E_1^*). The excited electron quickly loses energy and is lowered to another energy state (E_1). As the electron returns from E_1 to E_0, a photon is emitted. Since $E_1^* - E_0$ is > $E_1 - E_0$, the wavelength of the emitted photon is longer than that of the one absorbed. The difference between the absorption and emission maxima is known as the Stokes shift.[36]

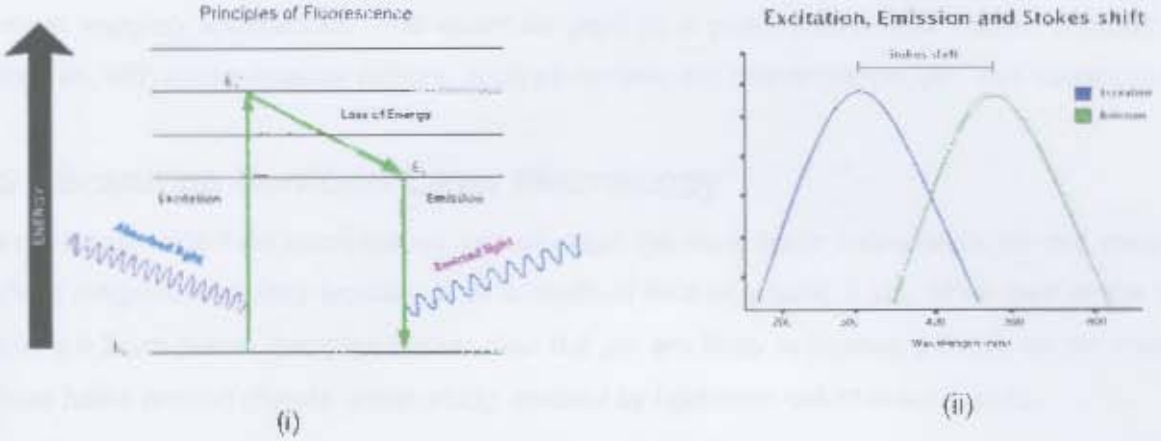

(i) (ii)

Figure 5: (i) A Perin-Jablonski Diagram showing an overview of fluorescence; (ii) Example of excitation, emission and Stokes shift associated with fluorescence

The small fluorescent markers used today mostly comprise aromatic and electron-rich conjugated systems (see Figure 6). These molecules offer a convenient and relatively quick way to tag biologically active molecules. Much effort has been made to link these markers to biological macromolecules such as proteins or nucleic acids, therefore facilitating localization within a specific structural region, such as the cytoskeleton, mitochondria, endoplasmic reticulum, and nucleus. Fluorescent dyes are also useful in monitoring cellular integrity (live versus dead and apoptosis), endocytosis, exocytosis, membrane fluidity, protein trafficking, signal transduction, and enzymatic activity. In addition, fluorescent probes have been widely applied to genetic mapping and chromosome analysis.[37]

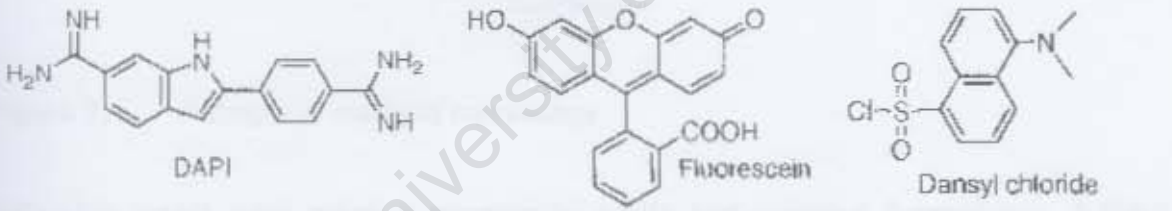

λ_{ex} 258 nm; λ_{em} 463 nm λ_{ex} 490 nm; λ_{em} 521 nm λ_{ex} 330 nm; λ_{em} 572 nm

Figure 6: Some Common fluorophores[38]

Careful consideration should be taken when choosing a fluorophore, as each possesses its own unique fluorescent properties such as the wavelengths of maximum absorbance (λ_{ex}) and emission (λ_{em}). One of the most useful quantitative parameters for characterizing absorption spectra is the molar extinction coefficient, a direct measure of the ability of a molecule to absorb light. The quantum yield of a fluorophore represents the probability that a given excited fluorophore will emit a photon. It is therefore a quantitative measure of fluorescence emission efficiency and can be expressed as the number of photons emitted to the number of photons absorbed. The technique is highly sensitive and thus accommodates fluorophores with varying quantum yields. In general, a high quantum yield is desirable

in most imaging applications. The quantum yield of a given fluorophore varies, sometimes to large extremes, with environmental factors, such as metallic ion concentration, pH, and solvent polarity.[37b]

1.9 Scanning Confocal Laser Microscopy

Conventional wide-field microscopes are amongst the most basic instruments for cell imaging. At their highest magnification they typically offer a depth of field of around 2 μm, while their range of focus lies within a 0.2 μm plane. Samples thicker than 0.2 μm are likely to impose artifacts on the image, such as diffuse halos around objects under study, caused by light from out-of-focus planes.

Confocal microscopy eliminates these undesirable artifacts by generating thin submicron slices of thick samples, comprised only from light in the desired focal plane (see Figure 7). This ability to exclude light from out-of-focus planes results in images of high resolution. The wide range of focus makes confocal microscopy ideal for live cell imaging. It is an invaluable tool for the analysis of the structure and physiology of live cells.

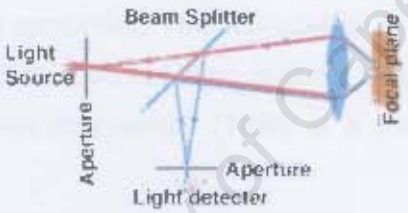

Figure 7: Principle of confocal microscopy

UV-visible lasers have made it possible to excite and visualise fluorophores in living cells using confocal microscopy. This technique has become increasingly valuable, but is typically limited to fluorophores that are excitable in the visible spectrum. UV-excitable molecules are avoided as the light required for excitation is damaging to living cells and tissues.

Two-photon excitation is a technique allowing for the use of UV-excitable fluorophores in living cells, using non-harmful visible or IR light. The excitation of the fluorophore is effected by the absorption of two lower-energy photons, equivalent to that of one high-energy photon (see Figure 8) exciting a fluorophore in one quantum event. Each photon carries approximately half the energy necessary to excite the molecule. An excitation results in the subsequent emission of a fluorescence photon, typically at a higher energy than either of the two excitatory photons. The probability of the near-simultaneous absorption of two photons is extremely low. Therefore a high flux of excitation photons is typically required, usually a femtosecond laser.[39]

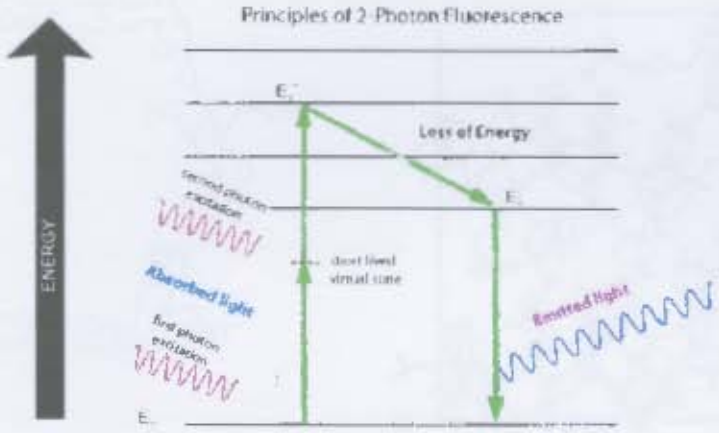

Figure 8: Jablonski diagram showing the excitation by two photons

1.10 Transmission Electron Microscopy

Light microscopes are subject to physical limitations. The magnification of samples is limited by the wavelength of visible light and typically cannot exceed two thousand times. Electron Microscopes function exactly as their optical counterparts except that they utilize a focused beam of electrons instead of light to "image" the specimen. The wavelength of an electron beam is (typically a hundred thousand times) shorter than that of visible light, making magnifications of up to a million fold possible. Thus, the transmission electron microscopy (TEM) is a powerful tool for studying cell or organelle morphology.[40]

1.11 Cyclodextrin Inclusion

Cyclodextrins are cyclic molecules comprising α-1,4-linked D-glucopyranose units. The most common amongst these macrocyclic molecules are the 6, 7, and 8 membered rings, appropriately named α- (see Figure 9 i), β- and γ-cyclodextrin. The cyclodextrins conform to a hollow truncated cone, with the hydrophilic hydroxyl groups displayed along the outside. Their cavity is lined with hydrogen atoms and glycosidic oxygens, with one of their non-bonding electron lone-pairs directed inwards towards the cavity. This gives the cavity its Lewis-base character and makes it a hydrophobic environment.[41]

Cyclodextrins are capable of forming host-guest complex, with many hydrophobic small molecules. There is usually a marked increase in water solubility of these complexes as compared with the native guest, making this a useful technique in the practical delivery of pharmaceuticals. When developing a new drug, poor aqueous solubility is one of the common shortcomings. This often results in poor drug bioavailability. Cyclodextrin inclusions offer a solution to many such drugs, and have been investigated for ajoene in this project.

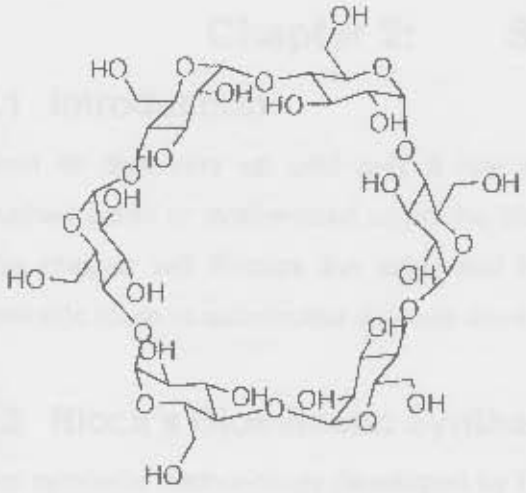

α-Cyclodextrin

(i)

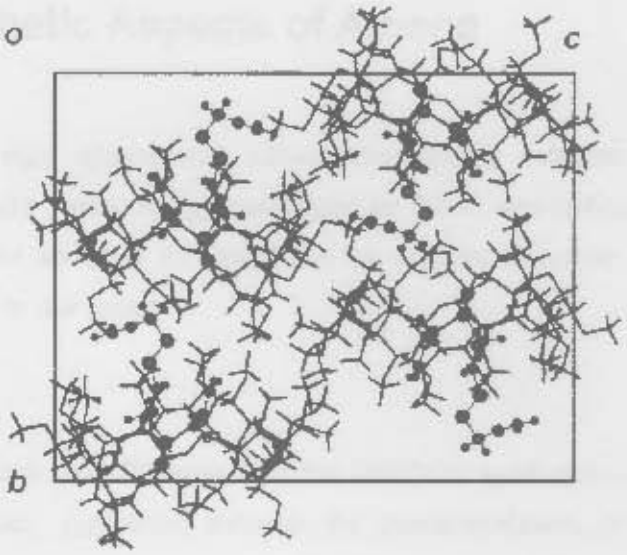

(ii)

Figure 9: (i) α-Cyclodextrin comprising 6 glucose units; (ii) Projection of the crystal packing in the inclusion complex of TRIMEB and *Z*-ajoene.

Caira *et al.* showed in 2004 that ajoene, individually as *E*- and *Z*-isomers, could be accommodated within the methylated heptakis(2,3,6-tri-O-methyl)-β-cyclodextrin (TRIMEB) host cavity to form inclusion complexes. It was found that the conformation of the ajoene molecule was such that the hydrophobic host-guest interactions in these complexes were responsible for the complexation. Each isomer formed its own distinct complex with TRIMEB, in 1: 1 host: guest ratio. TRIMEB•*Z*-ajoene complexed in the space group $P2_12_12_1$ (see Figure 9 ii), while TRIMEB•*E*-ajoene complexed in the space group $P2_1$.[42]

Chapter 2: Synthetic Aspects of Ajoene

2.1 Introduction

From its discovery up until only a few years ago, ajoene was either painstakingly extracted from crushed garlic or synthesized using the biomimetic methodology developed by Block and colleagues.[8] This chapter will discuss the latter and highlight some of its limitations as well as describe a new synthetic route to substituted ajoenes developed in our group.

2.2 Block's Biomimetic Synthesis

The synthetic methodology developed by Eric Block (see Scheme 4) in the 1980's to synthesize ajoene involves the biomimetic rearrangement of allicin (prepared through the mono-oxidation of diallyl disulfide), as it occurs in nature. Heating allicin in aqueous acetone facilitates the reaction, via the mechanism shown in Scheme 4, which has already been discussed.[8]

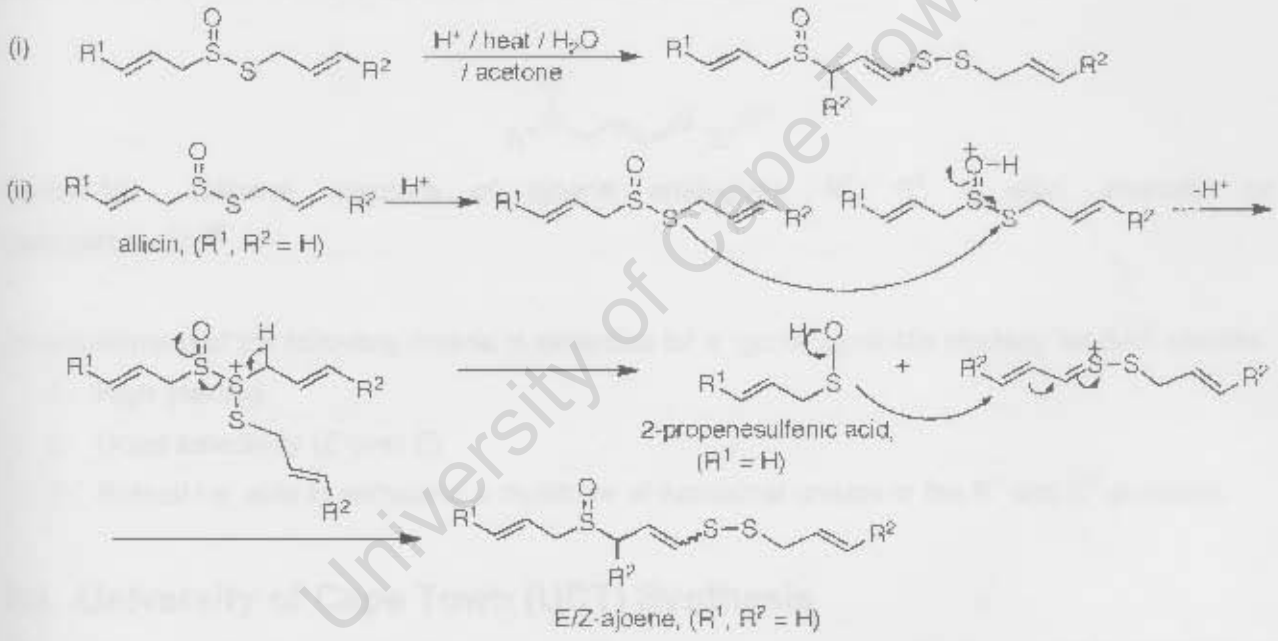

Scheme 4: Thermal rearrangement of allicin into ajoene – (i) Overview of reaction; (ii) Mechanism.

Block's synthesis, although elegant, has several disadvantages. It is not amenable to synthesizing ajoene analogues devoid of allyl and with R^1 and R^2 groups that are different (Scheme 4). Moreover, the overall yield of ajoene using this synthetic route is low (around 35%) and the ratio of *E*: *Z* is reported to be 4: 1.[8] As the *Z*-isomer is more active than the *E*-isomer as an anti-thrombotic and anti-cancer agent, higher yielding, geometrically selective synthesis is required.[43]

2.3 Functionalized Ajoenes

Modern medicinal chemistry is based primarily on establishing a SAR (structure-activity relationship) analysis by creating and testing libraries of similar and varying molecules in which groups of interest are systematically varied. In order to create a library of ajoene analogues, one must utilize a synthetic strategy that retains the biologically active pharmacophore. In the ajoene molecule, there is strong evidence that the pharmacophore lies within the vinyl disulfide group, making it an essential part of any target molecule. The allyl groups on each end can thus be replaced with various functional groups, suggesting the general structure of an ajoene analogue as shown in Figure 10.[43]

Convention in this project dictates the ajoene analogues be drawn such that the sulfoxide lies on the left-hand side of the molecule and the disulfide on the right (see Figure 10). Thus the term "left-hand side of the molecule" refers to the R^1 group closest to the sulfoxide, while the term "right-hand side of the molecule" refers to the R^2 group closest to the disulfide.

Figure 10: General structure of ajoene analogues. R^1, R^2 = alkyl, aromatic or heteroaromatic.[43]

Thus fulfillment of the following criteria is essential for a "good" synthetic strategy for SAR studies:

1. High yielding.
2. Good selectivity (*Z* over *E*)
3. Robust i.e. able to withstand a multitude of functional groups in the R^1 and R^2 positions.

2.4 University of Cape Town (UCT) Synthesis

A synthetic route has been developed at UCT as Block's ajoene synthesis cannot be used to access substituted analogues where R^1 and R^2 are other than allyl (see Scheme 4). A retrosynthetic analysis of the generalized ajoene is shown in Scheme 5 below.[43]

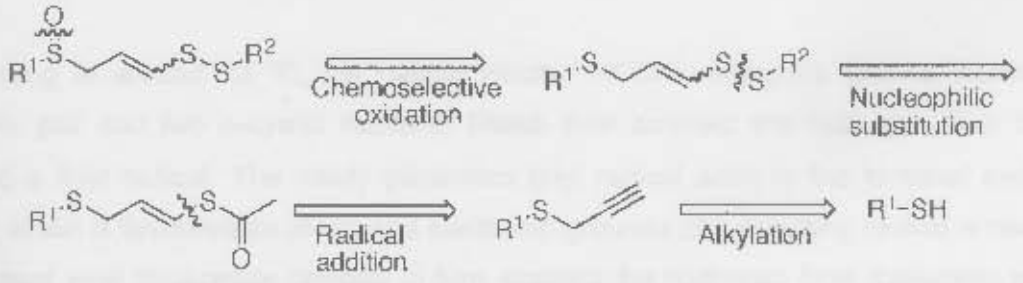

Scheme 5: The UCT retrosynthesis of a disubstituted ajoene.

2.4.1 Propargylation

The first step involves the propargylation of a thiol, either obtained commercially or synthesized via thiourea chemistry (see Scheme 6). Step (i) illustrates the latter via the reaction of an appropriate alkyl halide with thiourea to form an isothiouronium salt. The latter, when hydrolysed by potassium hydroxide, forms a thiol, potassium chloride and urea, allowing for a one-pot, *in situ* propargylation to form the desired propargyl sulfide by adding propargyl bromide in step (ii).

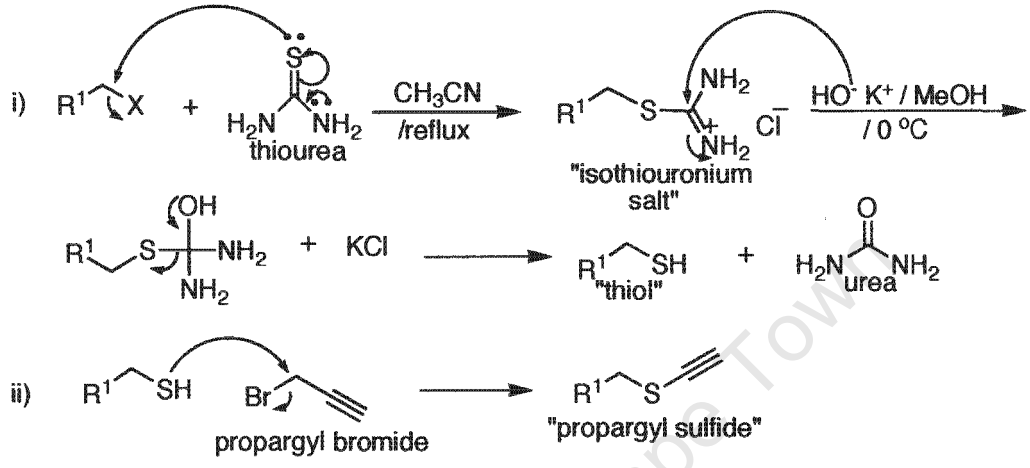

Scheme 6: (i) Preparation of substituted thiol R^1SH; (ii) Propargylation of thiol

2.4.2 Radical Addition

A regioselective radical addition was the reaction used in the second step to establish a vinylthio fragment. This section offers a brief overview of the rationale behind the chosen radical addition and some insight into its mechanism.

A radical addition developed in the 1950's by H. Behringer, H. Bader, K. A. Kampmeier, G. Chen and colleagues, forms the cornerstone of the UCT synthesis. This process involves a free radical addition of thiolacetic acid to 1-hexyne resulting in regioselective addition of an acetylthio radical to the terminal end of the alkyne terminus. The reaction follows the typical initiation, propagation and termination sequence associated with radical additions (see Scheme 7).

Upon heating at around 70 °C, the radical initiator ACCN undergoes thermal homolytic cleavage, yielding N_2 gas and two α-cyano radicals. These then abstract the hydrogen from thiolacetic acid, generating a thiyl radical. The newly generated thiyl radical adds to the terminal end of the alkyne terminus, which is favoured on steric and electronic grounds (the resulting radical is more stable). The newly formed vinyl thioacetate radicals in turn abstract the hydrogen from thiolacetic acid, generating the vinyl thioacetate and another acetylthio radical. Termination of the radical addition sequence

involves dimerization of the thiyl radicals, forming a disulfide diacetate. Although the *E*-vinyl thioacetate radical intermediate is lower in energy than that of the *Z*-isomer, the *Z*-vinyl radical provides easier access for the abstraction of the hydrogen in the second propagation step. Thus, the *Z*-vinyl thioacetate is kinetically favoured, typically in a ratio of 2: 1.

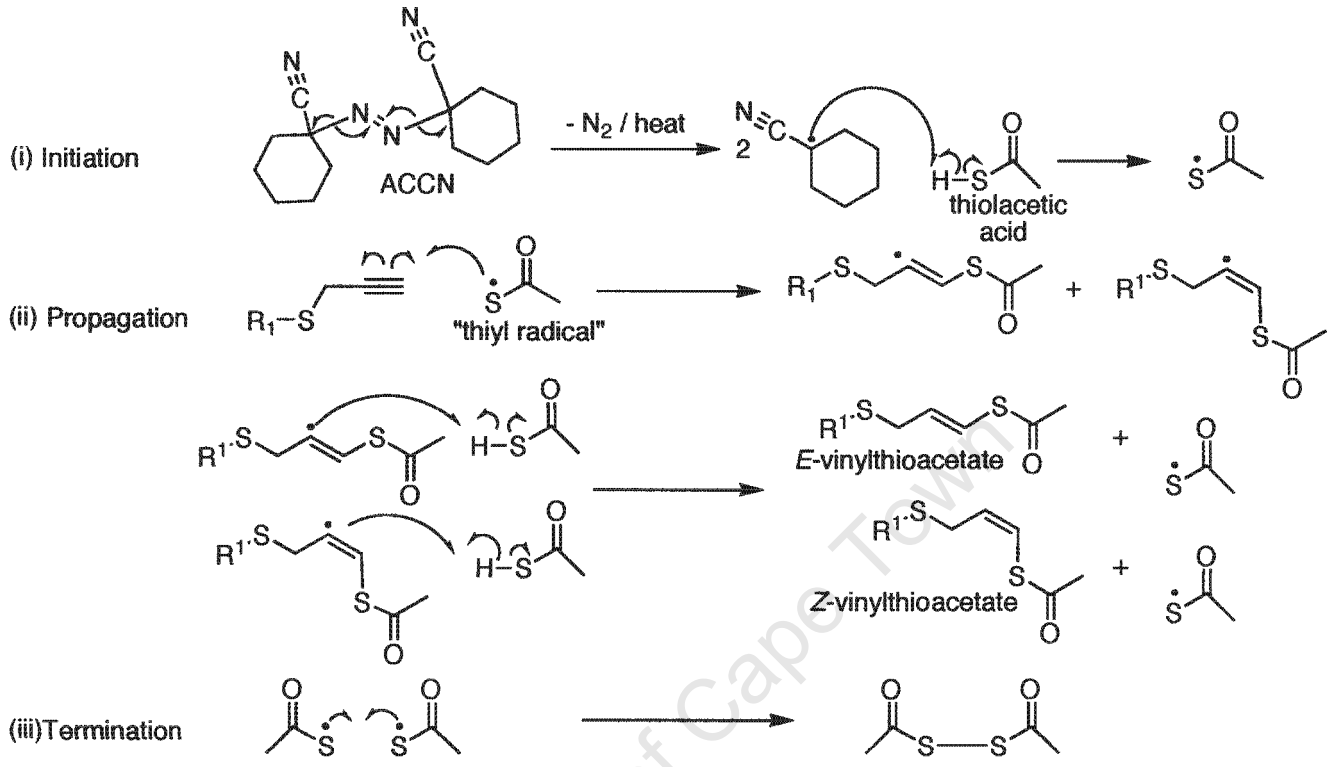

Scheme 7: Radical addition mechanism: (i) Initiation; (ii) Propagation; (iii) Termination

2.4.3 Sulfenylating Agent

The "right-hand" side of the molecule is constructed by sulfenylation using a sulfenylating agent (see Scheme 8). The thiosulfonate grouping, -S(SO_2)-R, is analogous to the *O*-sulfonate ester (e.g. tosylate) in S_N2 reactions. The important difference between the two groups is that the thiotosylate sulfur provides the electrophilic site for nucleophilic attack instead of the adjacent carbon, as observed in the analogous sulfonate ester, -O(SO_2)-R. This phenomenon involves the thiosulfonate acting as a soft sulfenylating agent towards a sulfur-nucleophile.

Typically, the sulfenylating agents are synthesized via nucleophilic substitution of the appropriate R^2-halide with a thiotosylate. In the instance of too much thiotosylate and/or applied heat, further substitutions can occur, as depicted in Scheme 8 ii.

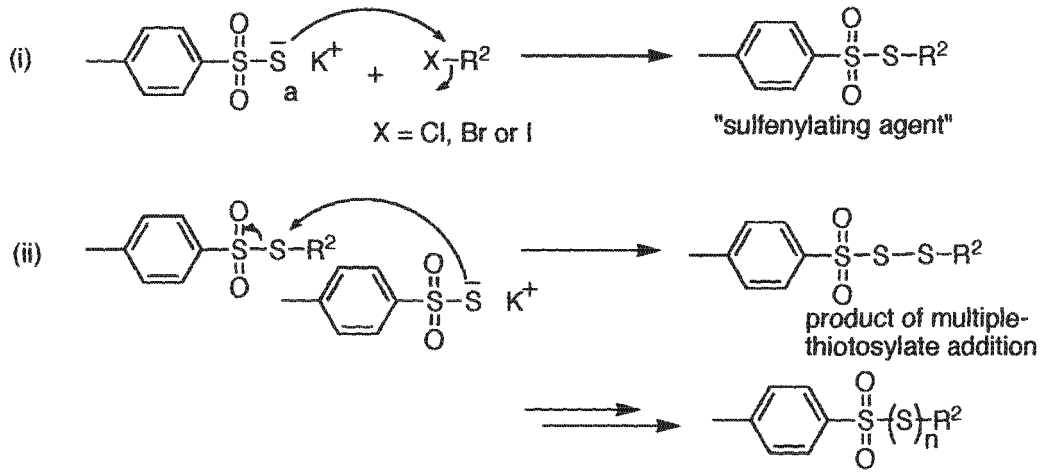

Scheme 8: Synthesis of the sulfenylating agent

2.4.4 Coupling

Hard-soft acid base theory predicts the observed chemoselectivity when the vinyl thioacetate and the sulfenylating agent are coupled to form the desired disulfide precursor to the ajoene target (Scheme 9). The vinyl thioacetate is deprotected to its enethiolate using potassium hydroxide in methanol. The reaction is carried out at -40 °C initially and then cooled to -78 °C before adding the sulfenylating agent in order to minimize geometric isomerization from *Z*- to its more thermodynamically stable *E*-isomer. The enethiolate rapidly displaces the S-tosyl leaving group, forming the desired disulfide bond in a textbook example of the "soft-soft" principle.

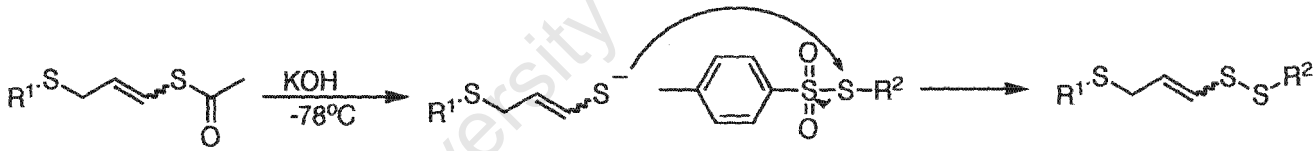

Scheme 9: Coupling reaction

2.4.5 Oxidation

The final step involves chemoselective oxidation of the sulfide of the vinyl disulfide using 1.1 equivalents *m*-CPBA as the oxidizing agent. Chemoselectivity is achieved through the maintenance of a reaction temperature below -30 °C and by limiting the oxidant to one equivalent, ensuring that only the more nucleophilic sulfide is oxidized.

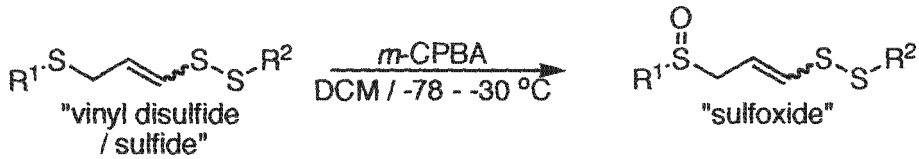

Scheme 10: Oxidation

2.5 Comments and Summary of Synthesis

The synthetic route (see Scheme 11) is a summary of Section 2.4 and summarizes the overall synthesis of substituted ajoenes. This synthesis cannot be used to synthesize ajoene itself as the allyl group on the "left-hand side" (R^1) of the molecule participates in the radical addition.

Ajoene and its analogues are relatively stable and can be subjected to silica-gel column chromatography to separate the *E*- and *Z*-isomers. It has been observed that small substituents (such as propyl) in the R^1 and R^2 position result in isomers that are separable, while large substituents (such as benzyl or *t*-butyl) result in inseparable isomers.

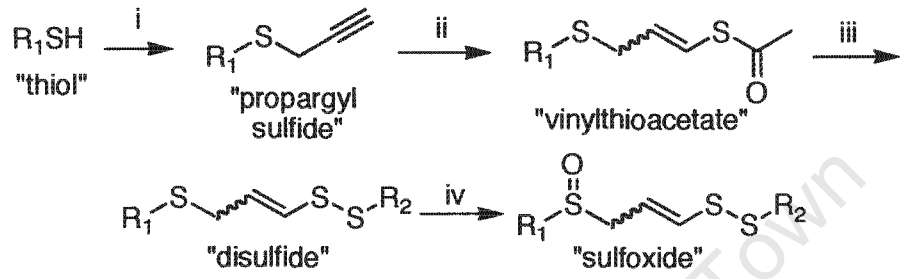

Scheme 11: UCT synthesis: reagents and conditions: (i) KOH, MeOH, propargyl bromide; (ii) thiolacetic acid (1.1 equiv), ACCN (2 mol%), toluene, 80 °C; (iii) (a) KOH (1.05 equiv), MeOH, -40 °C; (b) *p*-$TolSO_2SR^2$ (1.1 equiv), -78 to 0 °C; (iv) *m*-CPBA (1.1 equiv), DCM, -78 °C to room temperature

Chapter 3: Bis-*p*-methoxybenzyl Ajoene

3.1 Introduction

At the inception of this project, a small library of ajoene analogues of general structure **1** had already been synthesized and tested for activity against several cancer cell-lines. Below, in Tables 1 and 2, are the results of this SAR study, in which the R^1 and R^2 functional groups (see Figure 10) on the ajoene scaffold were independently varied. The data for the second SAR study (Table 2) presented was obtained using a WHCO1 oesophogeal cell-line, while the first study (Table 1) was carried out using CT1 lung-fibroblasts.[43]

Table 1: IC_{50} (μM) of ajoene derivatives of **1** against CT-1 fibroblast cells[43]

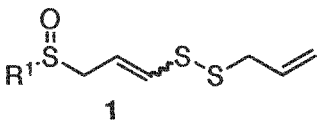

1

	Name	R^1	IC_{50}
i	*E*-ajoene		17.6
ii	*Z*-ajoene		15.5
iii	*E*-propyl		26.7

** *E/Z* ratio 2 : 3 [43]

	Name	-R^1	IC_{50}
iv	*Z*-propyl		17.0
v	*E/Z*-benzyl**	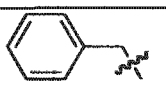	16.6
vi	*E/Z*-PMB**	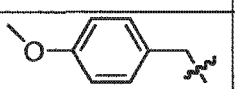	12.0

Examining activity trends in target **1 i - vi** (see Table 1), the following is presented in order of decreasing activity: PMB > benzyl > allyl > propyl as reflected by an increasing IC_{50}. When chromatographic separation was possible, the *E*- and *Z*-isomers were tested separately, with the latter exhibiting greater activity in every instance. When inseparable isomeric mixtures were isolated, they were tested as such. From the results, it became apparent that a *p*-methoxybenzyl substituent in the R^1 position provided optimal anti-cancer activity. This was then carried through to the next SAR study, which involved the scaffold **2** shown in Table 2. A similar trend of activity was observed when varying the functionality of the right-hand side (R^2) of the molecule, with the highest activity resulting from the benzyl group.

Table 2: IC_{50} (μM) of ajoene derivatives of **2** i - iii against WHCO1 oesophogeal cells[44]

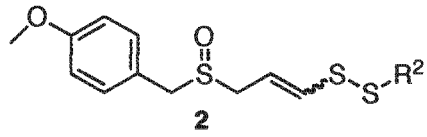

2

	Name	-R^2	IC_{50}
i	*E/Z*-allyl**		7.5
ii	*E/Z*-benzyl**	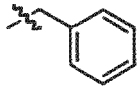	3.3

	Name	-R^2	IC_{50}
iii	*E/Z*-PFB**	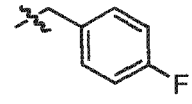	17.0

** *E/Z* ratio 2 : 3 [44]

The data obtained suggested that aromatic substituents in the R^1 and R^2 position increases the activity of the drug,[44] possibly related to increased lipophilicity, providing better permeation into the cell. It is interesting to note that the analogue containing the *para*-positioned fluorine (See Table 2, iii) displayed a marked decrease in activity compared to the other analogues in the series. Therefore some sort of activation through electron donation into the pharmacophore may be responsible for the increase in activity. Thus, structure-activity trends pointed towards a bis-*p*-methoxybenzyl analogue as being the most promising lead. This Chapter will discuss in detail the synthesis, characterization and biological activity of the bis-*p*-methoxybenzyl ajoene target, **17** shown in Figure 11.

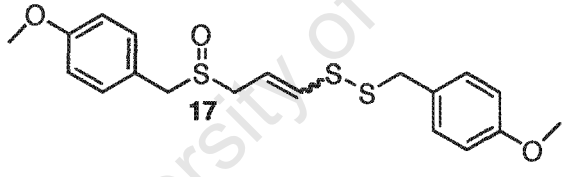

17

Figure 11: bis-*p*-methoxybenzyl ajoene, **17**

3.2 PMB Alkyne, 9[45]

Following the UCT synthesis described in Chapter 2, the synthesis (see Scheme 12) of the target molecule **17** began with the preparation of *p*-methoxybenzyl thiol **6**, which was synthesized from commercially available *p*-methoxybenzyl chloride **3**, utilizing thiourea chemistry. The transformation was achieved by refluxing *p*-methoxybenzyl chloride **3** and thiourea **4** (1.2 equivalents) in acetonitrile. Donation of the nitrogen lone pair in thiourea facilitates the nucleophilic substitution of the chloride, producing the *p*-methoxybenzyl isothiouronium salt **5**. The salt proved to be very polar and only moved on TLC in a polar medium such as MeOH in EtOAc in ratios greater than 1: 20. The reaction was monitored by the disappearance of the chloride and had reached completion within the first hour. Upon cooling, the salt rapidly crystallized out of solution, which was then filtered and washed with cold acetonitrile. The isothiouronium salt **5** was then dissolved in MeOH containing two equivalents of KOH at 0 °C. Propargyl bromide **8** was added to facilitate the *in situ* propargylation of the thiol. Urea **7** was

produced as a by-product. Two equivalents of KOH were needed to hydrolyze the isothiouronium salt to the thiol as well as to neutralize the HBr generated from the propargylation. The propargylation of the thiol was rapid, reaching completion (as determined by TLC) within 45 minutes. Purification using column chromatography afforded the resulting alkyne as a sweet-smelling yellow oil in a 77 % yield over the two steps.

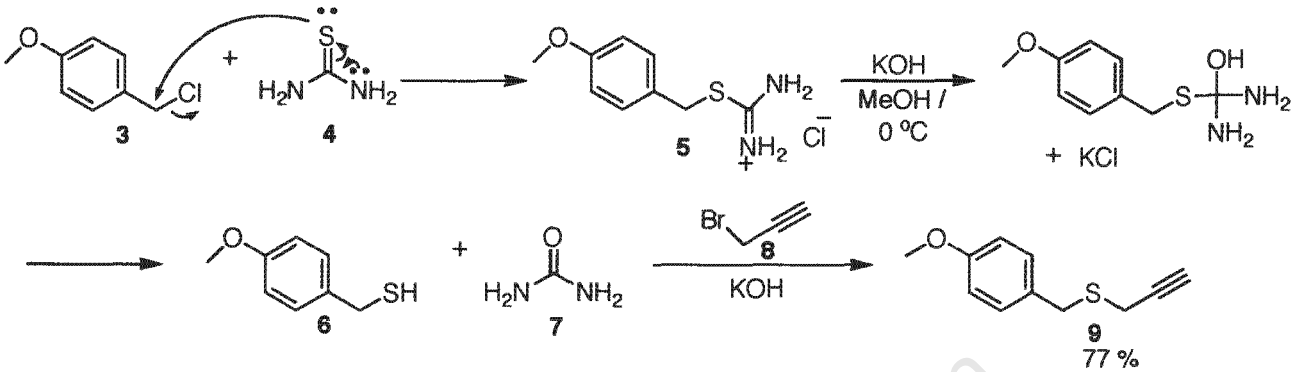

Scheme 12: Preparation of propargyl sulfide **9**. The isothiouronium salt **5** was generated from *p*-methoxybenzyl chloride and thiourea, after which it was deprotected to its thiol and propargylated *in situ* to give **9**.

The ^{1}H NMR spectrum of **9** revealed a pair of AB doublets characteristic of *para*-substituted phenyl groups. The singlet observed at 3.83 ppm integrating for two protons was identified as H-5 (see Figure 12), deshielded by being benzylic. A singlet, corresponding to the CH_3 of the methoxy-group was observed at 3.78 ppm. Strong evidence for the propargylation was given by the appearance of a doublet integrating for two protons for H-6 at 3.15 ppm, as well as a triplet integrating for one proton (H-8) at 2.72 ppm. The two signals were found to have a reciprocal splitting of 2.8 Hz via coupling through the triple bond.

Analysis of the ^{13}C NMR spectrum of **9** revealed a downfield peak at 160.0 ppm corresponding to C-1. Signals for C-2 and C-3 were observed at 114.9 ppm and 131.1 ppm respectively. C-3 appeared downfield to C-2 due to the shielding effect brought about by the mesomeric donation of the methoxy oxygen into the phenyl ring (see Figure 13). Peaks at 81.0 ppm and 72.8 ppm indicating the presence of alkynyl carbons, corresponded to C-7 and C-8 respectively.

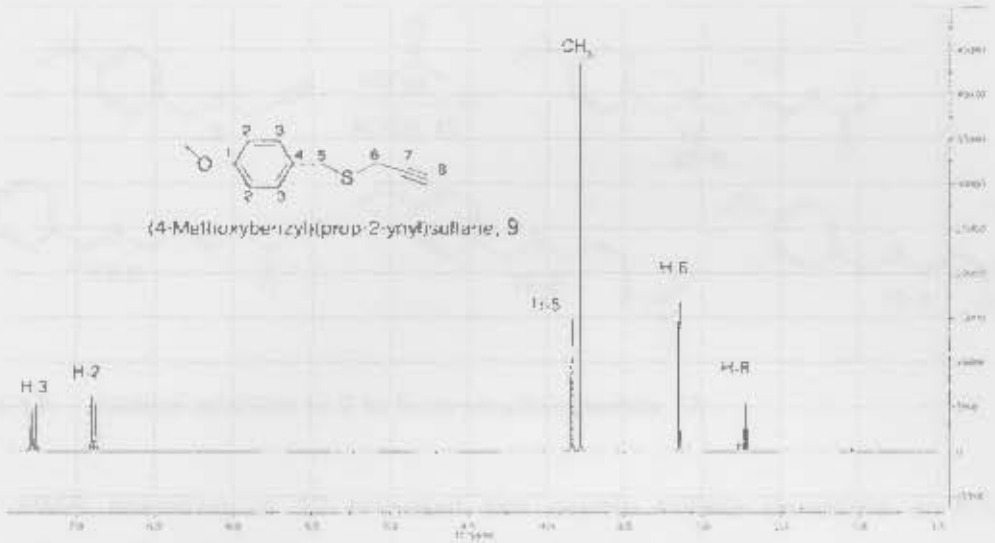

Figure 12: ^{1}H NMR spectrum of **9** in acetone-d_6

Figure 13: Mesomeric effect in the PMB ring

3.3 PMB Vinylthioacetate, 12

The next step in the synthesis involved the regioselective addition of thiolacetic acid **10** to the triple bond of compound **9** (see Scheme 13). The reaction was performed by dissolving compound **9** in dry, degassed toluene and heating to 85 °C under N_2. The radical initiator ACCN **11** (0.1 equivalents) was added directly as a solid, followed by the addition of thiolacetic acid (1.5 equivalents) in toluene over twenty minutes using a dropping funnel. The temperature of the mixture was restricted to 85 °C, as refluxing temperatures were feared to promote multiple addition of thiolacetic acid to form the saturated bis-thioacetate **12-*b***. After 2 hours, TLC analysis revealed a considerable depletion of the alkyne starting material and the appearance of a more polar product. The solution was cooled and saturated aqueous sodium carbonate was added to quench any remaining thiolacetic acid. The toluene solvent was then removed on the rotary evaporator, after which the residue was extracted into DCM and dried over $MgSO_4$. Purification on a silica-gel column gave compound **12** in a yield of 68 % as a 4: 3 mixture of *Z*: *E* stereoisomers that could not be separated. The stereoselectivity of the reaction (see Chapter 2.4.2) is explained by the kinetic product **12-*Z*** being favoured over the thermodynamically favoured product **12-*E***. Such kinetic behavior is due to the *Z*-vinyl radical intermediate reducing faster than the *E*-vinyl radical on steric grounds.

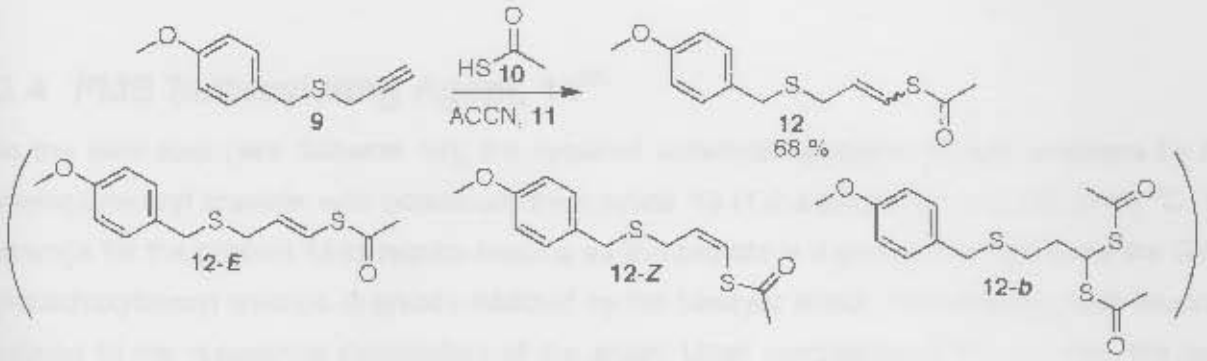

Scheme 13: Radical addition to **9** to form vinylthioacetate **12**

The ^{1}H NMR spectrum of **12** revealed two double triplets downfield at 6.50 and 6.67 ppm corresponding to H-3 of the *E*- and *Z*-stereoisomers respectively (see Figure 14 for numbering). The isomers were distinguished by their vicinal coupling constants, which were 15.2 Hz and 9.5 Hz respectively. The 4 : 3 ratio of *Z*/*E*-isomers was determined by comparison of the integration of the corresponding H-3 peaks. The H-4 resonances of both isomers presented as overlapping double triplets between 5.89 and 5.78 ppm. H-5 appeared as a double doublet for each of the isomers based on vicinal and allylic coupling with H-4 and H-3. Other diagnostic peaks used to identify and discern the isomers included pairs of methoxy and methyl acetyl singlets and the characteristic *para*-substituted phenyl signals.

The ^{13}C NMR spectrum revealed resonances at 192.8 and 191.1 ppm corresponding to the carbonyl (C-2) of the *E*- and *Z*-isomers respectively. Four aromatic, two vinyl and three aliphatic resonances were also observed, accounting for the required 13 carbons present. Because of the non-separable mixture of isomers, the spectrum was only fully assigned with the aid of HSQC, and the remaining resonances satisfactorily related to the ^{1}H resonances.

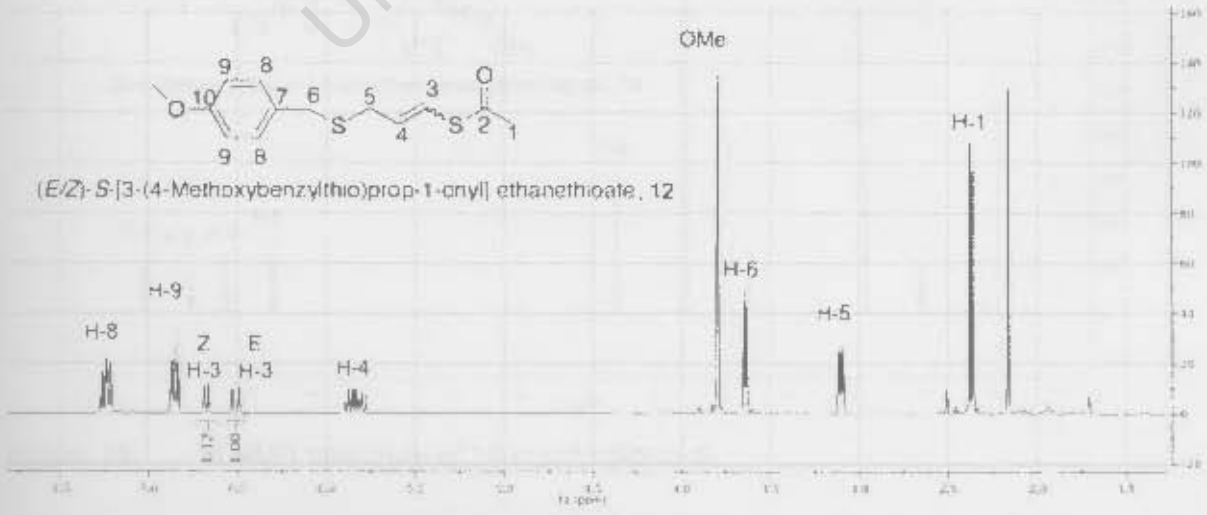

Figure 14: ^{1}H NMR spectrum of **12** as a mixture of *Z*/*E*-isomers in chloroform-d_3

3.4 PMB Sulfenylating Agent, 14[46]

In the next step (see Scheme 14), the required sulfenylating agent **14** was prepared by heating *p*-methoxybenzyl chloride with potassium thiotosylate **13** (1.2 equivalents) in DMF to 65 °C. It seemed strange for the product **14** to require heating as thiotosylate is a good nucleophile and the Cl-C bond in *p*-methoxybenzyl chloride is greatly labilized by the benzylic effect; The need for such heating may be related to the resonance stabilization of the anion. Upon completion of the reaction, the solvent was removed under vacuum, after which the residue was extracted into DCM and washed thoroughly with water to remove any remaining DMF. Recrystallization from EtOAc and hexane afforded **14** in a 74% yield.

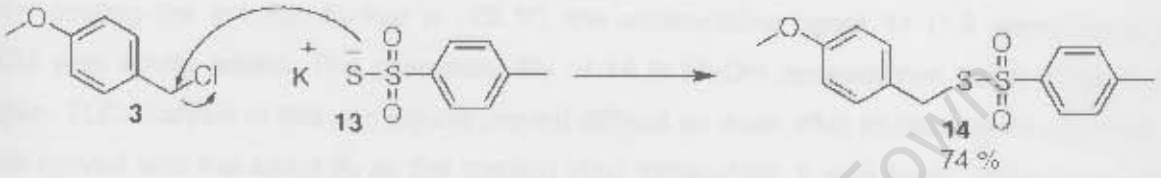

Scheme 14: PMB sulfenylating agent **14**

The ^{1}H NMR spectrum of **14** (see Figure 15) revealed four doublets in the aromatic region, corresponding to the two AB systems associated with H-3, H-4, H-8 and H-9 (see Figure 15 for numbering). Singlets at 4.28 ppm, 3.78 ppm and 2.45 ppm confirmed the presence of H-6, OCH_3 and H-1 respectively.

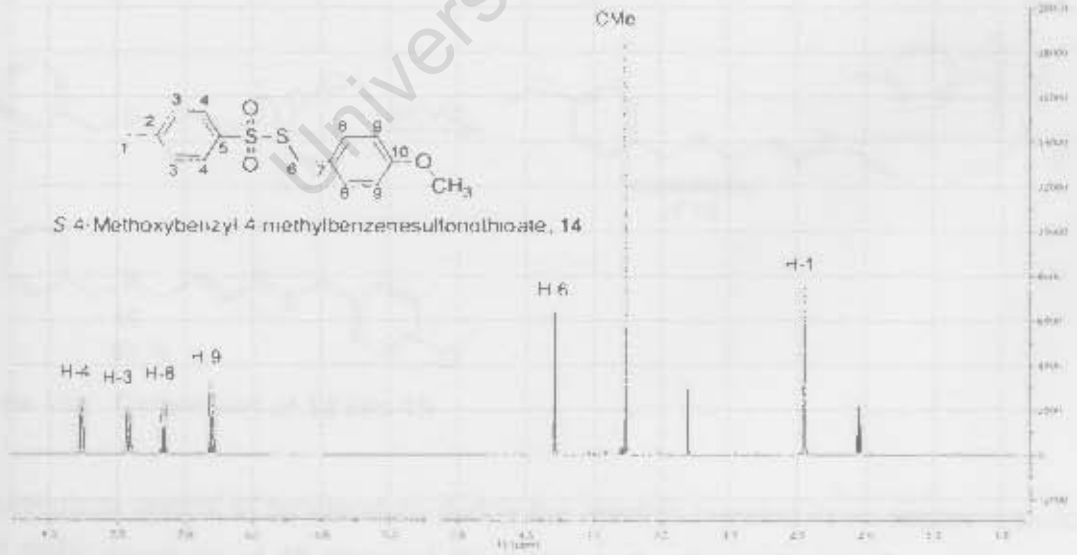

Figure 15: ^{1}H NMR spectrum of **14** in chloroform-d_3

3.5 Bis-PMB Disulfide, 15

The coupling (Scheme 15) of the protected enethiol (vinyl thioacetate **12**) with the sulfenylating agent to form the disulfide product is a critical step in the synthetic pathway to the target molecule. To this end the vinyl thioacetate **12** was deprotected to its enethiolate anion by hydrolysis with KOH in MeOH. The reaction temperatures for this step were kept below -40 °C to prevent the highly reactive enethiolate of **12** from forming side products or tautomerizing (discussed at length in Chapter 4, Scheme 30), to the thermodynamically favoured *E*-isomer. The low reaction temperature also demonstrates the weakness of the C-S bond in the thioacetyl group. The enethiolate/thiol was not observed on TLC, but it was found that 45 minutes at -40 °C was adequate for good product yields.

After cooling the solution further to -78 °C, the sulfenylating agent **14** (1.3 equivalents) dissolved in DCM was slowly added. The poor solubility of **14** in MeOH necessitated using DCM as a cosolvent. Again, TLC analysis of this compound proved difficult as even after multiple developments, the product spot moved with the same R_f as the starting vinyl thioacetate. It was found that an hour was sufficient for good yields. The reaction was quenched at -10 °C with saturated aqueous ammonium chloride and allowed to warm to room temperature before being extracted and isolated by column chromatography (ethyl acetate: hexane = 1: 4) to afford the disulfide **15** as a pleasant-smelling grey oil in an 83% yield.

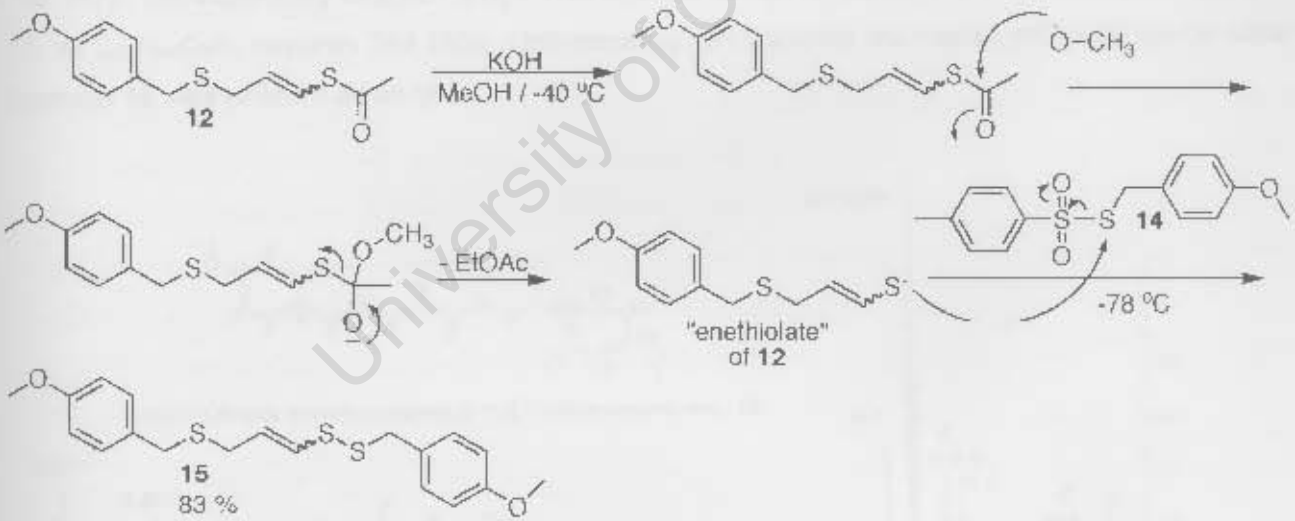

Scheme 15: Conversion of **12** into **15**

The meticulous control of temperature during the reaction resulted in no apparent tautomerization, as the ^{1}H NMR spectrum of **15** revealed the same 4: 3 ratio of *Z*- and *E*-isomers observed for vinyl thioacetate **12**. The isomers were inseparable by chromatography and despite the presence of two *p*-methoxybenzyl groups for each, resonances for each isomer could be assigned.

The ^{1}H NMR spectrum (See Figure 16) of **15** revealed the loss of the acetyl singlets observed in **12** at 2.35 ppm and 2.38 ppm for the two isomers. Pairs of singlets corresponding to the two methoxy groups in each isomer were observed; 3.78 ppm and 3.80 ppm for the *E*-isomer, and 3.81 and 3.80 for the *Z*-isomer respectively. The benzylic protons, H-5, appeared as a singlet at 3.60 and 3.68 for the *E*- and *Z*-isomers respectively, and was flagged as it was expected to shift downfield after the subsequent oxidation to the sulfoxide. The other benzylic protons H-1, situated next to the deshielding disulfide was observed slightly downfield to H-5 at 3.90 for both isomers. For the *E*-isomer, H-2 appeared as a doublet at 5.93 ppm with a coupling constant of 14.8 Hz, while H-3 appeared as a double triplet at 5.82 ppm with coupling constants of 14.8 and 7.1 Hz. For the *Z*-isomer, H-2 appeared as a doublet at 6.01 ppm with a coupling of 9.3 Hz, while H-3 appeared as a double triplet at 5.62 ppm with a coupling of 9.3 and 7.6 Hz. It is interesting to note that H-2 of the *Z*-isomer lies downfield to that of the *E*-isomer, while the trend is reversed for that of H-3. These trends may be rationalized by the shielding effect of the two sulfurs around the double bond.

Because the two isomers could not be separated, the ^{13}C NMR spectrum of **15** appeared as a set of double resonances. Downfield, in the vinyl and aromatic region of the ^{13}C NMR spectrum, nine signals were observed as C-8 and C-12 coincided at the same chemical shift, while upfield four distinct signals were observed. Because the two methoxy-carbons presented with identical chemical shifts, all nineteen carbons could be distinguished. High resolution mass spectrometry (EI) revealed a molecular ion at 789.1478, corresponding to $[2M + 2O]^+$. This offered further evidence for the formation of the product **15**, as $C_{38}H_{44}O_6S_6$ requires 789.1500. Unfortunately, an accurate microanalysis could not be obtained, because **15** was isolated as an oil.

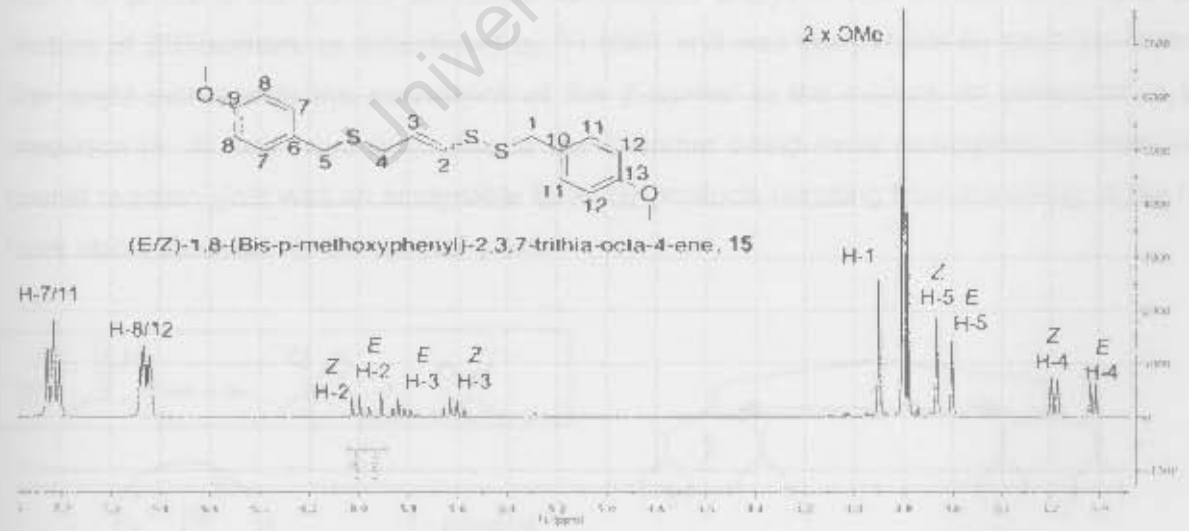

Figure 16: ^{1}H NMR spectrum of **15** as a mixture of *Z*/*E*-isomers in chloroform-d_3

3.6 Bis-PMB Sulfoxide, 17

In the final step of the synthetic sequence (see Scheme 16), **15** was chemoselectively oxidized to the target sulfoxide **17** (see Figure 11). The oxidizing agent, *m*-CPBA (*meta*-chloroperbenzoic acid, **16**), revealed selectivity towards the sulfide over the disulfide functionality, presumably because of its greater nucleophilicity.

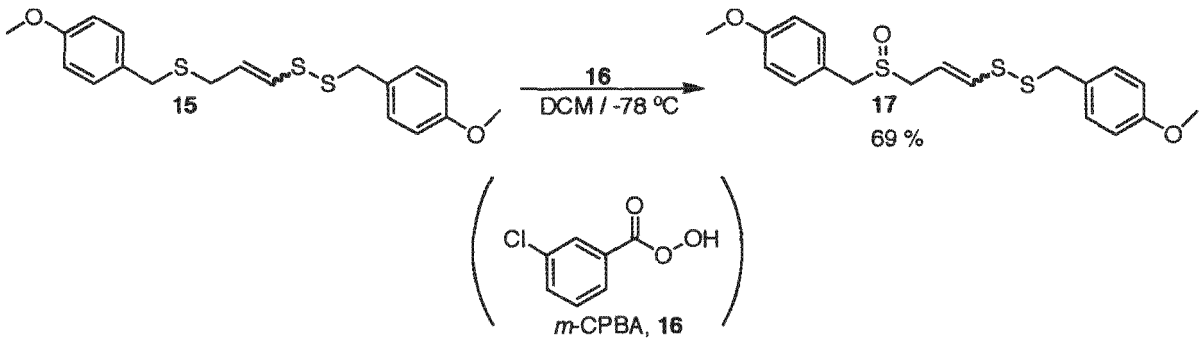

Scheme 16: Chemoselective oxidation of **15** to sulfoxide **17**

One equivalent of *m*-CPBA did not see the reaction go to completion, so a slight excess was added as a means of increasing the reaction yield. This however required the temperature to be kept below -60 °C to prevent over oxidation. TLC revealed a single polar spot corresponding to the sulfoxide, and the disappearance of **15**. The reaction was quenched by adding saturated aqueous sodium carbonate, which immediately resulted in the solution solidifying, so the reaction was left to warm to room temperature. After extraction of the residue, purification using silica-gel column chromatography (ethyl acetate: hexane = 1: 1) afforded the sulfoxide **17** as a white solid, which was further recrystalized from EtOH to produce the correct elemental combustion analysis. The product was found to be a 5: 4 mixture of *Z*/*E*-isomers as determined by ^{1}H NMR and was inseparable by silica-gel chromatography. The slight increase in the prevalence of the *E*-isomer in the mixture as compared to the disulfide precursor (4: 3) may have been due to the *Z*-isomer being more susceptible to over-oxidation. The overall reaction yield was an acceptable 69%. By-products resulting from the acidity of the reaction may have also accounted for the modest yield.

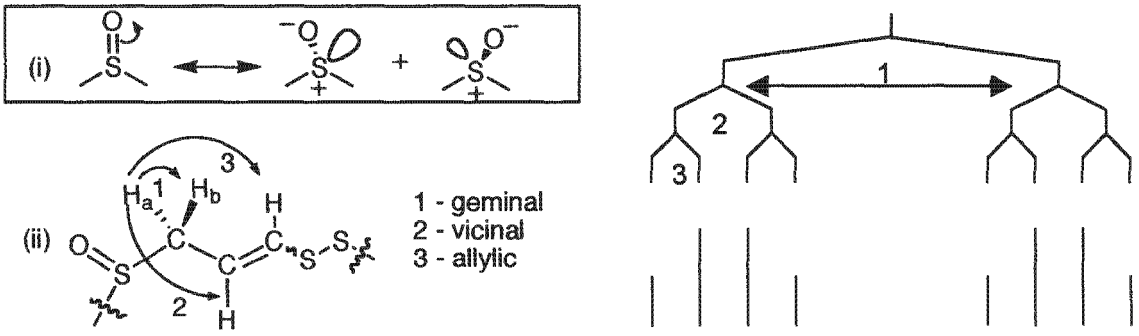

Figure 17: (i) Chirality in sulfoxide; (ii) Diastereotopic protons H_a and H_b

Comparing the ^{1}H NMR spectrum of **17** (see Figure 19 and Table 3) to that of its precursor **15** (see Figure 16 and Table 3), a downfield shift of the peaks corresponding to H-5, from δ = 3.60 ppm for the *E*- and δ = 3.68 ppm for the *Z*-isomer, to a multiplet centred at δ = 3.98 ppm for both was observed. This provided evidence for the oxidation in view of the sulfoxide sulfur's greater deshielding effect. In the disulfide precursor **15**, the H-4 protons are enantiotopic, appearing as doublets at δ = 3.02 ppm and δ = 3.19 ppm for the *E*- and *Z*-isomers respectively, owing to vicinal coupling with H-3. Because of the chirality of the sulfoxide (see Figure 17 **i**), the protons on C-4, labeled H-4_a and H-4_b (see Figure 19 for numbering), are in non-equivalent environments and hence geminally couple as diastereotopic protons. Thus, both H-4_a and H-4_b appeared as a double doublet of doublets (see Figure 17 **ii**) based on geminal, vicinal and allylic coupling. Although the protons on C-5 are also diastereotopic (by virtue of being α to the chiral sulfoxide), they are not split into the expected AB doublets. Upon oxidation, several key shifts in the ^{13}C NMR spectrum were noted (see Table 3) and comprised a trend that would be observed in the oxidation of all the ajoene-analogues, namely: The downfield shift of the methylene carbons α- to the new sulfoxide (C-4 and C-5) as well as to the vinyl carbon α- to the disulfide (C-2). There was also an upfield shift of the carbon β- to the disulfide due to the shielding effect of the sulfoxide's oxygen. The ^{13}C NMR spectrum was complicated by the presence of the two isomers, however the required nineteen carbons were observed. The *Z*- and *E*-isomers produced some distinct and some shared peaks, but with the aid of HSQC, all peaks could be identified.

High-resolution mass spectrometry (EI) revealed a peak (Figure 18) at 417.0630 corresponding to $[M + Na]^+$, providing confirmatory evidence for the formation of the product, as $C_{19}H_{22}NaO_3S_3$ requires 417.0629.

Biological results will be given in Chapter 6.

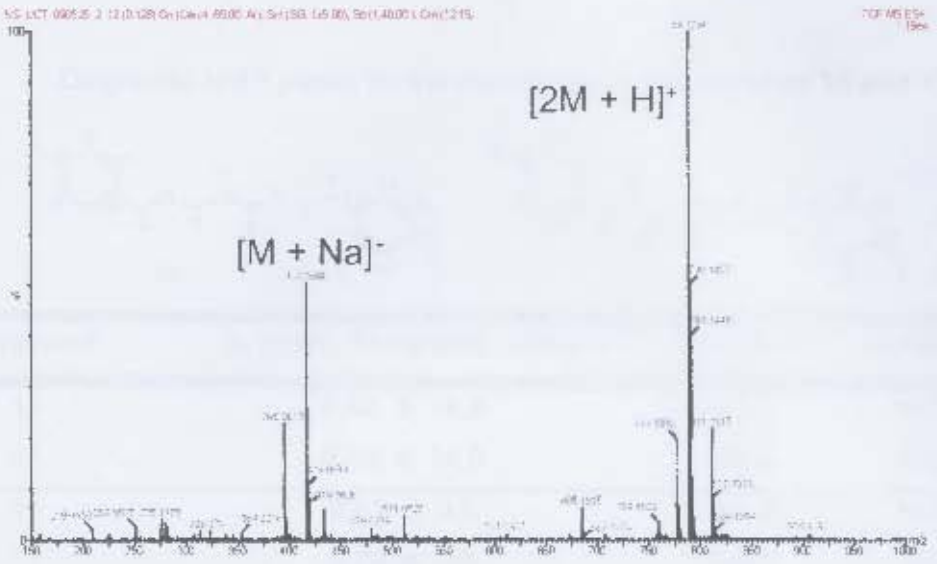

Figure 18: High-resolution mass spectrum of **17**

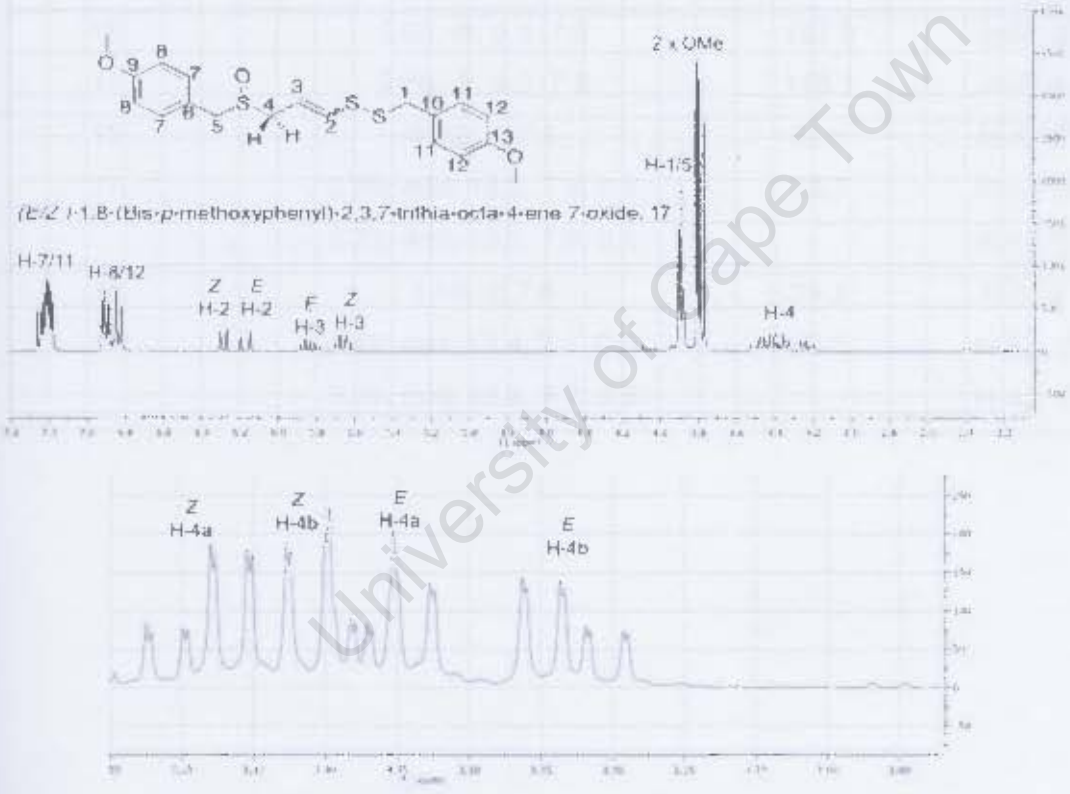

Figure 19: ^{1}H NMR spectrum of **17** as a mixture of *Z*/*E*-isomers in chloroform-d_3

Table 3: Diagnostic NMR peaks for the identification of compounds **15** and **17**

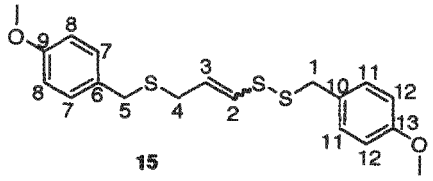

15

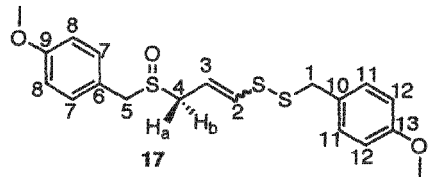

17

Compound	δ_H (ppm); Multiplicity; *J* (Hz)	δ_C (ppm)	Assignment
15	5.93; d; 14.8	127.7	H-2; *E*
17	6.18; d; 14.8	134.2	H-2; *E*
15	6.01; d; 9.3	131.8	H-2; Z
17	6.28; d; 9.5	138.0	H-2; Z
15	5.82; dt; 14.8, 7.1	127.8	H-3; *E*
17	5.83; dt; 14.8, 7.7	117.0	H-3; *E*
15	5.62; dt; 9.3, 7.6	127.9	H-3; Z
17	5.66; dt; 9.5, 7.8	118.1	H-3; Z
15	3.02; d; 7.1	32.6	H-4; *E*
17	3.36; ddd; 13.2, 7.9, 0.9	52.7	$H\text{-}4_a$; *E*
	3.23; ddd; 13.2, 7.9, 0.9		$H\text{-}4_b$; E
15	3.19; d; 7.6	29.2	H-4; Z
17	3.49; ddd; 13.4, 7.7, 0.9	49.5	$H\text{-}4_a$; *Z*
	3.29; ddd; 13.4, 7.7, 0.9		$H\text{-}4_b$; Z

Chapter 4: Fluorescent Ajoenes

4.1 Introduction

This dissertation concerns the synthesis and application of fluorescent ajoene analogues. These tagged molecules must not only possess fluorescent properties, but also the biological function of ajoene. The latter would be aided by the use of small fluorophores rather than larger macro-molecules such as fluorescent proteins. The λ_{ex} of the molecules was also an important factor to be taken into consideration, as *in vivo* studies are subject to the cells' sensitivity to high-energy light. Typically, λ_{ex} < 380 nm damages cells so is ill-suited for such studies.

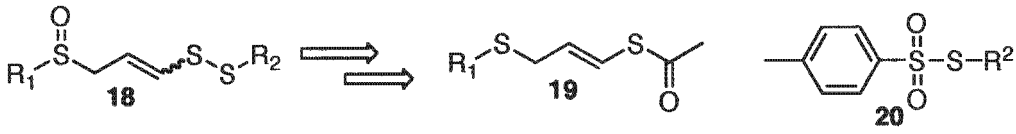

Scheme 17: A retrosynthetic overview of a substituted ajoene

According to the UCT synthesis, a generic ajoene-analogue **18** can be retrosynthetically broken down into a vinyl thioacetate **19** and thiosulfonate **20** (see Scheme 17). Careful consideration is needed when deciding where to place the fluorophore, ie in R^1 or R^2, as its position may prove to be incompatible with one or more of the synthetic steps. The radical addition was the step of highest concern as the unsaturated fluorophore might also undergo reaction. Thus, it was decided that the fluorophore should be placed on the R^2 group in the thiosulfonate sulfenylating agent **20**, in order to avoid the potentially troublesome radical addition.[43] The greater nucleophilicity of ajoene's allyl-S over its vinyl-S supports the placement of the fluorophore in the R^2 position in the preliminary strategy.

A dansyl fluorophore was selected first as the fluorescent marker. Being readily available and affordable, dansyl chloride seemed the ideal choice for developing the skills and methodology needed to synthesize a fluorescent analogue. The dansyl fluorophore is widely used in fluorescent tagging as it has a high fluorescent intensity, typically absorbing at around 330 nm. The λ_{ex} fell below the recommended range for live-cell imaging, but it was hoped that having a 2-photon laser system would prove suitable for the project.

The dansyl-tagged targets chosen, **30** and **32**, as well as their required sulfenylating agent **27** and vinyl thioacetates **23** and **12** respectively, can be seen in Scheme 18 parts **i** and **ii**. The propyl and PMB functional groups were chosen for R^1, as other ajoene analogues with these groups had been shown to possess biological activity comparable (or superior) to that of ajoene. The required vinyl thioacetates were attractive intermediates as their synthesis and characterization was well established within our group.

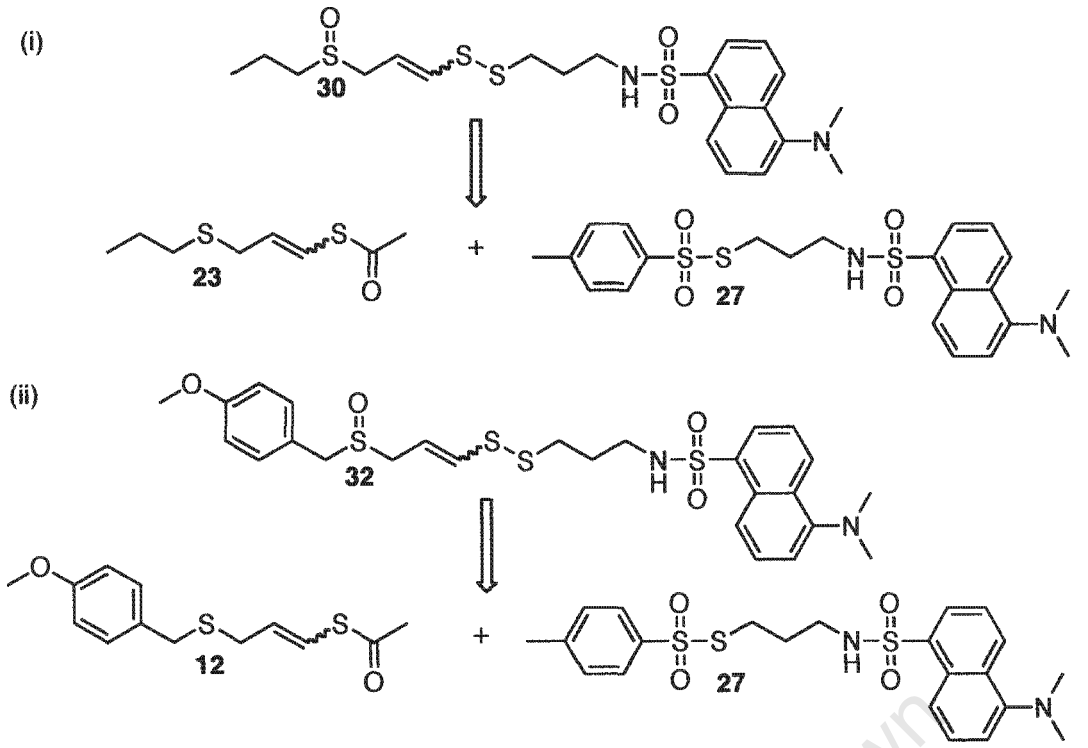

Scheme 18: Dansyl-tagged ajoene targets **30** and **32** with their respective intermediates

4.2 Propyl Propargyl Sulfide, 22[47]

The synthesis of the tagged analogue **30** will be discussed first: The synthesis of the propyl propargyl sulfide **22** (Scheme 19) involved an S_N2-type nucleophilic substitution between commercially available 1-propanethiol **21**, and propargyl bromide **8**. The 1-propanethiol **21** was dissolved in degassed methanol at 0 °C under N_2, after which potassium hydroxide (1.3 equivalents) was added to generate the corresponding thiolate. Propargyl bromide was added drop-wise to avoid a rapid rise in temperature due to the exothermic substitution. Upon adding the propargyl bromide, the solution became opaque as potassium bromide was formed. TLC revealed a new UV-active product that was less polar than the starting propargyl bromide. The methanol was then removed under vacuum on the rotary evaporator and the resulting residue extracted into diethyl ether, which was dried over $MgSO_4$ and the solvent removed under vacuum. The residue was purified by distillation under vacuum (water-pressure generated) to give **22** in a yield of 81 % and as a light-orange oil that smelled strongly of onion.

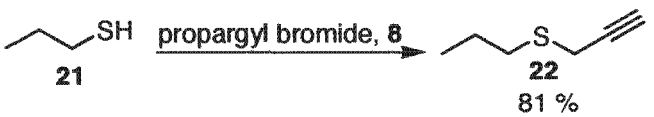

Scheme 19: Synthesis of propyl propargyl sulfide **22**.

The ^{1}H NMR spectrum of **22** (see Figure 20) confirmed the correct product by virtue of the presence of an alkyne methine hydrogen triplet (H-1) at δ = 2.21 ppm and a propargyl, i.e. methylene doublet (H-3) at δ = 3.22 ppm. The ^{13}C spectrum revealed the six expected resonances, including those at δ = 80.1 ppm and 70.7 ppm corresponding to the two alkynyl carbons C-2 and C-1 respectively.

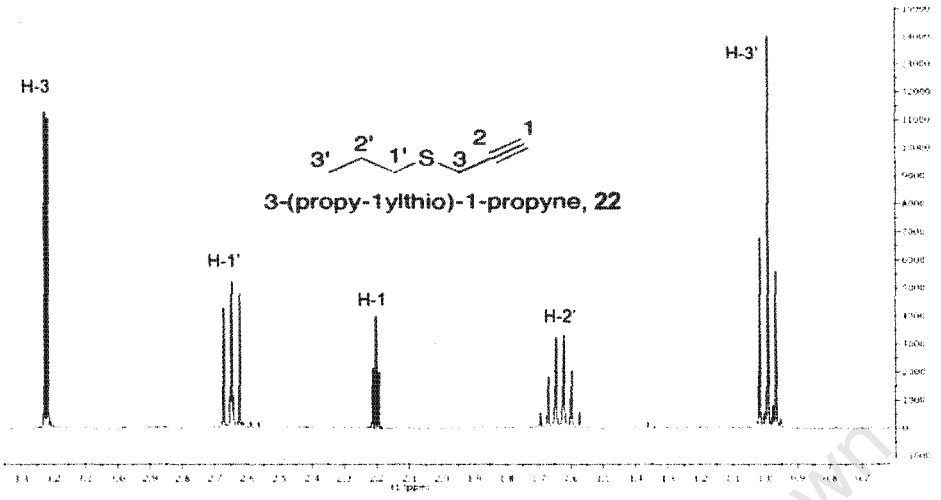

Figure 20: ^{1}H NMR spectrum of **22** in chloroform-d_3

4.3 Propyl Vinyl thioacetate, 23[43]

The propargyl sulfide **22** was next subjected to the regioselective addition of thiolacetic acid (see Scheme 20), using the same procedure to synthesize **13**. It was found that less than 10% (0.1 equivalents) of ACCN was required for the reaction to proceed to completion, resulting in the formation of the vinyl thioacetate **23** as a 5: 3 mixture of *Z/E* stereoisomers in an overall yield of 67 %.

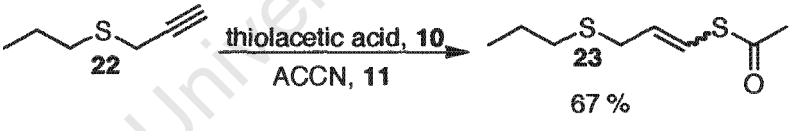

Scheme 20: Synthesis of vinyl thioacetate **23**.

Once again, evidence for the successful addition of thiolacetic acid came from the ^{1}H NMR spectrum of **23** (see Figure 21), as the product presented signals in the vinyl region corresponding to H-3, as well as acetyl singlets for the *E*- and *Z*-stereoisomers respectively. The signal for the H-3 resonance of the *E*-isomer appeared as a double triplet at δ = 6.51 ppm, with coupling constants of *J* = 15.6 (trans) and 1.2 Hz (allylic coupling), while for the *Z*-isomer it appeared at δ = 6.64 ppm, with coupling constants of *J* = 9.5 (cis) and 1.1 Hz. Double triplets were observed for H-4, showing the expected reciprocal large vicinal coupling experienced with H-3. ^{13}C NMR spectroscopy revealed eight distinct resonances for each isomer.

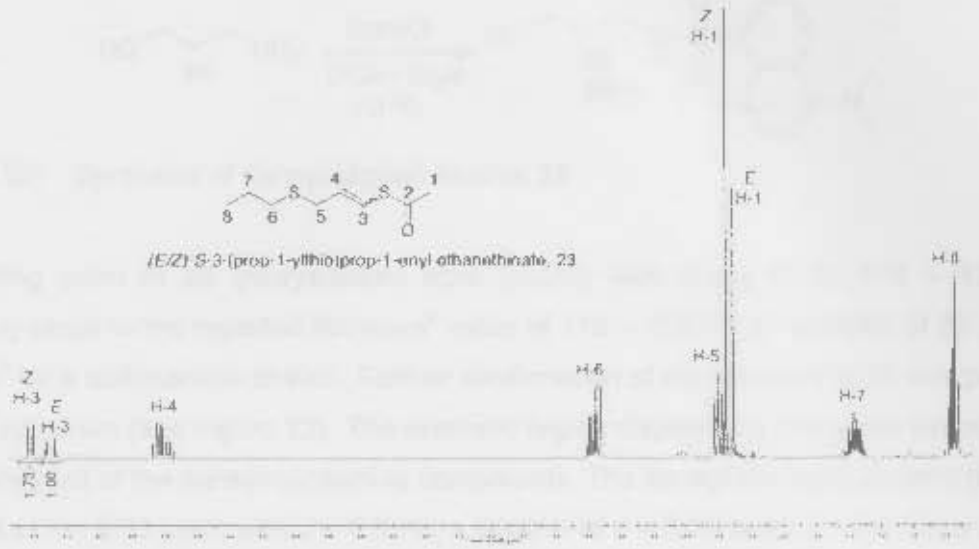

Figure 21: ^{1}H NMR of **23** as a mixture of *Z*/*E*-isomers in chloroform-d_3

4.4 Dansyl-tagged Sulfenylating Agent, 27

The dansyl-tagged sulfenylating agent **27**, was envisaged via the route outlined in Scheme 21. The synthesis targeted the chemoselective nucleophilic substitution of dansyl chloride by 3-aminopropan-1-ol **24** to produce the dansyl-tagged alcohol **25**. The hydroxyl of **25** would later be converted into a mesyl leaving group and it was thought that this would be sufficiently labile to promote substitution by thiotosylate **13** to form the dansyl-tagged sulfenylating agent **27**.

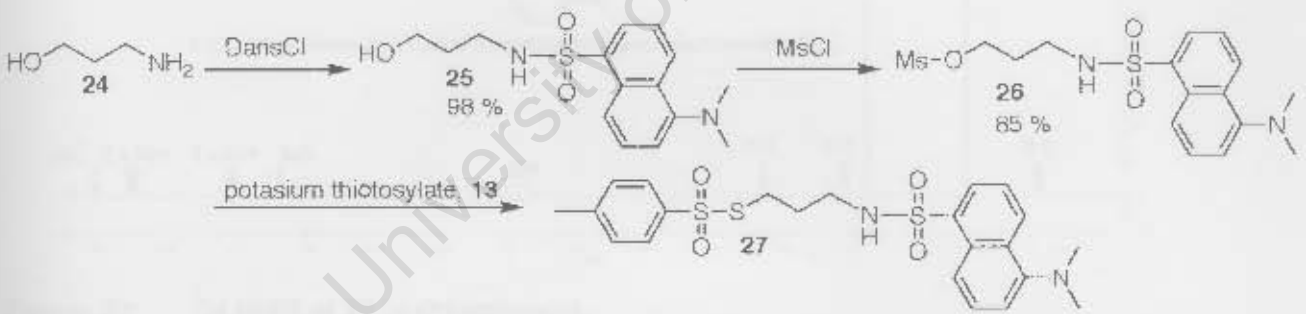

Scheme 21: Proposed synthesis of dansyl-tagged sulfenylating agent **27**

4.4.1 Dansyl-tagged alcohol, 25[48]

The synthesis of dansyl-tagged alcohol **25** (see Scheme 22) began by the drop-wise addition of 3-aminopropan-1-ol **24** into a solution of dansyl chloride and triethylamine in DCM. The latter was used to neutralize the HCl formed during the reaction. The greater nucleophilicity of the amine nitrogen in **24** over the hydroxyl oxygen, resulted in a rapid chemoselective reaction and almost total conversion to product **25**. The product was extractively worked-up and the residue was subjected to column chromatography using ethyl acetate and hexane mixtures to afford the dansyl-tagged alcohol **25** in 98 % yield.

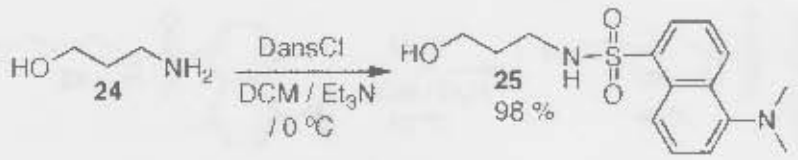

Scheme 22: Synthesis of dansyl-tagged alcohol **25**

The melting point of **25** (recrystalized from EtOAc) was found to be 118 – 120 °C, which was acceptably close to the reported literature[x] value of 119 – 120 °C. IR analysis of **25** revealed a peak at 1270 cm^{-1} for a sulfonamide stretch. Further confirmation of the structure of **25** was provided through its ^1H NMR spectrum (see Figure 22). The aromatic region displayed a distinctive set of signals that would be present in all of the dansyl-containing compounds. The dansyl-aromatic-protons (DAP) appeared as: a doublet at δ = 8.53 ppm with J = 8.6 Hz, a doublet at δ = 8.28 ppm, J = 8.6 Hz, a doublet at δ = 8.21 ppm with J = 7.3 Hz, a multiplet at δ = 7.53 ppm for two hydrogens and a doublet at δ = 7.17 ppm with J = 7.3 Hz. The NMe_2 presented as a singlet at δ = 2.88 ppm. The sulfonamide hydrogen appeared at δ = 5.36. The three methylene signals of **25** were observed for H-1, H-3 and H-2 at δ = 3.64 ppm, δ = 3.04 ppm and δ = 1.63 ppm respectively. The ^{13}C NMR spectrum displayed the ten aromatic and four aliphatic resonances corresponding to the fifteen carbons present. Notably, the NMe_2 appeared as one signal at δ = 45.4 ppm due to free rotation around the C_{Ar}-N bond.

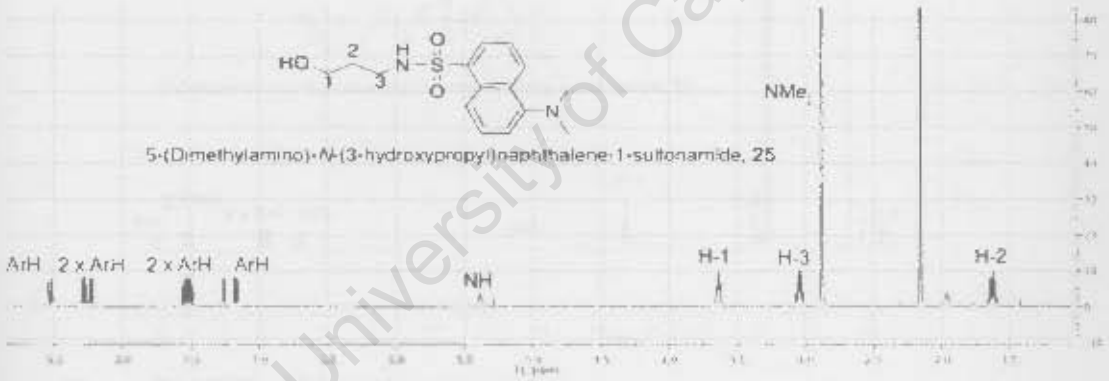

Figure 22: ^1H NMR of **25** in chloroform-d_3

4.4.2 Dansyl-tagged mesylate, 26

In order to generate the S-tosylate of the primary alcohol **25**, it was first necessary to convert the hydroxyl (OH) into a suitable *leaving group* (see Scheme 23), as the hydroxyl group functions poorly in this regard. The group chosen was the mesylate (methylsulfonate ester), which was formed by slowly adding mesyl chloride to a solution of **25** and triethylamine in anhydrous DCM at 0 °C. After 20 minutes, TLC analysis indicated the total consumption of the starting material and the formation of a new fluorescent spot that was less polar than the starting **25**. After extraction, drying over $MgSO_4$ and removal of solvent, the residue was subjected to column chromatography (EtOAc) to afford **26** as a luminous-green oil in an 85 % yield.

Scheme 23: Synthesis of dansyl-tagged mesylate **26**

IR analysis of the product **26** revealed an absorbance at 1270 cm^{-1} corresponding to the sulfonamide. The characteristic DAP-peaks were also present in the ^1H NMR spectrum. Introduction of the mesylate was verified by a notable shift downfield of the methylene peak for H-1 closest to the oxygen as well as a three-hydrogen singlet for the mesyl group at δ 2.93 ppm. The ^{13}C NMR spectrum of **26** was similar to that of **25**, but with an additional aliphatic carbon, lending support to a successful mesylation. The downfield shift of C-1, from 60.5 ppm in the alcohol **25**, to 66.9 ppm in the mesylate **26**, gave further evidence for the formation of the product (see Table 4).

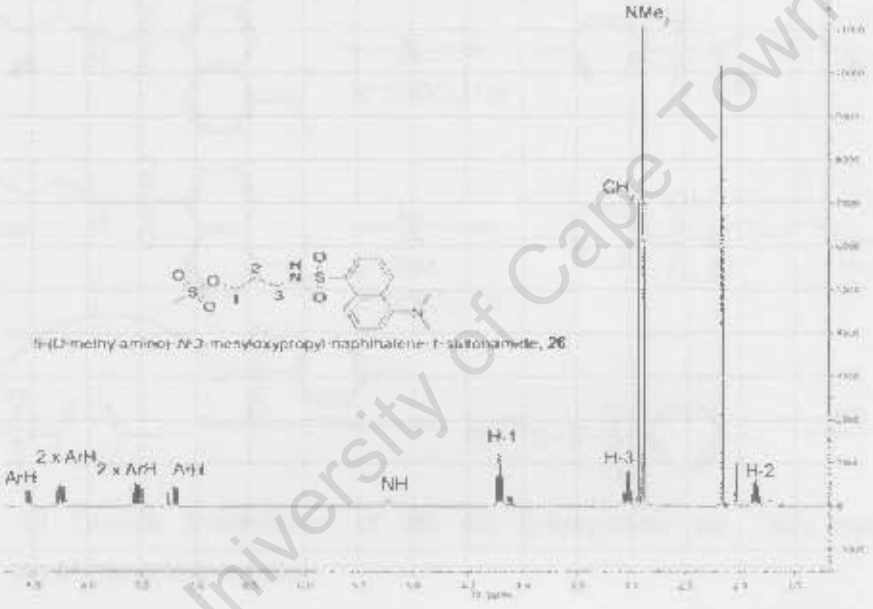

Figure 23: ^1H NMR of **26** in chloroform-d_3

Table 4: Diagnostic NMR shifts of H-1 and C-1 of **25**, **26** and **28**

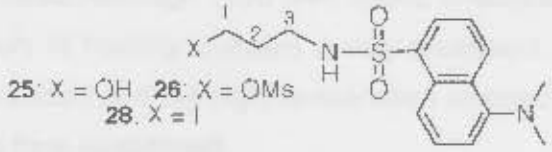

Compound	H-1:	C-1:
	δ_H (ppm); Multiplicity; J (Hz)	δ_C (ppm)
25	3.64, t, 5.4	60.5
26	4.21, t, 5.4	66.9
28	2.96, t, 5.3	30.9

4.4.3 Dansyl-tagged Iodide, 28

For conversion of mesylate **26** to its S-tosylate **27**, direct S_N2 substitution was initially attempted with potassium *p*-toluenethiosulfonate (see Scheme 24 i). The reaction required heating, with products only becoming visible on TLC above 50 °C and after 6 hours. TLC analysis revealed incomplete consumption of the starting material as well as two assumed product spots in the reaction mixture, which were inseparable by column chromatography. It is believed that upon heating, one cannot control further substitutions of the thioate to the desired product, as the sulfur of the thiosulfonate ester is a soft electrophile and is susceptible to attack by the residual S-tosylate (see Scheme 24 iii). Therefore, it was concluded that the sulfonate ester was not suitable and that the mesyl group would have to be exchanged for a more labile leaving group.

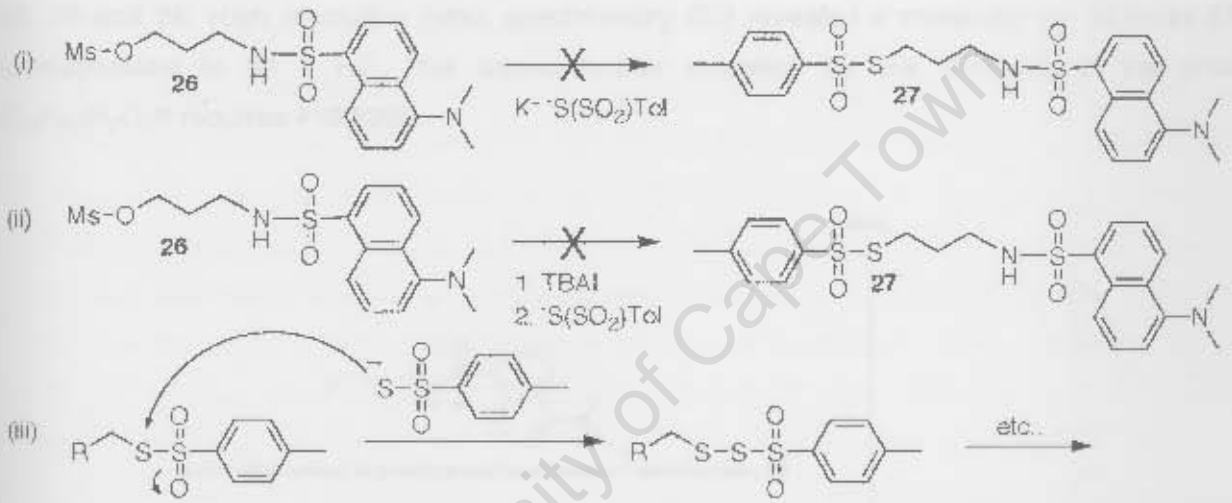

Scheme 24: (i) Directs S-tosylation of **26**; (ii) S-tosylation via TBAI generated iodide intermediate; (iii) Multiple S-tosylation

It was thus decided to exchange the mesylate group of **26** for an iodide, using tetrabutylammonium iodide (TBAI) in refluxing acetonitrile, and then to try the S-tosylation (see Scheme 24 ii). This approach was also problematic. Although TBAI was added in excess to drive the reaction towards full iodination, TLC after 2 hours of heating revealed a very prominent spot corresponding to the starting mesylate. The thioate was added and the high temperature resulted in the same breakdown observed before. The procedure was thus abandoned.

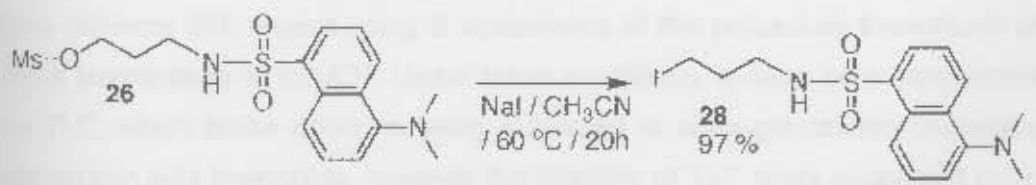

Scheme 25: Synthesis of dansyl-tagged iodide **28**

A modification of the approach was then adopted. Thus, mesylate **26** was heated with 20 equivalents of NaI in acetonitrile for 20 hours at 60 °C (see Scheme 25). Successful generation of the iodide **28**, which was less polar than the mesylate, was followed by TLC. Purification by silica-gel column chromatography afforded the desired iodide **28** as a luminous-green oil in a yield of 97 %.

The ^{1}H NMR spectrum of **28** (see Figure 24) showed a definite "up-field" shift of the H-1 methylene signal, from δ = 4.21 ppm in mesylate **26** to around 3.05 ppm (observed as a multiplet) in iodide **27**, demonstrating the lower deshielding effect of iodine over a sulfonate ester. The typical dansyl proton signals were observed in the ^{1}H NMR spectrum as well as the desired 14 carbon signals in the ^{13}C spectrum. There was the expected upfield shift of C-1, from 66.9 ppm in the mesylate, to 30.9 ppm, also indicating that exchange to the iodide had taken place. Table 4 offers evidence for the various transformations by highlighting the chemical shifts for H-1 and C-1 for the dansyl-tagged intermediates **25**, **26** and **28**. High resolution mass spectrometry (EI) revealed a molecular ion of mass 419.0273, corresponding to [M + H]$^{+}$. This added further evidence for the formation of the product, as $C_{15}H_{20}IN_2O_2S$ requires 419.0290.

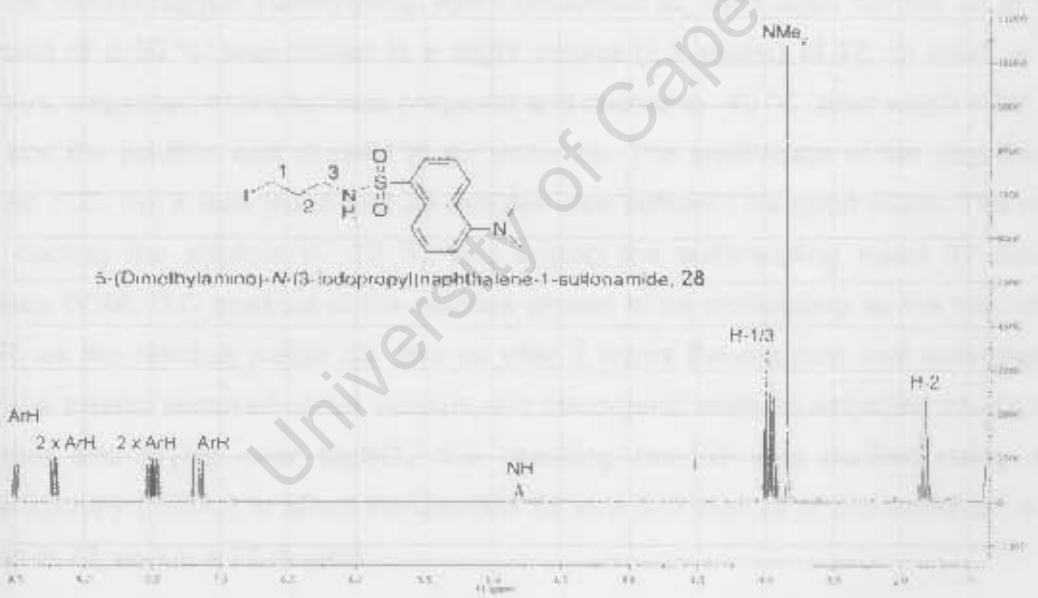

Figure 24: ^{1}H NMR of **28** in chloroform-d_3

4.4.4 Dansyl-tagged thiosulfonate

With the iodide **28** in hand, substitution with potassium *p*-toluenethiosulfonate was attempted as before (see Scheme 26), except using 8 equivalents of the potassium thiosulfonic acid salt for 20 hours at room temperature in CH_3CN. Under these conditions, a more polar fluorescent product was observed on TLC, which broke down on being subjected to silica-gel column chromatography. Quantifying the conversion was impossible, however the intensity of TLC spots suggested more than 50 % conversion. The use of such a high number of equivalents of the thiosulfonate salt was intended to drive conversion

to the thioate **27**. When left for longer periods (greater than 20 hours), in an attempt to increase the yield of **27**, decomposition was noticed, reflected as streaking as well as extra (polar and non-polar) spots on TLC. Thus, after 20 hours, the solvent was removed under vacuum, the organic residue extracted into EtOAc, washed with water to remove traces of salt, afterwhich it was washed further with brine, dried over $MgSO_4$ and the solvent removed under vacuum. Characterization of **27** was not performed due to the crude nature of the mixture as well as the instability of the product. Instead **27**, was used directly in the synthesis of disulfides **29** and **31**.

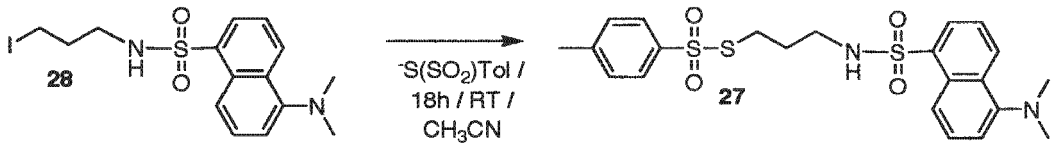

Scheme 26: Synthesis of dansyl-tagged sulfenylating agent **27**

4.5 Dansyl-propyl Disulfide, 29

The next step involved coupling the vinylthioacetate **23** with dansyl-tagged sulfenylating agent **27** (see Scheme 27). The reaction was carried out in a similar fashion to that described in Chapter 3.5, except the crude dansyl-tagged sulfenylating agent (assumed to have been formed as in Scheme 26 to a conversion of ± 50 %) was added to a slight excess (1.2 equiv.) of **23**. In short, a solution of **23** in anhydrous, degassed methanol was prepared and cooled to -40 °C, after which KOH in methanol was added and the solution was allowed to stir under N_2. The enethiolate of the vinyl thioacetate was not visible on TLC, but it was found that 30 minutes was sufficient for good yields. The next step involved further cooling the solution to -78 °C and adding the sulfenylating agent **27** dissolved in a little anhydrous DCM. TLC analysis of the reaction proved to be challenging as the product moved with the same R_f as the residual iodide **28**, and so after 2 hours the reaction was quenched using aqueous NH_4Cl, the solvent removed under vacuum and the organic material extracted into DCM. After washing with brine and drying over $MgSO_4$, the resulting residue was purified using silica-gel column chromatography (EtOAc) to afford the disulfide **29** as a 5: 3 mixture of *Z/E*-isomers, i.e. with retention of *E/Z*-ratio in **23**, and in a 71 % yield.

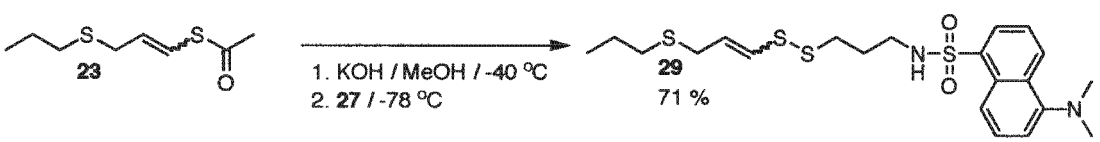

Scheme 27: Synthesis of disulfide **29**

The major product was the disulfide, indicating that the iodide did not react with the enethiolate to afford a vinyl sulfide entity (see Scheme 28). This implies electrophilic carbon C-1 α to the iodine, typically considered to be a soft electrophilic centre, was suitably hard as compared to the S-tosylate, providing the reaction with the desired chemoselectivity owing to sulfur being softer than carbon. The weaker S-S

bond compared to the C-I bond also assisted with the selectivity. This further illustrates the robust chemoselective properties of the sulfenylation step in forming vinyl disulfide functionality.

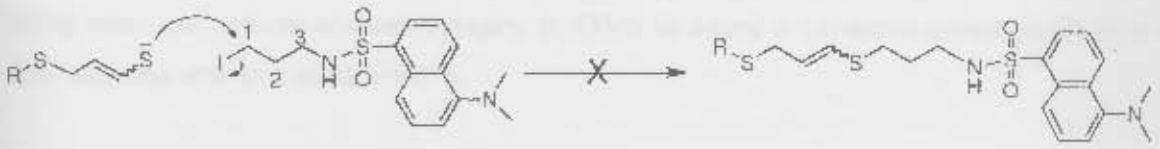

Scheme 28: Potential S-alkylation side reaction

The ^{1}H NMR spectrum for the disulfide **29** (see Figure 25) confirmed that the desired coupling had been achieved, owing to signals from both coupling partners being observed. The expected dansyl signals were present and the vinyl protons H-4 and H-5 appeared seperately for the *E*- and *Z*-isomers. In the ^{13}C NMR spectrum, twelve downfield vinyl and aromatic signals were observed, with two resonances coinciding at the same chemical shift. As expected, eight aliphatic signals were detected upfield, lending support to a product containing twenty-one carbons. High resolution mass spectrometry revealed a molecular ion of 471.1274, corresponding to $[M + H]^+$ as $C_{21}H_{31}N_2O_2S_4$ requires 471.1268. Unfortunately an accurate microanalysis could not be obtained as the product was an oil.

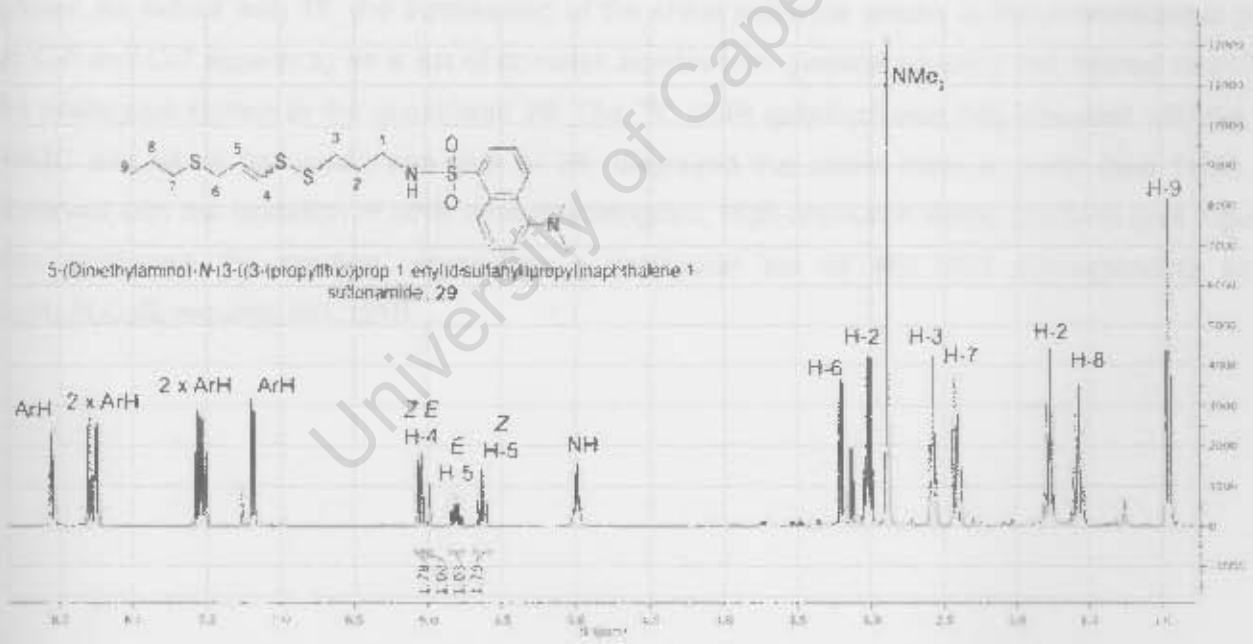

Figure 25: ^{1}H NMR of **29** as a mixture of *Z*/*E*-isomers in chloroform-d_3

4.6 Dansyl-propyl Ajoene, 30

With the disulfide **29** in hand, the final step in the synthetic sequence towards the target **30** was the chemoselective oxidation of the sulfide to its sulfoxide (see Scheme 29). The procedure was similar to that for **17**. Thus, the reaction was performed by adding 1.3 equivalents of *m*-CPBA to a solution of the disulfide **29** in DCM (see Scheme 29). Care was taken to ensure that the temperature of the solution was kept below -60 °C, and TLC analysis revealed the formation of a single product spot. After 2 hours,

saturated aqueous Na_2CO_3 was added to the rapidly stirring solution to quench the reaction. The solution was allowed to warm enough for the aqueous layer to melt, after which the organic material was extracted into DCM. After drying over $MgSO_4$ and removing the solvent, the residue was purified using silica-gel column chromatography (EtOAc) to afford a luminous-green oil **30** as a 5: 3 mixture of *Z*/*E*- isomers and in a yield of 66 %.

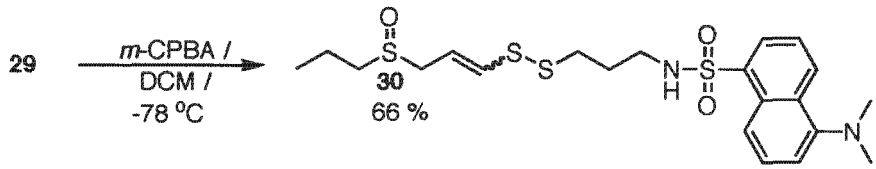

Scheme 29: Oxidation of disulfide **29** to sulfoxide **30**

The ^1H NMR spectrum of **30** (see Figure 26) revealed the expected dansyl signals. The sulfonamido NH of the *E*- and *Z*-isomers resonated with different chemical shifts. The NH appeared as a single peak at δ = 4.99 ppm for the disulfide **29**, but upon oxidation to the sulfoxide **30**, appeared as two peaks, at δ = 6.02 ppm and δ = 5.63 ppm for the *E*- and *Z*-isomers respectively. It is also interesting that the NH of the Z-isomer appeared upfield to that of the *E*-isomer, possibly due to greater H-bonding in the *Z*-isomer. As before with **17**, the introduction of the chiral sulfoxide results in the diastereotopic protons on C-6 and C-7 appearing as a set of complex signals with geminal coupling that appear downfield to the analogous signals in the unoxidised **29**. The ^{13}C NMR spectrum was fully assigned with the aid of HSQC and when compared with that of **29**, displayed the same trend in shifts (see Table 5) as observed with the oxidation of other ajoene-analogues. High-resolution mass spectrum (see Figure 27) also confirmed the product, presenting a molecular ion of 487.1221 corresponding to $[M]^+$; $C_{21}H_{31}N_2O_3S_4$ requires 487.1218.

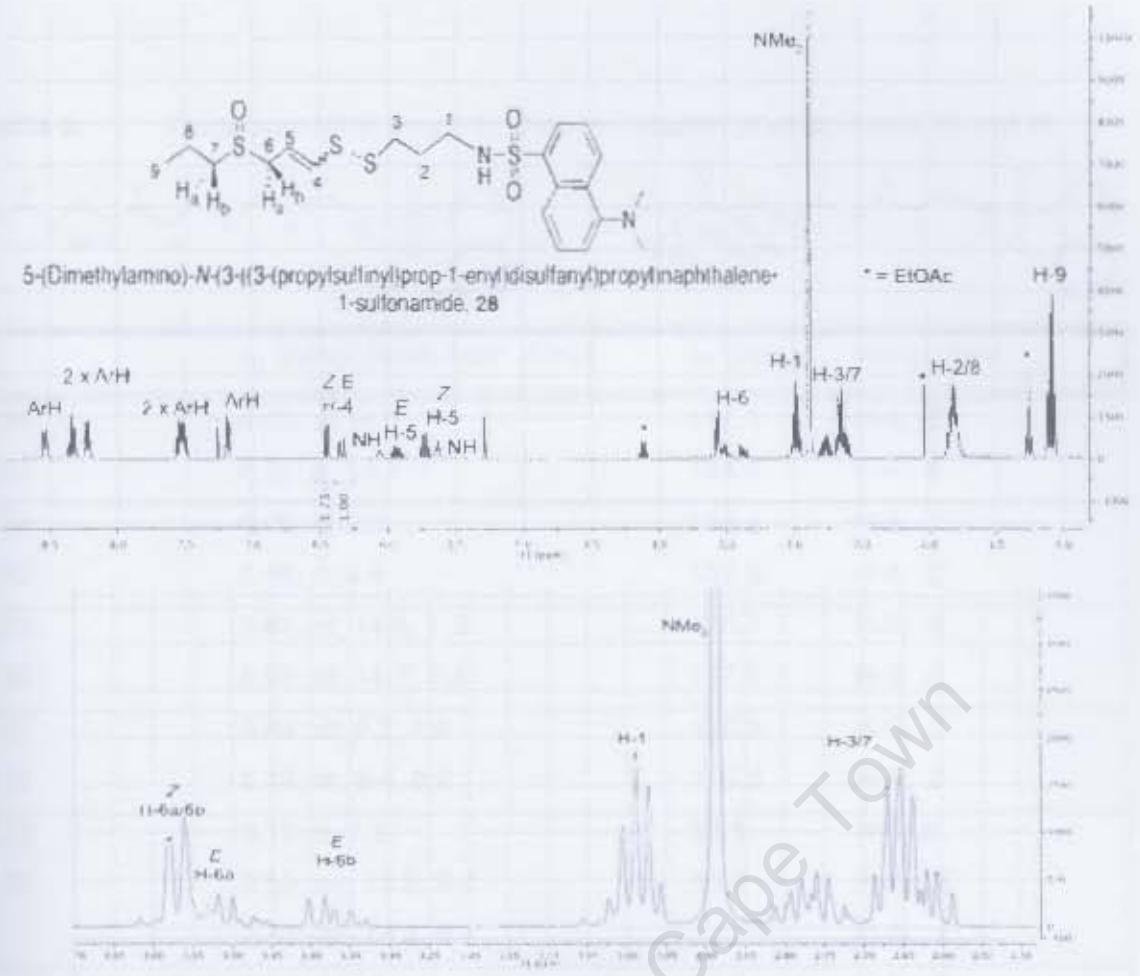

Figure 26: ^{1}H NMR of **30** as a mixture of *Z*/*E*-isomers in chloroform-d_3

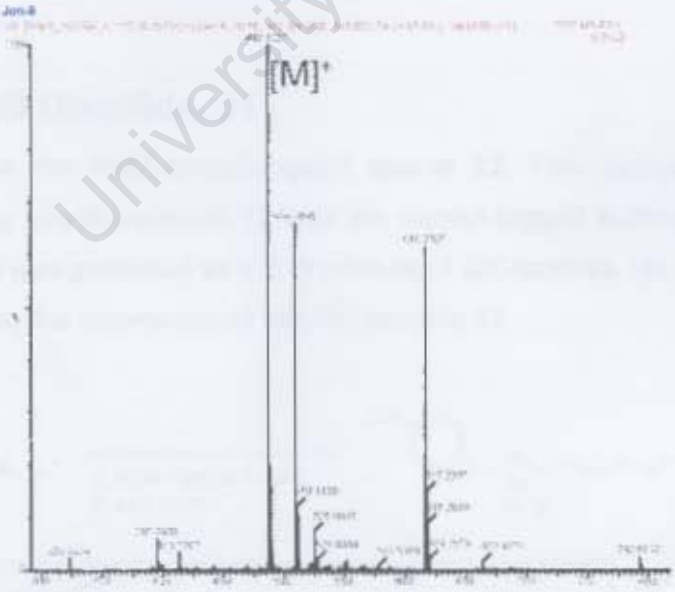

Figure 27: High resolution mass spectrometry of **30**

Table 5: Diagnostic NMR peaks for the identification of compounds **29** and **30**

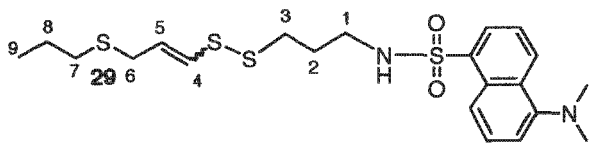

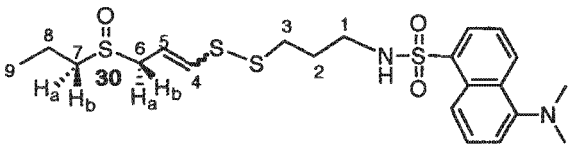

	δ_H (ppm); Multiplicity; *J* (Hz)	δ_C (ppm)	Assignment
29	6.02; d; 14.6	127.1	H-4; *E*
30	6.32; d; 14.7	134.6	H-4; *E*
29	6.06; d; 9.2	131.2	H-4; *Z*
30	6.46; d; 9.4	137.8	H-4; *Z*
29	5.81; dt; 14.6, 7.3	128.7	H-5; *E*
30	5.93; dt; 14.7, 7.4	117.5	H-5; *E*
29	5.64; dt; 9.2, 7.8	128.9	H-5; *Z*
30	5.73; dt; 9.4, 8.2	119.5	H-5; *Z*
29	3.13; d; 7.3	33.1	H-6; *E*
30	3.53; dd; 13.2, 8.4	53.9	H-6_a; *E*
	3.38; dd; 13.2, 8.4		H-6_b; *E*
29	3.19; d; 7.8	29.3	H-6; *Z*
30	3.57; d; 8.9	50.9	H-6_a and H-6_b; *Z*

4.7 Dansyl-PMB Disulfide, 31

The next target was the PMB-dansyl-tagged ajoene **32**. The dansyl-tagged intermediate **31** was prepared by coupling vinylthioacetate **12** with the dansyl-tagged sulfenylating agent **27** (see Scheme 30). The disulfide **29** was produced as a 6: 5 mixture of *Z/E*-isomers (as determined by ^{1}H NMR) and in a 90 % yield based on the conversion of vinylthioacetate **12**.

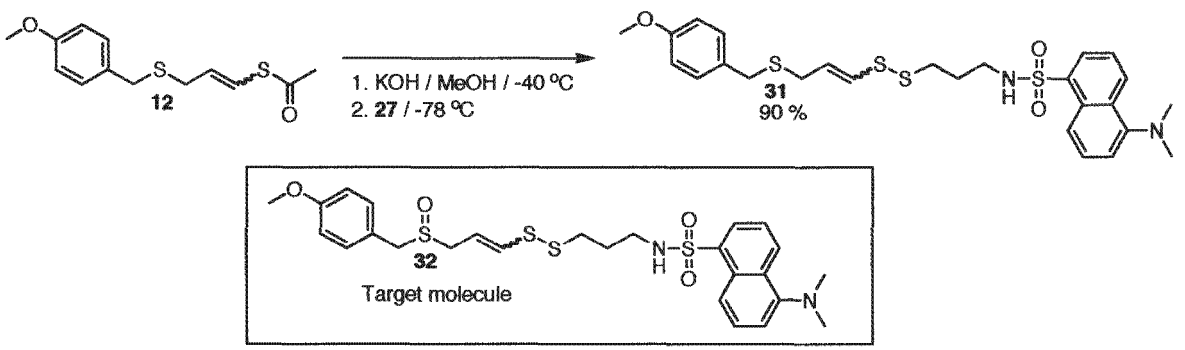

Scheme 30: Synthesis of disulfide **31**

There appears to be a marginal reversal of the geometry about the double bond, from 4: 3 *Z: E* in the precursor **12** to 6: 5 in the disulfide **31**, which did not occur in the synthesis of the disulfide **15** (see Scheme 15). The following (see Scheme 31) is a proposed pathway that illustrates how an equilibrium may be established: The enethiolate may be protonated by MeOH to form the enethiol, which in turn may tautomerize to form the corresponding thioaldehyde. The next step would involve a rotation about the C-1/C-2 single bond, reducing steric strain. The next step involves the tautomerization to form the more stable *E*-enethiol, which could then be deprotonated by methoxide, producing the *E*-enethiolate. The net effect of this proposed pathway is the transformation of the more-abundant *Z*- to its thermodynamically favoured *E*-isomer.

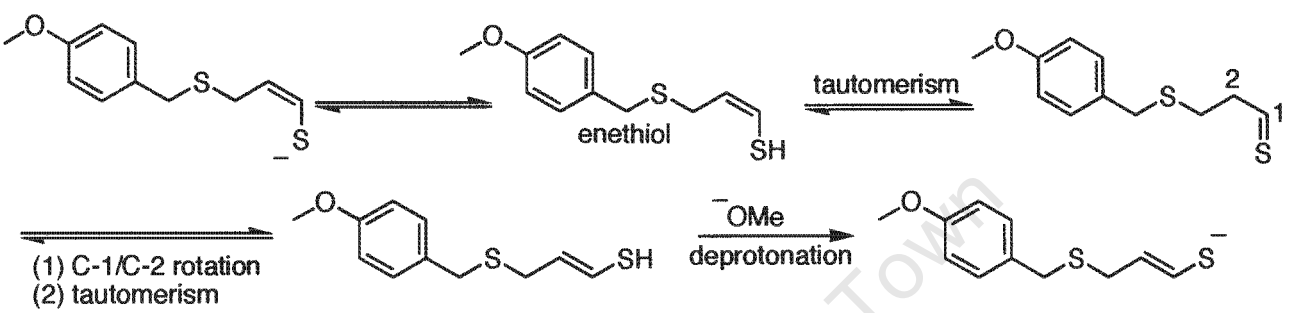

Scheme 31: A mechanism for the tautomerism of enethiolates

The structure of the disulfide **31** was confirmed by its ^{1}H NMR spectrum, which revealed signals from both coupling partners and possessed the typical dansyl aromatic proton signals. An overlap between H-9 and one of the dansyl aromatic protons obscured the signals at around δ = 7.21 ppm. The presence of *E*- and *Z*-isomers was apparent from the typical resonances expected from such a mixture. Thus, for the double bond, the *E*-isomer presented a doublet at δ = 5.98 ppm and a double triplet at δ = 5.80 ppm with coupling constants J = 14.6 Hz and J = 14.6, 7.3 Hz respectively, while the *Z*-isomer presented a doublet at δ = 6.08 ppm and a double triplet at δ = 5.64 ppm with coupling constants J = 9.2 Hz and J = 9.2, 7.8 Hz respectively. The ^{13}C spectrum was fully characterized with the aid of an HSQC spectrum, which revealed the expected 26 resonances for each isomer; however it must be noted that several resonances, namely C-9 and ArC_{qu} (dansyl) as well as ArC (dansyl) and C-5 (*E*) coincided at 130.0 ppm and 128.4 ppm respectively. Table 6 contains some of the diagnostic ^{1}H and ^{13}C NMR peaks for **31**.

A high-resolution mass spectrum (EI) revealed a molecular ion of *m/z* 549.1385, corresponding to $[M + H]^+$, offering further evidence for the formation of **31**, as $C_{26}H_{33}N_2O_3S_4$ requires 549.1374.

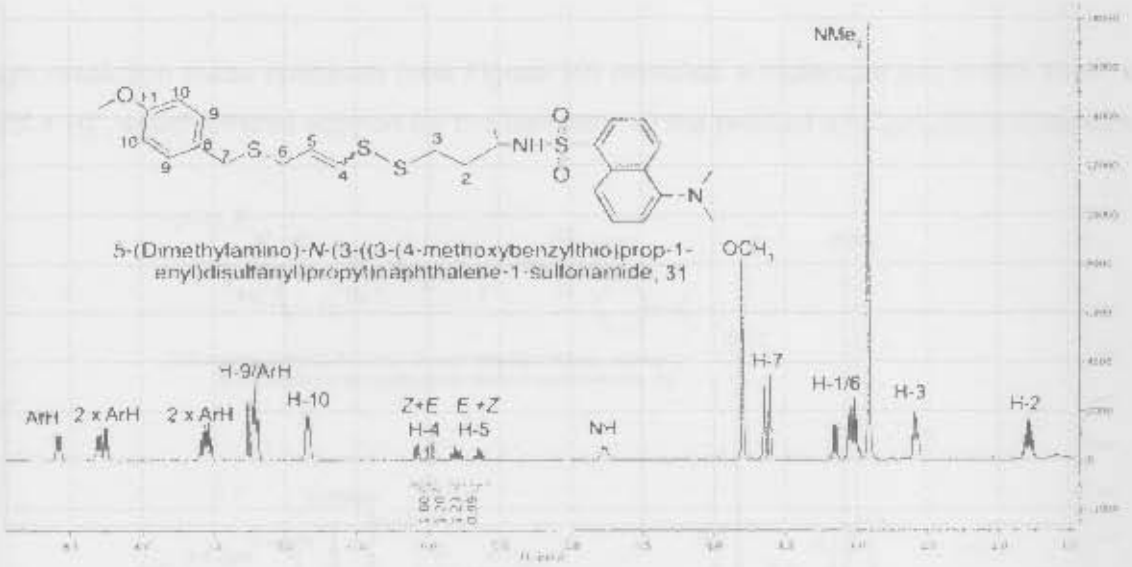

Figure 28: ^{1}H NMR of **31** as a mixture of *Z*/*E*-isomers in chloroform-d_3

4.8 Dansyl-PMB Ajoene, 32

The final step in the synthetic sequence towards the dansyl-tagged target **32** was the chemoselective oxidation of the sulfide to its sulfoxide (see Scheme 32). The procedure used was similar to that of **15** and **30**. The product **32** was produced in a yield of 72 % and as a 6: 5 mixture of *E*/*Z*- isomers (as determined by ^{1}H NMR), indicating a retention of stereo-integrity from **31**.

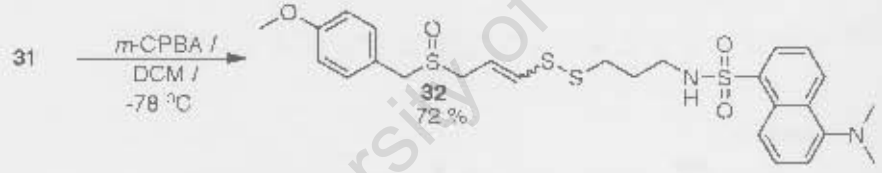

Scheme 32: Oxidation of disulfide **31** to sulfoxide **32**

The oxidation to the sulfoxide **32** was supported by its ^{1}H (see Figure 29 i) and ^{13}C NMR spectra. The peaks for both **H-6** and **H-7** shifted downfield (from their chemical shift in **31**) as a result of the deshielding effect of the sulfoxide. As before, the introduction of the sulfoxide created different magnetic environments for the diastereotopic protons on C-6 and C-7, causing them to appear as separate signals. The **NH** signal was observed to experience a similar shift upon oxidation as observed in **30**. Thus, the NH signal appeared at δ = 4.77 ppm for both isomers in the disulfide **31**, but presented as two separate signals in the oxidized product **32**, both down field, at δ = 6.08 ppm for the *E*- and δ = 5.69 ppm for the *Z*-isomer. The aromatic region, from around δ = 8.7 ppm through to δ = 6.7 ppm, contained all of the expected dansyl and phenyl aromatic signals. The ^{13}C spectrum was fully characterized with the aid of HSQC (see Figure 29 ii) and revealed the expected changes in chemical shifts (see Table 6) that adhered to the previously described trend, namely: the downfield shift of C-4, C-6 and C-7, as well as the upfield shift of C-5 upon oxidation.

High resolution mass spectrum (see Figure 30) revealed a molecular ion at 565.1331, corresponding to $[M + H]^+$, which offered support for the formation of the product as $C_{26}H_{33}N_2O_4S_4$ requires 565.1323.

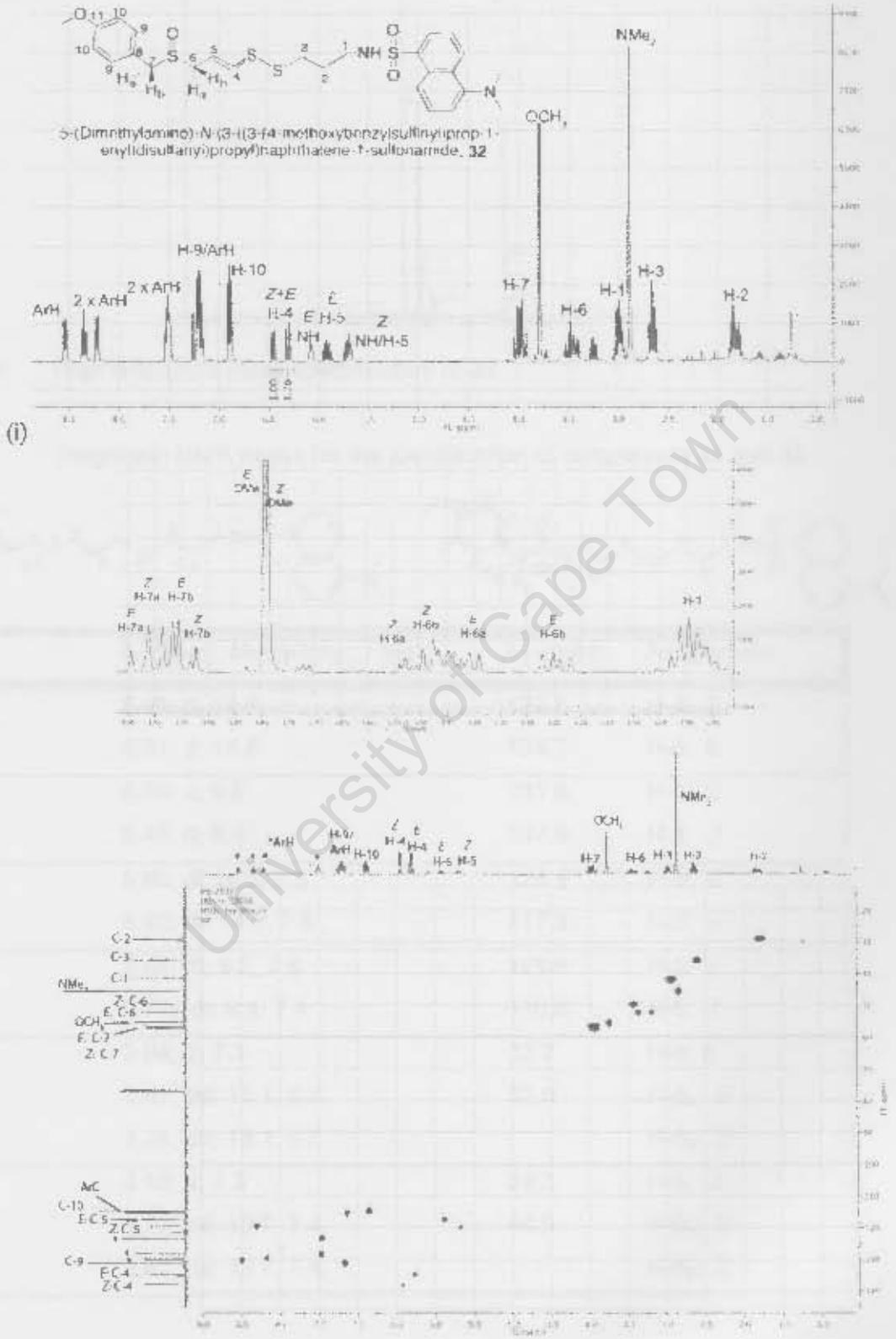

Figure 29: (i) ^{1}H NMR of **32** as a mixture of *Z*/*E*-isomers in chloroform-d_3; (ii) HSQC of **32** as a mixture of *Z*/*E*-isomers in chloroform-d_3.

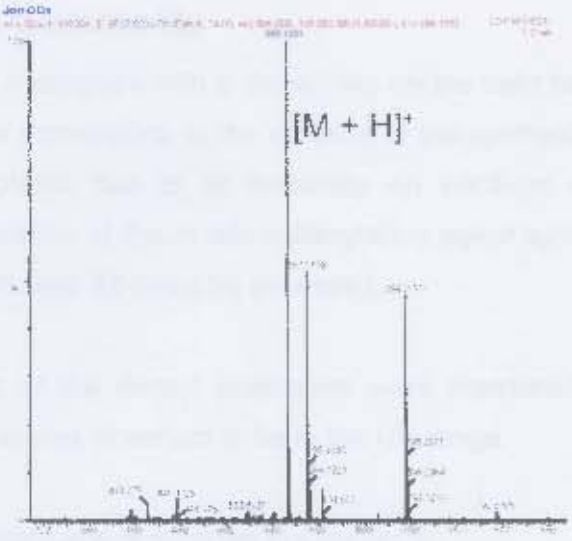

Figure 30: High resolution mass spectrometry of **32**

Table 6: Diagnostic NMR peaks for the identification of compounds **31** and **32**

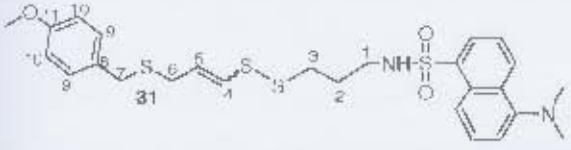

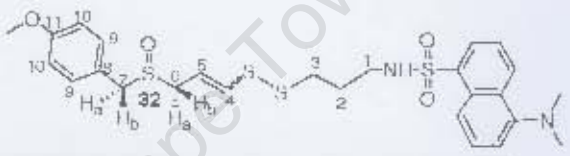

	δ_H (ppm); Multiplicity; *J* (Hz)	δ_C (ppm)	Assignment
31	5.98; d; 14.6	127.5	H-4; *E*
32	6.31; d; 14.8	134.7	H-4; *E*
31	6.08; d; 9.2	131.6	H-4; *Z*
32	6.45; d; 9.4	137.9	H-4; *Z*
31	5.80; dt 14.6, 7.3	128.4	H-5; *E*
32	5.92, dt, 14.8, 7.6	117.3	H-5; *E*
31	5.64; dt; 9.2, 7.8	128.6	H-5; *Z*
32	5.71; dt; 9.4, 7.4	119.6	H-5; *Z*
31	3.04; d; 7.3	32.7	H-6; *E*
32	3.42; dd; 13.1, 6.7	52.0	$H\text{-}6_a$; *E*
	3.24; dd; 13.1, 6.7		$H\text{-}6_b$; *E*
31	3.15; d; 7.8	29.3	H-6; *Z*
32	3.52; dd; 13.7, 7.4	49.5	$H\text{-}6_a$; *Z*
	3.47; dd; 13.7, 7.4		$H\text{-}6_b$; *Z*

4.9 Overview and Comments

The synthesis of ajoene analogues with a dansyl-tag on the right hand side of the molecule proved to be a non-trivial task. The cornerstone to the success of the synthesis lay in the sulfenylating agent **27**, which could not be isolated due to its instability on silica-gel columns. Nevertheless, once the development and optimization of the *in situ* sulfenylating agent synthesis had been achieved, the two dansyl tagged ajoenes **30** and **32** could be accessed.

The fluorescent spectra of the dansyl analogues were measured and are reported at the end of Chapter 5. The absorption was observed to be in the UV range.

Biological activity was tested and is reported in Chapter 6.

Chapter 5: A Fluorescein-tagged Ajoene

5.1 Introduction

The second fluorophore chosen for the fluorescent-ajoene derivatives was fluorescein. Fluorescein is a xanthene dye first synthesized by Baeyer in the 1870's. Despite its antiquity, fluorescein remains one of the most widely utilized fluorophores in modern medicinal, biological, and biochemical research. Its value can be attributed to its excellent spectral properties and its well established synthetic chemistry.[49] Fluorescein provides a modular scaffold that is well-suited for modification to create various molecular tools, including ion indicators, fluorogenic enzyme substrates, and fluorescent labels for biomolecules and pharmaceuticals.[50 51 52]

The synthetic strategy involved synthesizing a fluorescein-tagged sulfenylating agent (much like the dansyl-tagged **27**) to synthesize an ajoene with the fluorophore on the "right hand side". The expensive, but commercially available fluorescein isothiocyanate **33** was first considered as a potential starting material. A possible synthetic route in shown in Scheme 33, whereby a fluorescein-tagged sulfenylating agent is generated by linking an amine **34** (where n = 2 or 3, X = OH) to the isothiocyanate **33**, followed by the activation of X to a leaving group. The strategy was considered flawed as the sulfur in the thiourea moiety in **35** is nucleophilic and could promote intramolecular cyclization to afford **36a** upon activation of X from OH to a leaving group for conversion into the desired thiosulfinate **36b** (see Scheme 33).

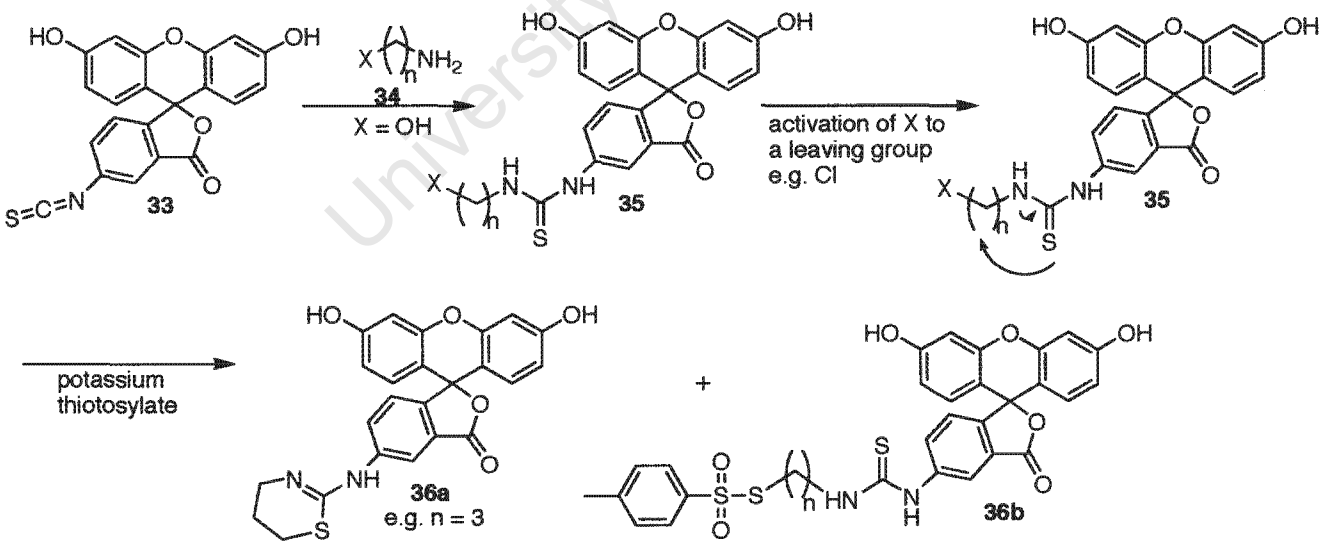

Scheme 33: Potential problem with fluorescein isothiocyanate

Conversely, 5-aminofluorescein **37**, which could be prepared from affordable and commercially available starting materials, seemed to be a better alternative for accessing the tagged-sulfenylating agent. It has been cited countless times in the literature and used for many aminofluorescein-based

fluorescent tags.[49, 51, 53] It was thought that coupling the aminofluorescein to chloroacetyl chloride would produce the amide intermediate **38** that could be substituted with the required thiotosylate to form the sulfenylating agent **39**. The stability of the amide bond in **38** made the sequence shown in Scheme 34 attractive.

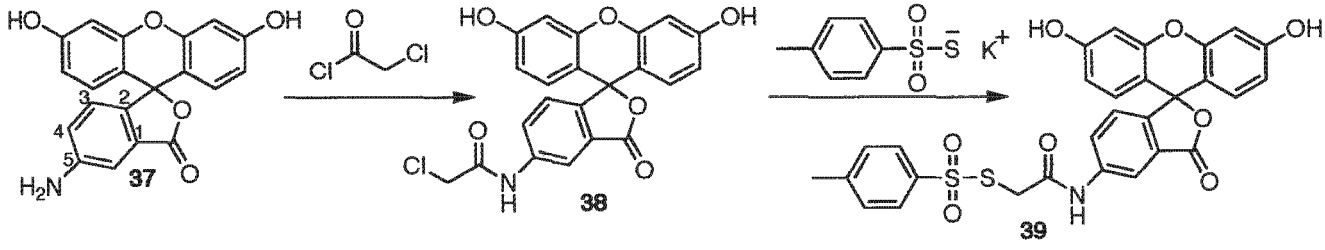

Scheme 34: Proposed synthesis of fluorescein-tagged thiotosylate

Using a well-documented procedure,[51] 4-nitrophthalic acid **40** and 2 equivalents of resorcinol **41** were heated to a melt in an open Erlenmeyer flask to produce a dark, red-brown mass after 3 hours (Scheme 35 **i**). In this reaction, three water molecules are eliminated (see Scheme 35 **ii**). The solid material was then ground to a fine powder with a pestle and mortar, after which it was refluxed in 0.5 M HCl for 1 hour to dissolve any unreacted starting materials. The solid material was then collected with a Büchner funnel and dried under vacuum at 80 °C.

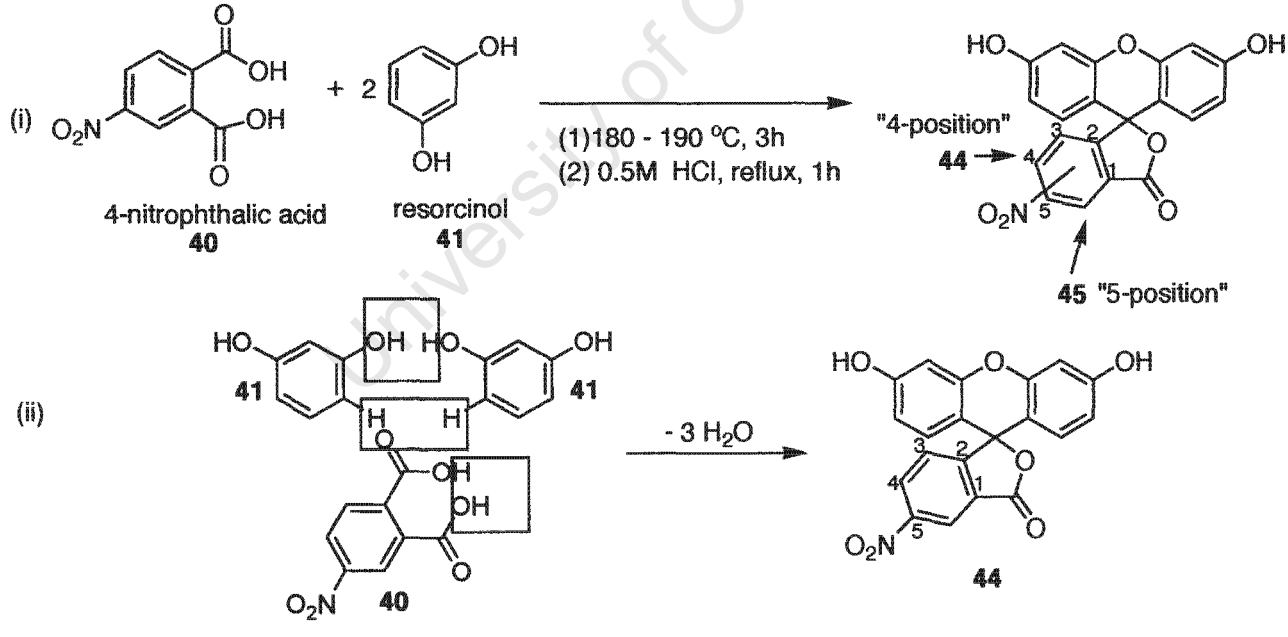

Scheme 35: (i) Synthesis of 4- and 5-nitrofluoresceins **44** and **45**; (ii) overview of the fusion reaction used to produce 4-nitrofluorescein **44**.

The product was a mixture of 4-nitro and 5-nitrofluorescein **44** and **45**, which could not be separated easily using conventional methods. The literature reports that fractional recrystallization is an effective method to separate the regioisomers and this was performed by refluxing the mixture in Ac_2O for 3

hours, filtering hot through a sintered glass funnel and storing at -20 °C for 4 days for the 5-nitrofluorescein diacetate **42** to crystallize (see Scheme 36 **i**).[51]

Crystals of 5-nitrofluorescein diacetate **42** crystals were collected and the mother liquor was concentrated to one quarter of its original volume and again stored at -20 °C overnight for further crystallization to occur. The crystals were collected, combined with the previous batch and recrystallized twice from Ac_2O to yield pure 5-nitrofluorescein diacetate in an overall yield of 17 %. The melting point (Ac_2O) was found to be 216 – 218 °C, and in agreement with the literature melting point (Ac_2O) of 215 – 218 °C.[51]

Subsequently, the mother liquor was then heated under vacuum to remove all of the remaining Ac_2O. The resulting viscous brown-syrup was dissolved into hot toluene, which formed needle-like crystals of the 4-nitrofluorescein diacetate **43** upon cooling. A further two recrystallizations from hot toluene yielded 4-nitrofluorescein diacetate in a yield of 18 %. The melting point (toluene) was found to be 189 - 190 °C, agreeing with the literature melting point (toluene) of 190 °C.[51]

Both deacetylated nitrofluorescein isomers, **44** and **45**, were produced (see Scheme 36 **ii**) by heating their corresponding diacetates independently in a mixture of 10 % aqueous sodium hydroxide and methanol until a dark red homogenous solution was obtained. Each warm solution was then diluted with water, acidified with glacial acetic acid and heated again until boiling. Upon cooling in an icebox for 3 hours, the resulting precipitates were collected using a Büchner funnel, washed with water and dried under vacuum at 80 °C. Both **44** and **45** were determined to be pure on account of their melting points in close agreement with the values from the literature.[51] See experimental section for details.

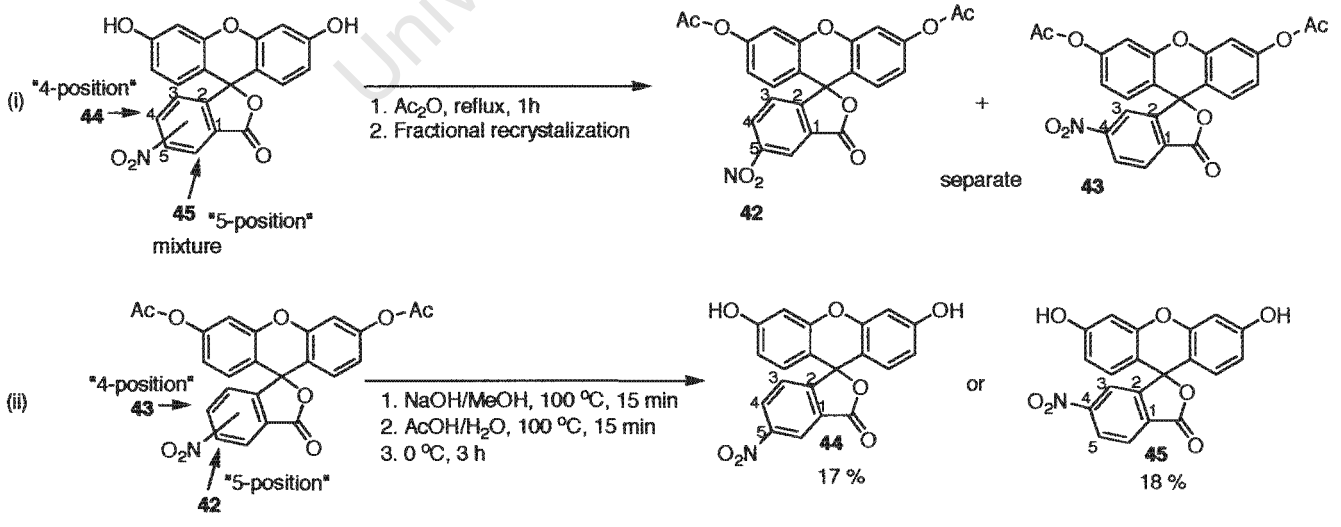

Scheme 36: (i) Fractional recrystallization used to separate 4- and 5-nitro fluorescein isomers **44** and **45** through acetylating to diacetates **42** and **43**; (ii) deacetylation of **42** and **43** to **44** and **45** respectively.

5-Nitrofluorescein was chosen over 4-nitrofluorescein as the preferred intermediate as the former was afforded first from the fractional recrystallization. Thus, the next step (see Scheme 37) involved the reduction of 5-nitrofluorescein **44** to 5-aminofluorescein **37** using a well-documented procedure for reducing aromatic-nitro compounds to their corresponding amines. The reduction involved refluxing **44**, Na_2S and NaSH in water for 24 hours, which resulted in an 80 % yield of amine **37**. Its structure as shown in Scheme 37 was confirmed from the ^1H NMR spectrum, which agreed completely with literature data for this compound.[51]

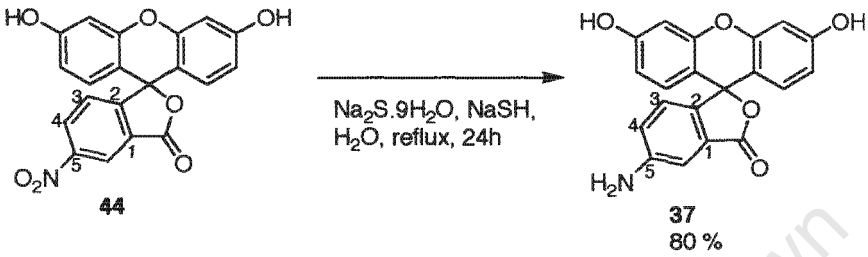

Scheme 37: Reduction of 5-nitrofluorescein **44** to 5-aminofluorescein **37**

Conversion of **37** to its chloroacetamide **38** was successfully achieved using both DCC and acid chloride methodologies (see Scheme 38), with the former producing the highest yields. The structures were confirmed using ^1H NMR spectroscopy.[53a]

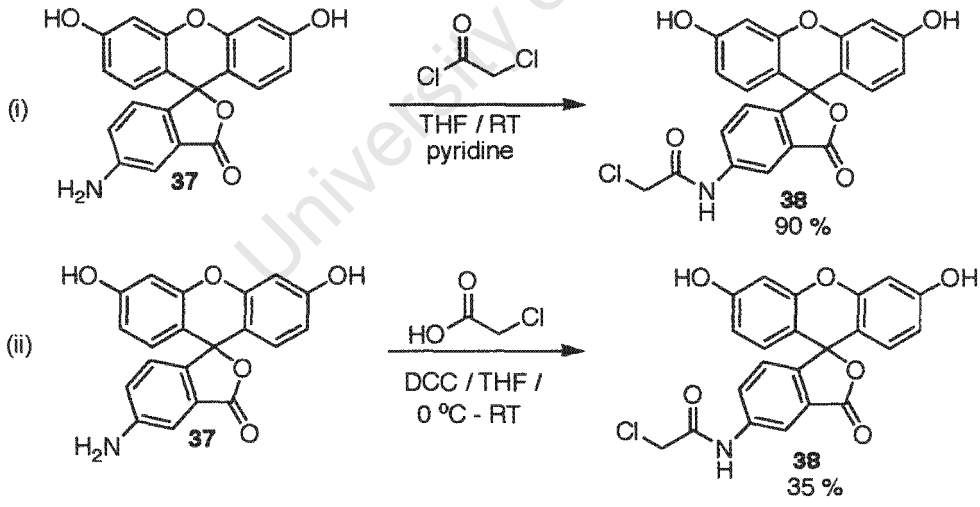

Scheme 38: Synthesis of halo-fluoresceinamide **38** via: (i) acid chloride methodology; (ii) DCC coupling with chloroacetic acid.

The final step towards the required sulfenylating agent involved reacting **38** with potassium thiotosylate. This proved to be problematic and similar to the case with mesylate **26**. Despite mild heating, the reaction did not proceed (see Scheme 39 i). It was thought that the C-Cl bond was too strong, so it was decided to exchange the chloride to an iodide. *In situ* exchange with TBAI was attempted initially, but

was ultimately unsuccessful (see Scheme 39 **ii**). This prompted complete iodide exchange, which involved refluxing **38** and NaI (10 equivalents) in acetone overnight. The iodide[53a] (see Scheme 38 **iii**) was recovered in a modest yield (70 %) as evidenced by the upfield shift of the methylene singlet in the ^{1}H NMR spectrum, but upon reacting with the thiotosylate **13**, did not produce the desired product either.

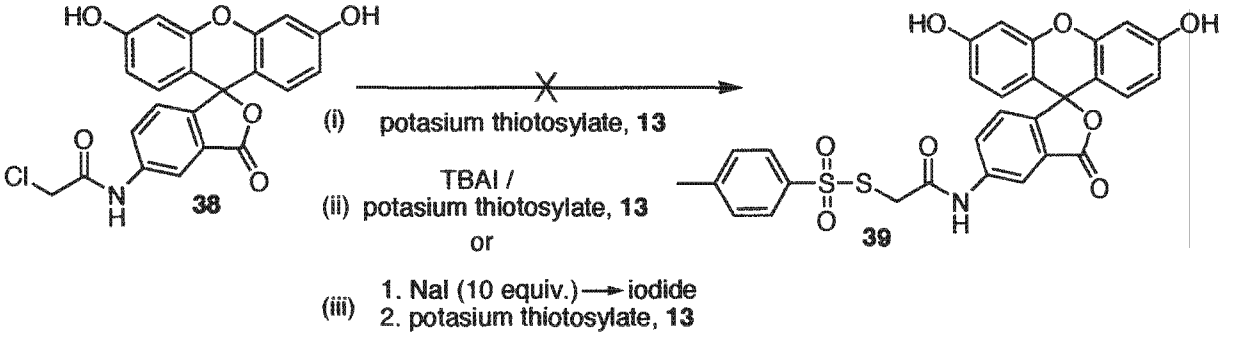

Scheme 39: (i) Coupling fluorescein chloroacetamide **38** directly with thiotosylate **13**; (ii) coupling **38** with **13** using TBAI to generate iodoacetamide *in situ*; (iii) generation of fluorescein iodoacetamide, followed by coupling with **13**

It is well known that fluorescein exists both in a "closed" lactone form and an "open" carboxylic acid form as illustrated in Scheme 40.[53a] A concern throughout the synthesis was the ever-present polar spot observed on TLC. This was thought to correspond to the fluorescein in its open and polar carboxylic acid form. It was thought that if **39** was generated, it likely existed in its carboxylic acid form and could not be extracted into organic solvent on account of its highly polar nature. Steps were thus taken to accommodate this possibility.

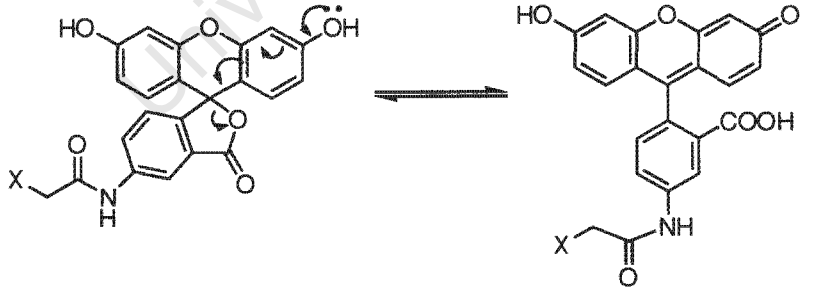

Scheme 40: Equilibrium possible within the aminofluorescein structure

5.2 Fluorescein Methyl Ester, 47

It was decided to develop a new synthetic route based on lactone esterification of the 4-nitrofluorescein derivative **45**. The 4-nitrofluorescein **45** was recovered as a by-product of the 5-nitrofluorescein synthesis and was available in gram quantities. It should be noted that upon opening of the lactone, the numbering around the ring was adjusted to give the product **47** as "5-nitrofluorescein methyl ester".

To this end (see Scheme 41), 4-nitrofluorescein **45** was refluxed in dry methanol with a catalytic amount of sulfuric acid for 48 hours. The resulting yellow solution was diluted with Et_2O and left in the freezer for a further 48 hours for crystallization. The resulting brown precipitate was filtered with a Büchner funnel yielding a solid in 89 % yield, thought to be the bisulfate phenolic ester **46**. Hydrolysis of the monosulfate ester was achieved by suspending **46** in a 1: 1 mixture of water and methanol, adding aqueous Na_2PO_4 (10 %) to adjust the pH to 5, and after stirring for 20 minutes, collecting the dark red precipitate on a Büchner funnel and drying the solid on the bench overnight. The final yield of the free phenol **47** was 75 %.

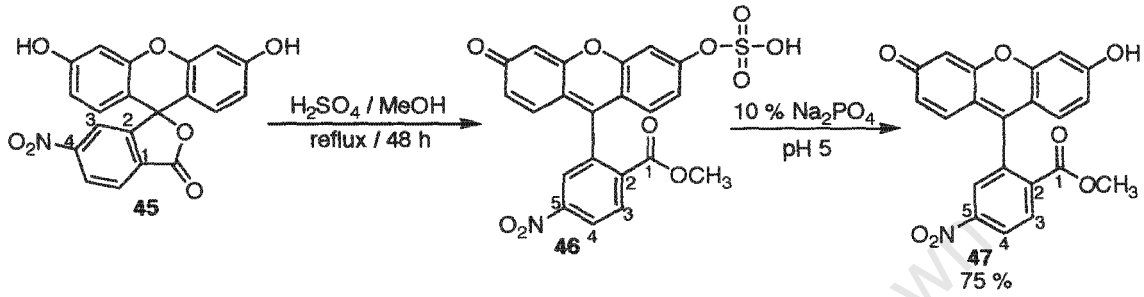

Scheme 41: Synthesis of 5-nitrofluorescein methyl ester **47**

The ^1H NMR spectrum for **47** (see Figure 31 i) revealed all of the expected resonances. The resonances for H-1' and H-8', H-2' and H-7' as well as H-4' and H-5' resonated in pairs with identical chemical shifts (see Figure 31). This is most likely due to rapid tautomerization as depicted in Scheme 42, resulting in the averaging of resonances. In the aromatic region, H-4 could be observed as a double doublet due to ortho- and meta-coupling to H-3 and H-4 respectively, while H-3 and H-6 appeared as doublets. The proposed symmetry in the xanthene ring system is illustrated in Figure 31 ii, which shows the equivalent protons signals for H-1'/8' and H-2'/4'/5'/7' each correlating to one distinct carbon resonance. Thus, only fifteen distinguishable resonances were observed in the ^{13}C NMR spectrum of **47**, of which HSQC showed seven to be quaternary. A single methoxy signal in the aliphatic region supported the presence of the methylester **47**. High resolution mass spectrum (EI) offered further evidence for the formation of the product as it provided a molecular ion peak of 392.0760 corresponding to $[M + H]^+$, for which $C_{21}H_{14}NO_7$ requires 392.0770.

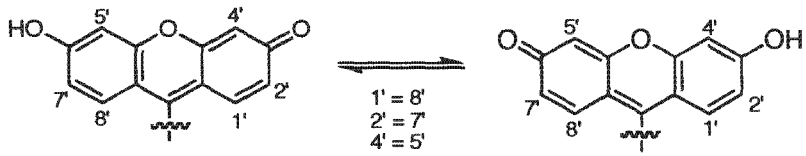

Scheme 42: Possible tautomerization within fluorescein methyl ester **47**

(i)

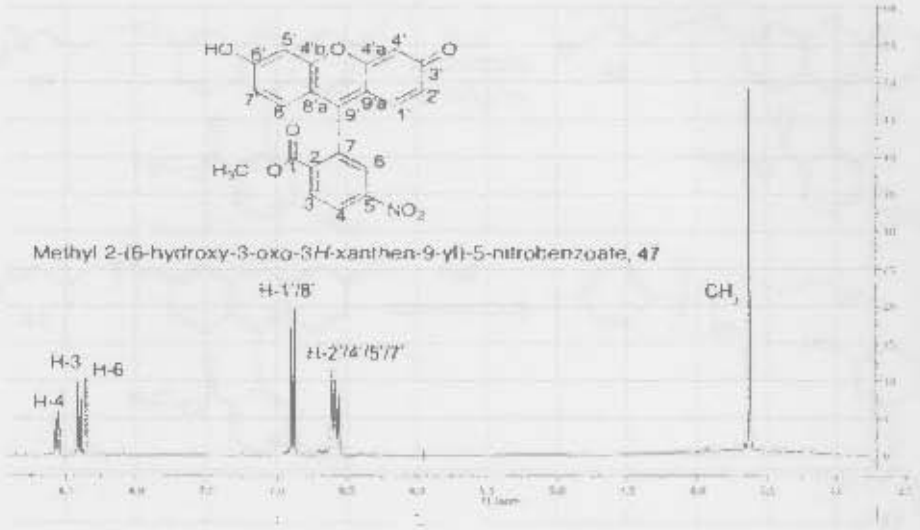

(ii)

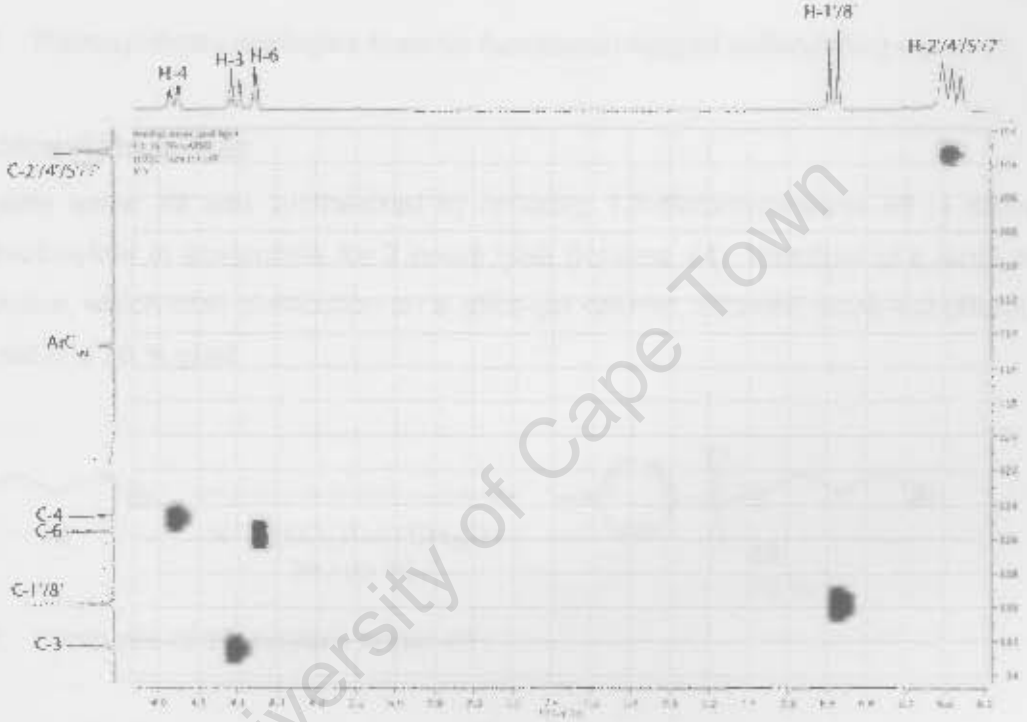

Figure 31: (i) ^{1}H NMR spectrum of **47** in DMSO-d_6; (ii) HSQC expansion of **47** in DMSO-d_6

5.3 Fluorescein-tagged Sulfenylating Agent, 51

In the next step, two synthetic approaches were considered for the synthesis of fluorescein-tagged sulfenylating agent **51**. The first approach (see Scheme 43 **i**) envisaged thiotosylation of the fluorescein-tagged alkyl halide **50**. Mindful of the difficulties encountered whilst synthesizing the dansyl-tagged sulfenylating agent **27**, it was feared upon heating that multiple S-tosyl additions may occur as described earlier (Scheme 24 **iii**). The second strategy considered (see Scheme 43 **ii**) envisaged incorporating the thiotosylate group into the alkyl halide **49**, which would need to be coupled to the fluorescein via an S_N2 reaction. Such a coupling would necessitate a chemoselective alkylation at the relatively harder bromide end of **49**. Ultimately, it was decided to pursue strategy ii.

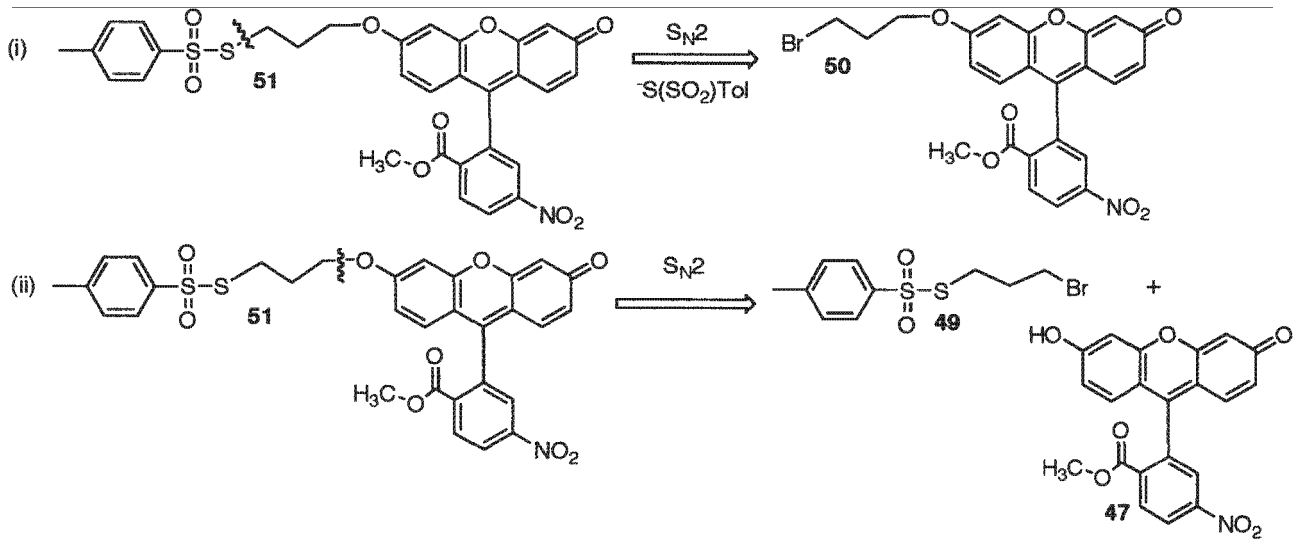

Scheme 43: Retrosynthetic strategies towards fluorescein-tagged sulfenylating agent **48**

5.3.1 Thiotosylate tether

The thiotosylate tether **49** was synthesized by refluxing 1,3-dibromopropane **48** (4 equivalents) and potassium thiotosylate in acetonitrile for 2 hours (see Scheme 44). Reaction of a large excess of **48** yielded a residue, which after purification on a silica-gel column, afforded mono-substituted product **49** as a semi-solid in a 76 % yield.

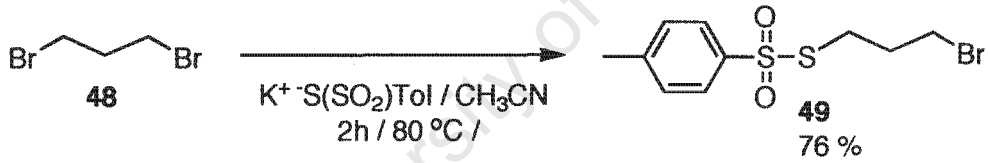

Scheme 44: Synthesis of thiotosylate tether **49**

The structure of **49** was confirmed with ^1H and ^{13}C NMR spectroscopy (see Figure 31), both of which revealed all of the expected resonances. Several attempts made to obtain a high resolution mass spectrum failed to give intelligible data. The ^{13}C NMR spectrum (see Figure 32 **ii**) revealed the expected four aromatic and four aliphatic signals.

(i)

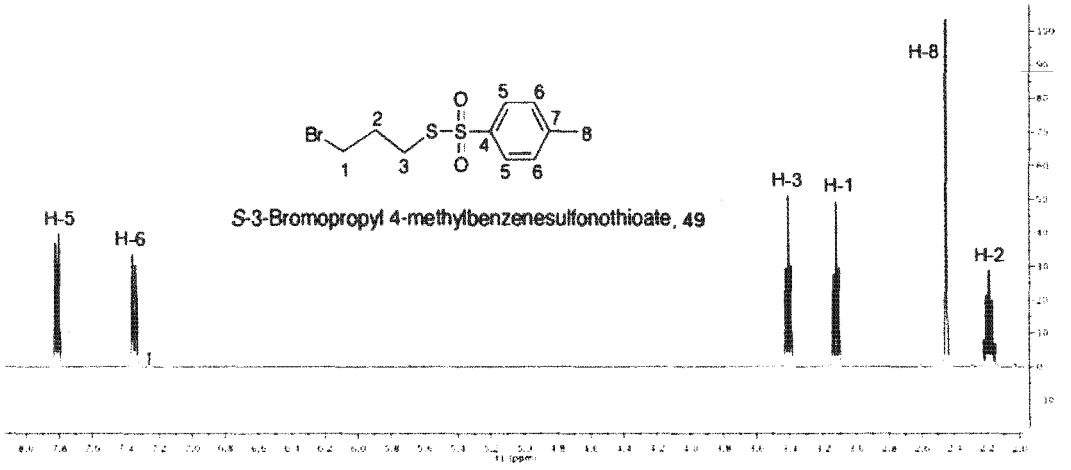

(ii)

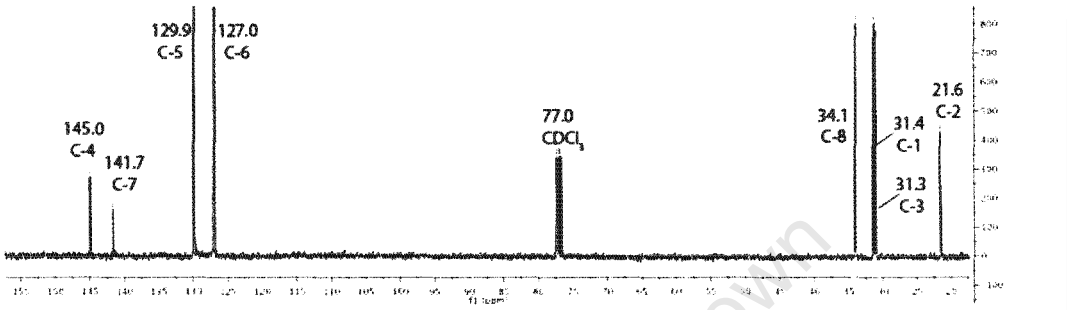

Figure 32: (i) ^{1}H NMR spectrum of **49** in chloroform-d_3; (ii) ^{13}C NMR spectrum of **49** in chloroform-d_3

5.3.2 Fluorescein-tagged sulfenylating agent, 51

The next step involved the coupling of the nitrofluorescein methyl ester **47** with the thiotosylate tether **49** (see Scheme 45). The phenoxide of **47** was generated using K_2CO_3 as a base in refluxing acetonitrile. Potassium phenoxides have a level of hardness based on oxygen and it was hoped that this would be sufficient to distinguish between the carbon and sulfur electrophilic centres. In the event, the desired fluorescein-tagged sulfenylating agent **51** was generated as the major product in a 58 % yield, marking a triumph of hard and soft acid-base theory.

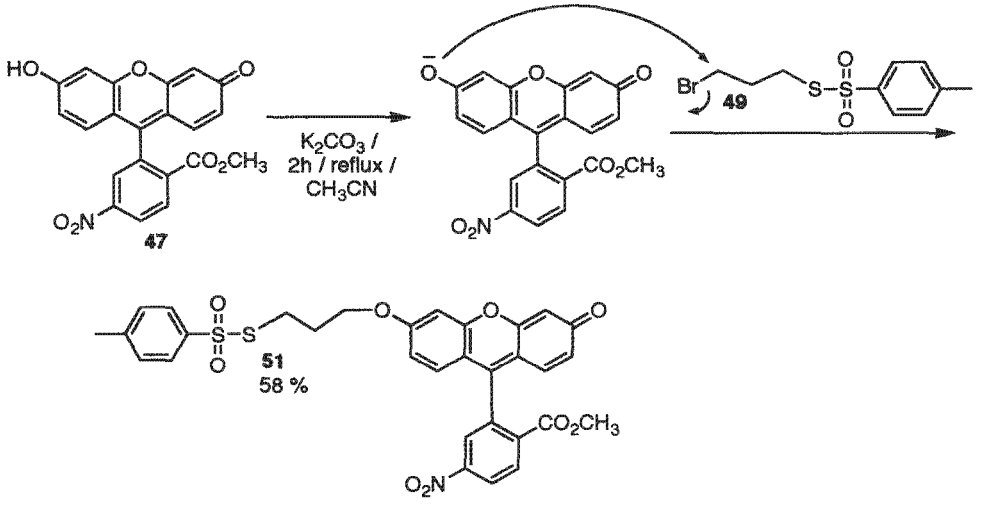

Scheme 45: Synthesis of fluorescein-tagged sulfenylating agent **51**

All of the expected resonances of the fluorescein-tagged sulfenylating agent product **51** were observed in both the ^{1}H and ^{13}C spectra. The ^{1}H NMR spectrum is shown in Figure 33 and clearly shows signals from both coupling partners that offers evidence for successful coupling. The equivalence between H-1'/8', as well as between H-2'/7' and H-4'/5' observed in **47** was lost as a result of functionalizing the phenol group, thus supporting the tautomerization suggested previously (see Scheme 42). An "AB" system of doublets (J = 8.2 Hz) was observed in the aromatic region corresponding to H-5" and H-6" of the tosyl group, indicating that the phenoxide attacked the bromide end of the precursor **49**, since an attack on the sulfur would have displaced the SO_2Tol group. The downfield shift of C-1" due to the oxygen also supports the formation of **51**. The ^{13}C NMR spectrum displayed twenty-four resonances in the aromatic region and five in the aliphatic. High resolution mass spectrometry provided further evidence for the formation of the product, providing a molecular ion of 620.1057 corresponding to $[M + H]^+$, since $C_{31}H_{26}NO_9S_2$ requires 620.1049.

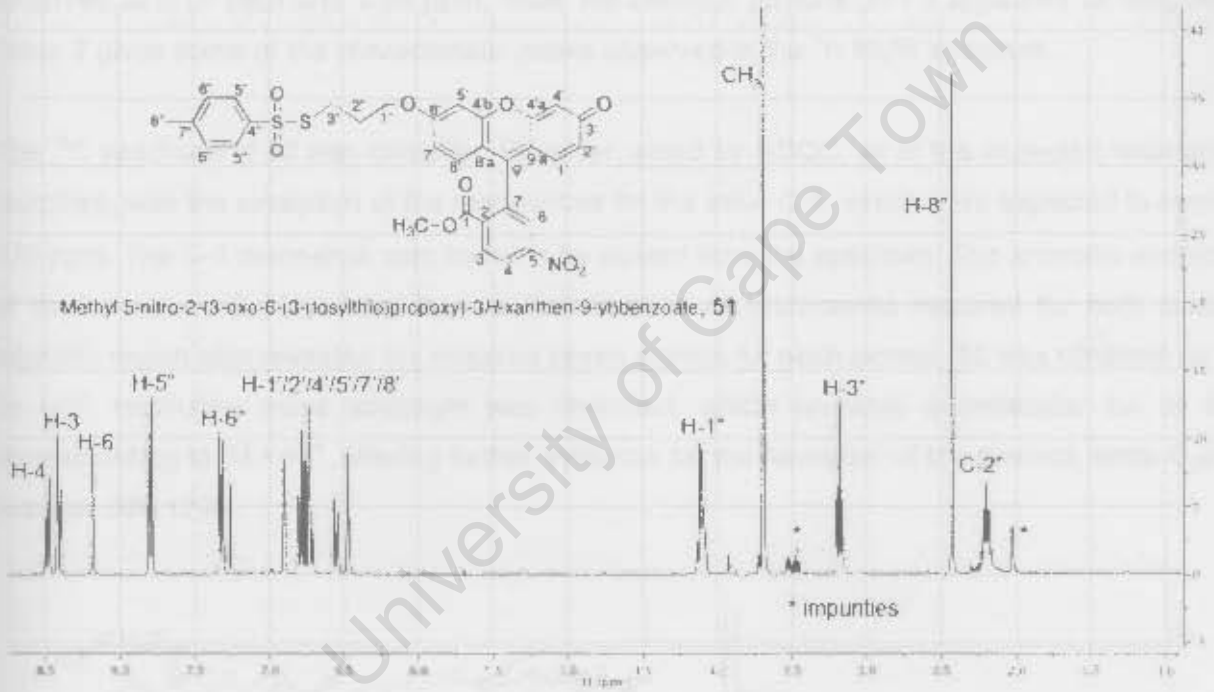

Figure 33: ^{1}H NMR spectrum for **51** in chloroform-d_3

5.4 Fluorescein-tagged Disulfide, 52

The synthesis of the fluorescein-tagged disulfide **52** (see Scheme 46) was performed by coupling PMB-vinylthioacetate **12** (1.2 equivalents) with the fluorescein-tagged sulfenylating agent **51** in a fashion similar to the coupling described in Chapter 3.5. In this instance it was decided to use the sulfenylating agent as the limiting reagent for the reaction so as to maximize its utility. The disulfide product **52** was obtained in a 86 % yield based on **51** and as a 1: 1 mixture of *Z/E*-isomers as determined by ^{1}H NMR spectroscopy, which was different from the **4**: 3 ratio observed in the vinyl thioacetate precursor **12**. A proposed mechanism for the tautomerism may be seen in Chapter 4, Scheme 31. The isomers were inseparable by chromatography, but were fully characterizable in their native mixture.

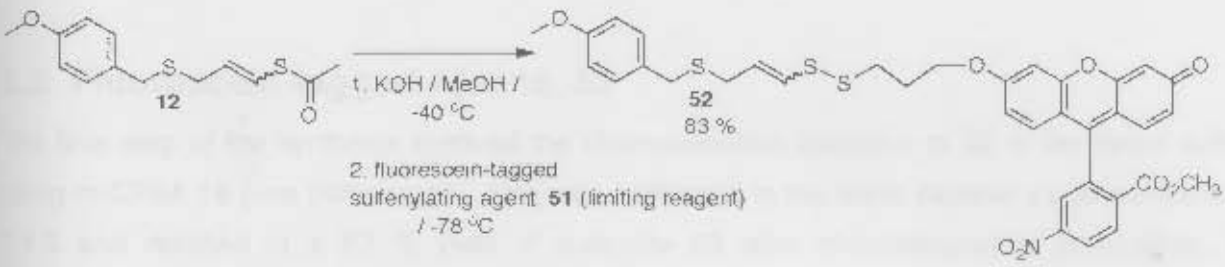

Scheme 46: Synthesis of fluorescein-tagged disulfide **52**

The ^{1}H NMR spectrum (See Figure 34) of disulfide **52** revealed contributions from both coupling partners as well as the loss of the acetyl singlets observed in **12** at 2.35 ppm and 2.38 ppm. As expected, the vinyl protons H-4" and H-5" were observed as a set of doublets and double triplets for both isomers respectively. For both isomers, singlets corresponding to the two methoxy groups were observed at 3.77 ppm and 3.68 ppm, while the benzylic protons (H-7") appeared as singlets at 3.66. Table 7 gives some of the characteristic peaks observed in the ^{1}H NMR spectrum.

The ^{13}C spectrum of **52** was complex. However, aided by HSQC, all of the expected resonances were identified, with the exception of the resonances for the ester C-1, which were expected to occur at $\delta = \pm$ 170 ppm. The C-1 resonance was found to be absent from the spectrum. The aromatic and vinyl region of the spectrum displayed twenty-five distinct pairs of resonances required for both isomers. The aliphatic region also revealed the required seven signals for each isomer. **52** was obtained as an oil, so its high resolution mass spectrum was recorded, which revealed a molecular ion at 690.1307, corresponding to $[M + H]^+$, offering further evidence for the formation of the product, since $C_{35}H_{32}NO_8S_3$ requires 690.1290.

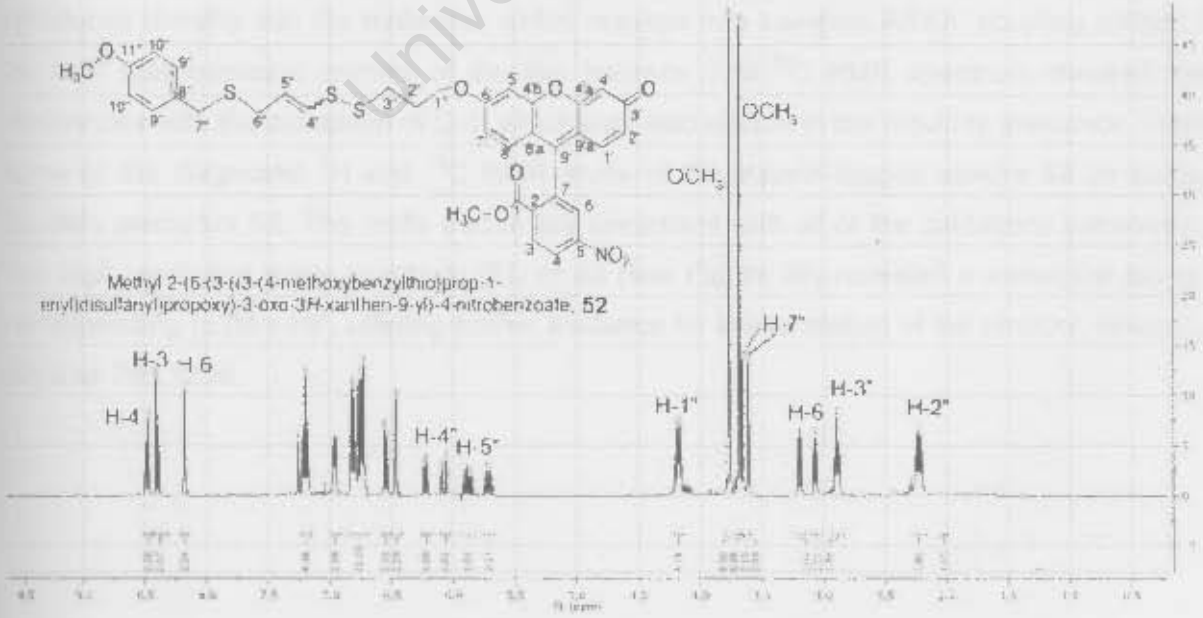

Figure 34: ^{1}H NMR spectrum of **52** as a mixture of *Z/E*-isomers in chloroform-d_3

5.5 Fluorescein-tagged Ajoene, 53

The final step of the synthesis involved the chemoselective oxidation of **52** to the target sulfoxide **53** using *m*-CPBA **16** (see Scheme 47). This was performed in the same manner as described in Chapter 2.4.5 and resulted in a 62 % yield of sulfoxide **53** after chromatographic purification. ^{1}H NMR spectroscopy was used to determine the *Z/E* ratio as 3: 4. The slight increase in the prevalence of the *E*-isomer in the mixture as compared to the disulfide precursor (1: 1) may have been due to the *Z*-isomer being more susceptible to over-oxidation. The increase in *E*-isomer may also be attributed to an artifact of chromatographic enrichment during purification.

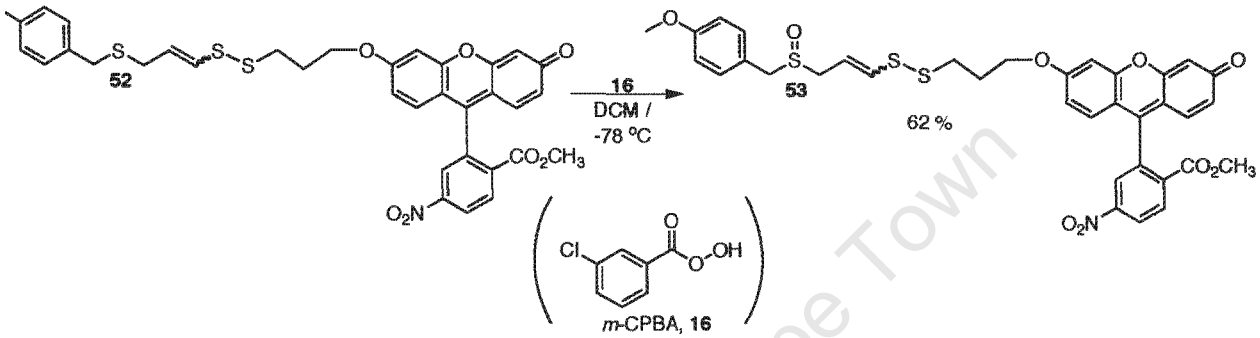

Scheme 47: Oxidation of fluorescein-tagged disulfide **52** to sulfoxide **53**

The ^{1}H NMR spectrum of **53** (see Figure 35) revealed all of the expected resonances based on previous trends for other sulfoxide targets. Table 7 illustrates the key signals used to confirm that the transformation from **52** to **53** had occurred. The methylene peaks α to the newly formed sulfoxide were observed downfield to their analogous peaks in the disulfide precursor **52**. The newly formed sulfoxide introduced chirality into the molecule, which resulted in a complex ABXX' coupling pattern for each of the H-6" diastereotopic protons of the two isomers. The ^{13}C NMR spectrum revealed the expected resonances with the exception of C-1, which was also absent in the disulfide precursor. Table 7 reflects some of the diagnostic ^{1}H and ^{13}C NMR shifts of fluorescein-tagged ajoene **53** as compared to its disulfide precursor **52**. The shifts trends are consistent with all of the oxidations previously described. The high resolution mass spectrum (EI) of **53** (see Figure 36) revealed a molecular ion at 706.1258, corresponding to $[M + H]^{+}$, offering further evidence for the formation of the product, since $C_{35}H_{32}NO_9S_3$ requires 706.1239.

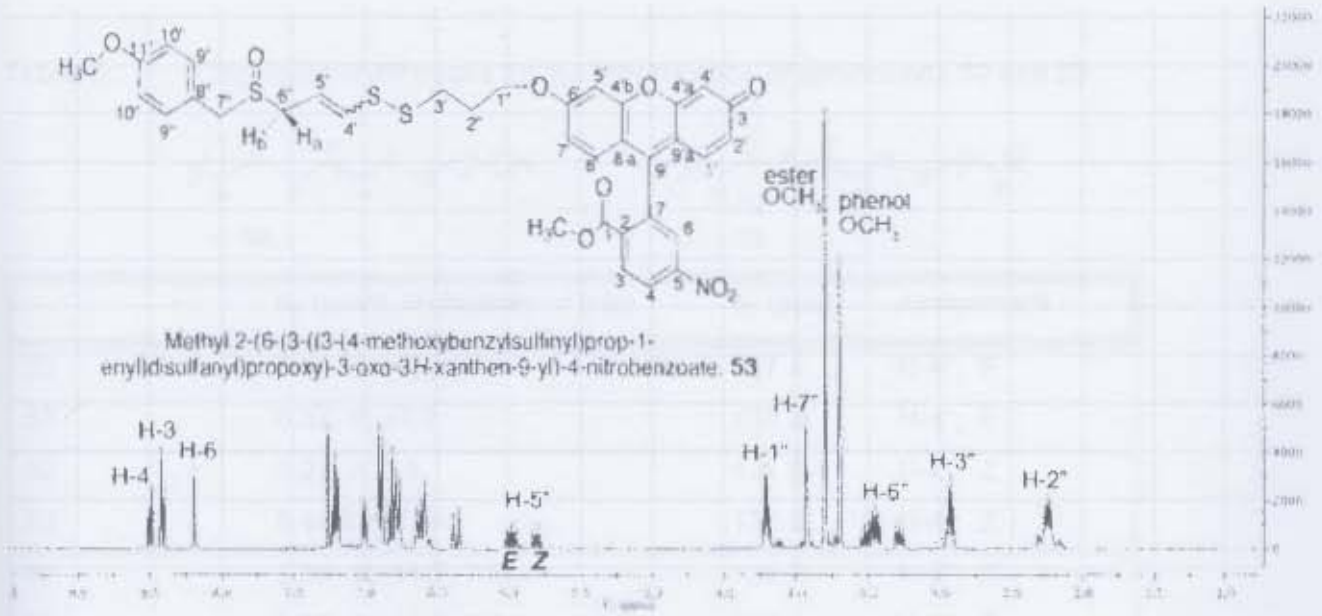

Figure 35: ^{1}H NMR spectrum of **53** as a mixture of *Z*/*E*-isomers in chloroform-d_3

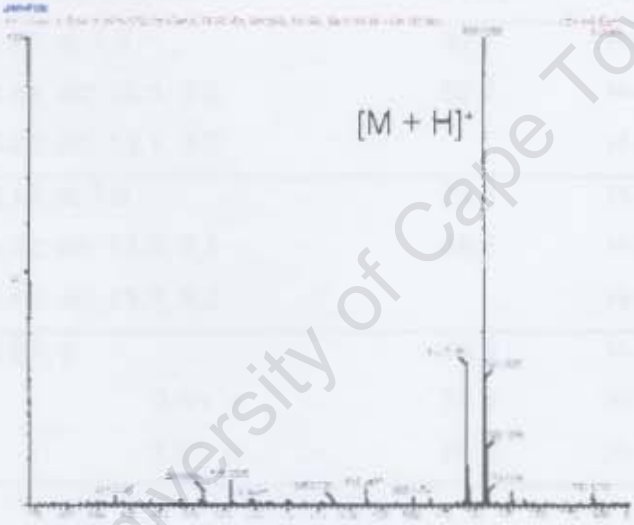

Figure 36: High-resolution mass spectrum of **53**

Table 7: Diagnostic NMR peaks for the identification of compounds **52** and **53**

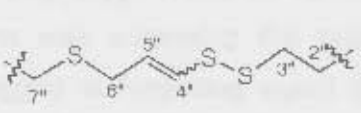

52

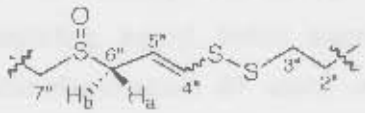

53

	δ_H (ppm), Multiplicity; J (Hz)	δ_C (ppm)	Assignment
52	6.08; d; 14.6	127.4	H-4"; *E*
53	6.37; d; 14.7	133.8	H-4"; *E*
52	6.23; d; 9.3	131.5	H-4"; *Z*
53	6.64-6.55; m	137.8	H-4"; *Z*
52	5.88; dt; 14.6, 7.3	129.7	H-5"; *E*
53	5.98; dt; 14.7, 7.2	117.9	H-5"; *E*
52	5.72; dt; 9.3, 7.6	128.8	H-5"; *Z*
53	5.81; dt; 9.0, 8.2	119.2	H-5"; *Z*
52	3.07; d; 7.3	32.7	H-6"; *E*
53	3.44; dd; 13.1, 8.2	52.7	$H\text{-}6''_a$; *E*
	3.28; dd; 13.1, 8.2		$H\text{-}6''_b$; *E*
52	3.19; d; 7.6	29.3	H-6"; *Z*
53	3.52; dd; 13.5, 8.2	49.5	$H\text{-}6''_a$; *Z*
	3.48; dd; 13.5, 8.2		$H\text{-}6''_b$; *Z*
52	3.66; s	35.5	H-7"; *E*
52	3.61; s	34.9	H-7"; Z
53	3.93; m	56.6	H-7"; *E* + Z

5.6 Conclusions

As with the dansyl-tagged ajoenes **30** and **32**, the most crucial part of the synthesis of the fluorescein-tagged ajoene was accessing the tagged sulfenylating agent. Initial attempts at synthesizing a fluorescein-tagged sulfenylating agent through aminofluorescein **37** were unsuccessful. The labile nature of fluorescein's lactone made recovery of products difficult. The synthesis of novel 5-nitrofluorescein methyl ester **47** was the breakthrough needed for accessing the sulfenylating agent. The decision to first couple potassium thiotosylate with 1,3-dibromopropane **48** (see Scheme 49) eliminated concerns regarding multiple thiotosylate addition (see Scheme 24 **iii**) experienced in the synthesis of **27**. The coupling of thiotosylate tag **49** with methyl ester **47** resulted in the successful generation of sulfenylating agent **51**, which was used to access fluorescein-tagged ajoene **53**.

The fluorescent spectra of all of the fluorescently-tagged ajoenes **30**, **32** and **53** were measured and are reported in the next section. The biological activities of all the tagged-analogues were measured and are reported on in Chapter 6.

5.7 Fluorescence – Absorption and Emission

The absorption and emission spectra (see Figure 37 and Table 8) for the fluorescent ajoene analogues were measured using 0.1 mM solutions in ethanol. The λ_{ex} and λ_{em} values for all compounds are summarized in Table 8.

The fluorescein-tagged analogue **53** had a maximum excitation peak at 460 nm (blue) and a maximum emission at 546 nm (green). Fluorescent data is not available for the nitrofluorescein methylester **47** as it is was insoluble in ethanol or DMSO. However, fluorescein is reported to experience its maximum absorption at 495 nm (blue-green) and its maximum emission at 520 nm (green). The λ_{em} observed in fluorescein was found to be a shorter wavelength than that of fluorescein-tagged ajoene **53**. This can be explained (in part) by the effect of the electron withdrawing nitro-group, which is thought to lower the energy of the excited state, thus effecting the emission of a photon of longer wave length (bathochromic shift).

The dansyl-tagged analogues **30** and **32** had their maximum absorbances at 331 nm (UV) and 321 nm (UV) respectively. Their maximum emissions were observed at 515 nm (green) and 518 nm (green) respectively. Dansyl chloride is reported to have its maximum absorbance and emission at 337 nm (UV) and 481 nm (green) respectively.

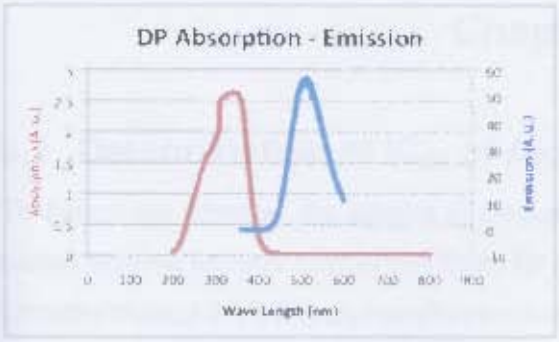

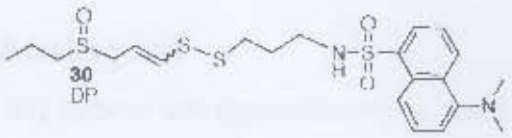

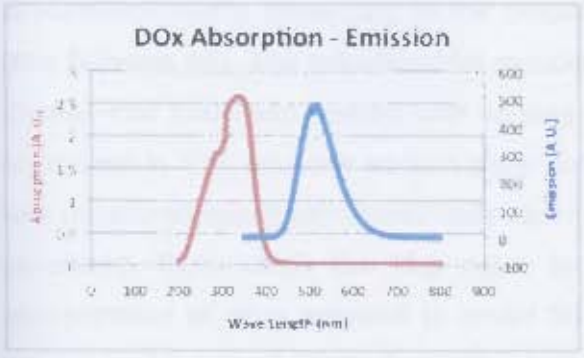

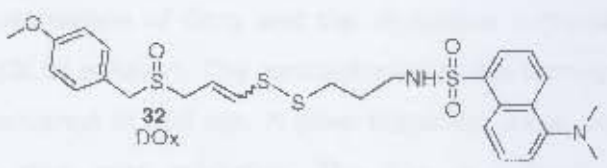

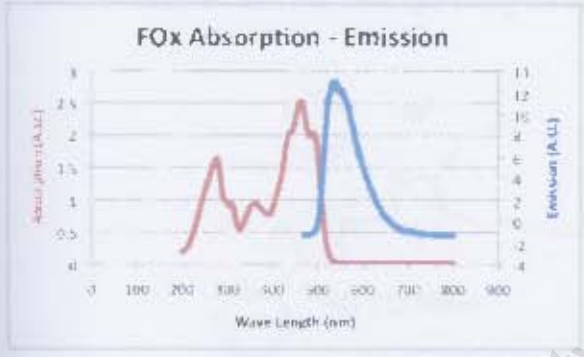

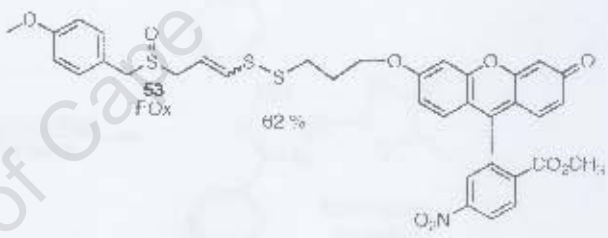

Figure 37: Absorption-Emission spectra for the fluorescent ajoenes

Table 8: Summary of λ_{ex} and λ_{em} for all fluorescent ajoenes

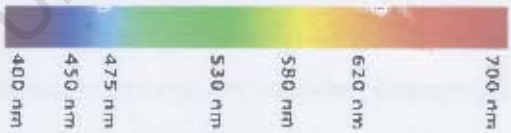

	λ_{ex} (nm)	λ_{em} (nm)
FOx, 53	460	546
DP, 30	331	515
DOx, 32	321	518
Fluorescein[54]	495	520
Dansyl chloride[55]	337	481

Chapter 6: Biology

6.1 Determination of IC_{50} of Ajoene Analogues

To determine whether the ajoene analogues had any tumour cell cytotoxic activity, each analogue was tested against several cancer cell lines for its ability to inhibit cell proliferation. The assay utilized 3-(4,5-Dimethylthiazol-2-yl)-2,5-diphenyltetrazolium bromide (MTT) to assess cell viability by spectrophotometric measuring of the reduction of tetrazolium MTT (yellow) to the formazan (purple) (see Scheme 48). The mitochondrial reductase enzyme facilitates this reduction. MTT dye was added to cells that had been treated with varying concentrations of drug and the crystalline formazan was solubilized in 10% aqueous sodium lauryl sulfate (SLS) solution. The concentration of the formazan dye was measured spectrophotometrically as an absorbance at 595 nm. A dose response curve was then generated, from which the IC_{50} value for the drug was extracted. The IC_{50} is defined as the concentration of drug required to inhibit 50 % of the cell growth. It should be noted that this is an indirect measurement not distinguishing between apoptotic or necrotic cell death.[56]

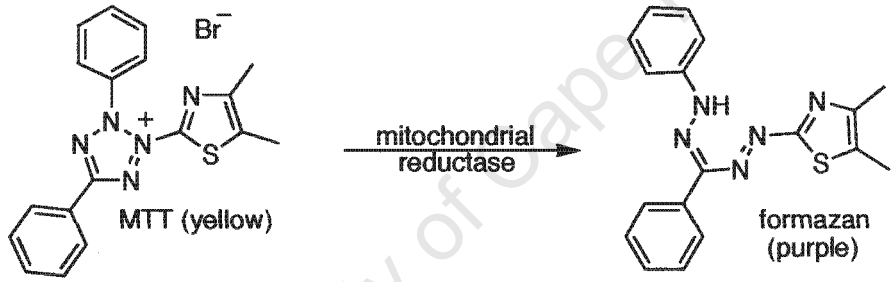

Scheme 48: The reduction of MTT by mitochondrial reductase

The synthetic analogues were assayed for their ability to inhibit cell proliferation in two cancer cell-lines, namely: MDA-MB-231 breast tumour epithelial cell-line and the WHCO1 oesophogeal epithelial cancer cell-line. The ajoene analogues were synthesized as non-separable mixtures of *E/Z*-isomers and were tested as such. The IC_{50} values for ajoene are reported separately for each isomer.

The IC_{50} values for all of the ajoene analogues prepared are shown in Table 9. All of the synthesized analogues (see Figure 38) had activity comparable to that of ajoene. The results of the assay were found to depend on cell density as treating cells that had achieved (or were near to achieving) confluence appeared to produce a less pronounced effect. This supports the notion that the drug is selective for mitotic cells.[57] Therefore, all of the IC_{50} values were determined only on growing cells and comparable to ajoene.

The IC_{50} values obtained for the modified ajoenes are in agreement with data from *Hunter et al.*[43] in that the anti-cancer activity of ajoene appears to reside within the vinyl disulfide/sulfoxide core. Here it was

previously shown that analogues bear a certain amount of tolerance towards replacing the allyl (R^1,R^2) groups with other substituents (see Table 9). In agreement with this finding, substitution of R^2 with a bulky fluorescein-tag (FOx, **53**) did not reduce the drug's efficacy as FOx's activity was in fact found to be equivalent to that of ajoene for MDA-MB-231 cells and superior in the case of WHCO1 (*Z*-ajoene = 25 μM, FOx = 7.4 μM). These findings lent credibility to using these synthetically derived fluorescent ajoenes to track the localization and movement of this class of compounds in living MDA-MB-231 cancer cells.

BPMB **17** is the most active ajoene analogue that has been generated to date. Again it retains the central vinyl disulfide/sulfoxide core but the two termini comprise lipophilic and electron donating *para*-methoxyphenyl groups. This compound was found to be roughly 15 times more active at inhibiting tumour cell growth than ajoene on MDA-MB-231 cells (*Z*-ajoene = 13.70 μM, **17** = 0.83 μM). In agreement with the *para*-methoxyphenyl substitution being more active than propyl substitution on WHCO1 cells[44], DOx **32** containing *para*-methoxyphenyl substitution was slightly more active than the propyl-substituted DP **30** (see Table 9 and Table 10 for representative IC_{50} curves)

Table 9: IC_{50} Data for Ajoene Analogues (in μM)

	MDA-MB-231	WHCO1
E –ajoene	15.59 ± 2.40[58]	34.78 ± 1.03[58]
Z–ajoene	13.70 ± 2.02[58]	25.21 ± 2.84[58]
E/Z-FOx, **53**	14.65 ± 1.14; $^{n=3}$	7.76 ± 4.60; $^{n=3}$
E/Z-DOx, **32**	14.07 ± 2.18; $^{n=5}$	9.20 ± 6.34; $^{n=3}$
E/Z-DP, **30**	20.87 ± 6.20; $^{n=4}$	14.59 ± 4.24; $^{n=4}$
E/Z-BPMB, **17**	0.83 ± 0.20[58]	1.97 ± 0.42[58]

FOx, fluorescein-tagged ajoene; DOx, dansyl-*p*-methoxybenzyl ajoene; DP, dansyl-propyl ajoene; BPMB, bis-*p*-methoxybenzyl ajoene; n = number of repeated experiments;

Table 10: Representative dose-response Curves for the Fluorescent Ajoene Analogues

	MDA-MB-231	WHCO1
E/Z-FOx 53	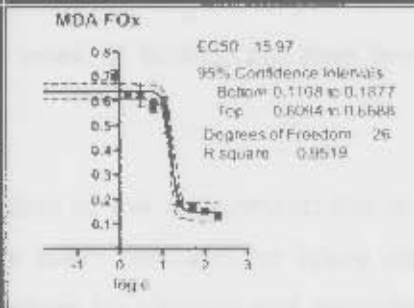	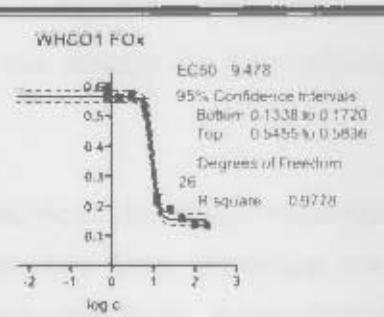
E/Z-DOx 32	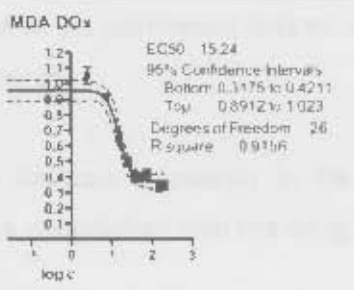	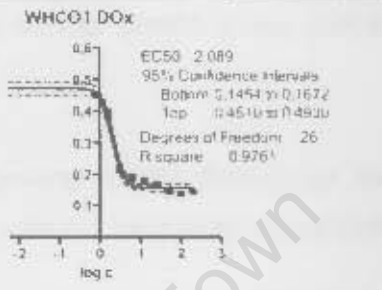
E/Z-DP 30	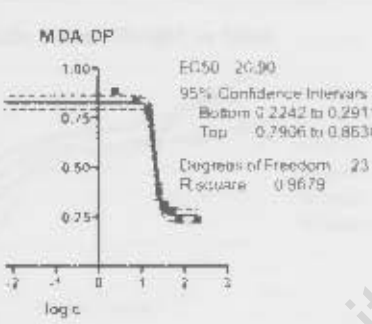	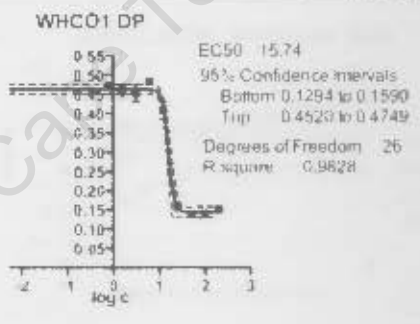

6.2 Animal Studies

6.2.1 Study 1

The first animal study utilized an immune-suppressed "nude-mouse" and a "Balb/C" laboratory mouse. The study was aimed at testing the efficacy of BPMB 17 in inhibiting tumour growth of MDA-MB-231 cancer cells and establishing tolerable doses for treatment. The 24 nude mice each received a subcutaneous injection, delivering 1.47 x 10^6 MDA-MB-231 cells (in 100 µL of PBS) into their hind right quarter, whilst the 24 Balb/C mice received the same volume of PBS alone. Both nude- and Balb/C mice were randomized into 4 cages A-D and each mouse was labeled 1-6 using a standard ear clipping technique.

The drug was aqueous insoluble and could therefore not be administered orally through dosing the water. Thus, the drug formulation was therefore made using (the fat emulsion) Intralipid. The doses administered to groups A, B, C and D were 1, 5, 45 and 0 µg/g (assuming an average mass of mouse to be 20 g). Treatments were administered every second day and the overall health and weight of the

mice were observed and recorded. Throughout the experiment, it became apparent that the nude mice were not developing tumours, despite the large number of MDA-MB-231 cells injected subcutaneously. Both mouse strains appeared healthy and gained weight throughout the experiment. The average weight of the mice receiving the largest dose (group-C, see Figure 39) of drug appeared to drop slightly over the first week of testing, but then proceeded to rise steadily for the remaining duration of the experiment.

Upon completion of the experiment, the mice were sacrificed (halothane inhalation), blood samples taken and the livers removed for future toxicological studies. Upon dissection, the nude mice were carefully examined for tumours and metastases, but none were found. It was determined that a model study would need to be performed first to optimize the tumour growth in the animals before the drug could be administered.

Since all of the animals appeared to be healthy, gaining weight throughout the duration of the experiment, it was established that the drug, BPMB 17, was not toxic in doses up to 45 μg/g.

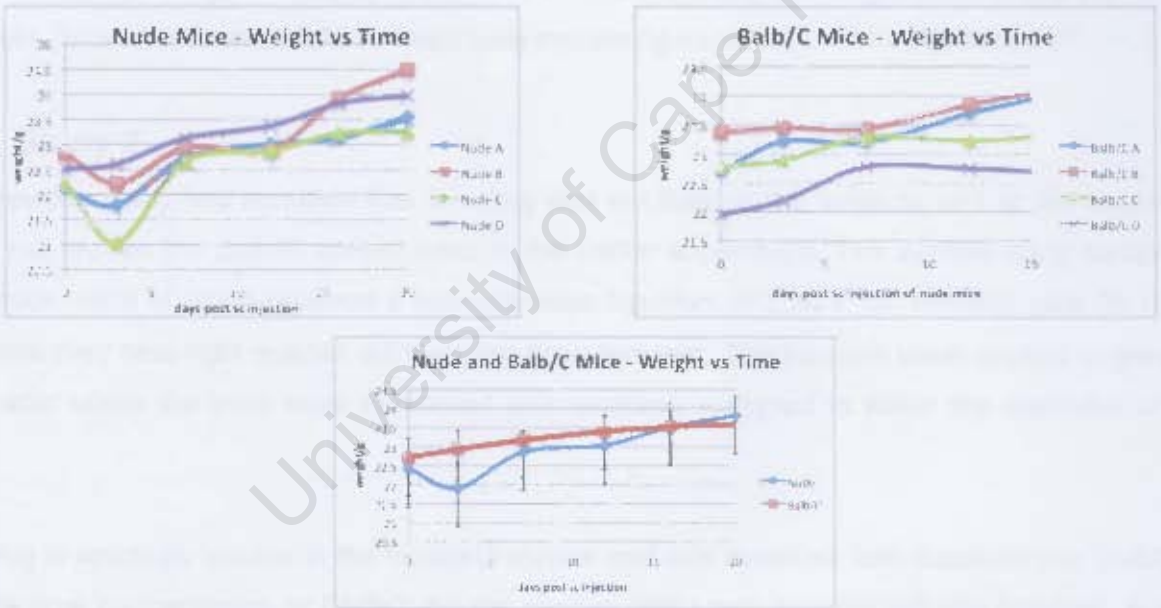

Figure 38: The weight of the mice, measured over the duration of the experiment, shows a steady increase, suggesting that the test subjects were healthy even at the highest administered dose of drug.

A model study was performed by Dr Catherine Kaschula to establish the optimal conditions for tumour growth in the nude mice. It was found that the MDA-MB-231 cells did not proliferate and form tumours in the mice, even when 5×10^6 cells were injected subcutaneously. The MDA-MB-231 cell-line was then replaced with the oesophogeal cancer cell line WHCO1, which were found to grow very readily. It was found that delivering 1×10^6 cells was sufficient for tumour growth and 5×10^6 cells resulted in large, aggressive growths. Biopsies from the WHCO1 tumours were taken for histological analysis (see

Figure 39). The tumours showed differentiation and post response desmoplasia, indicating that this was a good model for human cancer. Purple chromatin staining determined a mitotic count of one in ten fields (40X magnification).[44]

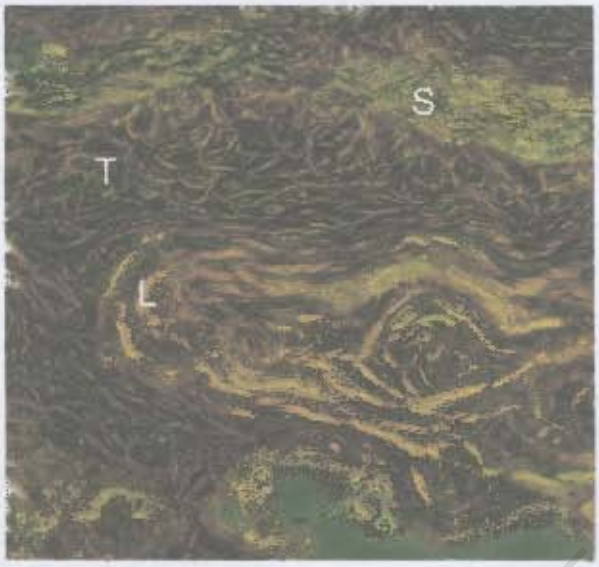

Figure 39: Histological sample taken from WHCO1 tumour, showing Tumour cells (T), host cells (S) and laminated differentiated cells containing keratin (L). 40X magnification[44]

6.2.2 Study 2

The previous study had revealed that the drug was not toxic to the subjects and so the second study would not require the Balb/C control used in the earlier experiment. The second study comprised 18 nude mice, each of which received a subcutaneous injection, of 2.50 x 10^6 WHCO1 cells (in 100 μL of PBS) into their hind right quarter. All the mice grew tumours. The tumours were allowed to grow for 11 days, after which the mice were numbered and randomly assigned to either the treatment or control group.

The drug is sparingly soluble in the Intralipid vehicle and was therefore first dissolved into DMSO (such that the final concentration of DMSO did not exceed 20%) and then diluted into Intralipid. Sonicating the solution for 5 minutes at 37 °C improved the homogeneity of the solution.

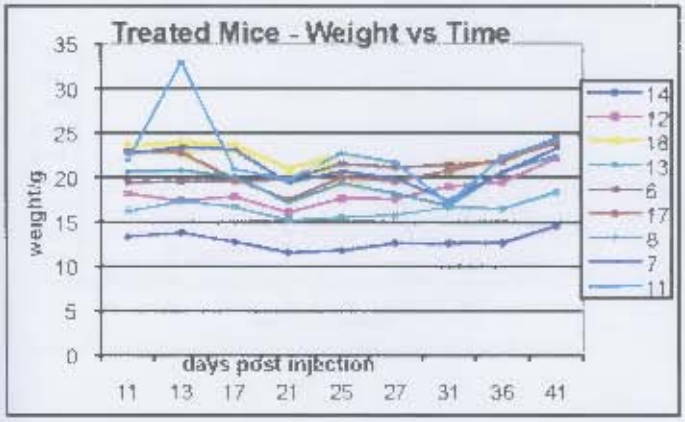

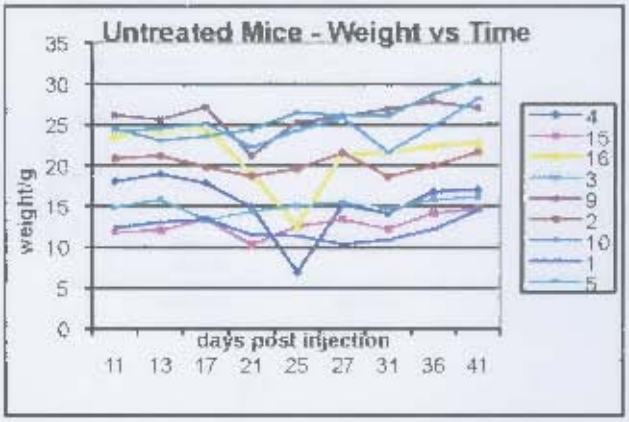

Figure 40: A steady increase of weight over the duration of the experiment was observed in the subjects belonging to both the treated and untreated groups, showing that that the mice were healthy.

(i)

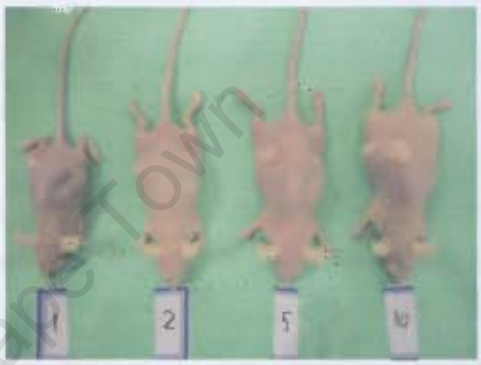

(ii)

Figure 41: Mouse 7, 8, 11 and 17 belonged to the treated group (i), while mouse 1, 2, 5 and 10 belonged to the untreated group (ii). Mice from both groups had similar tumour growth.

Some of the mice had swollen eyes and or growths that upon termination of the experiment, were determined to be abscesses. These infections did not impact the experiment as the mice were randomized and infections were present in both the control and treated groups.

The treatment had no significant effect on tumour growth (see Figure 42) when compared to the controls. From the data collected, there was no apparent reduction in tumour size observed in the treated mice compared to the untreated control. The tumours of both groups (see Figure 42 i) were observed to exhibit a steady growth over time. As observed in the earlier animal study, the drug appeared to have no apparent negative effect on the health of the subjects as each mouse gained weight and showed no obvious signs of discomfort.

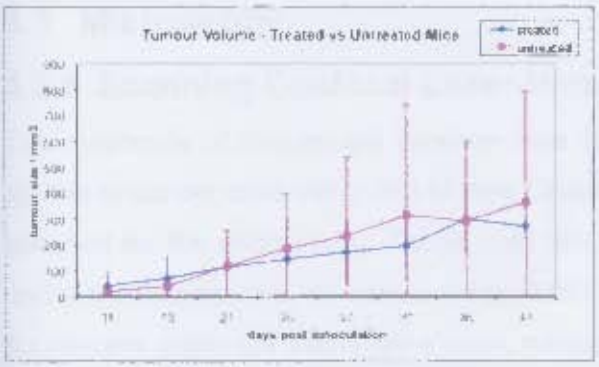

(i)

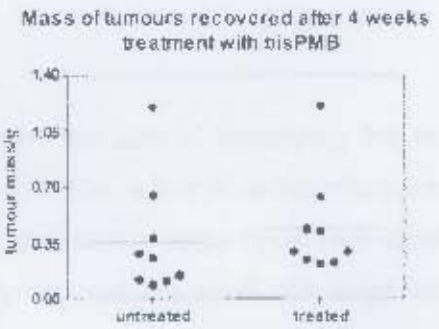

(ii)

Figure 42: (i) Growth of tumours - Treated vs Untreated. Tumour size were measured by calipers (volume calculated by: (length^2 x height)/2 [59]; (ii) Tumour size as measured by weight of tumour obtained from biopsy.

The drug, which was very active *in vitro*, was ineffective in reducing tumour size *in vivo*. This may be due to poor drug bio-availability as a result of poor solubility in Intralipid. Other methods need to be tried to solubilize the drug. It has been noted previously in our lab that increasing the lipophilicity of the drug increases *in vitro* activity,[43] but this likely limits the bioavailability *in vivo*. It is possible that a less lipophilic analogue, which exhibits lower *in vitro* activity, may be more active *in vivo*. It is also possible that administering the drug through intraperitoneal injection was not the best choice for drug-delivery and perhaps a topical application; oral or intravenous administration could prove superior. Administered topically directly to the tumour, the drug need only be absorbed through the skin and is likely to achieve its highest concentrations around the site of application. A drug administered orally may provide an alternate route for absorption, namely through the gut, but as the most practical oral delivery vehicle is the drinking water, the aqueous solubility of the drug would need to be improved. One might also look at the choice and position of the tumor grown. It may prove valuable to grow the tumour in the peritoneal cavity, which is currently the same site of the drug delivery (IP injection). This method may also maximize drug availability.

Ajoene has been shown to be a suitable guest for several cyclodextrins, forming inclusion complexes with enhanced aqueous solubility. With the addition of lipophilic side-groups, the water solubility and bioavailability of the drug diminishes. Cyclodextrin inclusion could offer a solution to this problem. Several attempts were made at forming inclusions with the BPMB-analogue, but none showed a noticeable increase in aqueous solubility. The results of these experiments are discussed at more length in the next chapter.

6.3 Microscopy

6.3.1 Scanning Confocal Laser Microscopy

The synthesis of fluorescent ajoenes was undertaken with the aim of identifying the localisation of ajoene in cancer cells using SCLM (see Chapter 1). MDA-MB-231, a line of neoplastic breast-cells, was selected for the microscopy. These cells are spread out and have a large cytoplasm ideal for viewing under the microscope, as compared to WHCO1, which by contrast are small with large nuclei. Several fluorescent organelle stains were used, namely: ER-tracker Red (Invitrogen E34250), Lyso-tracker Red (Invitrogen L7528), Mito-tracker Green (Invitrogen M7514) and DAPI (Invitrogen D3571). ER- Lyso- and mito-tracker are live cell dyes which accumulate in living cells and stain specific organelles. The nuclear stain DAPI does not permeate living cells, but stains the nuclei of dead cells and was hence used to differentiate living from dead cells. The cells were grown on chambered coverglass and kept in an incubated viewing chamber (CO_2 = 5 %, T = 37.5 °C) on the microscope. The fluorescent ajoenes were administered at 40 μM and the various organelle trackers were used as recommended by the manufacturer (see experimental section) to observe live cell imaging. The dansyl fluorophore is typically excited at around 350 nm, which lies within the UV region of the electromagnetic spectrum which is not suitable for studying live cells. UV-light would render any observations of localization invalid as the cells would be damaged by the this radiation. Using 2-photon excitation, it was possible to excite this fluorophore with near infrared light (700 nm), which is not harmful radiation to the cells. See Chapter 5.6 for fluorescent data on the analogues synthesized.

The SCLM images are presented as composites of the various colour channels, namely: red, green, blue and transmitted light. This makes it possible to visualize the individual signals in the cell, without interference from the others. It is then possible to overlay the channels to look for colocalization of the different fluorescent and transmitted-light signals.

Before examining the effects of the fluorescent-tagged ajoenes on the cells, it was first required to establish the controls to be used as a baseline for comparison. Figure 43 displays untreated MDA-MB-231 cells, showing that the cells are healthy, without background red or blue fluorescence emitted from these cells. All cells possess endogenous green fluorescence, but this was considered the baseline. Thus, any signal in the green channel superseding the base-fluorescence was due to the drug.

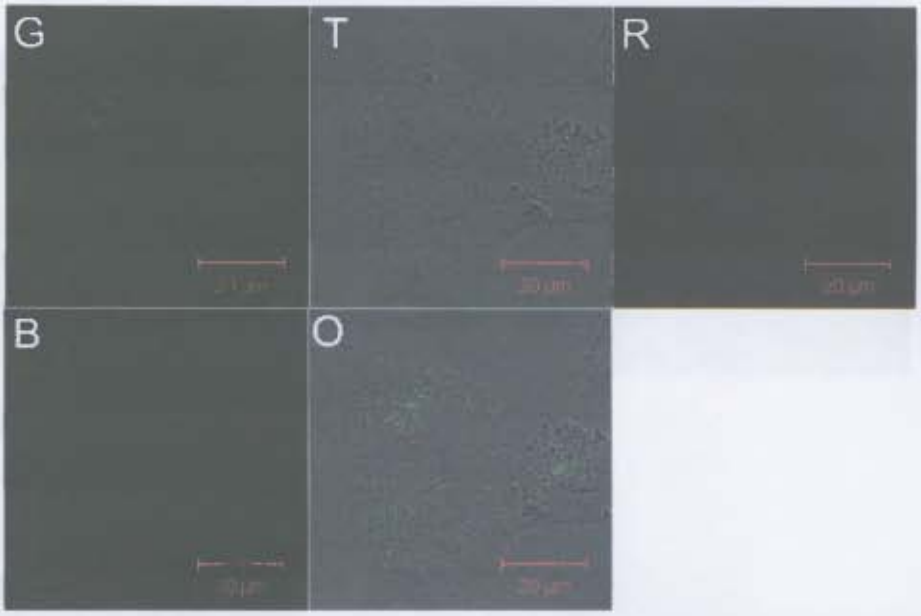

Figure 43: Untreated MDA-MB-231 cells exhibiting a weak endogenous green signal (G) as a result of endogenous cellular fluorescence. No red (R) or blue (B) fluorescence detected. Transmitted light channel (T) and overlay (O) reveal healthy cell morphology.

MDA-MB-231 cells treated with only the organelle trackers are shown in Figures 44 and 45. The images show that the organelle trackers only appear in the red channel and thus any red signal observed is due to the tracker. The transmitted light and overlay-images show cells that exhibit normal morphology and thus the organelle trackers do not appear to negatively affect the cells. The implication of the aforementioned controls is to note that any distress experienced by the cells would therefore be attributed to the ajoene drug alone.

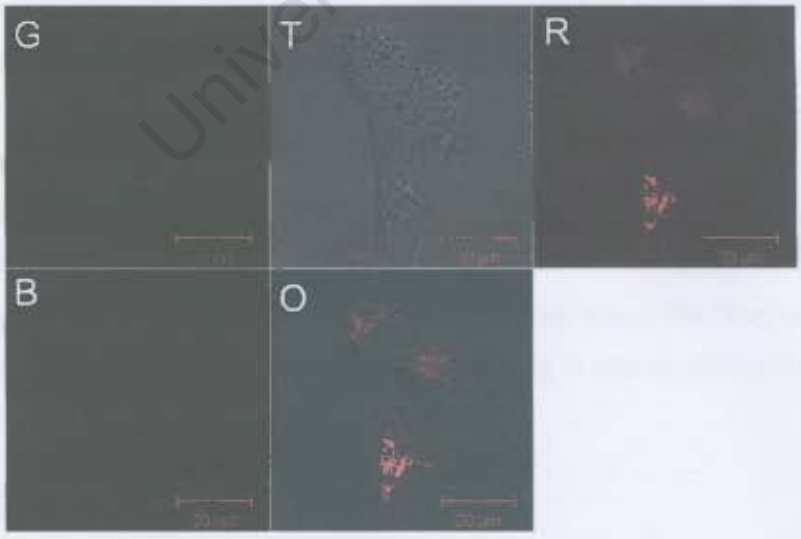

Figure 44: MDA-MB-231 cells treated with lyso-tracker alone. No green (G) or blue (B) fluorescent signal is detected. Strong staining of the lysosomes observed in the red (R) channel. Transmitted light channel (T) reveals healthy cell morphology and overlay (O) maps the location of the lysosomes in the cell.

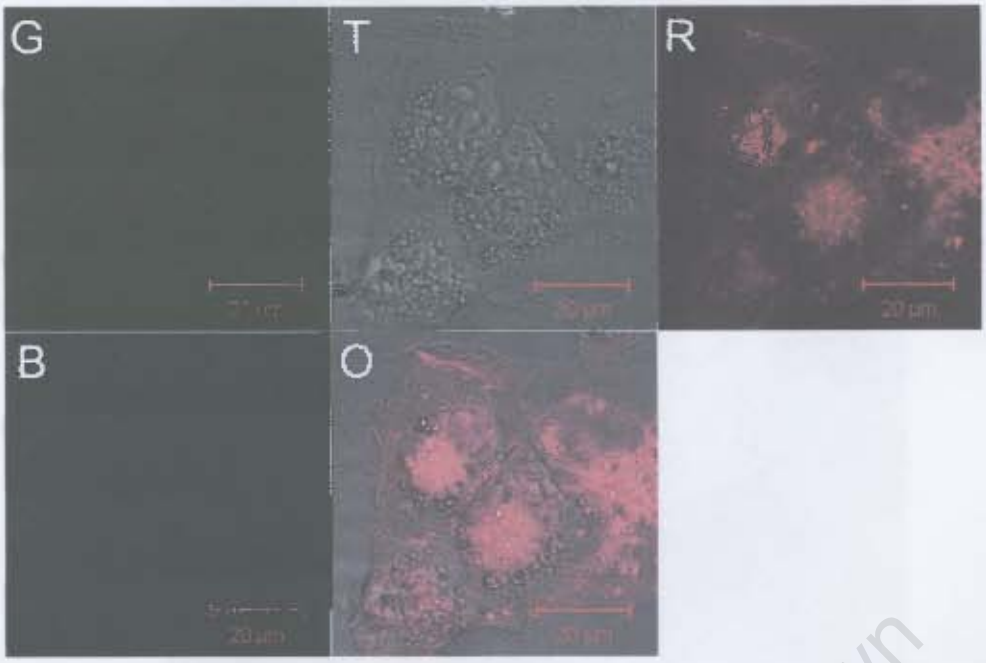

Figure 45: MDA-MB-231 cells treated with ER-tracker alone. No green (G) or blue (B) fluorescent signal is detected. Strong staining of the ER observed in the red (R) channel. Transmitted light channel (T) reveals healthy cell morphology and overlay (O) maps the location of the ER in the cell.

Cells treated with DP **30** exhibited blue fluorescence, which was observed within the first 30 minutes after adding compound to the cells (see Figure 46). When examining cells that had been treated with both ER-tracker and DP **30**, no colocalization with the ER-tracker or Lyso-tracker was observed (see Figure 47). DP also appears to localize in droplet-like structures, which appear as blue granular structures in the cytosol. Comparing the morphology of treated (see Figure 47) and untreated (see Figure 48) cells at 60 and 75 minutes respectively, the cytotoxic effect of the DP **30** is evident. The cells show signs of stress, presenting as membrane blebbing and leaking of the cytoplasm, indicative of apoptosis. After 240 minutes (see Figures 49 and 50), changes to the morphology of the treated cell's have become more pronounced while cells treated only with ER-tracker appear healthy with normal morphology (see Figure 50) supporting the idea that the stress experienced by the cell is caused by the drug. Where the drug localizes remains uncertain, however since the drug is lipophilic, the appearance of granular fluorescent bodies might suggest that the drug is accumulating in lipid bodies.

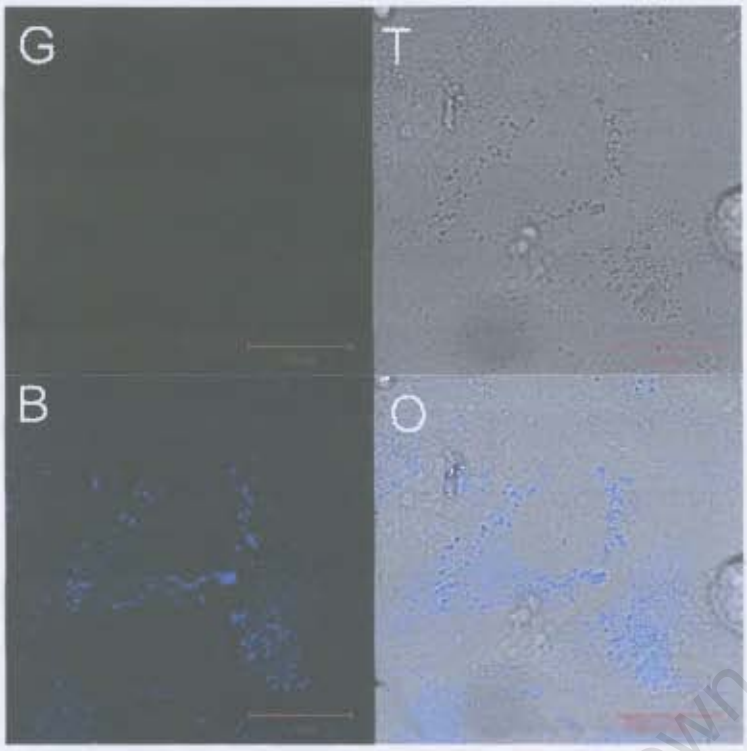

Figure 46: Treated MDA-MB-231 cells after incubation with DP **30**, 30 min, 2-photon laser. Weak blue fluorescence (B) detected, while no signal is observed in the green (G) fluorescent channel. Transmitted light channel (T) reveals cell morphology and overlay (O) maps the location of the DP in the cell.

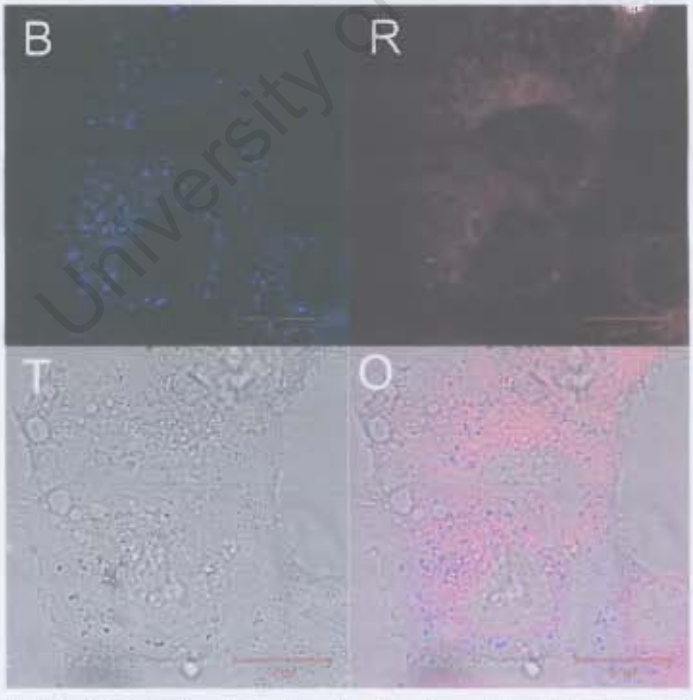

Figure 47: Treated MDA-MB-231 cells after incubation with DP **30** and ER-tracker, 60 min into the experiment, 2-photon laser. Weak blue fluorescence (B) detected and a stained ER in the red channel (R). The cell shows signs of distress, seen in the transmitted light channel (T). The overlay (O) shows no apparent colocalization between the drug and tracker.

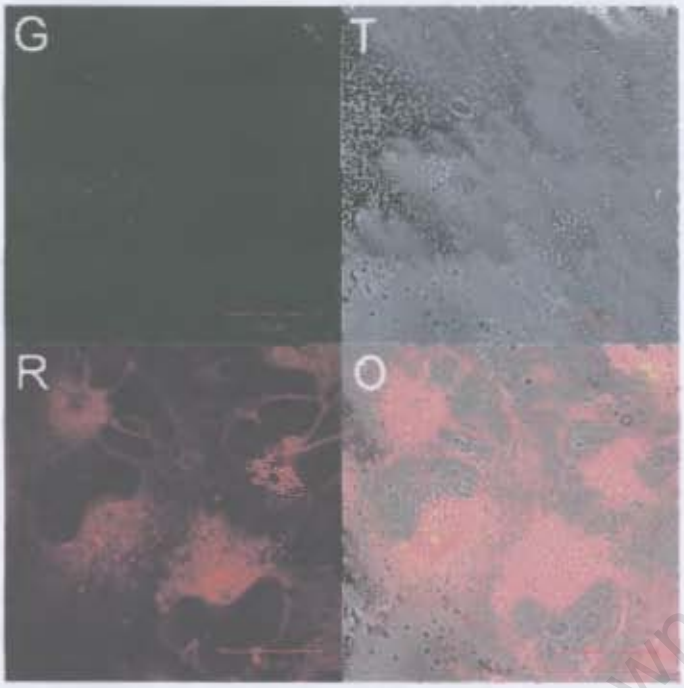

Figure 48: MDA-MB-231 cells incubated with ER-tracker, 75 minutes into the experiment. No green (G) fluorescent signal is detected. Strong staining of the ER observed in the red (R) channel. Transmitted light channel (T) reveals healthy cell morphology and overlay (O) maps the location of the ER in the cell.

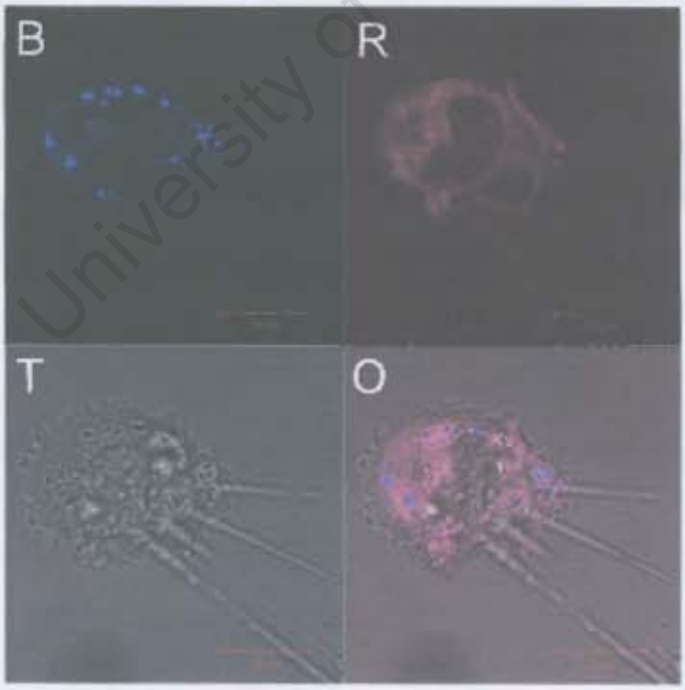

Figure 49: Treated MDA-MB-231 cells after incubation with DP **30** and ER-tracker, 240 min into the experiment, 2-photon laser. Blue fluorescence (B) detected and a stained ER in the red channel (R). The cell shows signs of distress, seen in the transmitted light channel (T). The overlay (O) shows possible colocalization between the drug and tracker.

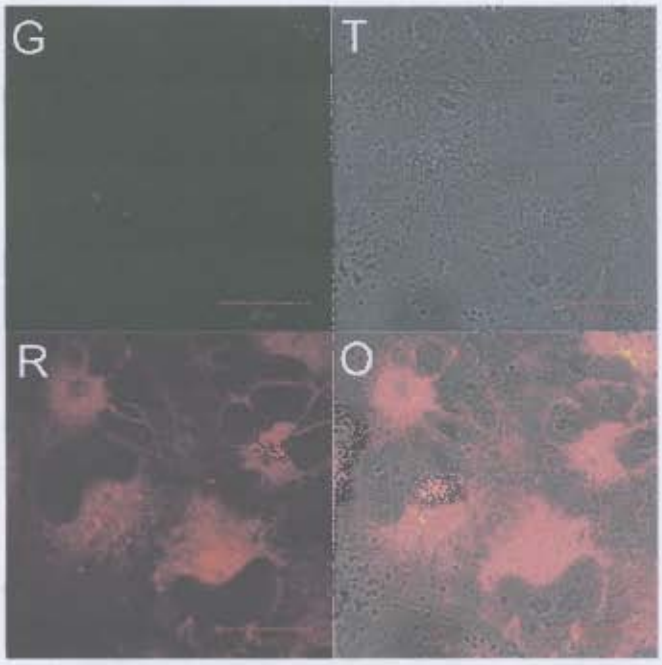

Figure 50: MDA-MB-231 cells incubated with ER-tracker, 240 minutes into the experiment. Slight endogenous green fluorescent (G) is observed. Strong staining of the ER observed in the red (R) channel. Transmitted light channel (T) reveals healthy cell morphology and overlay (O) maps the location of the ER in the cell.

Figure 51 shows the green fluorescence produced by the fluorescein-tagged ajoene FOx **53**. The drug was found to be insoluble in the medium and even with DMSO as a cosolvent, formed small particles on the chamber slide. The images shown in Figures 51 and 52 were taken after the drug, dissolved in DMSO and media, was added directly to the cells. The drug administered to the cells shown in Figures 53 – 56 was centrifuged first to remove the larger insoluble particles and hence resulted in fewer floating objects seen around the cells. The concentration of drug in these latter images was thus lower than calculated and required longer incubation for the cells to accumulate enough drug for fluorescence to be apparent.

We have previously shown the control (up to 240 minutes) for the MDA-MB-231 cells with ER- and Lyso-trackers, showing healthy morphology and no unaccountable background fluorescence. Figure 52 shows cells treated with FOx **53** and lyso-tracker and shows no signs of colocalization between the two. It is thus unlikely that the drug accumulates in the lysosomes. Some insoluble drug material is also seen.

Figures 53 – 56 show cells that have been treated with FOx **53** and ER-tracker. After 90 minutes (see Figure 53), a green fluorescent signal was observed, however no obvious colocalization was seen between the two signals (red and green). Comparing the images in Figure 53 and 54, it is apparent that the green signal is due to the drug and not to endogenous cellular fluorescence.

After 240 minutes, treated cells (see Figure 56) produced a strong green signal. In the overlay of the channels there appears to be good co-localization between drug and ER-tracker. This provides strong evidence that ajoene localizes in the ER.

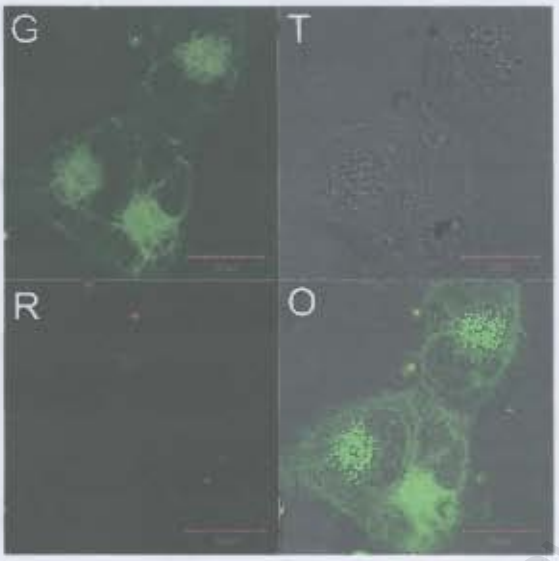

Figure 51: Treated MDA-MB-231 cells after incubation with FOx **53**, 120 min. Green fluorescence (G) is observed. No red fluorescence (R) detected. The cell shows signs of distress, seen in the transmitted light channel (T). The overlay (O) shows localization of the drug in the cell.

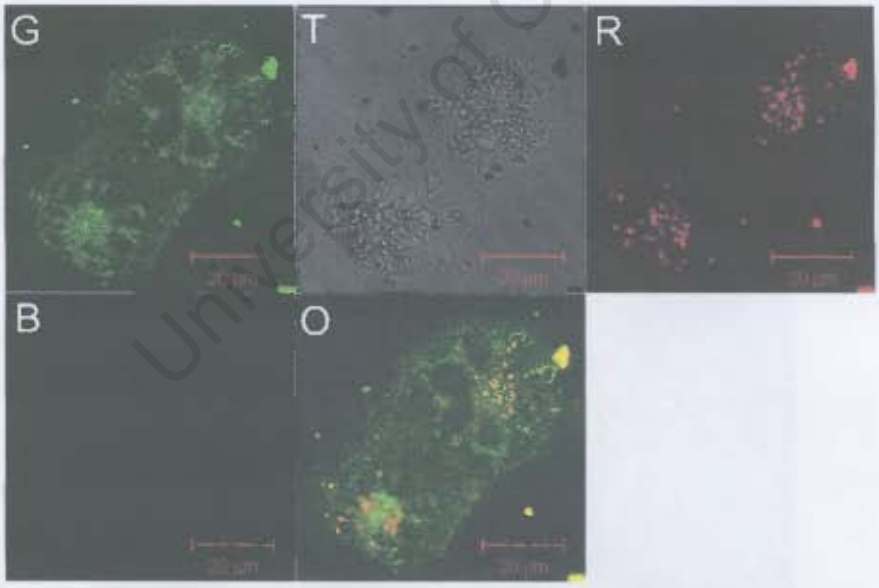

Figure 52: Treated MDA-MB-231 cells after incubation with FOx **53** and lyso-tracker, 45 min. Green fluorescence (G) is observed, resulting from the drug. Red fluorescence (R) is observed, resulting from the lyso-tracker. The transmitted light channel (T) shows the cell's morphology. The overlay (O) shows localization of the drug and tracker in the cell, with no colocalization detected.

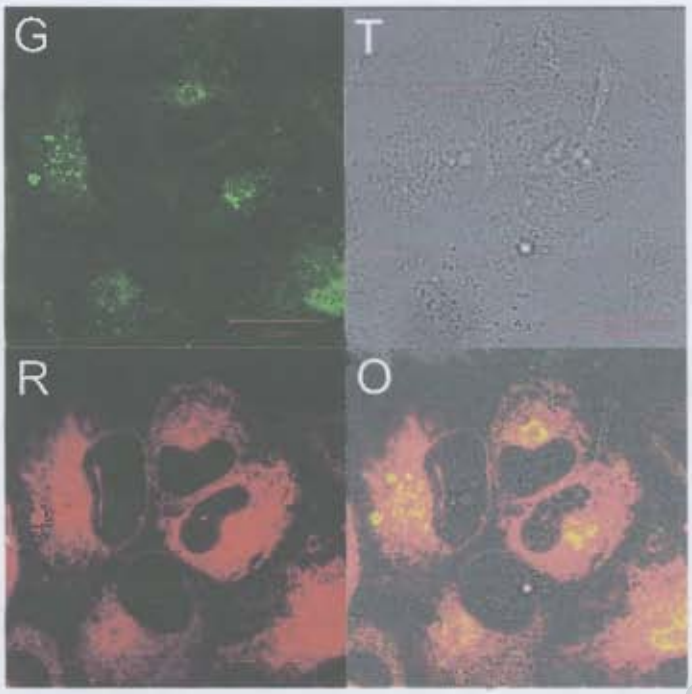

Figure 53: Treated MDA-MB-231 cells after incubation with FOx **53** and ER-tracker, 90 min. Green fluorescence (G) is observed, resulting from the drug. Red fluorescence (R) is observed, resulting from the ER-tracker. The transmitted light channel (T) shows the cell's morphology. The overlay (O) shows localization of the drug and tracker in the cell, with no apparent colocalization detected.

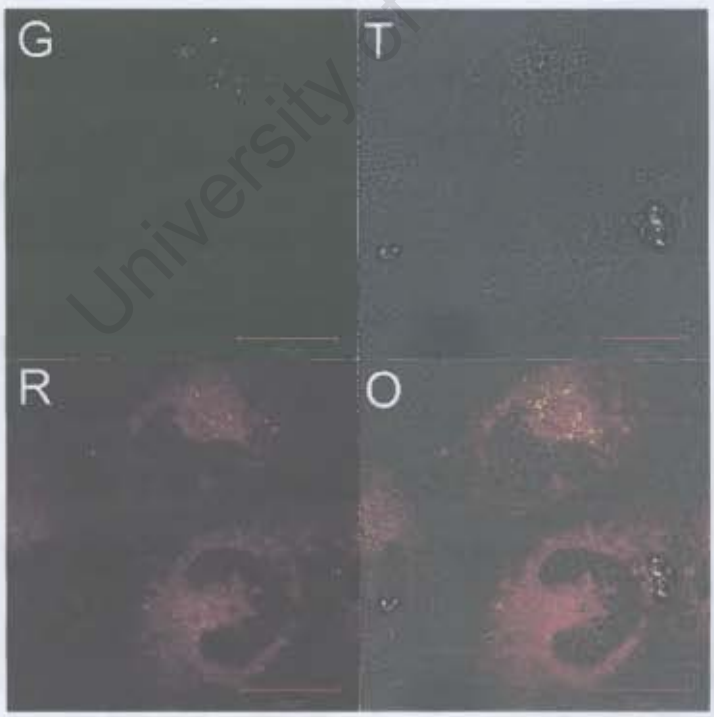

Figure 54: MDA-MB-231 cells incubated with ER-tracker, 90 minutes. No green (G) fluorescent signal is detected. Strong staining of the ER is observed in the red (R) channel. Transmitted light channel (T) reveals healthy cell morphology and overlay (O) maps the location of the ER in the cell.

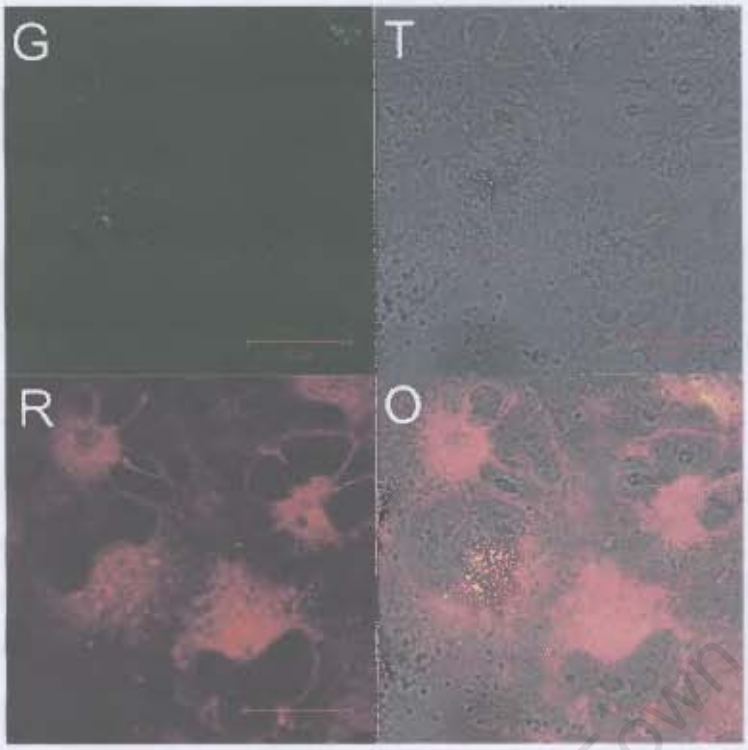

Figure 55: MDA-MB-231 cells incubated with ER-tracker, 240 minutes. No green (G) fluorescent signal is detected. Strong staining of the ER is observed in the red (R) channel. Transmitted light channel (T) reveals healthy cell morphology and overlay (O) maps the location of the ER in the cell.

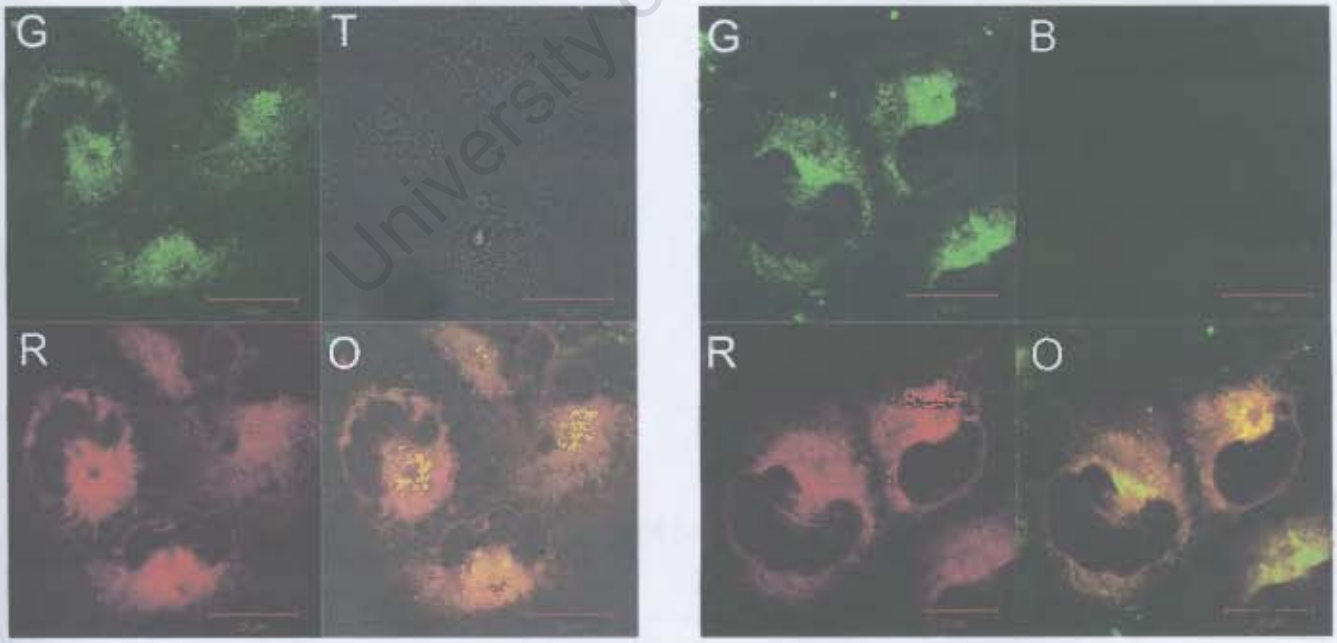

Figure 56: Treated MDA-MB-231 cells after incubation with FOx **53** and ER-tracker, 240 min. Green fluorescence (G) is observed, resulting from the drug. Red fluorescence (R) is observed, resulting from the ER-tracker. No blue fluorescence (B) is detected. The transmitted light channel (T) shows the cell's morphology. The overlay (O) shows colocalization of the drug and tracker in the cell.

6.3.2 Transmission Electron Microscopy

Our study using fluorescent ajoenes provided evidence that ajoene may localize to the ER. It was decided to use transmission electron microscopy (TEM) to examine more closely the morphological changes associated with ajoene treatment of MDA-MB-231cells over time. Figures 57 – 59 were taken using the TEM (Zeiss, 912 Omega EFTEM) at the University of Cape Town. The cells were treated with BPMB **17** (10 μM) for **1**, 3 and 24 hours. The cells were then prepared and sectioned as described in the experimental section.

When comparing cells treated for 24 hours with the untreated control (Figure 57), there are many differences. The untreated control cells (Figure 57 **i**) have intact mitochondria. The treated cells (Figure 57 **ii**) contain mitochondria appearing swollen and misshapen. The nuclear membrane of the treated cells (Figure 58) is also notably different to that of untreated cells. The treated cells exhibited condensed nucleoli and deformed nuclear membranes, indicative of bis-PMB **17** induced apoptosis.

It was not possible to draw conclusions from the TEM images about the effects of bis-PMB **17** on the ER which was not easily identifiable from these sections.

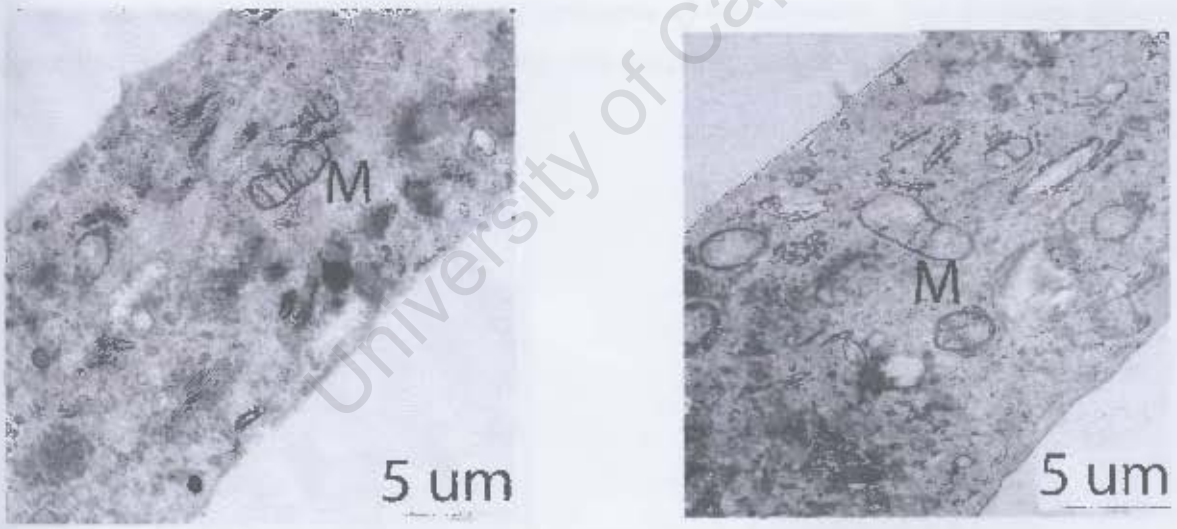

(i) (ii)

Figure 57: (i) Untreated MDA-MB-231 cells, 24 hours; (ii) MDA-MB-231 cells treated with BPMB **17**, 24 hours

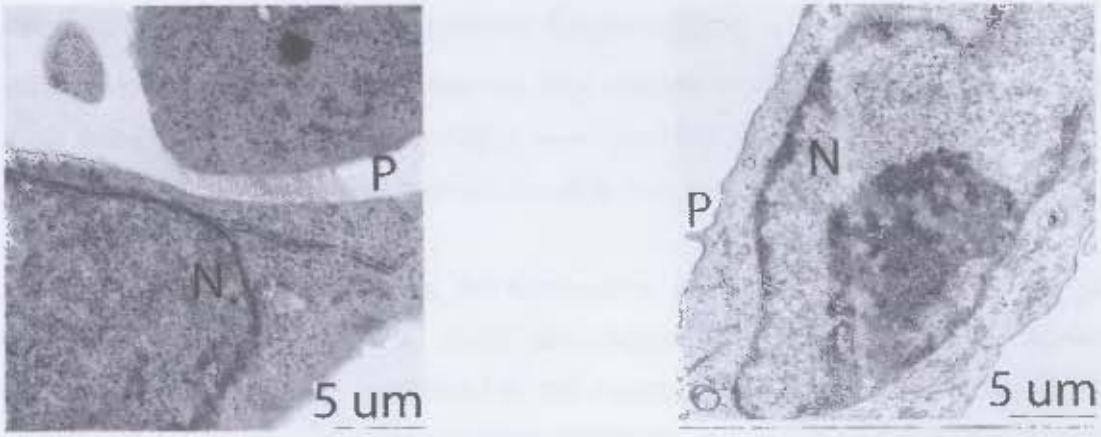

(i) (ii)

Figure 58: (i) Untreated MDA-MB-231 cells, 24 hours; (ii) MDA-MB-231 cells treated with BPMB **17**, 24 hours

Cells treated with BPMB exhibited similar morphological features to those treated with benzyl isothiocyanate, an organosulfur compound found in cruciferous vegetables also reported to have anti-cancer properties.[60] Figure 59 shows a representative transmission electron micrograph (10,000X magnification) following a 24 hour treatment with 10.0 μM BPMB (see Figure 59 **i**) and a 6-h treatment with 2.5 μM BITC (see Figure 59 **ii**). The abundance of membranous vacuoles in both images is denoted by **V** in Figure 59 **i** and the arrows in Figure 59 **ii**. These vacuoles, as suggested by Xiao *et al.*,[60] may be autophagosomes, containing remnants of mitochondria. The similarity between **i** and **ii** suggest that ajoene and BITC, both of which are lipophilic, may impose similar biochemical effects in cells.

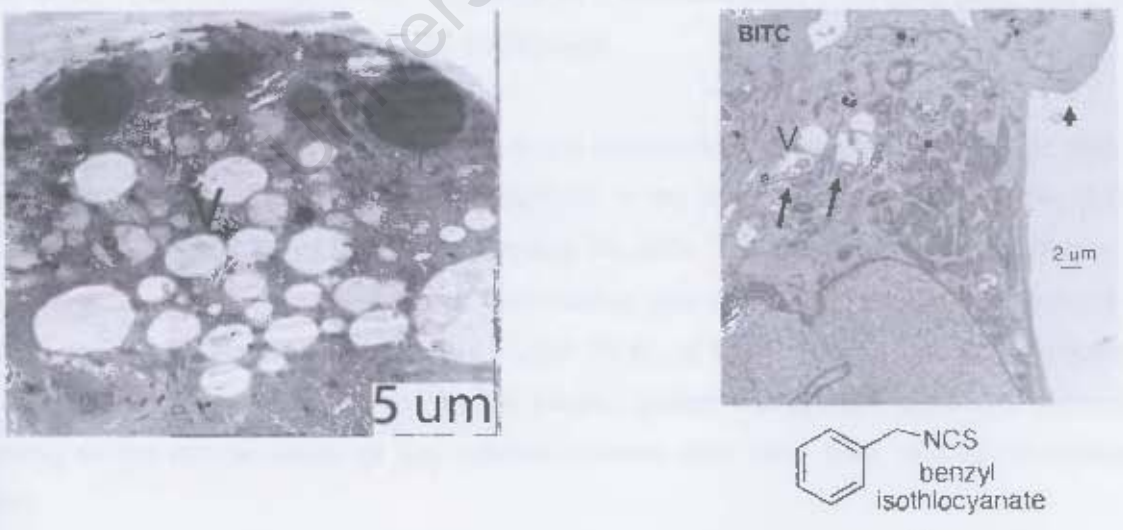

(i) (ii)

Figure 59: (i) MDA-MB-231 cells treated with BPMB **17**, 10 μM for 24 hours and (ii) MDA-MB-231 cells treated with benzyl isothiocyanate[60], 2.5 μM, 6 hours, both containing similar vacuole structures (V).

6.4 Protein Labeling and Cysteine Experiment

Previous research in our lab has identified the vinyl disulfide in ajoene as a critical structural feature for anti-cancer activity. It is therefore likely that ajoene (and structurally similar organo-sulfur compounds) inhibit cancer cell growth by forming a mixed disulfide with a protein.

For both the fluorescent ajoenes tested, the fluorophore was situated on the right hand (disulfide) side of the molecule. To date, there is much speculation about the reactivity of ajoene's disulfide pharmacophore. An experiment performed in the Hunter group showed that when BPMB-ajoene **17** was reacted with 1 equivalent of *N*-boc cysteine ethylester, it produced a mixed disulfide containing the right hand PMB group.[61] This experiment supports the notion that ajoene sulfenylates from its allyl-sulfur and hence this position is more electrophilic. The experiment was repeated using the dansyl-tagged analogue DOx **32**. To this end, DOx **32** was refluxed overnight with *N*-Boc cysteine ethylester (1 eq.) in THF, and produced a new fluorescent spot on TLC (see Figure 60 **i**), which could not be isolated. This evidence suggests that the right hand side of the molecule was a good choice for the fluorophore and that the observed localization of fluorescence may arise as a result of the fluorescent ajoene forming a mixed disulfide with a protein thereby forming a fluorescent-tagged protein in the ER. It is still premature to conjecture the exact mechanism of action, however the involvement of the ER and right-hand side of the ajoene is now implicated.

Thiols are highly reactive functional groups and it is likely that the secondary metabolites of ajoene also have biological activity. Evidence supports the notion that the left hand side of ajoene also plays a role in its biological activity. With the current set of fluorescent analogues it is impossible to track this part of the molecule. This motivates for the synthesis of a double-tagged molecule, such that the fate of the left hand side of the ajoene may also be determined.

One of the most pressing questions relating to the biochemistry of ajoene relates to its ability to interact with and modify proteins. The procedure (outlined in the experimental section) involved treating cells with 40 μM DP **30** for 2 hours, followed by lysing the cells. The total cell-lysates were run on 10 %, 12 % or 20 % acrylamide gels. In each case, the finished gels were photographed under a UV-light source and then stained with coomasie-blue (see Figure 60 **ii**). In each instance, the dansyl-labeled analogue appeared to run to the bottom the gel, but no labeled protein bands were observed. This result was not surprising as the concentration of any labeled proteins may have been too low for detection on this system.

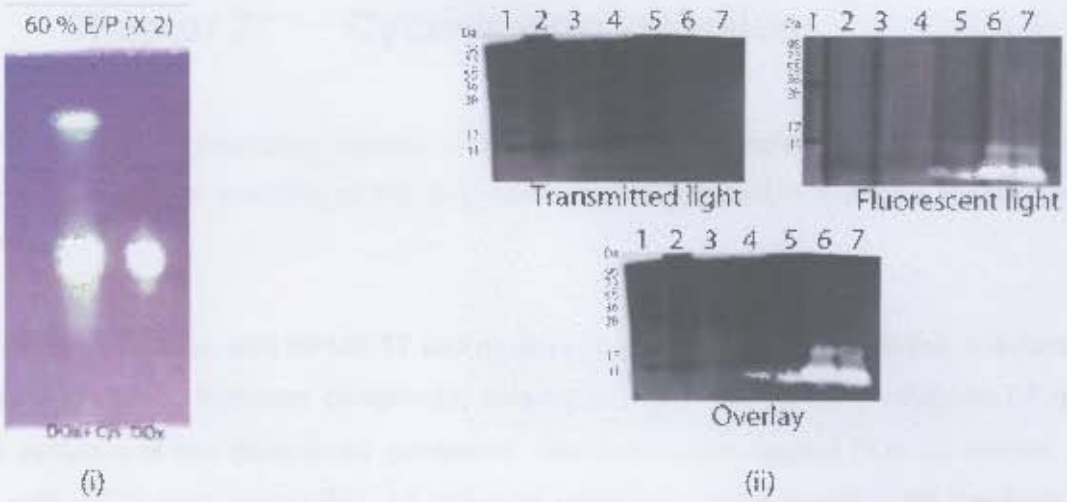

Figure 60: (i) TLC experiment with DOx **32** and 1 equivalent of *N*-Boc cysteine ethylester in THF (refluxed overnight), producing a new less-polar fluorescent spot. This implicated the "right-hand side" of the ajoene as the first site of attack; (ii) 12 % acrylamide gel of DP treated (40 μM, 3h) total cell lysates - Transmitted light, UV-fluorescence and overlay.

6.5 Conclusion

All of the synthesized ajoene analogues tested had *in vitro* anti-cancer activity comparable to that of ajoene itself. BPMB **17** was the most active analogue synthesized to date and seemed the ideal candidate for *in vivo* testing in the animal trials. The poor solubility of the drug proved to be problematic, with the treatment formulation not reducing or inhibiting tumour growth in the mice.

The animal trials show that the drug is tolerated by the mice in doses of up to 45 μg per gram and can thus be administered at this dose.

The SCLM offered a unique opportunity to visualize the movement and localization of ajoene in cancer cells. The subsequent discovery that ajoene localizes in the ER is both novel and valuable as one can now look closely at the specific ER proteins that may interact with ajoene. The images obtained from the TEM revealed the morphological changes exhibited by treated cells were typical of apoptosis. The appearance of the suspected autophagosomal bodies was an interesting and unexpected phenomenon, suggesting that there may be underlying similarity between the mode of action of ajoene and other organo-sulfur compounds.

Chapter 7: Cyclodextrin Inclusion

Ajoene offers an interesting and promising scaffold to new anti-cancer therapies, but with the addition of lipophilic side-groups, the water solubility of the drug diminishes. Cyclodextrin inclusion could offer a solution to this problem.

Preparation of inclusion complexes with BPMB **17** and several cyclodextrins was attempted. Ultimately, only two cyclodextrins produced inclusion complexes, namely β- and γ-CD. Below (in Figures 61 and 63) are the PXRD patterns of the complexes generated. The fluorescein tagged FOx **53** formed an inclusion complex with β-CD (see Figure 65). All inclusion complexes were found to be insoluble in water.

The term isostructural is used to describe a set of chemically distinct crystalline compounds or molecules, which share structural constituency. This method is used extensively by members of the Centre for Supramolecular Chemistry Research at the University of Cape Town, who have compiled and characterized a library of reference X-ray diffraction patterns for many cyclodextrin inclusion complexes. Two isostructural compounds will produce similar powder X-ray diffraction patterns, making it possible to extrapolate complex structural information from comparisons with known compounds.

Analysis of the PXRD pattern shown in Figure 61 revealed that the kneading of β-CD and **17** formed an inclusion complex, which conformed to the **B6** structure. Successful generation of single crystals must still be achieved; however, the isostructurality provides much information about the inclusion complex.

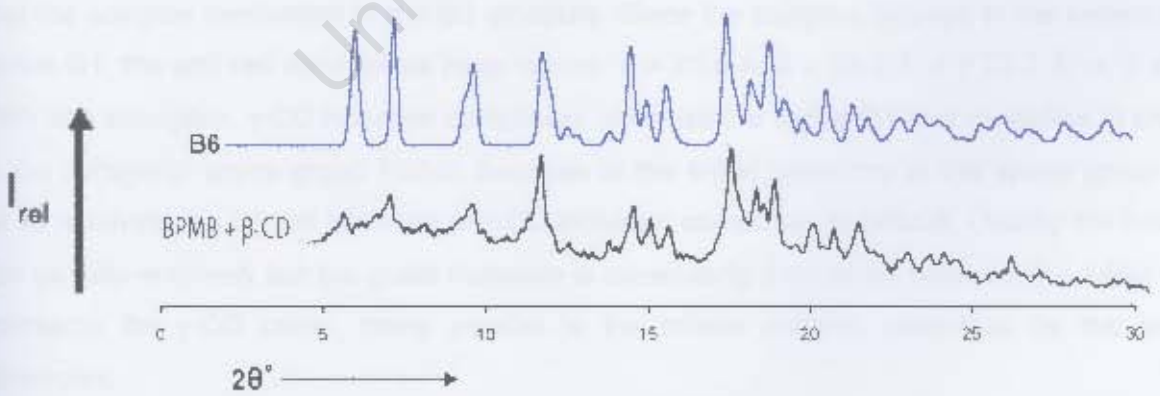

Figure 61: Isostructurality reveals that inclusion complex generated by kneading BPMB **17** with β-CD conforms to **B6** structure.

Since the complex belongs to the known isostructural series **B6**, the unit cell dimensions have values: $a \approx 19.4$ Å; $b \approx 24.5$ Å; $c = 15.9$ Å; $\beta = 109°$. **B6** forms a dimeric structure in the space group C2, typically encapsulating larger organic guests, in a channel type (**CH**) packing arrangement. An example of the **B6** structure is depicted below, showing the stacking of the β-CD molecules to form channels in which the guest resides.

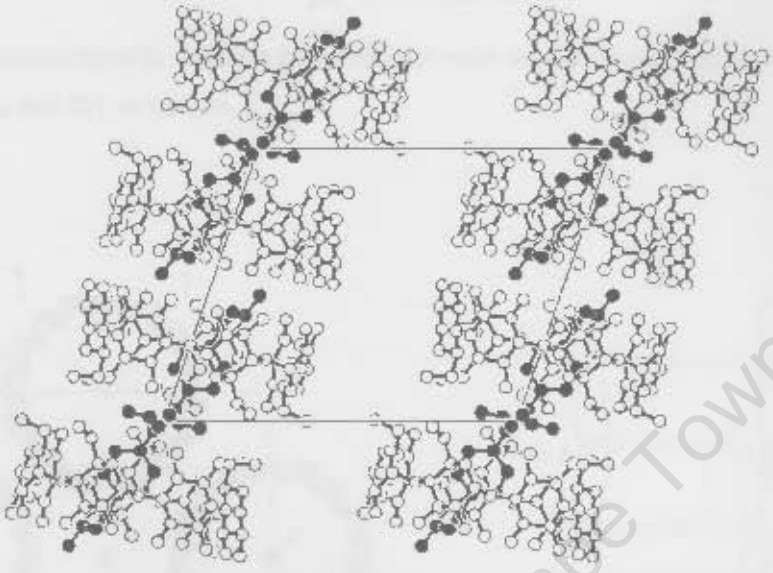

Figure 62: View of a **B6**-conforming inclusion complex showing a head-to-head dimer of β-CD molecules stacked along the crystallographic *c*-axis, thus forming a slightly tilted channel-type structure with 2-fold symmetry. In this example, the guest is the common analgesic ibuprofen.[62]

Analysis of the PXRD pattern generated from kneading BPMB **17** with γ-CD (see Figure 63) revealed that the complex conformed to the **G1** structure. Since the complex belongs to the known isostructural series **G1**, the unit cell dimensions have values: $a \approx 23.8$ Å; $b \approx 23.8$ Å; $c = 23.2$ Å; α, β and $\gamma = 90°$. With little exception, γ-CD inclusion complexes comprise the series **G1** and crystallize in channel-mode in the tetragonal space group $P42_12$. Because of the 4-fold symmetry in this space group (see Figure 64 **i**), resolving the crystal structure of γ-CD inclusion complexes is difficult. Usually the host molecules can be fully resolved, but the guest molecule is necessarily disordered because the 4-fold rotation axis intersects the γ-CD cavity, being parallel to the infinite channel generated by the stacked γ-CD molecules.

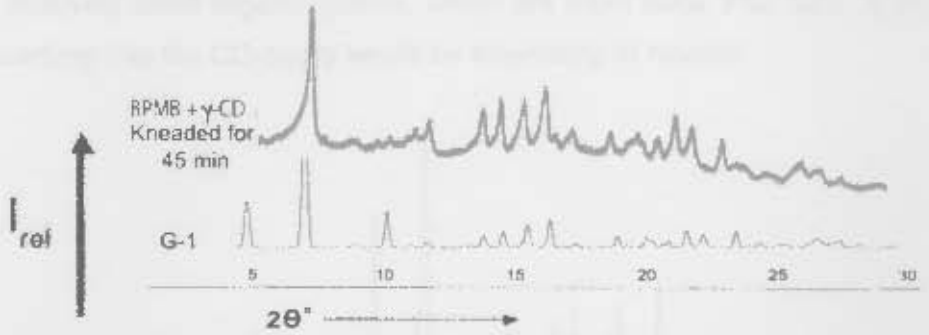

Figure 63: Isostructurality reveals that the inclusion complex generated by kneading BPMB **17** with γ-CD conforms to the **G1** structure.

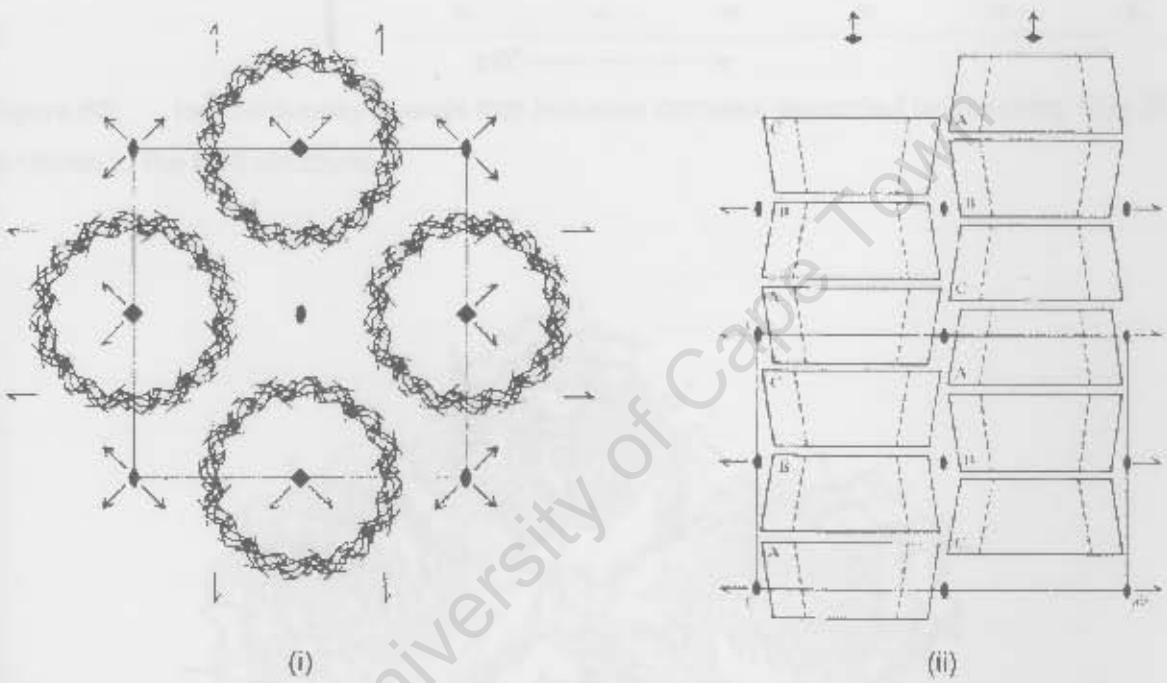

Figure 64: (i) **G1** structure results in crystal packing of the γ-CD complex shown in a projection in the *x,y* plane. The crystallographic symmetry elements of the space group $P42_12$ have been indicated;[63] (ii) Stacking sequence within the molecular columns and lateral contact between the columns shown schematically. The projection is on a diagonal plane of the unit cell.
63

Analysis of the PXRD pattern generated from kneading FOx **53** with β-CD (see Figure 65) revealed an inclusion complex conforming to the **B10** structural series. Thus, the unit cell dimensions have values: $a \approx 15.5$ Å; $b \approx 26.0$ Å; $c = 36.8$ Å; α, β and $\gamma = 90$ °. Complexes comprising series **B10** are monomeric with an asymmetric unit made of two CD molecules in a head-to-tail orientation. The monomeric β-CD molecules of the two complexes of series **B10** pack in anti-parallel head-to-tail screw channels along the *c*-axis. The **B10** isostructural series belongs to the space group $P2_12_12_1$ (see Figure 66) and

typically comprises relatively small organic guests, which are often salts. FOx **53** is a large molecule and thus its spatial packing into the CD-cavity would be interesting to resolve.

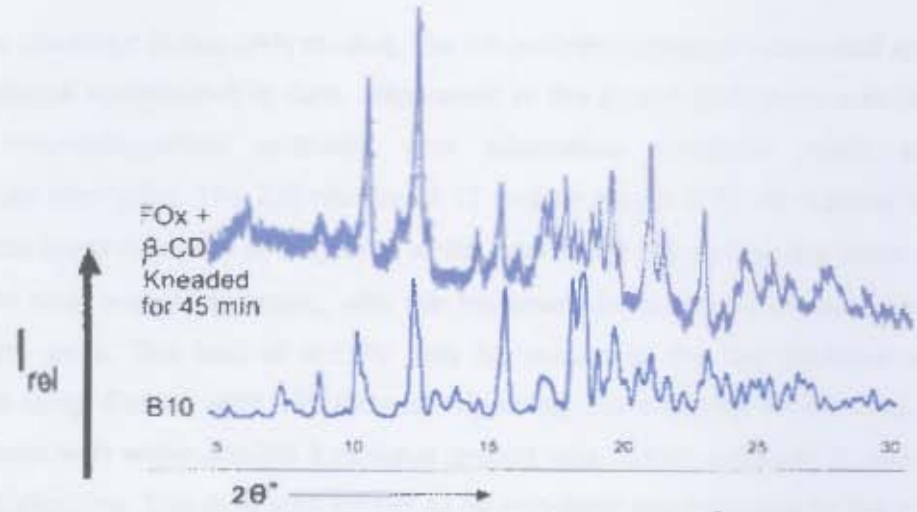

Figure 65: Isostructurality reveals that inclusion complex generated by kneading FOx **53** with β-CD conforms to the **B10** structure.

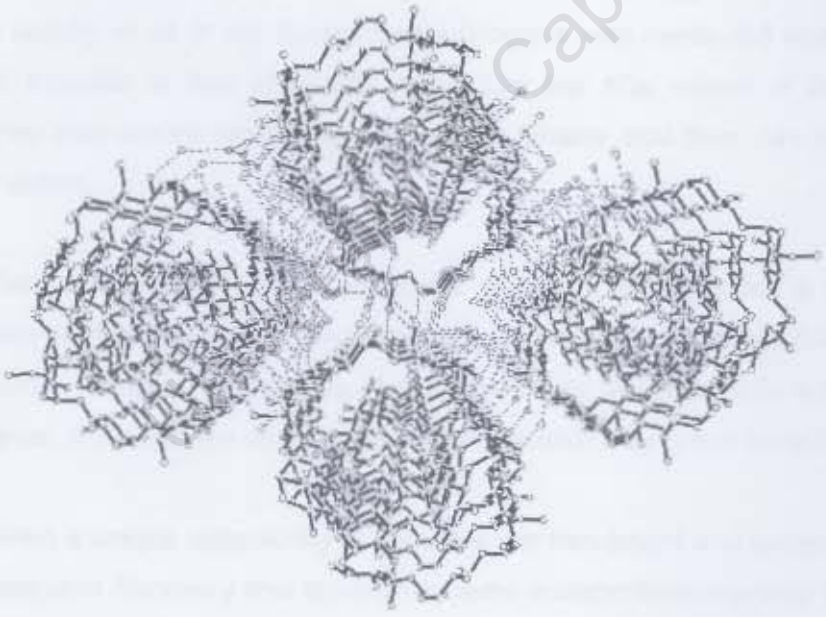

Figure 66: 3-dimensional helical columnar packing of β-CD in space group $P2_12_12_1$.[64]

Owing to the low aqueous solubility of the synthetic ajoene analogues, cyclodextrin inclusion still offers a practical and cost effective way to solubilize these compounds. PXRD analysis confirms that inclusion complexes have been generated and more work is required to improve solubility. To this end, amorphous CDs such as HP-β-CD and RAMEB continue to show promise as potential solubilizing agents in formulations containing the ajoene analogues.

Chapter 8: Summary and Future Work

Following the trends observed in our SAR studies, the bis-*p*-methoxyphenyl substituted ajoene **17** was the most active analogue synthesized to date. Separation of the *Z*- and *E*-isomers was not successful using traditional chromatographic methods, and alternative strategies such as fractional recrystallization will be attempted. The *Z/E* mixture of **17** had an IC_{50} of 0.83 μM against MDA-MB-231 cells, seventeen times lower than that of *Z*-ajoene, which was 13.70 μM against the same cell-line. The poor solubility of the drug was problematic, with the treatment formulation not reducing or inhibiting tumour growth in the mice. The lack of activity may be related to the low aqueous solubility and bioavailability of the drug. Future work will include improving the solubility of the drug through the synthesis of analogues with water-soluble functional groups and further attempts to include the drug into amorphous cyclodextrins. The drug was shown to be non-toxic and tolerated by the mice in doses of up to 45 μg per gram.

Three fluorescent ajoenes were successfully synthesized, utilizing dansyl and fluorescein fluorophores. The cornerstone to success in all cases was the fluorescently-tagged sulfenylating agents **27** and **51**. The biological activity of all of the fluorescent analogues was measured and all had activity that was comparable or superior to that of ajoene itself. The low IC_{50} values of the fluorescent analogues suggest that they may invoke similar biochemistry to ajoene, and thus, can be used to probe ajoene's mechanism of action.

The reaction between *N*-boc cysteine ethylester and DOx **32** produced a new fluorescent product, lending credibility to the choice of putting the fluorescent tag on the "right-hand side" of the molecule. Attempts to isolate proteins, specifically those that might be covalently modified, have not yielded success. However, enriching the cell lysates for ER material may prove beneficial.

The SCLM offered a unique opportunity to visualize the movement and localization of ajoene in cancer cells. The subsequent discovery that ajoene (or some metabolite comprising the right hand side of the molecule) localizes in the ER is both novel and valuable as one can now look closely at the specific ER proteins that may interact with ajoene. Using a double-tagged ajoene, the fate of both sides of the drug can be determined as they are tracked within the cell. A double-tagged fluorescent ajoene will be synthesized in the future, with a dansyl-tag at one end and the fluorescein-tag at the other. Below in Figure 67 is a proposed synthetic route towards a double-tagged ajoene.

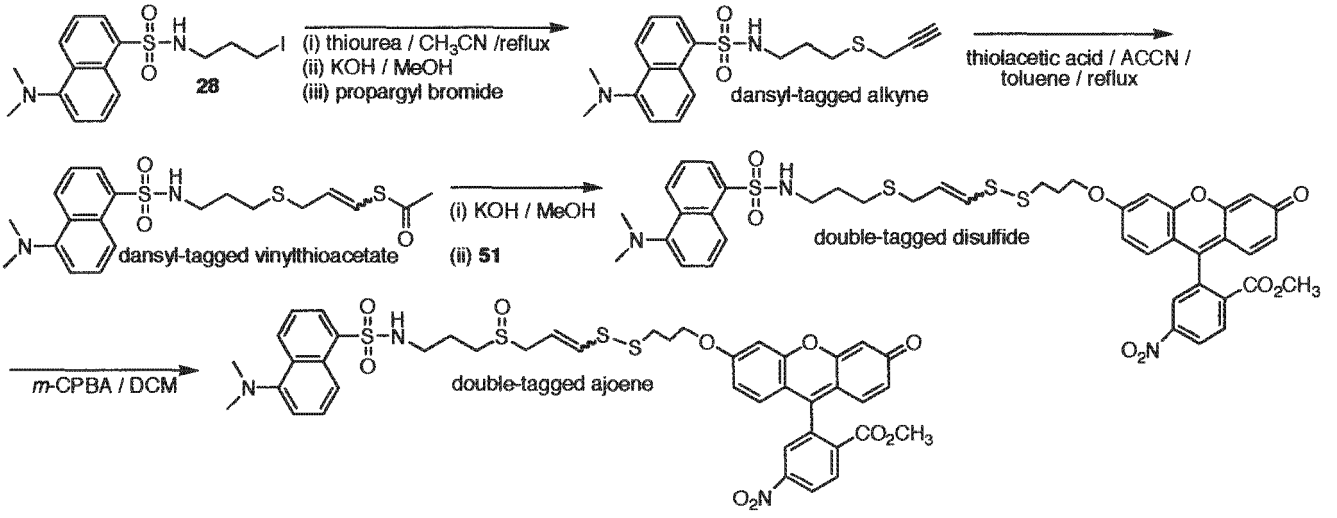

Figure 67: Proposed synthetic route towards a double-tagged ajoene*

*(Preliminary studies indicate the dansyl group placed on the "left-hand side" will indeed survive the radical addition)

Chapter 9: Experimental Section

9.1 General methods

All solvents were freshly distilled. Tetrahydrofuran was distilled under argon from first: lithium aluminium hydride and then sodium wire with benzophenone. Diethyl ether was distilled from lithium aluminium hydride under argon. Acetonitrile was distilled from calcium hydride under argon. Dichloromethane was distilled from phosphorus pentoxide under nitrogen. Other reagents were purified according to standard procedures.

Column chromatography was performed using silica-gel 60 (Merck 7734). Thin layer chromatography (TLC) was carried out on aluminium-backed Merck silica-gel 60 F_{254}. Compounds were visualized on TLC by using one or more of the following revealing techniques: UV lamp, iodine vapour, spraying with a 2.5% solution of anisaldehyde in a mixture of sulfuric acid and ethanol (1:10 v/v) and then heating at 250°C.

Infra-Red (IR) absorptions were measured on a Perkin Elmer Spectrum one FT-IR Spectrometer, with all absorptions measures in chloroform. Nuclear Magnetic Resonance spectra were recorded on a Varian Mercury 300 MHz (75.5 MHz for ^{13}C), Varian Unity 400 (100.6 MHz for ^{13}C) or Bruker Advance III 400 (100.6 MHz for ^{13}C) NMR instrument and were carried out in chloroform-d unless otherwise stated. Chemical shifts (δ) were recorded relative to residual chloroform (δ = 7.26 in ^{1}H NMR) and (δ = 77.00 in ^{13}C NMR), acetone (δ = 2.05 in ^{1}H NMR) and (δ = 206.26 in ^{13}C NMR) or dimethylsulfixide (δ = 2.50 in ^{1}H NMR) and (δ = 39.52 in ^{13}C NMR). All chemical shifts are reported in ppm and resonances are assigned according to IUPAC numbering, viz H-1 = H on C-1. High-resolution mass spectra were recorded on a Waters API Q-TOF Ultima machine, at the Mass Spectrometry Service, School of Chemistry, University of Stellenbosch.

Melting points were obtained using a Reichert-Jung Thermovar hot-stage microscope and are uncorrected. Elemental analyses were performed using a Fisons EA 1108 CHNS elemental analyzer. All reagents were purchased from Aldrich or Merck.

9.2 Synthetic chemistry

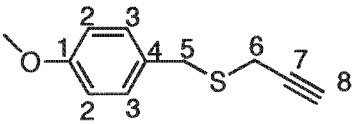

(4-Methoxybenzyl) prop-2-ynyl sulfane, **9**

Thiourea (293 mg, 3.84 mmol) was dissolved in acetonitrile (10 mL) under N_2 and 4-methoxybenzyl chloride (0.43 mL, 3.20 mmol) was added and the solution refluxed for 2 hours, by which time TLC showed a spot-to-spot conversion to a more polar product corresponding to the isothiouronium salt intermediate. The reaction was cooled in an ice-bath forming a solid product, that was filtered on a Büchner funnel. The product was then washed with ice-cold acetonitrile (30 mL) and dried on the pump to afford the crude isothiouronium salt (650 mg, 88 %), R_f = 0.1 (EtOAc: Hexane = 3: 2).

The isothiouronium salt (650 mg, 2.80 mmol) was added to a rapidly stirring solution of KOH (433 mg, 6.57 mmol) in methanol (10 mL) at 0°C. After 20 min a less polar spot was observed on TLC (EtOAc: Hexane = 5: 95) corresponding to the thiol. Propargyl bromide (0.51 mL, 80% in toluene, 4.7 mmol) was added drop-wise and the reaction was allowed to warm to room temperature. The reaction yielded one major product on TLC (EtOAc : Hexane = 5 : 95), which was less polar than the starting 4-methoxybenzyl chloride. The methanol was removed under vacuum, water (20 mL) was added and the residue extracted into DCM (3 x 20 mL). After drying the extracts over $MgSO_4$, the solvent was removed under vacuum and the residue chromatographed on silica-gel using ethyl acetate in hexane (5 : 95) to afford **9** as a pungent yellow oil, (474 mg, 77 %).

TLC: R_f = 0.4 (EtOAc: Hexane = 5: 95); ν_{max}/cm^{-1} ($CHCl_3$): 3304 (C-H alkyne); δ_H (400 MHz, d_6-Acetone)[45]: 7.27 (2H, d, *J* = 6.8 Hz, H-3), 6.88 (2H, d, *J* = 6.8 Hz, H-2), 3.83 (2H, s, H-5), 3.78 (3H, s, OMe), 3.15 (2H, d, *J* = 2.8 Hz, H-6), 2.72 (1H, t, *J* = 2.8 Hz, H-8); δ_C (100.6 MHz, d_6-Acetone): 160.0 (C-1), 131.1 (C-3), 130.7 (C-4), 114.9 (C-2), 81.0 (C-7), 72.8 (C-8), 55.7 (OCH_3), 35.5 (C-5), 19.0 (C-6); HRMS (*EI*): *m/z* 193.0701 $[M + H]^+$, $C_{11}H_{13}OS$ requires 193.0687.

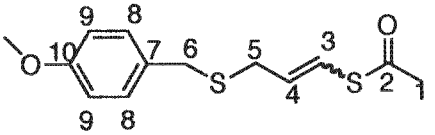

(E/Z)-S-[3-(4-Methoxybenzylthio)prop-1-enyl] ethanethioate, **12**

9 (1.50 g, 7.80 mmol) was dissolved in toluene (15 mL) and the solution heated to 85 °C under N_2. ACCN (195 mg, 0.78 mmol) as a radical initiator was added directly followed by the drop-wise addition of thiolacetic acid (0.66 mL, 9.36 mmol) in toluene (5 mL). The reaction was followed by TLC (EtOAc:

Hexane = 15: 85), which revealed a more polar spot corresponding to the vinyl thioacetate. After 1 hour, a second, more-polar spot began to form corresponding to the bis-substituted addition product, but the reaction was left until starting material had been fully consumed. The solution was allowed to cool, saturated sodium carbonate (20 mL) was then added to quench any remaining thiolacetic acid and the toluene removed under vacuum. The residue was extracted using DCM (3 x 20 mL), which was washed with brine (3 x 15 mL) and dried over $MgSO_4$. The solvent was removed under vacuum and the resulting residue purified by column chromatography (EtOAc: hexane = 5: 95) to afford **12** as a 4: 3 mixture of *Z: E* isomers and as a light-yellow oil (1.42 g, 68 %).

***(E/Z)* mixture**: TLC: R_f = 0.4 (EtOAc: Hexane = 15: 85); ν_{max} / cm^{-1}($CHCl_3$): 1700 (C=O), 663 (C-S); HRMS (EI): *m/z* 307.0404 $[M + NaO]^+$; $C_{13}H_{16}O_3S_2Na$ requires 307.0439 together with *m/z* 285.0636 $[M + H + O]^+$; $C_{13}H_{17}O_4S_2$ requires 285.0619.

***E*-isomer**: δ_H (400 MHz, $CDCl_3$): 7.23 (2H, d, *J* = 8.7 Hz, H-8), 6.85 (2H, d, *J* = 8.7 Hz, H-9), 6.50 (1H, dt, *J* = 15.2, 1.1 Hz, H-3), 5.83 (1H, dt, *J* = 15.2, 7.4 Hz, H-4), 3.80 (3H, s, OMe), 3.63 (2H, s, H-6), 3.08 (2H, dd, *J* = 7.4, 1.1 Hz, H-5), 2.35 (3H, s, H-1); δ_c (100.6 MHz, $CDCl_3$): 192.8 (C-2), 158.6 (C-10), 130.3 (C-4), 130.0 (C-8), 129.8 (C-7), 119.2 (C-3), 113.9 (C-9), 55.2 (OCH_3), 34.3 (C-6), 33.1 (C-5), 30.3 (C-1).

***Z*-isomer**: δ_H (400 MHz, $CDCl_3$): 7.23 (2H, d, *J* = 8.7 Hz, H-8), 6.85 (2H, d, *J* = 8.3 Hz, H-9), 6.67 (1H, dt, *J* = 9.5, 1.0 Hz, H-3), 5.86 (1H, dt, *J* = 9.5, 7.4 Hz, H-4), 3.80 (3H, s, OMe), 3.64 (2H, s, H-6), 3.10 (2H, dd, *J* = 7.4, 1.0 Hz, H-5), 2.38 (3H, s, H-1); δ_c (100.6 MHz, $CDCl_3$): 191.1 (C-2), 158.6 (C-10), 129.9 (C-8), 129.7 (C-7), 128.5 (C-4), 119.4 (C-3), 113.8 (C-9), 55.2 (OCH_3), 35.1 (C-6), 30.6 (C-5), 30.7 (C-1).

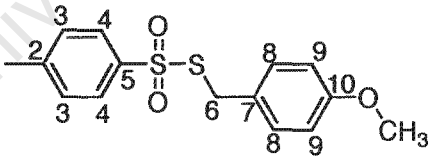

S-4-Methoxybenzyl 4-methylbenzenesulfonothioate, **14**

4-Methoxybenzyl chloride (0.43 mL, 3.2 mmol) and potassium thiotosylate (870 mg, 3.84 mmol) were dissolved in DMF (2 mL) and stirred at 65 °C under N_2. The reaction was allowed to proceed for 1 hour, whereupon a spot-to-spot conversion was observed on TLC (EtOAc: Hexane = 1: 9), with the resulting product more polar than the starting 4-methoxybenzyl chloride. The DMF was removed under vacuum and the residue suspended in water (10 mL), which was extracted with DCM (3 x 15 mL). The organic extracts were washed with water (3 x 15 mL) to remove residual DMF. Following drying and solvent evaporation, the residue was recrystallized using ethyl acetate and hexane to yield **14** as a colourless, crystalline solid, (880 mg, 74 %).

TLC: R_f = 0.3 (EtOAc: Hexane = 1: 9); Mp (MeOH): 58 - 60 °C; ν_{max} / cm^{-1}($CHCl_3$): 1325 (S=O); δ_H (400 MHz, d_6-Acetone)[46]: 7.76 (2H, d *J* = 8.5 Hz, H-4), 7.41 (2H, d, *J* = 8.5 Hz, H-3), 7.16 (2H, d, *J* = 8.8 Hz, H-8), 6.79 (2H, d, *J* = 8.8 Hz, H-9), 4.28 (2H, s, H-6), 3.78 (3H, s, OCH_3), 2.45 (3H, s, H-1); δ_C (100.6 MHz, d_6-Acetone): 160.6 (C-10), 145.9 (C-2), 143.7 (C-5), 131.4 (C-3/4), 130.9 (C-3/4), 128.0 (C-8), 127.1 (C-7), 115.1 (C-9), 55.8 (OCH_3), 40.7 (C-6), 19.7 (C-1).

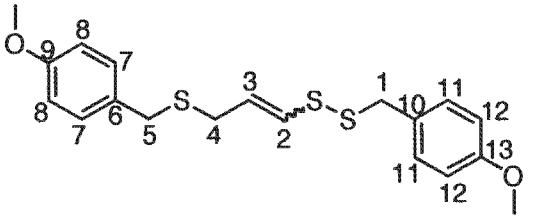

(*E/Z*)-1,8-(Bis-*p*-methoxyphenyl)-2,3,7-trithia-octa-4-ene, **15**

The vinyl thioacetate **12** (870 mg, 3.27 mmol) was dissolved in methanol (2 mL), cooled to -40 °C and stirred under nitrogen. KOH (220 mg, 3.92 mmol) in degassed methanol (1 mL) was added slowly and the reaction was left stirring for 45 minutes, after which it was cooled down to -78 °C. **14** (1.31 g, 4.25 mmol) dissolved in DCM (3 mL) was added and the reaction was allowed to stir for 1 hour at -78 °C before being allowed to warm up. The final product moved along the TLC plate with the same R_f as the vinyl thioacetate, making monitoring difficult. The reaction was quenched with saturated aqueous ammonium chloride (10 mL) at -10 °C, allowed to warm to room temperature and the solvents removed under vacuum on the rotary evaporator. The residue was extracted into DCM (3 x 20 mL), which was washed with brine (3 x 15 mL) and dried over $MgSO_4$. Purification using column chromatography with ethyl acetate in hexane (1: 4) as the eluent afforded **15** as a grey, sweet-smelling oil and as a 4: 3 mixture of *Z/E* isomers, (1.03 g, 83 %).

***(E/Z)* mixture**: TLC: R_f = 0.4 (EtOAc: Hexane 15: 85); ν_{max} / cm^{-1}($CHCl_3$): 450 (S-S); HRMS (EI): *m/z* 417.0629, $[M + Na + O]^+$, $C_{19}H_{22}NaO_3S_3$ requires 417.0629; 789.1478, $[2M + 2O]^+$; $C_{38}H_{44}O_6S_6$ requires 789.1500.

***E*-isomer**: δ_H (400 MHz, $CDCl_3$): 7.24 (4H, m, H-7/11), 6.86 (4H, m, H-8/12), 5.93 (1H, d, *J* = 14.8 Hz, H-2), 5.82, (1H, dt, *J* = 14.8, 7.1 Hz, H-3), 3.90 (2H, s, H-1), 3.80 (3H, s, OCH_3), 3.78 (3H, s, OCH_3), 3.60 (2H, s, H-5), 3.02 (2H, d, *J* = 7.1 Hz, H-4); δ_c (100.6 MHz, $CDCl_3$): 159.1 (C-9/13), 158.6 (C-9/13), 130.4 (C-7/11), 129.9 (C-7/11), 129.8 (C-6.10), 128.7 (C-6/10), 127.8 (C-3), 127.7 (C-2), 113.9 (C-8/12), 55.2 (2 x OCH_3), 42.2 (C-1), 34.5 (C-5), 32.6 (C-4).

***Z*-isomer**: δ_H (400 MHz, $CDCl_3$): 7.24 (4H, m, H-7/11), 6.86 (4H, m, H-8/12), 6.01 (1H, d, *J* = 9.3 Hz, H-2), 5.62, (1H, dt, *J* = 9.3, 7.6 Hz, H-3), 3.90 (2H, s, H-1), 3.81 (3H, s, OCH_3), 3.80 (3H, s, OCH_3), 3.68 (2H, s, H-5), 3.19 (2H, d, *J* = 7.6 Hz, H-4); δ_c (100.6 MHz, $CDCl_3$): 159.1(C-9/13), 158.6 (C-9/13),

131.8 (C-2), 130.4 (C-7/11), 129.9 (C-7/11), 129.8 (C-6/10), 128.7 (C-6/10), 127.9 (C-3), 113.9 (C-8/12), 55.2 (2 x OCH_3), 42.9 (C-1), 35.3 (C-5), 29.2 (C-4).

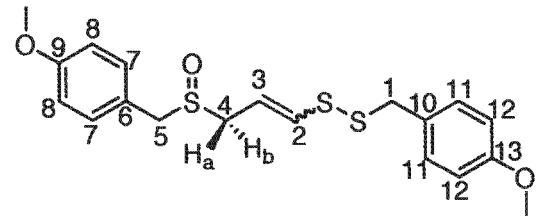

(E/Z)-1,8-(Bis-*p*-methoxyphenyl)-2,3,7-trithia-octa-4-ene 7-oxide, **17**

15 (185 mg, 0.49 mmol) was dissolved in DCM (5 mL) under N_2. The reaction vessel was cooled to -78 °C in a liquid N_2 / acetone bath, and *m*-CPBA (140 mg, 77 % in H_2O, 0.62 mmol) was added directly. The reaction was allowed to stir for 2 hours below -60 °C, producing a single product spot on TLC. Saturated aqueous Na_2CO_3 (10 mL) was added at -60 °C and the reaction was allowed to warm to room temperature. The residue was extracted into DCM (3 x 10 mL), which was washed with brine (3 x 10 mL) and dried over $MgSO_4$. Subsequent TLC analysis revealed an array of minor products formed during the work-up. The residue was purified using column chromatography with 1: 1 ethyl acetate in hexane as the eluent to afford **17** as a white, sweet-smelling solid, which was recrystallized using ethanol. The product was obtained as a 5: 4 mixture of *Z: E* isomers, (128 mg, 69 %).

***(E/Z)* mixture**: TLC: R_f = 0.6 (EtOAc: Hexane 1:1); Mp (EtOH): 111 - 113 °C; ν_{max}/cm^{-1} ($CHCl_3$): 1035 (S=O); HRMS (EI): *m/z* 789.1404 $[2M + H]^+$, $C_{38}H_{45}O_6S_6$ requires 789.1514; *m/z* 417.0630 $[M + Na]^+$, $C_{19}H_{22}NaO_3S_3$ requires 417.0629; CHN_{calc}: C 57.80, H 5.64, O 12.16, S 24.38; CHN_{exp}: C 57.87, H 5.51, O 12.46, S 24.16.

***E*-isomer**: δ_H (400 MHz, $CDCl_3$): 7.21 (4H, m, H-7/11), 6.90 (2H, m, H-8/12), 6.83 (2H, m, H-8/12), 6.18 (1H, d, *J* = 14.8 Hz, H-2), 5.83 (1H, dt, *J* = 14.8, 7.7 Hz, H-3), 3.91 – 3.87 (4H, m, H-1/5), 3.81 (3H, s, OCH_3), 3.77 (3H, s, OCH_3), 3.36 (1H, ddd, *J* = 13.2, 7.9, 0.9 Hz, H-4_a), 3.23 (1H, ddd, *J* = 13.2, 7.9, 0.9 Hz, H-4_b); δ_c (100.6 MHz, $CDCl_3$): 159.8 (C-9/13), 159.2 (C-9/13), 134.2 (C-2), 131.2 (C-7/11), 130.6 (C-7/11), 128.5 (C-6), 121.5 (C-10), 117.0 (C-3), 114.5 (C-8/12), 114.0 (C-8/12), 56.1 (C-5), 55.3 (2 x OCH_3), 52.7 (C-4), 42.2 (C-1).

***Z*-isomer**: δ_H (400 MHz, $CDCl_3$): 7.21 (4H, m, H-7/11), 6.88 (4H, m, H-8/12), 6.28 (1H, d, *J* = 9.5 Hz, H-2), 5.66 (1H, dt, *J* = 9.5, 7.8 Hz, H-3), 3.90-3.87 (2H, m, H-1/5), 3.80 (3H, s, OCH_3), 3.79 (3H, s, OCH_3), 3.49 (1H, ddd, *J* = 13.4, 7.7, 0.9 Hz, H-4_a), 3.39 (1H, ddd, *J* = 13.4, 7.7, 0.9 Hz, H-4_b); δ_c (100.6 MHz, $CDCl_3$): 159.8 (C-9/13), 159.2 (C-9/13), 138.0 (C-2), 131.2 (C-7/11), 130.6 (C-7/11), 128.5 (C-6), 121.6 (C-10), 118.1 (C-3), 114.5 (C-8/12), 114.0 (C-8/12), 56.8 (C-5), 55.3 (2 x OCH_3), 49.5 (C-4), 43.0 (C-1).

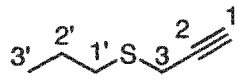

3-(propy-1ylthio)-1-propyne, **22**

Potassium hydroxide (9.70 g, 174.6 mmol) was dissolved in degassed methanol (30 mL) at 0°C under N_2. 1-Propanethiol (10.0 g, 131.3 mmol) was added drop-wise, followed by propargyl bromide (16.4 mL, 147.1 mmol, 80% in toluene) and the reaction was allowed to warm to room temperature, after which TLC (hexane) showed the formation of a less polar UV-active spot to the propargyl bromide. The methanol was then removed under vacuum using the rotary evaporator and the resulting residue extracted into diethyl ether (3 x 100 mL), which was washed with water (3 x 15 mL). The ether extract was dried with $MgSO_4$ and the solvent removed under vacuum to yield a yellow residue, which was purified by distillation (80 °C, 20 mm Hg) to give **22** as a yellow oil, (12.21 g, 81 %).

TLC: R_f = 0.8 (Hexane); ν_{max} / cm^{-1}($CHCl_3$): 3303 (C-H alkyne); δ_H (400 MHz, $CDCl_3$)[47]: 3.22 (2H, d, *J* = 2.6 Hz, H-3), 2.64 (2H, t, *J* = 7.4 Hz, H-1'), 2.21 (1H, t, *J* = 2.6 Hz, H-1), 1.63 (2H, m, H-2'), 0.98 (3H, t, *J* = 7.4 Hz, H-3'); δ_c (100 MHz, $CDCl_3$): 80.1 (C-2), 70.7 (C-1), 33.6 (C-1'), 22.2 (C-2'), 19.0 (C-3), 13.3 (C-3').

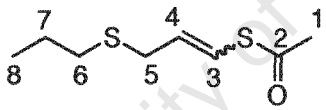

(E/Z)-S-3-(prop-1-ylthio)prop-1-enyl ethanethioate, **23**

22 (2.63 g, 23.0 mmol) was added to dry toluene (20 mL) at room temperature and the solution heated to 80 °C. ACCN (480 mg, 2.0 mmol) was added, followed by drop-wise addition of thiolacetic acid (3 mL, 42 mmol). The mixture was heated at 80 °C under N_2 for 2 hours, after which the solution was allowed to cool. Saturated sodium carbonate (20 mL) was then added to quench any remaining thiolacetic acid and the toluene removed under vacuum. The residue was extracted using DCM (3 x 30 mL), which was washed with brine (3 x 20 mL) and dried over $MgSO_4$. The solvent was removed under vacuum and the resulting orange residue purified by silica-gel chromatography (ethyl acetate: hexane = 1: 49) to give compound **23** as a yellow oil, and as a 5: 3 mixture of *Z / E* stereoisomers, (2.93 g, 67 %).

***(E/Z)* mixture**: TLC: R_f = 0.6 (EtOAc: Hexane = 1: 9); ν_{max} / cm^{-1}($CHCl_3$): 1701 (C=O carbonyl), 634 (C-S); HRMS (EI): m/z 190.0485 $[M]^+$; $C_8H_{14}OS_2$ requires 190.0486.

***E*-isomer**: δ_H (400 MHz, $CDCl_3$)[43]: 6.51 (1H, dt, *J* = 15.6, 1.2 Hz, H-3), 5.81 (1H, dt, *J* = 15.6, 7.6 Hz, H-4), 3.19 (2H, dd, *J* = 7.4, 1.2 Hz, H-5), 2.42 (2H, t, *J* = 7.5 Hz, H-6), 2.33 (3H, s, H-1), 1.58 (2H, m, H-

7), 0.95 (3H, t, J = 7.1Hz, H-8); δ_c (100 MHz, $CDCl_3$): 192.8 (C-2), 130.5 (C-4), 118.7 (C-3), 34.0 (C-5), 32.9 (C-6), 30.3 (C-1), 22.5 (C-7), 13.3 (C-8).

Z-isomer: δ_H (400 MHz, $CDCl_3$)[43]: 6.64 (1H, dt, J = 9.5, 1.1 Hz, H-3), 5.84 (1H, dt, J = 9.7, 7.4 Hz, H-4), 3.16 (2H, dd, J = 7.7, 1.0 Hz, H-5), 2.42 (2H, t, J = 7.1 Hz, H-6), 2.37 (3H, s, H-1), 1.58 (2H, m, H-7), 0.96 (3H, t, J = 7.2 Hz, H-8); δ_c (100 MHz, $CDCl_3$): 191.1 (C-2), 128.9 (C-4), 119.0 (C-3), 33.1 (C-6), 30.9 (C-5), 30.8 (C-1), 22.8 (C-7), 13.4 (C-8).

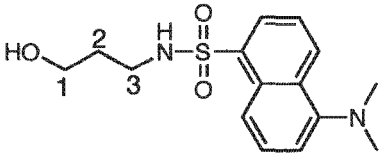

5-(Dimethylamino)-*N*-(3-hydroxypropyl)naphthalene-1-sulfonamide, **25**

3-Aminopropan-1-ol (42 mg, 0.56 mmol) in DCM (1 mL) was added drop-wise to a solution of dansyl chloride (100 mg, 0.37 mmol) and triethylamine (75 mg, 0.74 mmol) in DCM (3 mL) at 0°C, under N_2. The reaction was allowed to warm to room temperature, at which point TLC analysis showed a spot-to-spot conversion from the starting dansyl chloride to a less-polar, fluorescent product. DCM (30 mL) was added and the organic solution washed with saturated aqueous $NaHCO_3$ (15 mL) and dried over $MgSO_4$. Removal of the solvent under vacuum gave a residue, which was purified on a silica-gel column with ethyl acetate as the eluent to afford **25** as a solid, (113 mg, 98 %).

TLC: R_f = 0.6 (EtOAc: Hexane = 4: 1); Mp (EtOAc): 118 – 120 °C, lit[48] 119 – 120 °C; ν_{max} / cm^{-1} ($CHCl_3$): 3386 (OH), 3051 (C-H aromatic), 2957 (C-H aromatic), 1269 (S=O); δ_H (400 MHz, $CDCl_3$): 8.53 (1H, d, J = 8.6 Hz, ArH), 8.28 (1H, d, J = 8.6 Hz, ArH), 8.21 (1H, d, J = 7.3 Hz, ArH), 7.56 - 7.49 (2H, m, ArH), 7.17 (1H, d, J = 7.3 Hz, ArH), 5.36 (1H, t, NH), 3.64 (2H, t, J = 5.4 Hz, H-1), 3.04 (2H, q, J = 6.0 Hz, H-3), 2.88 (6H, s, NMe_2), 1.63 (2H, pent, J = 6.3 Hz, H-2); δ_C (100 MHz, $CDCl_3$): 152.0 (ArC_{qu}), 134.7 (ArC_{qu}), 130.4 (ArC), 129.9 (ArC_{qu}), 129.6 (ArC_{qu}), 129.5 (ArC), 128.3 (ArC), 123.1 (ArC), 118.7 (ArC), 115.2 (ArC), 60.5 (C-1), 45.4 (NMe_2), 41.1 (C-3), 31.5 (C-2).

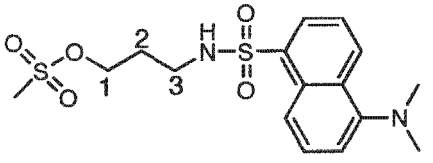

3-(5-(Dimethylamino)naphthalene-1-sulfonamido)propyl methanesulfonate, **26**

25 (250 mg, 0.81 mmol) and triethylamine (164 mg, 1.62 mmol) were dissolved in dry DCM (5 mL) under nitrogen, cooled to 0 °C and mesyl chloride (141 mg, 1.22 mmol) in DCM (1 mL) was slowly

added. The reaction vessel was allowed to reach ambient temperature, with TLC analysis (ethyl acetate: petroleum ether = 1: 1) indicating total conversion of the starting material after 20 minutes. Saturated aqueous $NaHCO_3$ (10 mL) was added, after which the organic material was extracted into DCM (3 x 20 mL). After drying the organic extracts over $MgSO_4$ and removing the solvent, the residue was subjected to column chromatography using ethyl acetate as an eluent to afford **26** as a luminous-green oil (267 mg, 85 %).

TLC: R_f = 0.7 (EtOAc: Hexane = 4: 1); ν_{max} /cm^{-1} ($CHCl_3$): 3051 (C-H aromatic), 2957 (C-H aromatic), 1270 (S=O); δ_H (400 MHz, $CDCl_3$): 8.55 (1H, d, *J* = 8.6 Hz, ArH), 8.25 (1H, d, *J* = 8.6 Hz, ArH), 8.22 (1H, d, *J* = 7.4 Hz, ArH), 7.59 – 7.49 (2H, m, ArH), 7.18 (1H, d, *J* = 7.4 Hz, ArH), 5.22 (1H, t, NH), 4.21 (2H, t, *J* = 5.8 Hz, H-1), 3.02 (2H, q, *J* = 6.4 Hz, H-3), 2.88 (6H, s, NMe_2), 2.16 (3H, s, CH_3), 1.85 (2H, pent, *J* = 6.3 Hz, H-2); δ_C (100 MHz, $CDCl_3$): 152.0 (ArC_{qu}), 134.5 (ArC_{qu}), 130.6 (ArC), 129.9 (ArC_{qu}), 129.5 (ArC_{qu}), 128.5 (ArC), 127.1 (ArC), 123.1 (ArC), 118.5 (ArC), 115.3 (ArC), 66.9 (C-1), 45.3 (NMe_2), 39.2 (C-3), 37.1 (CH_3), 29.3 (C-2).

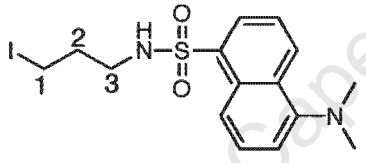

5-(Dimethylamino)-*N*-(3-iodopropyl)naphthalene-1-sulfonamide, **28**

26 (70 mg, 0.18 mmol) was dissolved in acetonitrile (15 mL) containing NaI (540 mg, 3.6 mmol) under nitrogen. The reaction was allowed to proceed at 60° C for 18 hours, after which TLC analysis indicated a spot-to-spot conversion of the mesylate to the less polar iodide. The solvent was removed under vacuum and saturated aqueous Na_2SO_3 (20 mL) was added and the organic material extracted into diethyl ether (3 x 20mL), which was washed with brine (3 x 10 mL). The ether layer was dried over $MgSO_4$, removed under vacuum and the residue purified on a silica-gel column (EtOAc: hexane = 1: 3) to afford **28** as a luminous-green wax, (74 mg, 97%).

TLC: R_f = 0.5 (EtOAc: Hexane = 3: 7); ν_{max} / cm^{-1} ($CHCl_3$): 1270 (S=O); HRMS (EI) *m/z*: 419.0273 [M + H]$^+$; $C_{15}H_{20}IN_2O_2S$ requires 419.0290; δ_H (400 MHz, $CDCl_3$): 8.55 (1H, d, *J* = 8.6 Hz, ArH), 8.29 (1H, d, *J* = 8.6 Hz, ArH), 8.27 (1H, d, *J* = 7.3 Hz, ArH), 7.59 – 7.51 (2H, m, ArH), 7.19 (1H, d, *J* = 7.3 Hz, ArH), 4.87 (1H, t, NH), 2.97 (2H, q, *J* = 6.5 Hz H-3), 2.96 (2H, t, *J* = 5.3 Hz H-1), 2.90 (6H, s, NMe_2), 1.88 (2H, pent, *J* = 6.0 Hz, H-2); δ_C (100 MHz, $CDCl_3$): 152.1 (ArC_{qu}), 134.5 (ArC_{qu}), 130.6 (ArC), 130.0 (ArC_{qu}), 129.8 (ArC), 129.6 (ArC_{qu}), 128.5 (ArC), 123.2 (ArC), 118.5 (ArC), 115.2 (ArC), 45.4 (NMe_2), 43.5 (C-3), 33.0 (C-2), 30.9 (C-1).

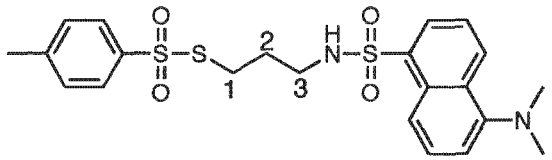

S-3-(5-(Dimethylamino)naphthalene-1-sulfonamido)propyl 4-methylbenzenesulfonothioate, **27**

Iodide **28** (0.20 g, 0.48 mmol) and potassium thiosulfonate (0.87 g, 3.82 mmol) were dissolved in acetonitrile (30 mL). The reaction was allowed to stir at room temperature overnight under N_2, after which TLC analysis indicated the formation of the thiotosylate product, appearing below the iodide on the plate. Despite the large excess of potassium thiosulfonate used, the reaction did not proceed to completion. The solvent was removed under vacuum and the organic material extracted into ethyl acetate (20 mL), which was washed with water (3 x 20 mL), followed by brine (1 x 20 mL) and dried over $MgSO_4$. Following the removal of the solvent under vacuum, purification using silica-gel column chromatography was avoided, as the resulting yellow-oil proved to be unstable and decompose. It was used directly in the syntheses of disulfides **29** and **31**, (184 mg, 80 %).

TLC: R_f = 0.3 (EtOAc: Hexane = 3: 7).

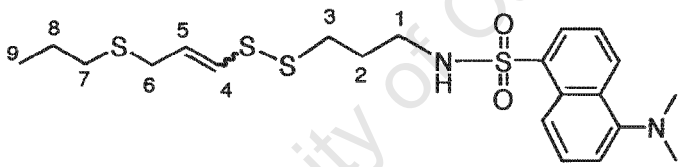

5-(Dimethylamino)-*N*-(3-((3-(propylthio)prop-1-enyl)disulfanyl)propyl)naphthalene-1-sulfonamide, **29**

A solution of **23** (78 mg, 0.40 mmol) in dry degassed methanol (1 mL) was prepared and cooled to -40 °C, under N_2. KOH (28 mg, 0.48 mmol) in methanol (1 mL) was added and after 30 minutes, the solution was further cooled to -78 °C. The unpurified sulfenylating agent **6** (300 mg, 0.63 mmol) in anhydrous DCM (1 mL) was added. The product moved with the same R_f as the iodide **5** (unreacted starting material of **6**) and so after 2 hours, saturated aqueous NH_4Cl (10 mL) was added, the solvent removed under vacuum and the product extracted into DCM (3 x 20 mL). The extracts were washed with brine (2 x 10 mL), dried over $MgSO_4$ and the solvent removed under vacuum. The resulting residue was purified using silica-gel column chromatography (EtOAc) to afford **29** as a 5: 3 mixture of Z/E-isomers and as a luminous-green oil (132 mg, 71 %).

***(E/Z)* mixture**: TLC: R_f = 0.7 (EtOAc: Hexane = 1: 4); ν_{max} / cm^{-1}($CHCl_3$): 1142 (sulfonamide), 541 (S-S); HRMS (EI): m/z, 471.1274 $[M + H]^+$; $C_{21}H_{31}N_2O_2S_4$ requires 471.1268.

***E*-isomer**: δ_H (400 MHz, $CDCl_3$): 8.54 (1H, d, *J* = 8.5 Hz, ArH), 8.29 (1H, d, *J* = 8.6 Hz, ArH), 8.25 (1H, d, *J* = 7.2 Hz, ArH), 7.54 (2H, m, ArH), 7.19 (1H, d, *J* = 7.5 Hz, ArH), 6.02 (1H, dt, *J* = 14.6, 1.0 Hz, H-4), 5.81 (1H, dt, *J* = 14.6, 7.3 Hz, H-5), 4.99 (1H, t, NH), 3.13 (2H, d, *J* = 7.3 Hz, H-6), 3.01 (2H, q, *J* = 6.5 Hz, H-1), 2.89 (6H, s, NMe_2), 2.57 (2H, t, *J* = 6.9 Hz, H-3), 2.41 (2H, t, *J* = 7.4 Hz, H-7), 1.78 (2H, pent, *J* = 6.8 Hz, H-2), 1.57 (2H, m, H-8), 0.96 (3H, t, *J* = 7.4 Hz, H-9); δ_C (100 MHz, $CDCl_3$): 152.0 (ArC_{qu}), 134.6 (ArC_{qu}), 130.5 (ArC), 129.9 (ArC_{qu}), 129.7 (ArC_{qu} and ArC), 128.7 (C-5), 128.4 (ArC), 127.1 (C-4), 123.2 (ArC), 118.6 (ArC), 115.2 (ArC), 45.4 (NMe_2), 41.6 (C-1), 34.8 (C-3), 33.4 (C-7), 33.1 (C-6), 28.7 (C-2), 22.6 (C-8), 13.4 (C-9).

***Z*-isomer**: δ_H (400 MHz, $CDCl_3$): 8.54 (1H, d, *J* = 8.5 Hz, ArH), 8.29 (1H, d, *J* = 8.6 Hz, ArH), 8.25 (1H, d, *J* = 7.2 Hz, ArH), 7.54 (2H, m, ArH), 7.19 (1H, d, *J* = 7.5 Hz, ArH), 6.06 (1H, d, *J* = 9.2 Hz, H-4), 5.64 (1H, dt, *J* = 9.2, 7.8 Hz, H-5), 4.99 (1H, t, NH), 3.19 (2H, d, *J* = 7.8 Hz, H-6), 3.01 (2H, q, *J* = 6.5 Hz, H-1), 2.89 (6H, s, NMe_2), 2.59 (2H, t, *J* = 6.9 Hz, H-3), 2.43 (2H, t, *J* = 7.4 Hz, H-7), 1.78 (2H, pent, *J* = 6.8 Hz, H-2), 1.57 (2H, m, H-8), 0.95 (3H, t, *J* = 7.4 Hz, H-9); δ_C (100 MHz, $CDCl_3$): 152.0 (ArC_{qu}), 134.6 (ArC_{qu}), 131.2 (C-4), 130.5 (ArC), 129.9 (ArC_{qu}), 129.7 (ArC_{qu} and ArC), 128.9 (C-5), 128.4 (ArC), 123.2 (ArC), 118.6 (ArC), 115.2 (ArC), 45.4 (NMe_2), 41.6 (C-1), 35.5 (C-3), 33.4 (C-7), 29.3 (C-6), 28.6 (C-2), 22.8 (C-8), 13.4 (C-9).

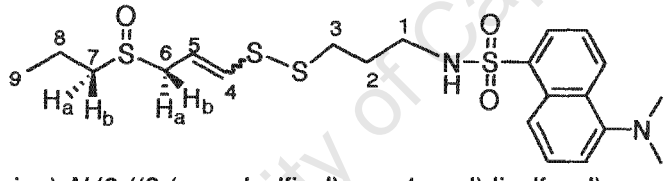

5-(Dimethylamino)-*N*-(3-((3-(propylsulfinyl)prop-1-enyl)disulfanyl)propyl)naphthalene-1-sulfonamide, **30**

Disulfide **29** (70 mg, 0.11 mmol) was dissolved in DCM (5 mL) under N_2. The reaction vessel was cooled to -78 °C in a liquid N_2 / acetone bath and *m*-CPBA (25 mg, 77 % in H_2O, 0.11 mmol) was added. The reaction was allowed to stir for 2 hours bellow -60 °C to produce a single spot on TLC. Saturated aqueous Na_2CO_3 (10 mL) was added at -60 °C and the reaction was allowed to warm to room temperature. The residue was extracted into DCM (3 x 20 mL), which was washed with brine (3 x 10 mL) and dried over $MgSO_4$. Subsequent TLC analysis revealed an array of minor products formed during the work up. Following solvent evaporation the residue was purified using column chromatography (EtOAc) to afford **30** as a luminous-green oil and as a 3: 2 mixture of *E/Z*- isomers, (48 mg, 66 %).

(*E/Z*) mixture: R_f = 0.2 (EtOAc: Hexane = 1: 1); ν_{max} / cm^{-1}($CHCl_3$): 1142 (sulfonamide), 1010 (sulfoxide), 541 (S-S); HRMS (EI): m/z 487.1221 $[M]^+$; $C_{21}H_{31}N_2O_3S_4$ requires 487.1218.

***E*-isomer**: δ_H (400 MHz, $CDCl_3$): 8.54 (1H, d, *J* = 8.5, Hz, ArH), 8.34 (1H, m, ArH), 8.22 (1H, m, ArH), 7.54 (2H, m, ArH), 7.19 (1H, m, ArH), 6.34 (1H, d, *J* = 14.7 Hz, H-4), 6.06 (1H, t, NH), 5.93 (1H, dt, *J* =

14.7, 7.4 Hz, H-5), 3.53 (1H, dd, J = 13.2, 8.4 Hz, H-6_a), 3.38 (1H, dd, J = 13.2, 8.4 Hz, H-6_b), 2.99 (2H, q, J = 6.5 Hz, H-1), 2.89 (6H, s, NMe_2), 2.79 – 2.59 (4H, m, H-3 and H-7), 1.81 (4H, m, H-2 and H-8), 1.08 (3H, t, J = 7.4 Hz, H-9); δ_C (100 MHz, $CDCl_3$): 151.9 (ArC_{qu}), 135.2 (ArC_{qu}), 134.6 (C-4), 130.2 (ArC), 130.0 (ArC_{qu}), 129.7 (ArC_{qu}), 129.3 (ArC), 128.2 (ArC), 123.2 (ArC), 119.1 (ArC), 117.5 (C-5), 115.2 (ArC), 53.9 (C-6), 53.3 (C-7), 45.4 (NMe_2), 41.5 (C-1), 35.7 (C-3), 29.0 (C-2), 16.4 (C-8), 13.4 (C-9).

***Z*-isomer**: δ_H (400 MHz, $CDCl_3$): 8.54 (1H, d, J = 8.5, Hz, ArH), 8.34 (1H, m, ArH), 8.22 (1H, m, ArH), 7.54 (2H, m, ArH), 7.19 (1H, m, ArH), 6.46 (1H, d, J = 9.4 Hz, H-4), 5.73 (1H, dt, J = 9.4, 8.2 Hz, H-5), 5.63 (1H, t, NH), 3.57 (2H, d, J = 8.9 Hz, H-6_a and H-6_b), 2.99 (2H, q, J = 6.5 Hz, H-1), 2.89 (6H, s, NMe_2), 2.79 – 2.59 (4H, m, H-3 and H-7), 1.81 (4H, m, H-2 and H-8), 1.08 (3H, t, J = 7.4 Hz, H-9); δ_C (100 MHz, $CDCl_3$): 152.0 (ArC_{qu}), 137.8 (C-4), 134.9 (ArC_{qu}), 130.4 (ArC), 130.0 (ArC_{qu}), 129.7 (ArC_{qu}), 129.5 (ArC), 128.3 (ArC), 123.2 (ArC), 119.5 (C-5), 118.9 (ArC), 115.2 (ArC), 53.6 (C-7), 50.9 (C-6), 45.4 (NMe_2), 41.6 (C-1), 35.6 (C-3), 28.9 (C-2), 16.4 (C-8), 13.4 (C-9).

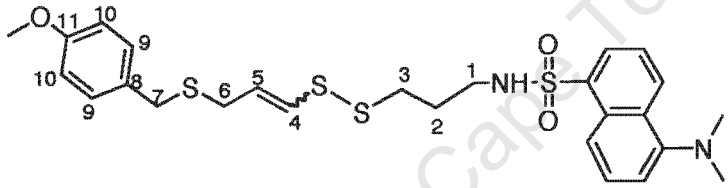

5-(Dimethylamino)-*N*-(3-((3-(4-methoxybenzylthio)prop-1-enyl)disulfanyl)propyl)naphthalene-1-sulfonamide, **31**

A solution of **12** (254 mg, 0.95 mmol) in dry degassed methanol (10 mL) was prepared and cooled to -40 °C under N_2. KOH (100 mg, 1.8 mmol) in methanol (5 mL) was added and after 30 minutes the reaction was further cooled to -78 °C, after which the crude dansyl sulfenylating agent **6** (960 mg, 2.0 mmol) in dry DCM (2 mL) was added. This resulted in the formation of the disulfide product as reflected by a fluorescent spot lying between the two starting materials on TLC after 30 minutes. After an hour, saturated aqueous NH_4Cl (10 mL) was added and the reaction was allowed to warm to room temperature, after which the organic material was extracted directly into DCM (3 x 20 mL). The organic extracts were washed with brine (3 x 20 mL), dried over $MgSO_4$ and the solvent removed under vacuum. The residue was purified using column chromatography (ethyl acetate: hexane = 3: 7) to afford **31** as a 6: 5 mixture of *E/Z*- isomers and as a green oil (470 mg, 90%).

(*E/Z*)-mixture: TLC: R_f = 0.7 (EtOAc: Hexane = 3: 7); ν_{max} / cm^{-1}($CHCl_3$): 517 (S-S); HRMS (EI): *m/z* 549.1385 $[M + H]^+$; $C_{26}H_{33}N_2O_3S_4$ requires 549.1374.

***E*-isomer**: δ_H (400 MHz, $CDCl_3$): 8.58 (1H, d, J = 8.6 Hz, ArH), 8.30 (1H, d, J = 8.6 Hz, ArH), 8.25 (1H, dd, J = 7.3 Hz, ArH), 7.55 (2H, m, ArH), 7.21 (3H, m, ArH and H-9), 6.84 (2H, m, H-10), 5.98 (1H, d, J = 14.6 Hz, H-4), 5.80 (1H, dt, J = 14.6, 7.3 Hz, H-5), 4.77 (1H, t, J = 6.5 Hz, NH), 3.80 (3H, s, OMe), 3.61

(2H, s, H-7), 3.04 (2H, d, J = 7.3 Hz, H-6), 3.01 (2H, m, H-1), 2.91 (6H, s, NMe_2), 2.59 (2H, t, J = 6.8 Hz, H-3), 1.78 (2H, m, H-2); δ_C (100 MHz, $CDCl_3$): 158.8 (C-11), 152.1 (ArC_{qu}), 134.7 (ArC_{qu}), 130.4 (ArC), 130.0 (C-9 and ArC_{qu}), 129.8 (ArC and C-8), 129.6 (ArC_{qu}), 128.4 (ArC and C-5), 127.5 (C-4), 123.5 (ArC), 119.2 (ArC), 115.5 (ArC), 114.0 (C-10), 55.3 (OCH_3), 45.5 (NMe_2), 41.7 (C-1), 35.5 (C-3), 34.9 (C-7), 32.7 (C-6), 28.9 (C-2).

***Z*-isomer**: δ_H (400 MHz, $CDCl_3$): 8.58 (1H, d, J = 8.6 Hz, ArH), 8.30 (1H, d, J = 8.6 Hz, ArH), 8.25 (1H, dd, J = 7.3 Hz, ArH), 7.55 (2H, m, ArH), 7.21 (3H, m, ArH and H-9) 6.84 (2H, m, H-10), 6.08 (1H, d, J = 9.2 Hz, H-4), 5.64 (1H, dt, J = 9.2, 7.8 Hz, H-5), 4.77 (1H, t, J = 6.5 Hz, NH), 3.80 (3H, s, O-CH_3), 3.65 (2H, s, H-7), 3.15 (2H, d, J = 7.8 Hz, H-6), 3.01 (2H, m, H-1), 2.91 (6H, s, NMe_2), 2.58 (2H, t, J = 7.0 Hz, H-3) 1.78 (2H, m, H-2); δ_C (100 MHz, $CDCl_3$): 158.8 (C-11), 152.1 (ArC_{qu}), 134.8 (ArC_{qu}), 131.6 (C-4), 130.4 (ArC), 130.0 (C-9 and ArC_{qu}), 129.8 (ArC and C-8), 129.6 (ArC_{qu}), 128.6 (C-5), 128.4 (ArC), 123.5 (ArC), 119.2 (ArC), 115.5 (ArC), 114.0 (C-10), 55.3 (OCH_3), 45.5 (NMe_2), 41.7 (C-1), 35.5 (C-3), 34.8 (C-7), 29.3 (C-6), 28.7 (C-2).

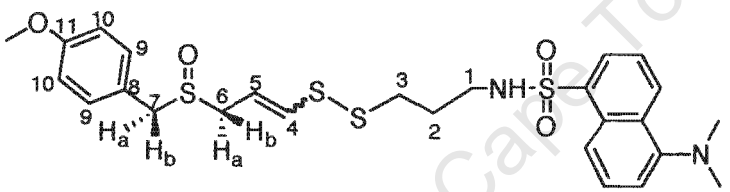

5-(Dimethylamino)-*N*-(3-((3-(4-methoxybenzylsulfinyl)prop-1-enyl)disulfanyl)propyl)naphthalene-1-sulfonamide, **32**

Disulfide **31** (420 mg, 0.59 mmol) was dissolved in DCM (10 mL) under N_2. The reaction vessel was cooled to -78 °C in a liquid N_2 / acetone bath and *m*-CPBA (150 mg, 77 % in H_2O, 0.67 mmol) was added directly as a solid. The reaction was allowed to stir for 2 hours below -60 °C, which produced a single polar product spot on TLC. Saturated aqueous Na_2CO_3 (10 mL) was added at -60 °C and the reaction was allowed to warm to room temperature. The residue was extracted into DCM (3 x 20 mL), which was washed with brine (3 x 10 mL) and dried over $MgSO_4$. Subsequent TLC analysis revealed an array of minor products formed during the work up. The residue was purified using column chromatography (ethyl acetate: hexane = 1: 1) to afford **32** as a luminous-green oil and in a 6: 5 mixture of *E/Z*- isomers (308 mg, 72%).

(*E/Z*)-mixture: TLC: R_f = 0.3 (EtOAc: Hexane = 2: 1); ν_{max} / cm^{-1}($CHCl_3$): 1033 (S=O); HRMS (EI): m/z 565.1331, $[M + H]^+$; $C_{26}H_{33}N_2O_4S_4$ requires 565.1323.

***E*-isomer**: δ_H (400 MHz, $CDCl_3$): 8.54 (1H, d, J = 8.5 Hz, ArH), 8.34 (1H, t, J = 7.8 Hz, ArH), 8.22 (1H, d, J = 7.2 Hz, ArH), 7.50 (2H, m, ArH), 7.21 (3H, m, ArH and H-9), 6.89 (2H, m, H-10), 6.31 (1H, d, J = 14.8 Hz, H-4), 6.08 (1H, t, J = 5.7 Hz, NH), 5.92 (1H, dt, J = 14.8, 7.6 Hz, H-5), 4.02 (1H, d, J = 13.0 Hz, H-7a), 3.94 (1H, d, J = 13.0 Hz, H-7b), 3.79 (3H, s, OCH_3), 3.42 (1H, dd, J = 13.1, 7.6 Hz, H-6a),

3.24 (1H, dd, J = 13.1, 7.6 Hz, H-6b), 2.98 (2H, m, H-1), 2.89 (6H, s, NMe_2), 2.67 (2H, t, *J* = 6.8 Hz, H-3), 1.85 (2H, m, H-2); δ_C (100 MHz, $CDCl_3$): 159.8 (C-11), 151.8 (ArC_{qu}), 135.2 (ArC_{qu}), 134.7 (C-4), 131.2 (C-9), 130.1 (ArC), 129.9 (ArC_{qu}), 129.7 (ArC_{qu}), 129.3 (ArC), 128.2 (ArC), 123.3 (ArC), 121.4 (C-8), 119.4 (ArC), 117.3 (C-5), 115.2 (ArC), 114.6 (C-10), 56.4 (C-7), 55.3 (OCH_3), 52.0 (C-6), 45.4 (NMe_2), 41.5 (C-1), 35.6 (C-3), 29.0 (C-2).

Z-isomer: δ_H (400 MHz, $CDCl_3$): 8.54 (1H, d, *J* = 8.5 Hz, ArH), 8.34 (1H, t, *J* = 7.8 Hz, ArH), 8.22 (1H, d, *J* = 7.2 Hz, ArH), 7.50 (2H, m, ArH), 7.21 (3H, m, ArH and H-9), 6.89 (2H, m, H-10), 6.45 (1H, d, *J* = 9.4 Hz, H-4), 5.71 (1H, dt, *J* = 9.4, 7.4 Hz, H-5), 5.69 (1H, t, *J* = 5.5 Hz, NH), 3.98 (1H, d, *J* = 12.5 Hz, H-7a), 3.94 (1H, d, *J* = 12.5 Hz, H-7b), 3.79 (3H, s, OCH_3), 3.52 (1H, dd, *J* = 11.3, 7.4 Hz, H-6a), 3.47 (1H, dd, *J* = 11.3, 7.4 Hz, H-6b), 2.99 (2H, t, *J* = 6.4 Hz, H-1,) 2.89 (6H, s, NMe_2), 2.64 (2H, t, *J* = 7.3 Hz, H-3), 1.79 (2H, m, H-2); δ_C (100 MHz, $CDCl_3$): 159.8 (C-11), 151.8 (ArC_{qu}), 137.9 (C-4), 135.0 (ArC_{qu}), 131.3 (C-9), 130.3 (ArC), 129.9 (ArC_{qu}), 129.7 (ArC_{qu}), 129.5 (ArC), 128.3 (ArC), 123.3 (ArC), 121.5 (C-8), 119.6 (C-5), 119.2 (ArC), 115.2 (ArC), 114.5 (C-10), 57.1 (C-7), 55.3 (OCH_3), 49.5 (C-6), 45.4 (NMe_2), 41.7 (C-1), 35.5 (C-3), 28.9 (C-2).

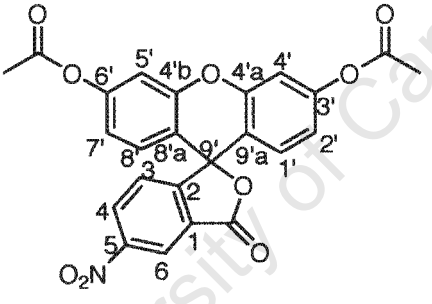

5-Nitro-3-oxo-3*H*-spiro[isobenzofuran-1,9'-xanthene]-3',6'-diyl diacetate, **42**

4-Nitrophthalic acid (7.0 g, 30.5 mmol) and resorcinol (7.7 g, 61 mmol) were combined in an open Erlenmeyer flask. The mixture was heated with stirring for 3 hours and kept between 180-190 °C, whereby the melt solidified into a dark red-brown mass. On cooling, the crude material was ground to a course powder with a pestel and mortar and refluxed in 0.5 M HCl (100 mL) for 1 hour to solubilize the unreacted starting materials. The solid material was then filtered with a Büchner funnel, washed with water (3 X 30 mL) and dried under vacuum at 80 °C. The solid material (9.9 g) was refluxed in Ac_2O (40 mL) for 3 hours, filtered hot through a sintered glass funnel and stored at -20 °C for 4 days for crystallization.

The 5-nitrofluorescein diacetate **42**[51] crystals were collected and the mother liquor was concentrated to one quarter of its original volume and again stored at -20 °C overnight for further crystallization. This afforded a second crop, which was collected and combined with the previous material. The combined material was recrystalized twice from Ac_2O to yield pure 5-nitrofluorescein diacetate **42**, (2.4 g, 17 %).

Mp_{lit}[51] (Ac_2O) 215 – 218 °C; Mp_{exp} (Ac_2O) 216 – 218 °C.

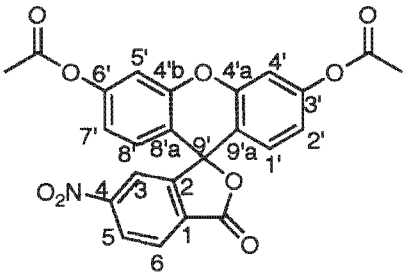

4-Nitro-3-oxo-3H-spiro[isobenzofuran-1,9'-xanthene]-3',6'-diyl diacetate, **43**

The 4-nitrofluorescein diacetate **43** was isolated by evaporating all of the Ac_2O from the mother liquor used to obtain the 5-nitro derivative. This afforded a brown-viscous syrup, which was then dissolved into hot toluene (15 mL) to give needle-like crystals upon cooling. A further recrystallization from hot toluene yielded 4-nitrofluorescein diacetate **43**, (2.6 g, 18 %).

Mp_{lit}[51] (toluene) 190 °C; Mp_{exp} (toluene) 189 – 190 °C.

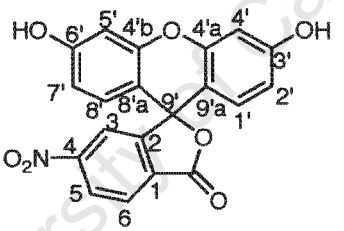

3',6'-Dihydroxy-6-nitro-3*H*-spiro[isobenzofuran-1,9'-xanthen]-3-one, **45**

4-Nitrofluorescein diacetates **43** (5.0 g, 10.2 mmol) was heated in a mixture of 10% aqueous sodium hydroxide (50 mL) and methanol (250 mL) until a dark red homogenous solution was obtained. The warm solution was diluted with water (75 mL), acidified with glacial acetic acid (25 mL) and heated again until boiling. The solution was allowed to cool slowly and then left in an icebox for 3 hours. The orange precipitate was collected using a Büchner funnel, washed with water (50 mL) and dried under vacuum at 80° C for 3 hours. The product **45** was an orange solid (3.03 g, 79%).

Mp_{lit}[51] > 250 °C (dec.); Mp_{exp} > 250 °C (dec.); δ_H[51] (400 MHz, d_6-DMSO): 10.26 (2H, br. S, OH), 8.48 (1H, dd, J = 8.4, 2.0 Hz, H-5), 8.24 (1H, d, J = 8.4 Hz, H-6), 8.08 (1H, d, J = 2.0 Hz, H-3), 6.67 (4H, m, H-1'/2'/7'/8'), 6.54 (2H, dd, J = 8.7, 2.3 Hz, H-4'/5').

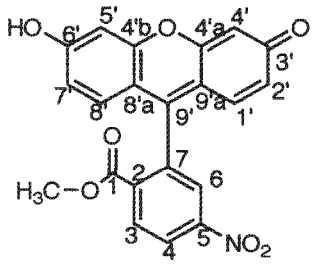

Methyl 2-(6-hydroxy-3-oxo-3*H*-xanthen-9-yl)-5-nitrobenzoate, **47**

4-Nitrofluorescein **45** (800 mg, 2.12 mmol), methanol (25 mL) and concentrated sulfuric acid (1 mL) were refluxed for 48 hours. The resulting yellow solution was diluted with Et_2O (40 mL) and left in the freezer for a further 48 hours to crystallize. The resulting brown precipitate was filtered with a Büchner funnel yielding a solid that was presumably the half bisulfate salt of the phenol, (920 mg, 89%).

The intermediate (560 mg, 1.1 mmol) was suspended in a 1:1 mixture of water and methanol (40 mL). Aqueous Na_2PO_4 (10 %) was added to adjust the pH to 5. The mixture was stirred for 20 minutes, the resulting dark-red precipitate collected with a Büchner funnel and dried on the bench overnight to afford the methyl ester **47**, (337 mg, 75%).

Mp > 275 °C (dec.); HRMS (*EI*): 392.0760 $[M + H]^+$; $C_{21}H_{14}NO_7$ requires 392.0770; CHN anal. Calc. for $C_{21}H_{13}NO_7$: C 64.45, H 3.35, N 3.50 %; Found: C 64.39, H 3.11, N 3.43 %; δ_H (400 MHz, d_6-DMSO): 8.55 (1H, dd, *J* = 8.7, 2.2 Hz, H-4), 8.40 (1H, d, *J* = 8.7 Hz, H-3), 8.34 (1H, d, *J* = 2.2 Hz, H-6), 6.88 (2H, d, *J* = 9.2 Hz, H-1'/8'), 6.60 (2H, br. s, H-4'/5'), 6.57 (2H, d, *J* = 9.2 Hz, 2'/7'), 3.62 (3H, s, CH_3); δ_C (100 MHz, d_6-DMSO): 206.3 (C-3'), 173.5 (C-1), 167.0 (ArC_{qu}), 164.1 (ArC_{qu}), 156.0 (ArC_{qu}), 149.8 (ArC_{qu}), 147.8 (ArC_{qu}), 135.3 (ArC_{qu}), 135.1 (ArC_{qu}), 132.4 (C-3), 129.9 (C-1'/8'), 125.6 (C-6), 124.7 (C-4), 121.5 (ArC_{qu}), 114.8 (ArC_{qu}), 103.4 (C-2'/4'/5'/7'), 52.8 (CH_3).

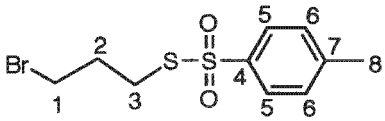

S-3-Bromopropyl 4-methylbenzenesulfonothioate, **49**

A solution of potassium thiotosylate (1.17 g, 5.17 mmol) and 1,3-dibromopropane (2.0 mL, 20.6 mmol), in acetonitrile (30 mL) was heated to 80 °C whilst stirring under N_2. After 2 hours, TLC analysis revealed complete consumption of the thiotosylate salt. The solvent was removed under vacuum, water (20 mL) was added and the organic material extracted into DCM (25 mL), which was washed with water (3 x 20 mL), brine (1 x 20 mL) and dried over $MgSO_4$. The residue was purified by column chromatography (EtOAc: hexane = 1: 9), yielding **49** as an opaque wax, (1.19 g, 76%).

TLC: R_f 0.3 (EtOAc: Hexane = 1: 9); ν_{max} / cm^{-1}($CHCl_3$): 740 (S-SO_2R), 590 (C-Br); CHN anal. Calc. for $C_{10}H_{13}O_2S_2Br$: C 38.84, H 4.24, S 20.74 %; Found: C 39.16, H 4.23, S 21.05 %; δ_H (400 MHz, $CDCl_3$): 7.81 (2H, d, *J* = 8.7 Hz, H-5), 7.35 (2H, d, *J* = 8.7 Hz, H-6), 3.41 (2H, t, *J* = 6.6 Hz, H-3), 3.12 (2H, t, *J* = 6.6 Hz, H-1), 2.45 (3H, s, H-8), 2.18 (2H, pent, *J* = 6.6 Hz, H-2); δ_C (100 MHz, $CDCl_3$): 145.0 (C-4), 141.7 (C-7), 129.9 (C-5), 127.0 (C-6), 34.1 (C-8), 31.4 (C-1), 31.1 (C-3), 21.6 (C-2).

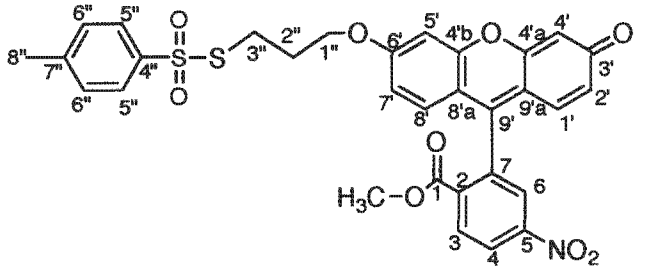

Methyl 5-nitro-2-(3-oxo-6-(3-(tosylthio)propoxy)-3*H*-xanthen-9-yl)benzoate, **51**

A solution of **49** (650 mg, 2.10 mmol), 5-nitrofluorescein methyl ester (800mg, 2.04 mmol) and K_2CO_3 (565 mg, 4.09 mmol) in acetonitrile (20 mL), was refluxed under N_2. TLC analysis after 2 hours revealed the full consumption of the methyl ester and the formation of a less-polar product. The solvent was removed under vacuum, water (30 mL) was added and the organic residue extracted into DCM (3 x 30 mL), which was washed with brine (3 x 20 mL) and dried over $MgSO_4$. Purification by silica-gel column chromatography (EtOAc: hexane = 7: 3) afforded **51** as an orange solid, (719 mg, 58 %).

TLC: R_f = 0.2 (EtOAc: Hexane = 4: 1); Mp (MeOH) 106 – 108 °C; ν_{max} / cm^{-1}($CHCl_3$): 1732 (CO_2CH_3); HRMS (EI): m/z 620.1057, $[M + H]^+$; $C_{31}H_{26}NO_9S_2$ requires 620.1049; CHN anal. Calc. for $C_{31}H_{25}NO_9S_2$: C 60.09, H 4.07, N 2.26, S 10.35 %; Found: C 59.68, H 4.03, N 2.06, S 10.32 %; δ_H (400 MHz, $CDCl_3$): 8.48 (1H, dd, *J* = 8.5, 2.2 Hz, H-4), 8.40 (1H, d, *J* = 8.5 Hz, H-3), 8.18 (1H, d, *J* = 2.2 Hz, H-6), 7.79 (2H, d, *J* = 8.2 Hz, H-5"), 7.32 (2H, d, *J* = 8.2 Hz, H-6"), 6.90 (1H, d, *J* = 2.3 Hz, H-5'), 6.79 (1H, d, *J* = 8.9 Hz, H-8'), 6.75 (1H, d, *J* = 9.7 Hz, H-1'), 6.72 (1H, dd, *J* = 8.9, 2.3 Hz, H-7'), 6.56 (1H, dd, *J* = 9.7, 1.9 Hz, H-2'), 6.47 (1H, d, *J* = 1.9 Hz, H-4'), 4.11 (2H, m, H-1"), 3.69 (3H, s, CO_2CH_3), 3.18 (2H, t, *J* = 6.7 Hz, H-3"), 2.43 (3H, s, H-8"), 2.21 (2H, pent, *J* = 6.5 Hz, H-2"); δ_C (100 MHz, $CDCl_3$): 185.2 (C-3'), 171.0 (C-1), 164.0 (ArC_{qu}), 163.2 (ArC_{qu}), 158.4 (ArC_{qu}), 154.2 (ArC_{qu}), 149.9 (ArC_{qu}), 146.4 (ArC_{qu}), 145.0 (ArC_{qu}), 141.7 (ArC_{qu}), 136.2 (ArC_{qu}), 135.9 (ArC_{qu}), 132.5 (C-3), 130.6 (ArC), 129.9 (C-6"), 129.3 (ArC), 128.3 (ArC), 127.0 (C-5"), 125.5 (C-6), 124.4 (C-4), 118.0 (ArC_{qu}), 113.8 (ArC), 106.2 (ArC), 101.3 (ArC), 66.4 (C-1"), 53.1 (OCH_3), 32.3 (C-3"), 28.4 (C-2"), 21.6 (C-8").

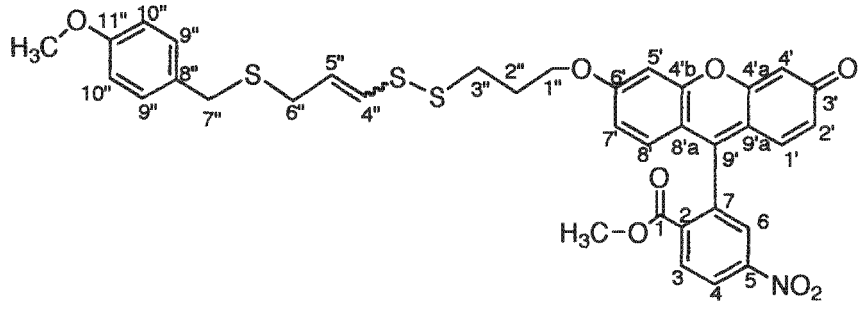

Methyl 2-(6-(3-((3-(4-methoxybenzylthio)prop-1-enyl)disulfanyl)propoxy)-3-oxo-3*H*-xanthen-9-yl)-4-nitrobenzoate, **52**

12 (205 mg, 0.76 mmol) was dissolved in dry degassed MeOH (10 mL) and the solution cooled to -40 °C under N_2. KOH (50 mg, 0.9 mmol) in MeOH (3 mL) was added, and after 30 minutes the solution was further cooled to -78 °C. **51** (380 mg, 0.61 mmol) in anhydrous DCM (2 mL) was added drop-wise and TLC analysis after 1 hour indicated the formation of the disulfide product as reflected by a fluorescent spot lying between the two starting materials as well as the total consumption of the starting sulfenylating agent. Saturated aqueous NH_4Cl (10 mL) was added and the solvent removed under vacuum. The organic and aqueous residues were extracted by DCM (3 x 30 mL), which was washed with brine (2 x 20 mL) and dried over $MgSO_4$. Purification using silica-gel column chromatography (EtOAc: hexane = 4: 1) afforded **52** as an orange oil, and as a 1: 1 mixture of *Z/E* stereoisomers, (354 mg, 84 %).

(*E/Z*)-mixture: TLC: R_f = 0.3 (EtOAc: Hexane = 7: 3); ν_{max} / cm^{-1}($CHCl_3$): 1730 (CO_2CH_3), 462 (S-S); MS: m/z 690.1307, $[M + H]^+$; $C_{35}H_{32}NO_8S_3$ requires 690.1290.

***E*-isomer**: δ_H (400 MHz, $CDCl_3$): 8.48 (1H, dd, *J* = 8.7, 2.2 Hz, H-4), 8.40 (1H, d, *J* = 8.7 Hz, H-3), 8.18 (1H, d, *J* = 2.2 Hz, H-6), 7.20 (2H, t, *J* = 8.6 Hz, H-9"), 6.96 (1H, dd, *J* = 5.5, 2.2 Hz H-5'), 6.84 – 6.72 (5H, m, H-1', H-7', H-8' and H-10"), 6.55 (1H, dd, *J* = 9.7, 1.8 Hz, H-2'), 6.47 (1H, s, H-4'), 6.08 (1H, d, *J* = 14.6 Hz, H-4"), 5.88 (1H, dt, *J* = 14.6, 7.3 Hz, H-5"), 4.18 (2H, m, H-1"), 3.77 (3H, s, OCH_3), 3.68 (3H, s, OCH_3), 3.66 (2H, s, H-7"), 3.07 (2H, d, *J* = 7.3 Hz, H-6"), 2.89 (2H, t, *J* = 6.9 Hz, H-3"), 2.23 (2H, m, H-2"); δ_C (100 MHz, $CDCl_3$): 185.0 (C-3'), 164.0 (ArC_{qu}), 163.6 (ArC_{qu}), 158.6 (C-11"), 158.4 (ArC_{qu}), 154.3 (ArC_{qu}), 149.8 (ArC_{qu}), 146.6 (ArC_{qu}), 136.2 (ArC_{qu}), 135.8 (ArC_{qu}), 132.5 (C-3), 130.5 (ArC), 129.9 (C-9"), 129.8 (C-8"), 129.7 (C-5"), 129.3 (ArC), 128.4 (ArC), 127.4 (C-4"), 125.5 (C-6), 124.4 (C-4), 117.9 (ArC_{qu}), 114.1 (ArC), 113.9 (C-10"), 106.2 (ArC), 101.2 (ArC), 66.7 (C-1"), 55.2 (OCH_3), 53.1 (OCH_3), 35.4 (C-7"), 34.1 (C-3"), 32.7 (C-6"), 28.1 (C-2");

***Z*-isomer**: δ_H (400 MHz, $CDCl_3$): 8.48 (1H, dd, *J* = 8.7, 2.2 Hz, H-4), 8.40 (1H, d, *J* = 8.7 Hz, H-3), 8.18 (1H, d, *J* = 2.2 Hz, H-6), 7.20 (2H, t, *J* = 8.6 Hz, H-9"), 6.96 (1H, dd, *J* = 5.5, 2.2 Hz H-5'), 6.84 – 6.72 (5H, m, H-1', H-7', H-8' and H-10"), 6.55 (1H, dd, *J* = 9.7, 1.8 Hz, H-2'), 6.47 (1H, s, H-4'), 6.23 (1H, d, *J* = 9.3 Hz, H-4"), 5.72 (1H, dt, *J* = 9.3, 7.6 Hz, H-5"), 4.18 (2H, m, H-1"), 3.77 (3H, s, OCH_3), 3.68 (3H, s, OCH_3), 3.61 (2H, s, H-7"), 3.19 (2H, d, *J* = 7.6 Hz, H-6"), 2.90 (2H, t, *J* = 6.9 Hz, H-3"), 2.22 (2H, m, H-2"); δ_C (100 MHz, $CDCl_3$): 185.0 (C-3'), 164.0 (ArC_{qu}), 163.6 (ArC_{qu}), 158.6 (C-11"), 158.4 (ArC_{qu}),

154.3 (ArC_{qu}), 149.8 (ArC_{qu}), 146.6 (ArC_{qu}), 136.2 (ArC_{qu}), 135.8 (ArC_{qu}), 132.5 (C-3), 131.5 (C-4"), 130.5 (ArC), 129.9 (C-9"), 129.8 (C-8"), 129.3 (ArC), 128.8 (C-5"), 128.2 (ArC), 125.5 (C-6), 124.4 (C-4), 117.9 (ArC_{qu}), 114.1 (ArC), 113.9 (C-10"), 106.2 (ArC), 101.2 (ArC), 66.7 (C-1"), 55.2 (OCH_3), 53.1 (OCH_3), 34.9 (C-7"), 34.1 (C-3"), 29.3 (C-6"), 28.1 (C-2").

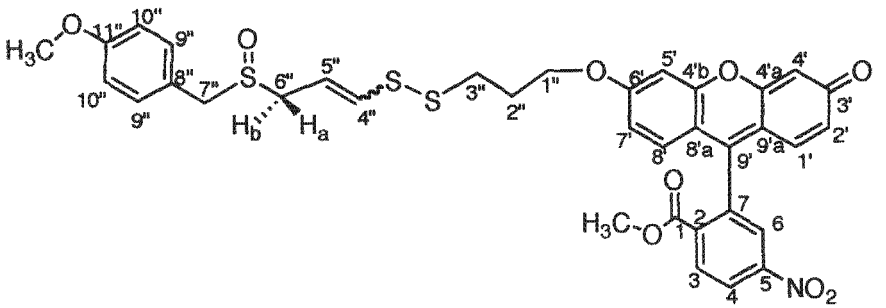

Methyl 2-(6-(3-((3-(4-methoxybenzylsulfinyl)prop-1-enyl)disulfanyl)propoxy)-3-oxo-3*H*-xanthen-9-yl)-4-nitrobenzoate, **53**

52 (355 mg, 0.51 mmol) was dissolved in DCM (5 mL) under N_2, after which the solution was cooled to -78 °C in a liquid N_2 / acetone bath. *m*-CPBA (138 mg, 0.61 mmol) was added directly as a solid and the reaction was allowed to stir for 2 hours below -60 °C, producing a single spot on TLC. Saturated aqueous Na_2CO_3 (10 mL) was added at -60 °C and the reaction was allowed to warm to room temperature. The organic material was extracted into DCM (20 mL), washed with brine (3 x 10mL) and dried over $MgSO_4$. Subsequent TLC analysis revealed an array of minor products formed during the work up. After the removal of solvent, the residue was purified using silica-gel column chromatography (EtOAc: hexane = 9: 1) to afford **53** as an orange-solid and as a 3: 4 mixture of *Z/E*-stereoisomers, (225 mg, 62 %).

(*E/Z*)-mixture: TLC: R_f = 0.15 (EtOAc); Mp (MeOH) 75 – 77 °C; ν_{max} / cm^{-1}($CHCl_3$): 1730 (CO_2CH_3), 1032 (S=O), 462 (S-S); MS: m/z 706.1258 , $[M + H]^+$; $C_{35}H_{32}NO_9S_3$ requires 706.1239; CHN anal. Calc. for $C_{35}H_{31}NO_9S_3$: C 59.56, H 4.43, N 1.98, S 13.63 %; Found: C 59.00, H 4.59, N 1.83, S 13.72 %;
***E*-isomer**: δ_H (400 MHz, $CDCl_3$): 8.50 (1H, dd, *J* = 8.8, 2.2 Hz, H-4), 8.41 (1H, d, *J* = 8.8 Hz, H-3), 8.19 (1H, d, *J* = 2.2 Hz, H-6), 7.20 (2H, d, *J* = 8.6 Hz, H-9"), 7.01 (2H, m, ArH), 6.89 (2H, d, *J* = 8.6 Hz, H-10"), 6.83 – 6.76 (3H, m, ArH), 6.64 – 6.55 (2H, m, ArH), 6.37 (1H, d, *J* = 14.7 Hz, H-4"), 5.98 (1H, dt, *J* = 14.7, 7.2 Hz, H-5"), 4.21 (2H, t, *J* = 6.0 Hz, H-1"), 3.93 (2H, m, H-7"), 3.80 (3H, s, OCH_3), 3.69 (3H, s, OCH_3), 3.44 (1H, dd, *J* = 13.1, 8.2 Hz, H-6_a"), 3.28 (1H, dd, *J* = 13.1, 8.2 Hz, H-6_b"), 2.92 (2H, t, *J* = 6.7 Hz, H-3"), 2.24 (2H, m, H-2"); δ_C (100 MHz, $CDCl_3$): 184.7 (C-3'), 164.0 (ArC_{qu}), 163.9 (ArC_{qu}), 159.8 (ArC_{qu}), 158.6 (C-11"), 154.5 (ArC_{qu}), 149.9 (ArC_{qu}), 136.2 (ArC_{qu}), 135.9 (ArC_{qu}), 133.8 (C-4"), 132.5 (C-3), 131.2 (C-9"), 130.6 (C-8"), 130.3 (ArC), 129.4 (ArC), 128.4 (ArC), 125.5 (C-6), 124.5 (C-4), 121.4

(ArC_{qu}), 118.0 (ArC_{qu}), 117.9 (C-5"), 114.5 (C-10"), 114.3 (ArC), 106.1 (ArC), 101.3 (ArC), 66.8 (C-1"), 56.6 (C-7"), 55.3 (OCH_3), 53.2 (OCH_3), 52.7 (C-6"), 34.3 (C-3"), 28.3 (C-2").

***Z*-isomer**: δ_H (400 MHz, $CDCl_3$): 8.50 (1H, dd, *J* = 8.8, 2.2 Hz, H-4), 8.41 (1H, d, *J* = 8.8 Hz, H-3), 8.19 (1H, d, *J* = 2.2 Hz, H-6), 7.20 (2H, d, *J* = 8.6 Hz, H-9"), 7.01 (2H, m, ArH), 6.89 (2H, d, *J* = 8.6 Hz, H-10"), 6.83 – 6.76 (3H, m, ArH), 6.64 – 6.55 (2H, m, ArH), 5.81 (1H, dt, *J* = 9.0, 8.2 Hz, H-5"), 4.20 (2H, t, *J* = 6.2 Hz, H-1"), 3.93 (2H, m, H-7"), 3.80 (3H, s, OCH_3), 3.69 (3H, s, OCH_3), 3.52 (1H, dd, *J* = 13.5, 8.2 Hz, H-6_a"), 3.48 (1H, dd, *J* = 13.5, 8.2 Hz, H-6_b"), 2.93 (2H, t, *J* = 5.8 Hz, H-3"), 2.24 (2H, m, H-2"); δ_C (100 MHz, $CDCl_3$): 184.7 (C-3'), 164.0 (ArC_{qu}), 163.9 (ArC_{qu}), 159.8 (ArC_{qu}), 158.6 (C-11"), 154.5 (ArC_{qu}), 149.9 (ArC_{qu}), 137.8 (C-4"), 136.2 (ArC_{qu}), 135.9 (ArC_{qu}), 133.8 (C-4"), 132.5 (C-3), 131.2 (C-9"), 130.6 (C-8"), 130.3 (ArC), 129.4 (ArC), 128.4 (ArC), 125.5 (C-6), 124.5 (C-4), 121.4 (ArC_{qu}), 119.2 (C-5"), 118.0 (ArC_{qu}), 114.5 (C-10"), 114.3 (ArC), 106.1 (ArC), 101.2 (ArC), 66.8 (C-1"), 57.0 (C-7"), 55.3 (OCH_3) 53.2 (OCH_3), 49.5 (C-6"), 35.1 (C-3"), 28.3 (C-2").

9.3 Fluorescent data

The UV/vis and fluorescent spectra were measured in quartz cuvettes using 100 μM ethanolic solutions of drug. The UV/vis spectrum was measured using a Varian Cary UV 100 spectrometer. The fluorescent spectra were measured using a Varian Cary-eclipse fluorescent spectrometer, with the following parameters set: excitation and emission slit set to 5 nm, medium scan control, medium PMT detector voltage, sample scanned from 200 – 800 nm.

Table 11: Summary of λ_{ex} and λ_{em} for all fluorescent ajoenes

	λ_{ex} (nm)	λ_{em} (nm)
FOx, 54	460	546
DP, 28	331	515
DOx, 30	321	518

9.4 Biological Experimental

9.4.1 General

The cells used were MDA-MB-231 breast tumour epithelial cell-line, CT1 transformed lung fibroblast cell-line and WHCO1 oesophogeal epithelial cell-line.

All cells were grown in Dulbecco's Modified Eagle Medium (DMEM) containing 10% heat-inactivated fetal bovine serum (FBS), 100 μg/ml penicillin and 100 μg/ml streptomycin. All media, buffers and reagents were pre-incubated (unless otherwise stated) to 37 °C in a thermostat-controlled water bath.

Generally, cells were cultured in 100 mm dishes to between 80 and 95 % confluence before splitting. The splitting procedure involved sucking off the growth media and washing with 7.4 phosphate buffer (PBS) (3 mL), followed by incubating the cells with 0.05% tripsin-EDTA (5 mL) for 3 - 4 minutes at 37 °C. The trypsin was then deactivated with the growth medium (3 mL), after which the cells were pelleted by centrifugation for 5 minutes at 40 000 rpm (Hettich EBA 20 centrifuge). The pellet was then resuspended in growth media (1 mL), using 20 % of the cells to propagate the culture.

Preparation of frozen stocks involved the steps described above, however instead of being replated, the cells were counted using a haemocytometer (Invitrogen Countess® Automated Cell counter), collected via centrifugation and resuspended at 1 x 10^6 cells/ml in a freeze medium containing 10% dimethyl sulfoxide (DMSO) and 70% DMEM and 20% FBS. The cell suspension was then transferred to 1ml ampules, which were stored at -80 °C for a week and then in liquid nitrogen for long-term storage. When required, the ampules were thawed at 37 °C and centrifuged for 5 minutes at 1000 x g. The cell pellet was collected, resuspended in growth medium and plated appropriately.

9.4.2 Cell proliferation analysis

The effect of the analogues on cell growth was measured using the MTT ((3-(4,5-Dimethylthiazol-2-yl)-2,5-diphenyltetrazolium bromide) cell proliferation kit (Roche, Mannheim, Germany). MTT is a yellow tetrazolium salt that is reduced by living cells to form a purple formazan, which can be quantified spectroscopically. The amount of purple formazan produced is proportional to the number of metabolically active cells. Each experiment was performed in triplicate, using 3 consecutive rows of a 96-well plate (Costar, Corning Inc., USA).

The cells were plated in 135 μl of media, in the following cell densities:

1. MDA – 3000 cells per well
2. WHCO1 – 2500 cells per well

After plating, the cells were allowed to settle and recover in an incubator overnight.

The following day a stock dilution series (see Table 12), ranging from 200 mM to 1.56 mM of drug in DMSO was prepared. Each dilution was further diluted 100 X into media, after which 15 μl of the new dilution was added to the cells (see table 13), giving a final dilution of 1000 X and 0.1 % DMSO. The cells were then incubated with the drug for 8 hours followed by the addition of 10μl of MTT solution to each well. Following a further 4 hour incubation at 37 °C, 10% SLS on 0.01 M HCl (100 μl) was added. The plate was further incubated at 37 °C over night.

Table 12: Dilution of drug stock

1	2	3	4	5	6	7	8	9	10	11
	200 mM	100 mM	50 mM	25 mM	12.5 mM	6.25 mM	3.125 mM	1.56 mM	0.753 mM	0 mM

Table 13: Final concentration of drug in each well

1	2	3	4	5	6	7	8	9	10	11
	200 μM	100 μM	50 μM	25 μM	12.5 μM	6.25 μM	3.125 μM	1.56 μM	0.75 μM	0

The following day, the plate was read on a plate reader (EL800, Biotek Instruments, Winsooki, USA) at 595 nm and the background absorbance of media, drug and MTT (no cells) was also obtained at 595 nm. The background absorbance was then subtracted from the readings. The data was converted into a spreadsheet and analyzed using Graphpad Prism 4, using non-linear regression analysis fitted to a sigmoidal dose-response curve (variable slope). The IC_{50} value was generated by the program and reported with a 95 % confidence interval.

9.4.3 Preparation of total cell lysate for SDS-page gel

The cells were plated in 10 cm dishes and allowed to grow to 80% confluence. The cells were treated with 1 ml of media containing DP (dansyl propyl ajoene) **30**, producing a final drug concentration of 40 μM and 0.01 % DMSO.

After 3 hours of incubation at 37 °C, the media was removed and the cells were gently washed with ice cold PBS (3 x 10 ml). After washing, RIPA buffer and protease inhibitor (200 μl) were added and the cells were harvested using mechanical scraping. The cells were collected in a 1 ml eppendorf tube, sonicated for 5 seconds and centrifuged at 15 000 x g for 15 minutes at 4 °C (Beckman Model TJ-6 Centrifuge, California, USA). After centrifugation, the supernatant was collected and the loading sample was prepared by mixing the lysate and loading buffer in a 5: 1 ratio. The samples were boiled for 10 minutes on a heating block at 99 °C and centrifuged again for 20 seconds, before loading onto the gel.

9.4.4 Protein assay using standard albumin curve

The BCA™ (Bicinchonic Acid) Protein Assay kit (Pierce, Illinois, USA) was used to quantify protein lysates from several cell extractions. The protocol was followed as described by the manufacturer, but a brief outline to follow: A standard curve was constructed using concentrations between 2000 and 0 μg/ml of bovine serum albumin (BSA) diluted in RIPA buffer or 0.9% saline. The protein lysates were

diluted ten fold and 25 μl of the test sample and each of the standards were pipetted into a Sero-Wel 96-well plate.

A working solution consisting of 50 parts A (sodium carbonate, sodium bicarbonate, BCA detection reagent, sodium tartrate in 0.1 M sodium hydroxide) to 1 part B (4% copper sulfate) was made and 200 μl was added to each well before incubating at 37 °C for 30 minutes. After cooling to room temperature, the absorbance at 595 nm was read using a 96-well plate reader (EL800, Biotek Instruments, Winsooki, USA) and the concentration of the protein extrapolated from the standard curve.

9.4.5 Non-denaturing gel electrophoresis

The gels were prepared using standard protocols: The separating gel was made using acrylamide concentrations of between 10 and 20 %, with the pH of 8.8 regulated by a tris buffer. The Stacking gel was made using acrylamide concentrations of 4%, with tris buffer regulated pH of 6.8. A molecular weight marker (PRN800 molecular weight marker, Amersham Bioschiences, Buckinghamshire, UK) was loaded in the first lane. The gel tank apparatus (Bio-Rad Mini-Protean 3 Cell Assembly) was filled with running buffer and the gels were run at 60 V while the proteins moving through the stacking gel. Once the dye front reached the running gel, the voltage was stepped up to 120 V for the remainder of the experiment.

9.4.6 Gel viewing and staining

The gels were fixed and stained for 2 hours in a solution containing 0.25% coomasie, 50% methanol, 10% acetic acid, in water. The destaining was performed over 48 hours using 10% methanol, 7.5% acetic acid in water.

9.4.7 Cysteine experiment

DOx **32** (30 mg, 0.050 mmol) and *N*-Boc cysteine ethylester (13 mg, 0.050 mmol) were refluxed over night in anhydrous THF. The reaction did not proceed to completion, but TLC revealed a new fluorescent product that was less polar than **32**. The solvent was removed under vacuum and the residue purified using silica-gel column chromatography (EtOAc: Hexane = 1: 1). The product was not obtained in quantities sufficient for analysis. The unreacted **32** (28 mg) was recovered from the column and confirmed to be pure by ^{1}H NMR spectroscopy and thus the reaction yield was estimated to be 7 %.

TLC: R_f = 0.60 (EtOAc: hexane = 3: 2)

9.4.8 Confocal microscopy

For the scanning laser confocal microscopy (Zeiss Axiovert 200m LSM 510 Meta Confocal Microscope). The confocal microscope was equipped with Argon laser lines (excitation at 458, 477, 488 and 514 nm; blue range), a solid state laser (561 nm; green range) and a HeNe laser (633 nm; red range). The cells were plated on chambered cover-glass dishes (Lab-Tek II, 1.5 borosilicate, 8 well) such that they would achieve approximately 80% confluence the following day. While using the confocal microscope, all dishes were kept in a 37 °C incubated chamber with 5% CO_2. Several organelle trackers were used in the manner outlined below:

All tracking substances were warmed to 37 °C and added to the cells at concentrations outlined by the manufacturers, after which the cells were incubated for 30 minutes. The media was then removed and replaced before the live-cell imaging could commence. The final DMSO concentration in each sample was < 0.1 %.

ER-tracker Red (Invitrogen E34250, stock = 1 mM in DMSO) – final concentration of 1 μM.
Lyso-tracker Red (Invitrogen L7528, stock = 1 mM in DMSO) – final concentration of 75 nM.
Mito-tracker Green (Invitrogen M7514, stock = 1 mM in DMSO) – final concentration of 250 nM.
DAPI (Invitrogen D3571, stock = 50 $\mu g.mL^{-1}$ in DMSO) – final concentration of 100ng. mL^{-1}.

The fluorescent analogues were added to the cells at 25 μM, after which the plates were immediately placed in an incubated chamber to maintain a healthy growing environment.

9.4.9 Transmission electron microscopy

MDA-MB-231 cells were plated in 145 mm dishes, containing 24 mL of DMEM media and grown to between 60 and 80% confluence. The treated samples were administered 1ml of media containing 1.25 μL of bis-PMB **17** (200 mM in DMSO stock), making the final concentration 10 μM in the cells. The control dishes were treated with 1 mL of media containing 1.25 μL DMSO (0.1 % DMSO). Samples were treated for 0, 1, 3 and 24 hours.

After the appropriate length of time, the media was removed by suction and the plates washed gently with ice-cold buffer (3 X 10ml), after which 2.5% gluteraldehyde in buffer (7 ml) was added to each dish. The dishes were left overnight to fix at 4 °C, after which the gluteraldehyde was removed and the cells harvested with gentle mechanical scraping. The cells were collected in 1 mL eppendorf tubes, centrifuged and after the supernatant had been removed, the pellet was resuspended 150 μl of low gelling agarose. The samples were stored at 4 °C for 2 hours to allow for the agarose to set. The gellified pellets were dissected into pieces of approximately 1 mm^3 and placed in 1 mL Epindorf tubes. Osmium tetroxide (1 % in PBS, 1 mL) was added to each sample and allowed to stand for 2 hours. The

Osmuim tetroxide solution was removed and the samples washed with PBS (500 μL, 5 min) and then water (2 X 500 μL, 5 min).

After removal of the water, the samples were dehydrated by subjection to increasing ethanolic solutions - 30 % ethanol (500 μL, 10 min), 50 % ethanol (500 μL, 10 min), 70 % ethanol (500 μL, 10 min), 80 % ethanol (500 μL, 10 min), 90 % ethanol (500 μL, 10 min), 95 % ethanol (500 μL, 10 min), 100 % ethanol (2 X 500 μL, 10 min), 100 % acetone (2 X 500 μL, 15 min).

The samples were then agitated in increasing concentrations of resin (in acetone) – 50 % (1 mL, 8 hours), 75 % (1 mL, 8 hours), 100 % (2 X 1 mL, 8 hours) – After the samples had spent a full 16 hours in 100 % resin, they were transferred to sample molds, labeled and placed in an oven at 60 °C over night for embedding.

The embedded samples were sectioned on a Leica Ultra-semi Microtome into 0.12 μm slices, which were collected on copper grids, post fixed with Uranyl acetate and Lead citrate and viewed on the transmission electron microscope (TEM).

9.4.10 Animal study 1

MDA cells were grown to 80% confluence, harvested and resuspended in PBS at 1.5 x 10^7 cells/mL. 100 μL of the suspension (1.5 x 10^6 cells) was injected subcutaneously into the right hind posterior each of the 24 female nude mice, aged between 4 and 8 weeks. The mice had been divided into 4 groups, each receiving a different dose of drug.

Immediately after the injection of the tumour cells, the first dose of bis-PMB **17** (100 μl dissolved in intralipid) was administered to each mouse via intraperitoneal injection. The control group consisting of 24 balb/C mice was similarly split into 4. The treatments (see Table 14) were administered every second day for 3 weeks, amounting to a total of 10 treatments.

Table 14: Dosage of treatments

Group	Dose (μg/g)
A	1
B	5
C	45
D	0

Upon completion of the experiment, the mice were sacrificed by halothane gas inhalation, followed by a C-2 – C-3 cervical dislocation. The mice were dissected and blood samples, tumors and livers were harvested.

9.4.11 Animal study 2:

WHCO1 cells were grown to 80% confluence, harvested and resuspended in PBS at 2.50 x 10^7 cells/ml. 100 μl of the suspension (2.50 x 10^6 cells) was injected subcutaneously into the right hind posterior each of the female nude mice, aged between 7 and 9 weeks. The mice were then left for 2 weeks to allow for tumour growth. The mice were numbered using the standard ear clipping numerical method and randomly divided (using Microsoft Excel to create random order) into two groups, each comprising two cages. The doses of BPMB **17** administered every second day, were prepared by dissolving the drug in DMSO (20% of total volume) and then into intralipid warmed to 37 °C. It was found that sonicating for 5 minutes at 37 °C also aided in the dissolution of drug. The doses of drug were administered as follows: 55.3 μg/g was administered for the first seven treatments, followed by 40.8 μg/g for the next five and 37.5 μg/g for the last four.

Treatments were administered every second day and the animals' health, weight and tumour size (measured with calipers) was carefully recorded. After 14 treatments, the mice were sacrificed using halothane and weighed. The tumors were carefully dissected, blood samples taken and the livers harvested. The volume of the tumour was determined as follows: (length^2 x height)/2.[57]

Stock solutions for all experiments were made as follows:

PBS 10 X solution: 1.37M NaCl 27 mM KCl 43 mM $Na_2HPO_4.2H_2O$ (pH 7.4) 14 mM KH_2PO_4	PBS 1 X solution: 1 part "PBS 10X" in 9 parts distilled H_2O – mixed, autoclaved and stored at 4 °C.
SLS – Solubilisation: 10% SLS in 0.01M HCl	The MTT solution: 100mg of MTT in 20 ml PBS buffer. Stored in the dark at 4 °C.
Glutaraldehyde: 2.5 % in PBS	Low gelling agarose: 0.3 % in d.H_2O
Osmium tetroxide: 1 % in PBS	

9.5 Powder X-ray diffraction

Powders generated from "kneading" were examined using powder X-ray diffraction (PXRD) and the traces compared to those for a library of known compounds. The powder was spread evenly on a thin layer of Paratone oil on a Mylar® film, which was fixed to an aluminum holder. The X-ray diffraction pattern was recorded using a Huber Imaging Plate camera 670 with nickel-filtered CuKα_1 radiation (λ = 1.5405981 Å), produced at 40 kV and 20 mA by a Philips (PW1120/00) generator, fitted with a Huber long fine-focus tube (PW 2273/20) and a Huber Guiner monochromator series (611/15). The pattern was recorded at steps of 0.005° over the 2θ range of 5 – 40°.

9.5.1 Host compounds

The host compounds β-CD, γ-CD, DIMEB, TRIMEB and TRIMEA were obtained from Cyclolab (Budapest, Hungary) and were used as received.

9.5.2 Guest compounds

An isomeric mixture of *E/Z* 1,8-(bis-*p*-methoxyphenyl)-2,3,7-trithia-octa-4-ene 7-oxide (BPMB, **17**) and *E/Z* Methyl 2-(6-(3-((3-(4-methoxybenzylsulfinyl)prop-1-enyl)disulfanyl)propoxy)-3-oxo-3*H*-xanthen-9-yl)-4-nitrobenzoate (FOx, **53**) were synthesized in Professor Roger Hunter's lab.

9.5.3 Complex preparation and crystal growth

Methylated cyclodextrins - Co-precipitation with the bis-*p*-methoxyphenyl ajoene **17** and DIMEB, TRIMEB and TRIMEA was attempted by vigorous overnight stirring of **17** (10 mg, 0.025 mmol) with cold solutions containing equimolar quantities of either DIMEB, TRIMEB or TRIMEA. Even after 24 hours of stirring, **17** did not fully dissolve and so the solutions were filtered using a 0.45 μm Teflon Millex-LCR filter into clean vials, left in an oven at 50 °C until crystals formed.

Native cyclodextrins - Co-precipitation with bis-*p*-methoxyphenyl ajoene **17** or fluorescein-tagged ajoene **53** and β-CD or γ-CD was attempted by vigorous overnight stirring of **17** (10 mg, 0.025 mmol) or **53** (10 mg, 0.015 mmol) with hot solutions containing equimolar quantities of either β-CD or γ-CD. The solutions were allowed to stir for 24 hours at 60 °C, after which it was noted that the guests failed to (completely) dissolve. The solutions were filtered using a 0.45 μm Teflon Millex-LCR filter into clean vials, left on the bench top for crystallization to occur. To date, no single crystals have been generated.

Kneading with native cyclodextrins – Inclusion complexes were prepared by vigorous mechanical kneading of **17** with equimolar quantities of β-CD or γ-CD for 45 minutes in an agate mortar using single drops of distilled water to ensure the mixture was a cohesive paste. The procedure was also performed using equimolar quantities of **53** and β-CD.

Chapter 10: References

1. Wilson, E. A.; Demmig-Adams, B., Antioxidant, Anti-Inflammatory, and Antimicrobial Properties of Garlic And Onions. *Nutrition & Food Science* **2007,** *37*, 178-183.

2. Yoshida, S.; Kasuga, S.; Hayashi, N.; Ushiroguchi, T.; Matsuura, H.; Nakagawa, S., Antifungal Activity of Ajoene Derived From Garlic. *Applied and Environmental Microbiology* **1987,** *53*, 615-7.

3. Lawson, L. D., Characterization of the Formation of Allicin and Other Thiosulfinates from Garlic. *Planta Med* **1992,** *58*, 345-350.

4. Block, E., The Organosulfur Chemistry of the Genus Allium - Implications for the Organic Chemistry of Sulfur. *Angewandte Chemie International Edition In English* **1992,** *31*, 1135-1174.

5. Argarwal, K. C., Theraputic Action of Garlic Constituents. *Med. Res. Rev* **1996,** *16*, 111-124.

6. Lawson, L. D., Composition, Stability and Bioavailability of Garlic Products Used in a Chemical Trial. *J. Agric. Food Chem.* **2005,** *53*, 6254-6261.

7. Block, E.; Ahmad, S., (E,Z)-Ajoene: A Potent Antithrombotic Agent from Garlic. *New York* **1984,** *106*, 8295-8296.

8. Block, E.; Ahmad, S.; Catalfamo, J. L.; Jain, M. K.; Apitz-Castrozd, R., Antithrombotic Organosulfur Compounds from Garlic. *J. Am. Chem. Soc.* **1986,** *108*, 7045-7055.

9. Gallwitz, H.; Bonse, S.; Martinez-Cruz, A.; Schlichting, I.; Schumacher, K.; Krauth-Siegel, R. L., Ajoene is an Inhibitor and Subversive Substrate of Human Glutathione Reductase and Trypanosoma Cruzi Trypanothione Reductase: Crystallographic, Kinetic, and Spectroscopic Studies. *Journal of Medicinal Chemistry* **1999,** *42*, 364-72.

10. Gargouri, Y.; Moreau, H.; Jain, M. K.; De Haas; G. H.; Verger, R., Ajoene Prevents Fat Digestion by Human Gastric Lipase in Vitro. *Biochim. Biophys. Acta* **1989,** *1006*, 137-139.

11. Cancer Statistics. Http://Www.Who.Int/Cancer/En/).

12. (A) Chemotharapy. Http://Www.Chemotherapy.Com/; (B) Breast Cancer Chemotherapy. Http://Www.Breastcancer.Org/Treatment/Chemotherapy/Medicines.Jsp.

13. Skalnikova, H.; J. M.; Hrabakova, R.; Halada, P.; Dziechciarkova, M.; Hajduch, M.; Gadher, S. J.; Hammar, A.; Enetoft, D.; Ekefjard, A.; Forsstrom-Olsson, O.; Kovarova, H. Cancer Drug-Resistance and a Look at Specific Proteins: Rho GDP-Dissociation Inhibitor 2, Y-Box Binding Protein 1 and HSP70/90 Organising Protein in Proteomics Clinical Application. *J. Proteome Res.* **2010**.

14. Sjöström, J.; Mäkelä, T., Apoptosis and the Cell Cycle in Human Disease. *Wiley Online Library* **2006**, 1-6.

15. Dirsch, V.; Antlsperger, D.; HENTZER, H.; Vollmar, A., Ajoene, an Experimental Anti-Leukemic Drug: Mechanism of Cell Death. *Leukemia* **2002,** *16*, 74-83.

16. Shiraishi, H.; Okamoto, H.; Yoshimura, A.; Yoshida, H., ER Stress-Induced Apoptosis and Caspase-12 Activation Occurs Downstream of Mitochondrial Apoptosis Involving Apaf-1. *Journal of Cell Science* **2006,** *119*, 3958-66.

17. Xu, C.; Baily-Maitre, B.; Reed, J. C., Endoplasmic Reticulum Stress: Cell Life and Death Decisions. *Journal Of Clinical Investigation* **2005,** *115*, 2656-2664.

18. (A) Fleischauer, A. T.; Arab, L., Garlic and Cancer: A Critical Review of the Epidemiologic Literature. *J. Nutr.* **2001,** 1032S–1040S; (B) Shukla, Y.; Kalra, N., Cancer Chemoprevention With Garlic and its Constituents. *Cancer Lett.* **2007,** *247*, 167–181.

19. Ishikawa, K.; Naganawa, R.; Yoshida, H.; Iwata, N.; Fukuda, H.; Fujino, T.; Suzuki, A., Antimutagenic Effects of Ajoene, an Organo-Sulfur Compound Derived from Garlic. *Biosci. Biotech. Biochem.* **1996,** *60*, 2086–2088.

20. Lawson, L. D.; Wang, Z. J., Pre-Hepatic Fate of the Organosulfur Compounds from Garlic (Allium Sativum). *Planta Med.* **1993** *59*, A688–A689.

21. Scharfenberg, K.; Wagner, R.; Wagner, K. G., The Cytotoxicity Effect of Ajoene, a Natural Product from Garlic, Investigated with Different Cell Lines. *Cancer Lett.* **1990,** *53*, 103–108.

22. Sundaram, S. G.; Milner, J. A., Impact of Organosulfur Compounds in Garlic on Canine Mammary Tumour Cells in Culture. *Cancer Lett.* **1993,** *74*, 85-90.

23. (A) Li, M.; Ciu, J.-R.; Ye, Y.; Min, J.-M.; Zhang, L.-H.; Wang, K.; Gares, M.; Cros, J.; Wright, M.; Leung-Tack, J., Antitumor Activity Of Z-Ajoene, A Natural Compound Purified from Garlic: Antimitotic and Microtubule-Interaction Properties. *Carcinogenesis* **2002,** *23*, 573-9; (B) Taylor, P.; Noriega, R.; Farah, C.; Abad, M.-J.; Arsenak, M.; Apitz, R., Ajoene Inhibits Both Primary Tumor Growth and Metastasis of B16/BL6 Melanoma Cells in C57BL/6 Mice. *Cancer Letters* **2006,** *239*, 298-304.

24. Dirsch, V. M.; Antlsperger, D. S. M.; Hentze, H.; Vollmar, A. M., Ajoene , An Experimental Anti-Leukemic Drug : Mechanism of Cell Death. *Leukemia* **2002**, 74-83.

25. Dirsch, V. M.; Gerbes, A. L.; Vollmar, A. M., Ajoene, a Compound of Garlic, Induces Apoptosis in Human Promyeloleukemic Cells, Accompanied by Generation of Reactive Oxygen Species and Activation of Nuclear Factor Kappab. *Molecular Pharmacology* **1998,** *53*, 402-7.

26. Tilli, C. M.; Stavast-Kooy, A. J. W.; Vuerstaek, J. D. D.; Thissen, M. R. T. M.; Krekels, G. A. M.; Ramaekers, F. C. S.; Neumann, H. A. M., The Garlic-Derived Organosulfur Component Ajoene Decreases Basal Cell Carcinoma Tumor Size by Inducing Apoptosis. *Archives Of Dermatological Research* **2003,** *295*, 117-23.

27. Laverick, N. A. L.; Sammons, J.; Zhang, H.; Maslin, D. J.; Hassan, H. T., Ajoene, a Garlic-Derived Natural Compound, Enhances Chemotherapy-Induced Apoptosis in Human Myeloid Leukemia CD-34-Positive Resistant Cells. *Anticancer Res.* **2001** *21*, 3519–3524.

28. Hassan, H. T., Ajoene (Natural Garlic Compound): A New Anti-Leukaemia Agent for AML Therapy. *Leukemia Research* **2004,** *28*, 667-71.

29. Antlsperger, D. S. M.; Dirsch, V. M.; Ferreira, D.; Su, J.-L.; Kuo, M.-L.; Vollmar, A. M., Ajoene-Induced Cell Death in Human Promyeloleukemic Cells Does Not Require JNK but is Amplified by the Inhibition of ERK. *Oncogene* **2003** *22*, 582–589.

30. Li, M.; Min, J.-M.; Cui, J.-R.; Zhang, L.-H.; Wang, K.; Valette, A.; Dav- Rinche, C.; Wright, M.; Leung-Tack, J., Z-Ajoene Induces Apoptosis of HL-60 Cells: Involvement of Bcl-2 Cleavage. *Nutr. Cancer* **2002** *42*, 241–247.

31. Munchberg, U.; Anwar, A.; Mecklenberg, S; Jacob, C., Polysulfides as Biologically Active Ingredients af Garlic. *Organic & Biomolecular Chemistry* **2007,** *5*, 1505-1518.

32. Ledezma, E.; Apitz-Castro, R.; Cardier, J., Apoptotic and Anti-adhesion Effect of Ajoene, a Garlic Derived Compound, on the Murine Melanoma B16F10 Cells: Possible Role of Caspase-3 and the Alpha(4)Beta(1) Integrin. *Cancer Letters* **2004,** *206*, 35-41.

33. Lawson, L. D.; Ransom, D. K.; Hughes, B. G.; Murdock, M., Inhibition of Whole Blood Platelet Aggregation by Compounds in Garilc Extracts and Commercial Garlic Products. *Thromb. Res* **1992,** *65*, 141-156.

34. Byron, B., Fluorescence Imaging of Tumors in Vivo. *Current Medicinal Chemistry* **2005**, 795-805.

35. Frisoli, J. K.; Tudor, E. G.; Flotte, T. J.; Hasan, T.; Deutsch, T. F.; Schomacker, K. T., L * Harmaco Kinetics of a Fluorescent Drug Using Laser-Induced Fluorescence. *Cancer Research* **1993,** *53*, 5954-5961.

36. Claxton, N. S.; Fellers, T. J.; Davidson, M. W., LASER SCANNING CONFOCAL MICROSCOPY. *Microscopy* **1979,** *1979*.

37. (A) Kapanidis, A. N.; Ebright, Y. W.; Ebright, R. H., Site-Specific Incorporation of Fluorescent Probes into Protein; *Health (San Francisco)* **2001,** *11*, 12123-12125; (B) Miller, L. W.; Cornish, V. W., Selective Chemical Labeling of Proteins in Living Cells. *Current Opinion in Chemical Biology* **2005,** *9*, 56-61; (C) Benito-Peña, E.; Moreno-Bondi, M. C.; Aparicio, S.; Orellana, G.; Cederfur, J.; Kempe, M., Molecular Engineering of Fluorescent Penicillins for Molecularly Imprinted Polymer Assays. *Analytical Chemistry* **2006,** *78*, 2019-27; (D) Zhang, Y.-H.; Gao, Z.-X.; Zhong, C.-L.; Zhou, H.-B.; Chen, L.; Wu, W.-M.; Peng, X.-J.; Yao, Z.-J., An Inexpensive Fluorescent Labeling Protocol for Bioactive Natural Products Utilizing Cu(I)-Catalyzed Huisgen Reaction. *Tetrahedron* **2007,** *63*, 6813-6821; (E) Tang, J.; Yin, H.; Qiu, J.; Tucker, M. J.; Degrado, W. F.; Gai, F., Using Two Fluorescent Probes to Dissect the Binding, Insertion, and Dimerization Kinetics af a Model Membrane Peptide. *Journal of The American Chemical Society* **2009,** *131*, 3816-7.

38. Olympus Microscopy. Http://Www.Olympusmicro.Com/Primer/Techniques/Confocal/Fluorophoresintro.Html.

39. Wang, X. F., *Fluorescence Imaging Spectroscopy And Microscopy*. 1996.

40. Bozzola, J. J., *Electron Microscopy*. Second Ed.; Jones And Bartlett Publishers: 1999.

41. Brewster, M. E., Cyclodextrins as Pharmaceutical Solubilizers. *Advanced Drug Delivery Reviews* **2007,** *59*, 645-666.

42. Caira, M. R.; Hunter, R.; Bourne, S. A.; Smith, V. J., Preparation, Thermal Behaviour and Solid-State Structures of Inclusion Complexes of Permethylated-B-Cyclodextrin with the Garlic-Derived Antithrombotics (E)- and (Z)-Ajoene. *Supramolecular Chemistry* **2004,** *16*, 395-403.

43. Hunter, R.; Kaschula, C. H.; Parker, I. M.; Caira, M. R.; Richards, P.; Travis, S.; Taute, F.; Qwebani, T., Substituted Ajoenes as Novel Anti-Cancer Agents. *Bioorganic & Medicinal Chemistry Letters* **2008,** *18*, 5277-9.

44. Kaschula, C. H., *Unpublished Data* **2010**.

45. Prabharasuth, R. A., *J. Org. Chem.* **2001,** *66*, 5256-5258.

46. Kimura, S.; Bill, E.; Bothe, E.; Weyhermuller T.; Wieghardt, K., *J. Am Chem. Soc.* **2001,** *123*, 6025-6039.

47. Tsutsumi, K.; Yabukami, T.; Fujimoto, K.; Kawase, T.; Morimoto, T.; Kakiuchi, K., Effects of a Bidentate Phosphine Ligand on Palladium-Catalyzed Nucleophilic Substitution Reactions of Propargyl and Allyl Halides with Thiol. *Organometallics* **2003,** 22, 2996-2999.

48. Mccabe, R. T.; Rhodes, C. A; Decosta, B. F., Characterization of Benzodiazapine Receptors with Fluorescent Ligands. *FASEB J.* **1990**, 11, 2934-2940

49. Mckinney, R. M., Nitrofluorescein Derivatives. *J. Chem. Soc.* **1949**, 3986-3988.

50. Coons, A. K., Melvin, Localization of Antigen in Tissue Cells. *Journal of Experimental Medicine* **1949**, 1-13.

51. Sigmund, H.; Pfleiderer, W., Nucleotides. Part LXXI. *Helvetica Chimica Acta* **2003,** *86*, 2299-2334.

52. Boga, C.; Puggioli, S.; Gherpelli, M.; Farruggia, G.; Pagnotta, E.; Masotti, L.; Neyroz, P., Fluorescein Conjugates Of 9- and 10-Hydroxystearic Acids: Synthetic Strategies, Photophysical Characterization, and Confocal Microscopy Applications. *Analytical Biochemistry* **2004,** *335*, 196-209.

53. (A) Lavis, L. D.; Rutkoski, T. J.; Raines, R. T., Tuning The Pk(A) of Fluorescein to Optimize Binding Assays. *Analytical Chemistry* **2007,** *79*, 6775-82; (B) Chen, S.-H.; Hsu, J.-L.; Lin, F.-S., Fluorescein as a Versatile Tag for Enhanced Selectivity in Analyzing Cysteine-Containing Proteins/Peptides Using Mass Spectrometry. *Analytical Chemistry* **2008,** *80*, 5251-9; (C) Cho, H. K.; Lone, S.; Kim, D. D.; Choi, J. H.; Choi, S. W.; Cho, J. H.; Kim, J. H.; Cheong, I. W., Synthesis and Characterization of Fluorescein Isothiocyanate (FITC)-Labeled PEO–PCL–PEO Triblock Copolymers for Topical Delivery. *Polymer* **2009,** *50*, 2357-2364.

54. Fluorescein Absorption and Emmission Spectra. Http://Www.Eurofinsdna.Com/Products-Services/Oligonucleotides0/Modified-Dna-Oligos/Dye-Modifications/Fluorescein-Dt.Html.

55. Dansyl Chloride Absorption and Emmission Spectra. Http://Www.Isogen-Lifescience.Com/Home/Fluorescent_Labeled.

56. Mosmann, T., Rapid Colorimetric Assay for Cellular Growth and Survival: Application to Proliferation and Cytotoxicity Assays. *Journal of Immunological Methods* **1983,** *65*, 55-63.

57. (A) Xiao, D.; Hrman-Antosiewicz, A.; Antosiewicz, J.; Xiao, H.; Brisson, M.; Lazo, J. S.; Singh, S. V., Diallyl Trisulfide-Induced G2-M Phase Arrest in Human Prostrate Cancer Cells is Caused by Reactive Oxygen Species-Dependent Destruction and Hyperphosphorylation of Cdc25C. *Oncogene* **2005** *24*, 6256–6268; (B) Xu, B.; Monsarrat, B.; Gairin, J. E.; Girbal-Neuhauser, E., Effect of Ajoene, a

Natural Antitumor Small Molecule, on Human 20S Proteasome Activity in Vitro and in Human Leukemic HL60 Cells. *Fundamental & Clinical Pharmacology.* **2004,** *18*, 171-80.

58. Kaschula, C. H., IC_{50} Values of Ajoene and BPMB. 2010.

59. Jensen, M.; Jorgensen, J.; Binderup, T.; Kjaer, A., Tumor Volume in Subcutaneous Mouse Xenografts Measured by Microct is More Accurate and Reproducible than Determined by 18F-FDG-Micropet or External Caliper. *BMC Medical Imaging* **2008,** *8* (1), 16.

60. Xiao, D.; Vogel, V.; Singh, S. V., Benzyl Isothiocyanate–Induced Apoptosis in Human Breast Cancer Cells is Initiated by Reactive Oxygen Species and Regulated by Bax and Bak. *Mol. Cancer Ther.* **2006,** *5*, 2931-2945.

61. Hunter, R., Unpublished Data. **2010**.

62. Braga, S. S.; Goncalves, I. S.; Herdtweckb, E.; Teixeira-Dias, J. J. C., Solid State Inclusion Compound of S-Ibuprofen in B-Cyclodextrin: Structure and Characterisation. *New J. Chem.* **200,** *27*, 597–601.

63. Steiner, T. S., Channel-Type Crystal Packing in the Very Rare Space Group P4212 with Z0 = 3/4: Crystal Structure Of The Complex -Cyclodextrin±Methanol±N-Hydrate2. *Acta Cryst.* **1998,** *54*, 450-455.

64. Yanli, Z. A. Y., L., Self-Assembly Behavior of Phenyl Modified B-Cyclodextrins. *Science in China: Series B Chemistry* **2006** *49* 230—237.